AD-A106 083 ROCKWELL INTERNATIONAL COLUMBUS OH NORTH AMERICAN AI--ETC F/G 20/1
INVESTIGATION OF ACOUSTIC INTERACTIONS IN JET THRUST AUGMENTING--ETC(U)
MAR 81 J R CAMPBELL, K D KORKAN, H VIETS N00019-79-C-0225
UNCLASSIFIED NR80H-50 NL

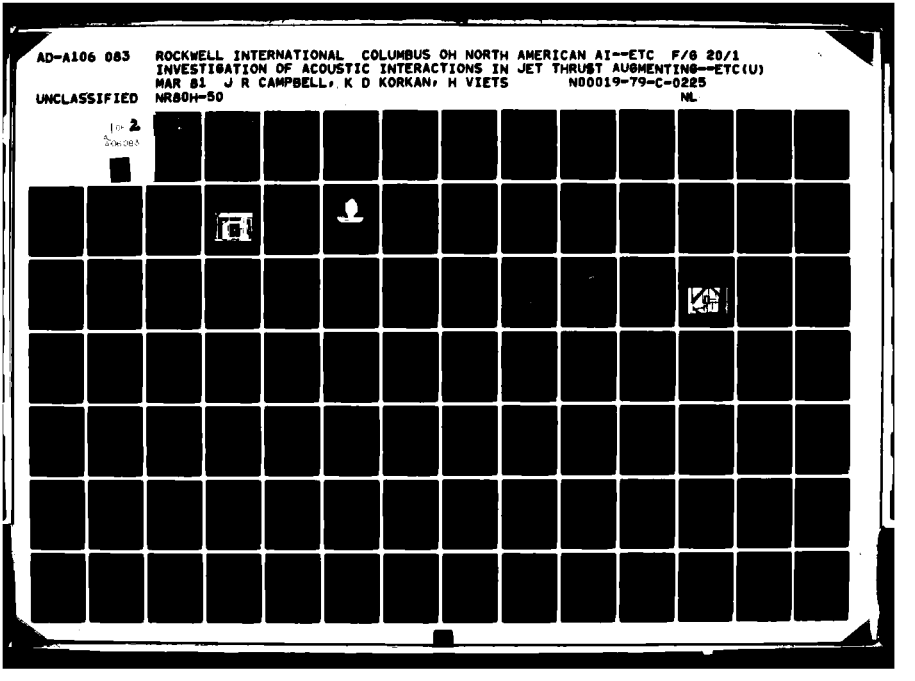

LEVEL II

NR80H-50

12

INVESTIGATION OF ACOUSTIC INTERACTIONS IN JET THRUST AUGMENTING EJECTORS

J. R. Campbell
Rockwell International
North American Aircraft Division
Columbus, Ohio 43216

K. D. Korkan
Ohio State University
Columbus, Ohio 43220

H. Viets
Wright State University
Dayton, Ohio 45431

Contract N00019-79-C-0225

5 March 1981

FINAL REPORT FOR PERIOD 1 January 1979–30 September 1980

PREPARED FOR THE
NAVAL AIR SYSTEMS COMMAND, DEPARTMENT OF THE NAVY, WASHINGTON, DC

X

01 10 23

UNCLASSIFIED

SECURITY CLASSIFICATION OF THIS PAGE *(When Data Entered)*

REPORT DOCUMENTATION PAGE

READ INSTRUCTIONS BEFORE COMPLETING FORM

1. REPORT NUMBER

2. GOVT ACCESSION NO. AD-A106 083

3. RECIPIENT'S CATALOG NUMBER

4. TITLE *(and Subtitle)*

(6) INVESTIGATION OF ACOUSTIC INTERACTIONS IN JET THRUST AUGMENTING EJECTORS.

5. TYPE OF REPORT & PERIOD COVERED

(9) FINAL REPORT. 1 JAN 79 — 30 SEP 80,

6. PERFORMING ORG. REPORT NUMBER

(14) NR804-50

7. AUTHOR(s)

(10) J. R. CAMPBELL, ROCKWELL INTERNATIONAL
K. D. KORKAN, OHIO STATE UNIVERSITY
H. VIETS, WRIGHT STATE UNIVERSITY

8. CONTRACT OR GRANT NUMBER(s)

(15) N00019-79-C-0225

9. PERFORMING ORGANIZATION NAME AND ADDRESS

ROCKWELL INTERNATIONAL CORPORATION
NORTH AMERICAN AIRCRAFT DIVISION
COLUMBUS, OHIO 43216

10. PROGRAM ELEMENT, PROJECT, TASK AREA & WORK UNIT NUMBERS

(12) 244

11. CONTROLLING OFFICE NAME AND ADDRESS

CODE AIR 320D
NAVAL AIR SYSTEMS COMMAND
WASHINGTON, D.C. 20361

12. REPORT DATE

30 SEPTEMBER 1980

13. NUMBER OF PAGES

139

14. MONITORING AGENCY NAME & ADDRESS*(if different from Controlling Office)*

15. SECURITY CLASS. *(of this report)*

UNCLASSIFIED

15a. DECLASSIFICATION DOWNGRADING SCHEDULE

16. DISTRIBUTION STATEMENT *(of this Report)*

(11) 30 SEP 80

17. DISTRIBUTION STATEMENT *(of the abstract entered in Block 20, if different from Report)*

18. SUPPLEMENTARY NOTES

19. KEY WORDS *(Continue on reverse side if necessary and identify by block number)*

JET SCREECH, AXISYMMETRIC EJECTOR, RECTANGULAR EJECTOR, ACOUSTIC EFFECTS, IMPROVED MIXING

20. ABSTRACT *(Continue on reverse side if necessary and identify by block number)*

The performance of a constant area rectangular ejector with varying mixing length was investigated to determine the aeroacoustics interaction effects. The rectangular ejector investigation was conducted in two phases. The phase one investigation involved the testing of three different aspect ratio rectangular convergent nozzles at pressure between 15-45 psig to determine the acoustic and jet spreading characteristics. From these data a rectangular ejector incorporating endwall and ejector flap blowing was

DD FORM 1 JAN 73 1473 EDITION OF 1 NOV 65 IS OBSOLETE

UNCLASSIFIED 407 290

SECURITY CLASSIFICATION OF THIS PAGE *(When Data Entered)*

fabricated and investigated at pressure ratios between 2.0 and 5.0. These investigations were conducted at ejector flap length (L) to ejector throat widths (W), L/W of 11.0, 9.5, 8.0, 6.5, 5.0, 3.5, 2.0, and 0.9 to determine the ejector performance.

The data for the rectangular ejector configuration investigated showed an aeroacoustic interaction in the pressure ratio range of 3.3 - 3.8. However, the resulting performance was not improved to the degree experienced with axisymmetric ejectors.

ABSTRACT

The performance of a constant area rectangular ejector with varying mixing length was investigated to determine the aeroacoustics interaction effects. The rectangular ejector investigation was conducted in two phases. The phase one investigation involved the testing of three different aspect ratio rectangular convergent nozzles at pressure between 15-45 psig to determine the acoustic and jet spreading characteristics. From these data a rectangular ejector incorporating endwall and ejector flap blowing was fabricated and investigated at pressure ratios between 2.0 and 5.0. These investigations were conducted at ejector flap length (L) to ejector throat widths (W), L/W of 11.0, 9.5, 8.0, 6.5, 5.0, 3.5, 2.0, and 0.9 to determine the ejector performance.

Based on previous investigation of axisymmetric ejectors it was anticipated that the rectangular ejector performance at short mixing lengths (L/W's) would as a result of aeroacoustic interaction exhibit increased mixing thereby improving performance of the short ejector to rival an ejector of a mixing length with nearly fully mixed flow.

The data for the rectangular ejector configuration investigated showed an aeroacoustic interaction in the pressure ratio range of 3.3 - 3.8. However, the resulting performance was not improved to the degree experienced with the axisymmetric ejector.

PREFACE

This report describes work performed by the North American Aircraft Division of Rockwell International during the period 1 January 1979 to 30 September 1980.

We would like to acknowledge the contributions of Mr. Paul Cole and Mr. James Baldwin, who conducted the isolated jet test and Mr. Rick Freuler, who developed the data acquisition routines which were employed.

TABLE OF CONTENTS

LIST OF FIGURES

LIST OF FIGURES (CONT'D)

LIST OF FIGURES (CONT'D)

LIST OF FIGURES (CONT'D)

LIST OF FIGURES (CONT'D)

LIST OF FIGURES (CONT'D)

INTRODUCTION

Background

The fact that a jet interacts with acoustic waves has been known and studied since the last century. Three of the more recent studies are presented in References 1 through 3. The changes in the jet behavior (in particular, the mixing rate) can be rather large and therefore lead to a consideration of potential applications.

When the stagnation pressure of the jet is increased beyond the point of reaching choked flow in a convergent nozzle (i.e., the flow limited by Mach number equal to unity in the nozzle), the noise produced by the jet is often dominated by a single frequency tone. This tone is called the jet screech tone and was first studied in detail by Powell.[4,5] The screech occurs when small disturbances are amplified by the jet velocity field, causing the jet to oscillate on a large scale. The unsteady jet then acts as a stronger noise source. Thus, an interaction is produced between the velocity and acoustic fields. This increases the jet mixing.

Powell's work concerned itself with axisymmetric and low aspect ratio rectangular choked jets. Hammitt,[6] on the other hand, was concerned with higher aspect ratio (approximately 12.5) rectangular jets. As in the axisymmetric case, the choked and underexpanded jet produced a dominant screech tone and the acoustic interaction between that tone and the jet caused the jet to oscillate. Besides measuring the acoustic properties of the jet, Hammitt was able to photograph the acoustic waves emanating from the unsteady jet structure farther downstream.

Glass[7] demonstrated that jet screech was not limited to the underexpanded jets from convergent nozzles when he found the same effect in supersonic jets from convergent-divergent nozzles operated at off-design pressure ratios. As in the earlier expeiments, the unsteady jets produced by the interaction result in a very substantial increase in the rate with which the jet mixes with its surroundings.

From the point of view of ejectors, the interest in aeroacoustic interactions of jets stems simply from the potential for increased mixing. The thrust performance of an ejector device is strongly coupled to the degree of mixing between the primary and secondary flows.[8,9] This is especially true for short ejectors where complete mixing (i.e., a uniform exit velocity profile) is difficult to achieve.

The first attempt to correlate the ejector performance with the jet acoustic interaction was performed by Quinn[10] in an axisymmetric ejector with a single axisymmetric nozzle on the centerline. He found that the mass flow through the ejector was increased whenever there was an acoustic interaction between the jet and the ejector shroud. He also showed that the acoustic structure of the axisymmetric choked jet flow was drastically modified by the presence of the ejector shroud about it. He compared his ejector results with the results of Rosfjord and Toms[11] who studied the acoustic properties of the nozzle alone.

A more complete description of the acoustic interaction present in an axisymmetric ejector is described by Quinn in Reference 12 and related comments appear in his study of temperature effects.[13] Of particular interest is Quinn's observation that the more beneficial acoustic interactions (from the point of view of increased mass flow) are the jet modes in which the jet oscillates from side to side so that the pressure oscillations on opposite sides of the jet are out of phase with each other.

Thus, the performance of axisymmetric ejectors has been shown to be improved by an acoustic interaction between the jet and the shroud. Since both round and rectangular jets have been observed to screech, it seems likely that the performance of rectangular ejectors may also be improved by an acoustic interaction. The purpose of this study was to determine the nature and magnitude of this interaction.

Because it was not known whether the increase in ejector performance was due to amplification of the jet or duct acoustics, the experiments were performed in two parts. First, the free jets from a series of rectangular nozzles were tested to determine their acoustic and mixing characteristics. Then, a rectangular ejector was tested to determine if there was an acoustic effect on performance. The magnitude of the effect was found to be small in the case of the ejector studied, and was primarily due to amplification of the isolated jet screech by the duct.

FREE JET TESTS

The objective of the free jet tests described in this report is to identify the screech tones generated by the nozzle geometries and conditions chosen, and to determine the basic effect of nozzle aspect ratio on the acoustic structure. The modification of this structure by the presence of the shroud and the overall ejector performance are then determined in the following section.

Experimental Facilities

The initial free jet nozzle tests were performed at the Aero-Thermodynamics Laboratory of the North American Aircraft Division of Rockwell

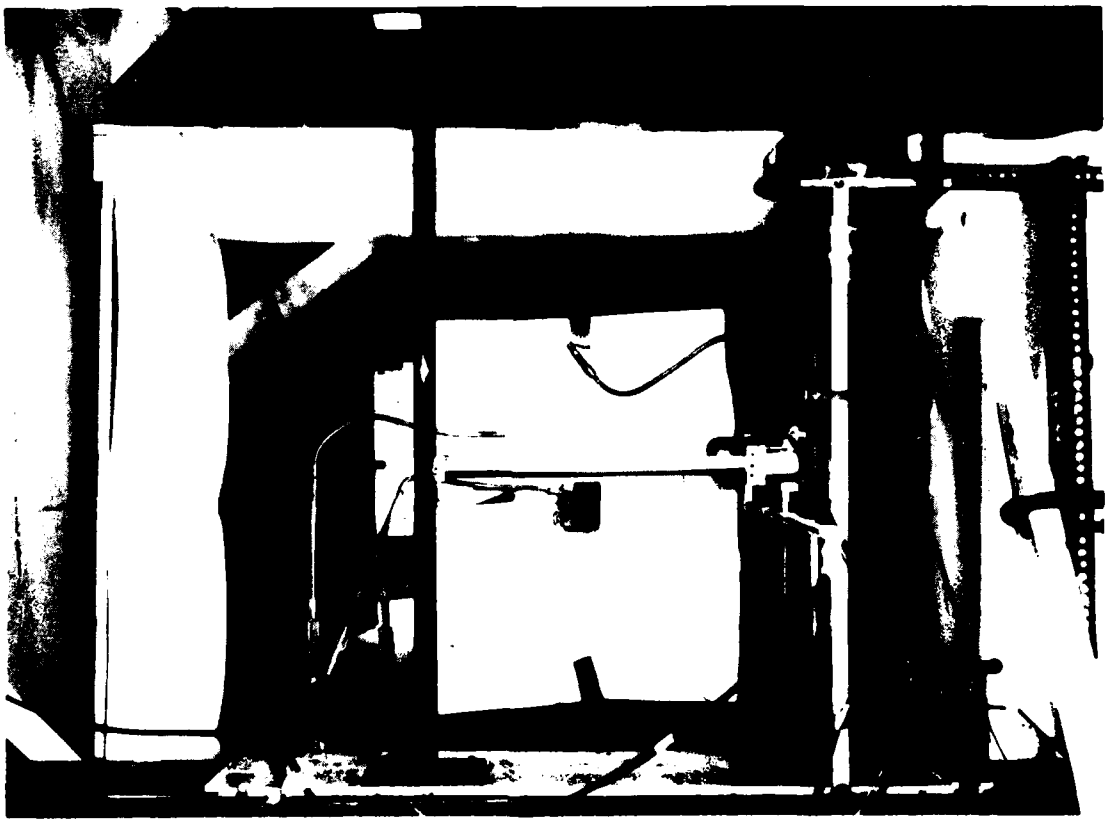

Figure 1. Free Jet Test Facility Rockwell International

International in Columbus, Ohio (Figure 1). The nozzles to be tested were mounted on the flat wall of a 20-inch diameter stagnation chamber. Both the chamber and the nozzle were enclosed on the sides, top and bottom, by a tent-like wood frame structure lined with 2-inch thick polyurethane foam to isolate the acoustic structure. The upstream and downstream ends of the enclosure were left open in order to avoid blocking the flow. The enclosure was 6 feet square and 3.3 feet long.

The acoustic data were measured by five Altec Lansing Corporation type 21BR-150 condenser microphone systems and a Gulton MBQ2151 crystal microphone system. The jet pressure profiles were measured by a conventional total pressure probe mounted on a two-axis traversing system. The entire experimental facility is shown in Figure 1 looking upstream at a rectangular nozzle mounted on the stagnation chamber.

Nozzle Geometries

The initial free jet tests were performed on three simple rectangular convergent nozzles of aspect ratio (length/width ratio of the nozzle exit) AR = 2, 5 and 16. The nozzles were designed to have the same nominal exit areas but the actual devices have a small variation as shown in Table I. A photograph of the AR = 5 test nozzle is shown in Figure 2 and illustrates the construction of the three nozzles.

Table I. Test Nozzle Exit Dimensions - Inches

L Length	W Width	A Area	AR Aspect Ratio
2.24	1.175	2.8	2.0
3.81	.768	2.9	5.0
6.58	.403	2.7	16.0

Figure 2. Aspect Ratio 5.0 Test Nozzle

Acoustic Characteristics

In order to insure that the experiment is not affected by noise generated in the settling chamber, acoustic waves were generated in the chamber employing both a sine wave oscillator and a white noise generator. Spectral peaks were eliminated by lining the settling chamber with 1-inch thick polyurethane foam. This left only a broad maximum near a frequency of 1.1 KHz.

The acoustic results should be independent of the characteristics of the microphone system; but, some dependence on the microphone and its orientation cannot be entirely eliminated. In the present case, the AR = 2 nozzle was examined with both condenser and crystal microphone systems. Typical results are shown in Figures 3 and 4 for a nozzle pressure of 40 psig. The dominant frequency of about 2750 Hz is clearly identified by both methods. Thus, in the subsequent tests, the acoustic data was gathered employing only a condenser microphone.

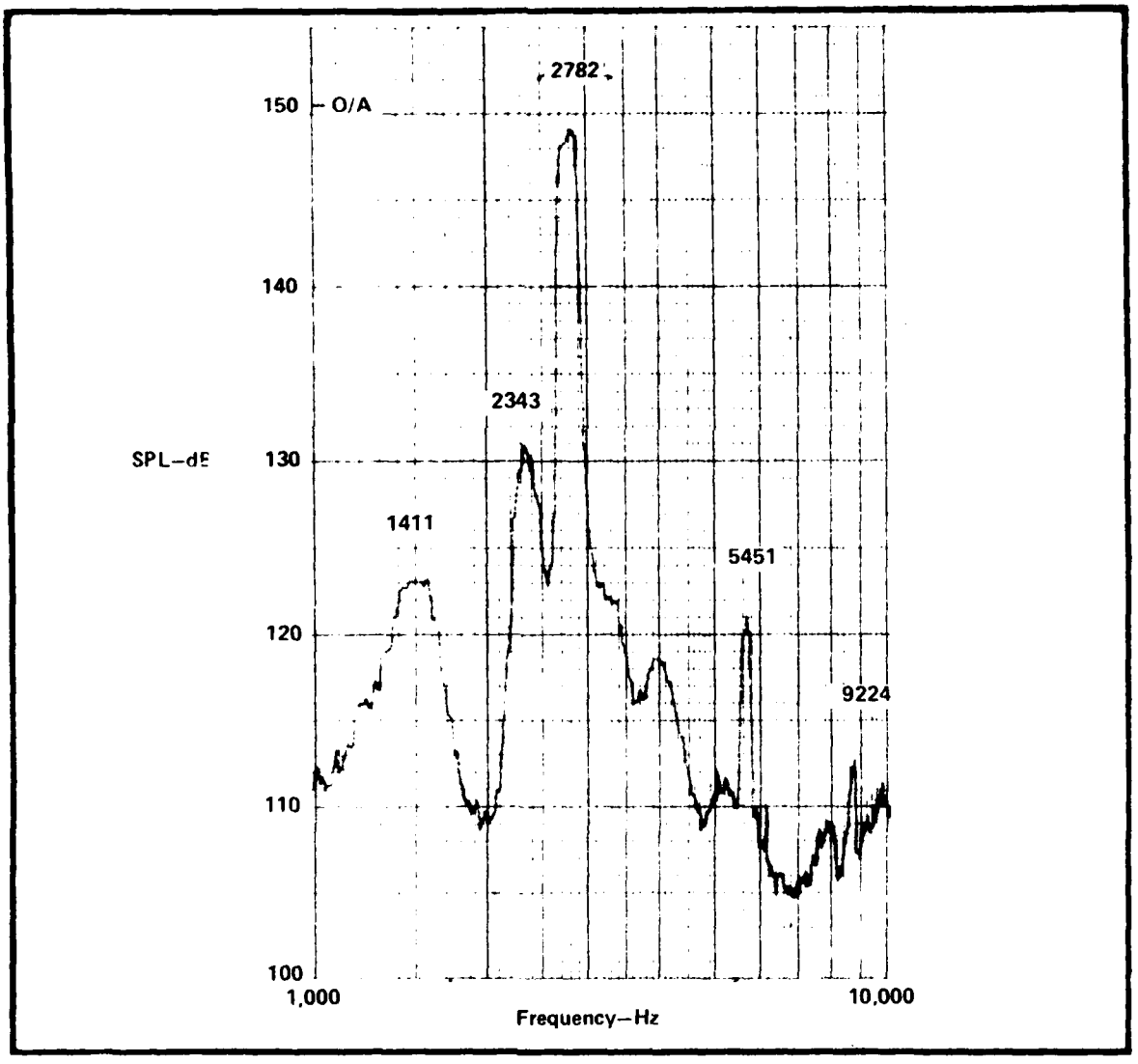

Figure 3. Aspect Ratio 2.0 Condenser Microphone Acoustic Data - Nozzle Pressure 40 psig

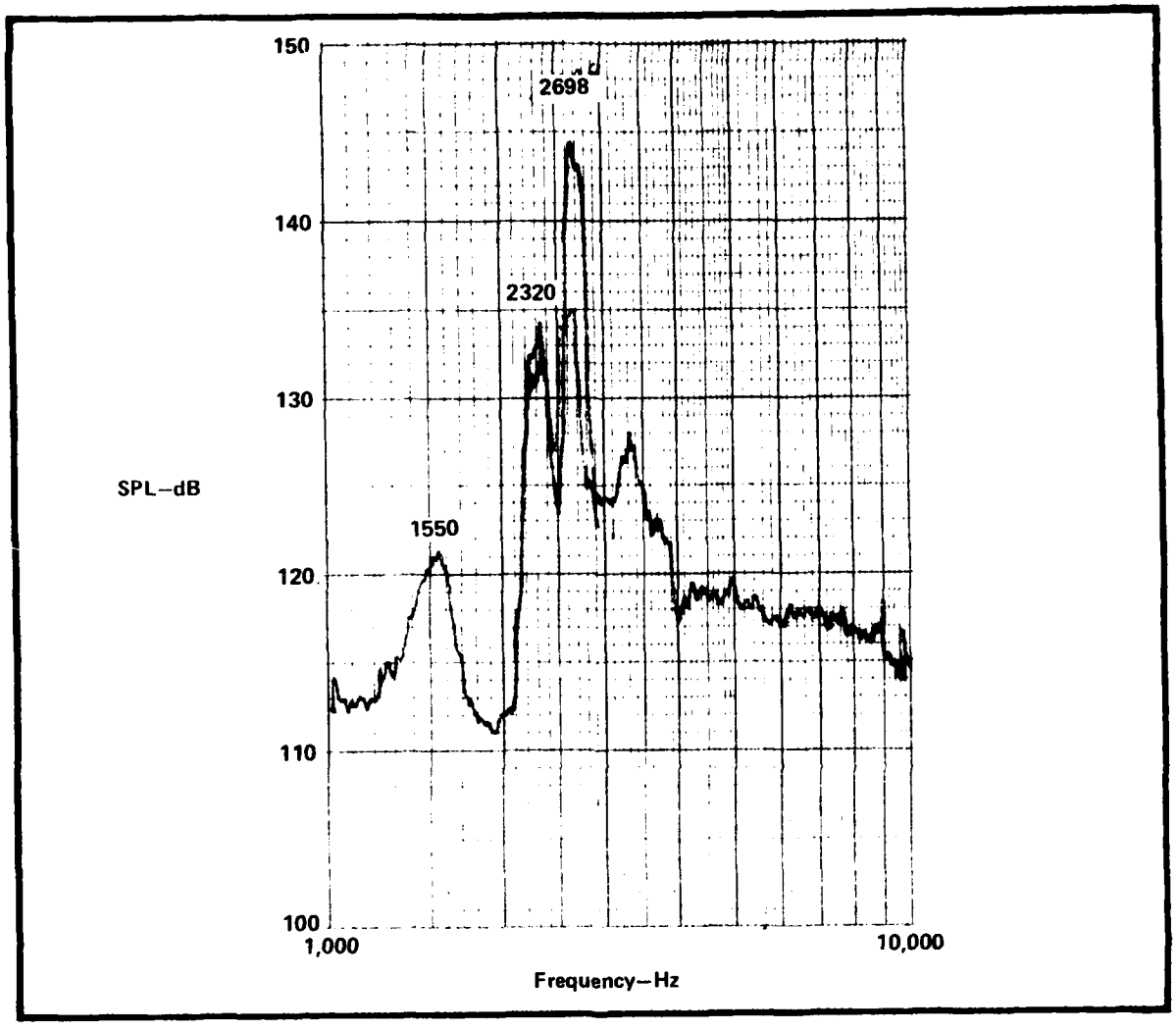

Figure 4. Aspect Ratio 2.0 Crystal Microphone Acoustic Data - Nozzle Pressure 40 psig

The acoustic tests were conducted at 1 psi intervals between pressures of 15 and 45 psig. The dominant frequency was determined at each pressure level and was interpreted as the "screech" frequency of the jet in Powell's[4,5] terminology. For the AR = 2 nozzle, the variation of the screech frequency with nozzle stagnation pressure is shown in Figure 5. There are distinct jumps in the screech frequency which are consistent with the variations observed by Powell,[4,5] Quinn[10,12], Rosfjord, and Toms[11] for axisymmetric jets as well as by Hammitt[6] for a rectangular jet.

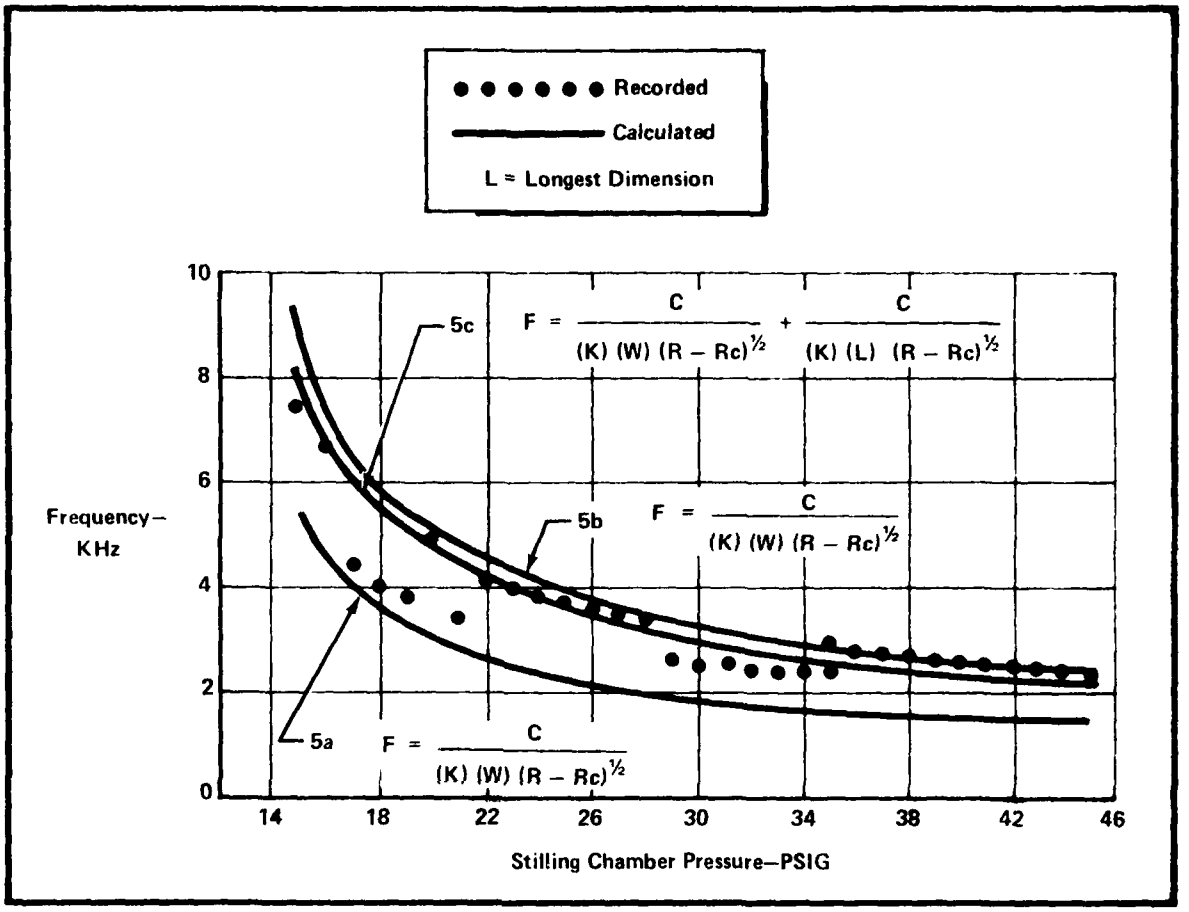

Figure 5. Aspect Ratio 2.0 Comparison of the Recorded and Estimated Screech Frequency

Several attempts were made to fit the data with an empirical relation developed by Powell,[5] from tests of a nozzle with AR = 12.5. This relation is:

$$\delta = \frac{C}{WK(R - R_c)^{\frac{1}{2}}} \qquad (1)$$

where: δ = screech frequency

C = speed of sound

K = empirical constant
= 5.0 rectangular jet
= 3.0 circular jet

R = nozzle pressure ratio

R_c = critical pressure ratio for choked flow

W = minor axis of rectangular exit or diameter of axisymmetric exit

Curve 5a employs Powell's equation with the recommended coefficient of five and leads to predictions which are lower than the data. Recognizing that the AR = 2.0 jet is close to round, the predictions are improved by the use of the axisymmetric coefficient as shown by Curve 5b. An additional possibility is that the dominant screech frequency is composed of beat frequencies caused by the existence of two exit dimensions. The frequency given by the sum of the frequencies due to each exit dimension as shown by Curve 5c. The sum of the terms, employing a coefficient of five, is shown by Curve 5c yields a reasonable prediction of the observed screech frequency.

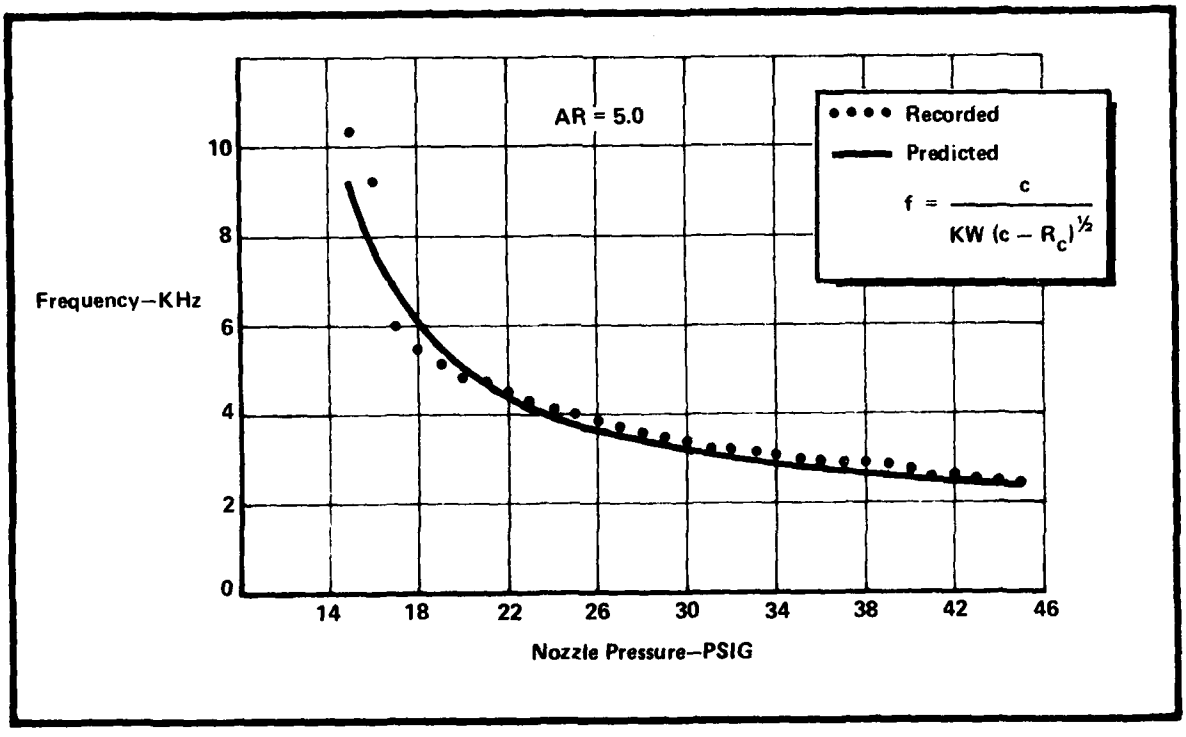

Figure 6. Aspect Ratio 5.0 Comparison of the Recorded and Estimated Screech Frequency

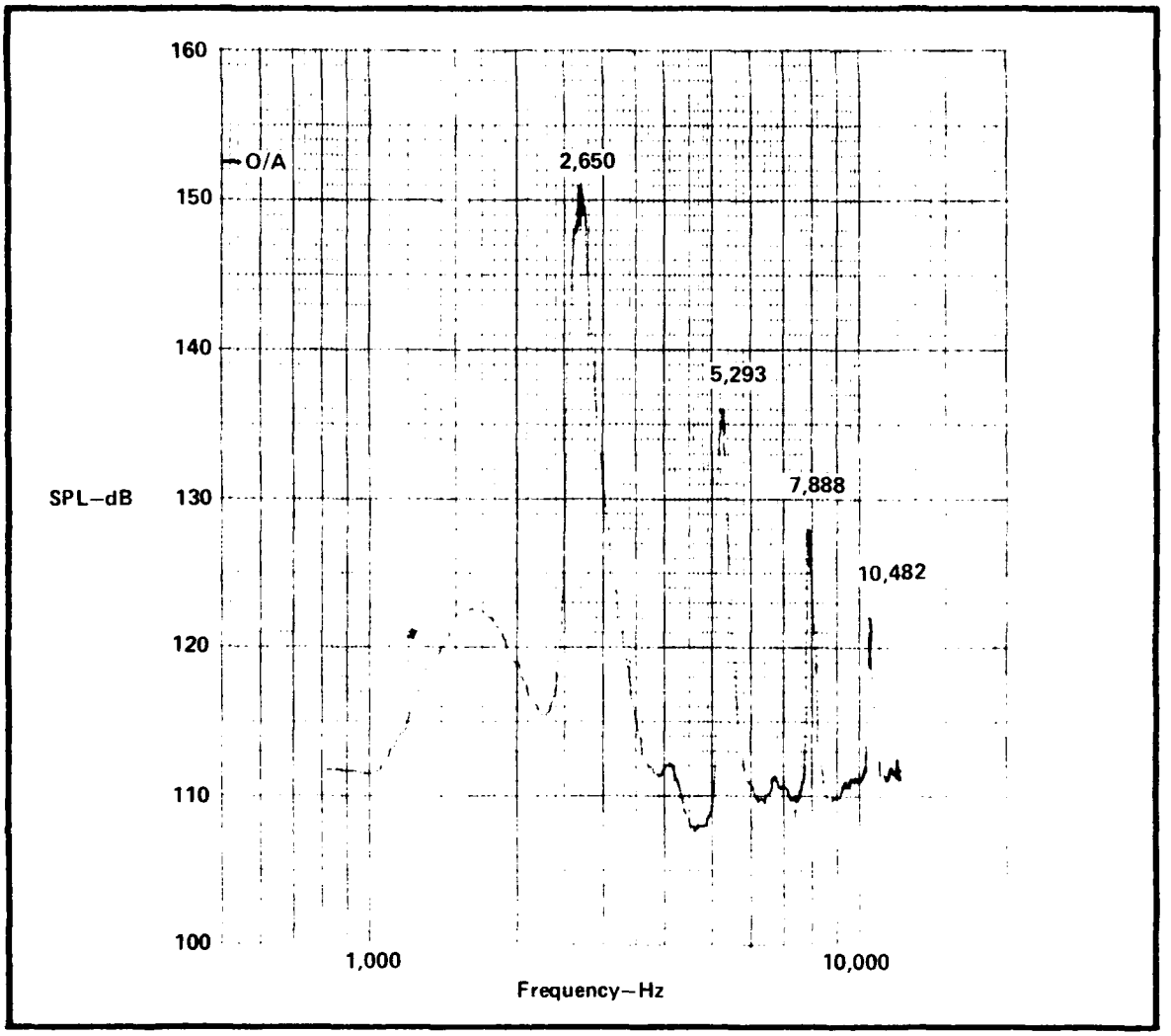

Figure 7. Aspect Ratio 5.0 Acoustic Data - Nozzle Pressure 40 psi

Similar tests were conducted employing the AR = 5.0 nozzle and the composite results of frequency as a function of chamber pressure are shown in Figure 6. In this case the predictions of Equation (1) employing the rectangular coefficient of five lead to acceptable results. A typical example of the frequency spectrum is shown in Figure 7 and exhibits an additional feature. The higher order harmonics can be clearly identified in this case.

Applying the same equation to the screech frequency data presented by Hammitt,[6] leads to the conclusion that the best prediction is obtained

from the rectangular jet coefficient of five. Including both exit dimensions as in the prediction of Curve 5c results in a less accurate frequency prediction.

Higher Harmonics

Repeating the above experiment with an AR = 16 nozzle results in the composite curve of Figure 8. Again the bulk of the data is well

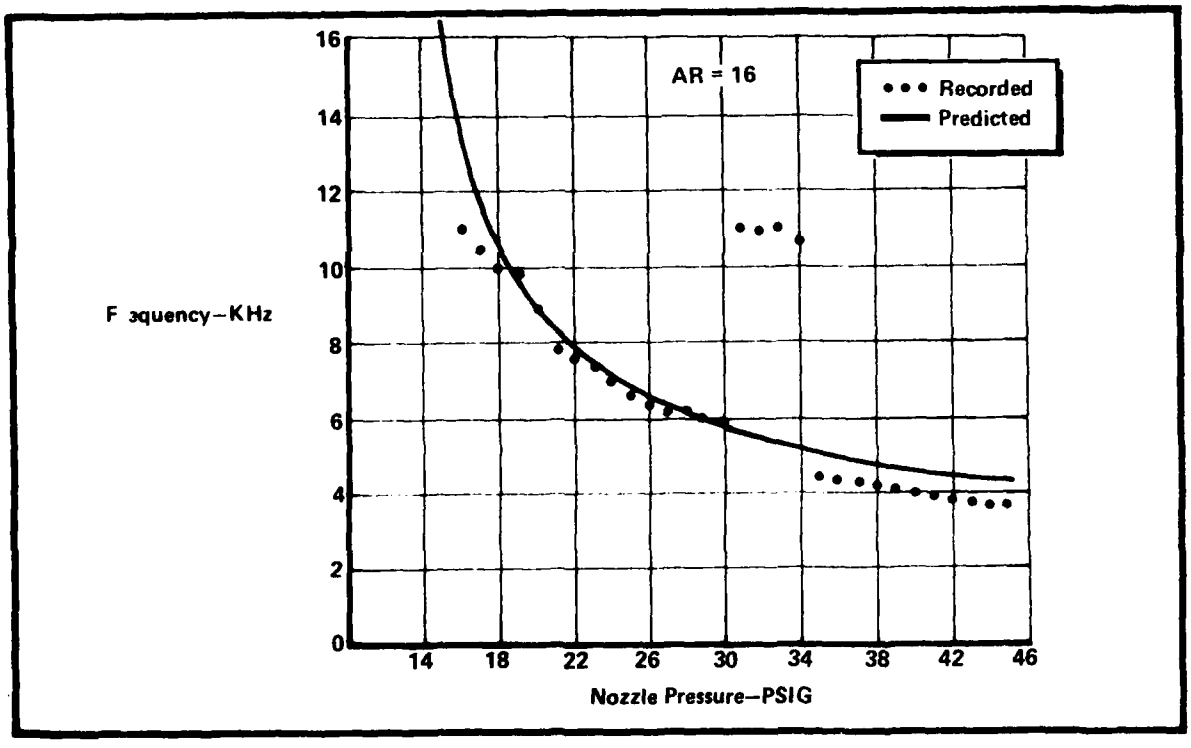

Figure 8. Aspect Ratio 16.0 Comparison of Recorded and Estimated Screech Frequency

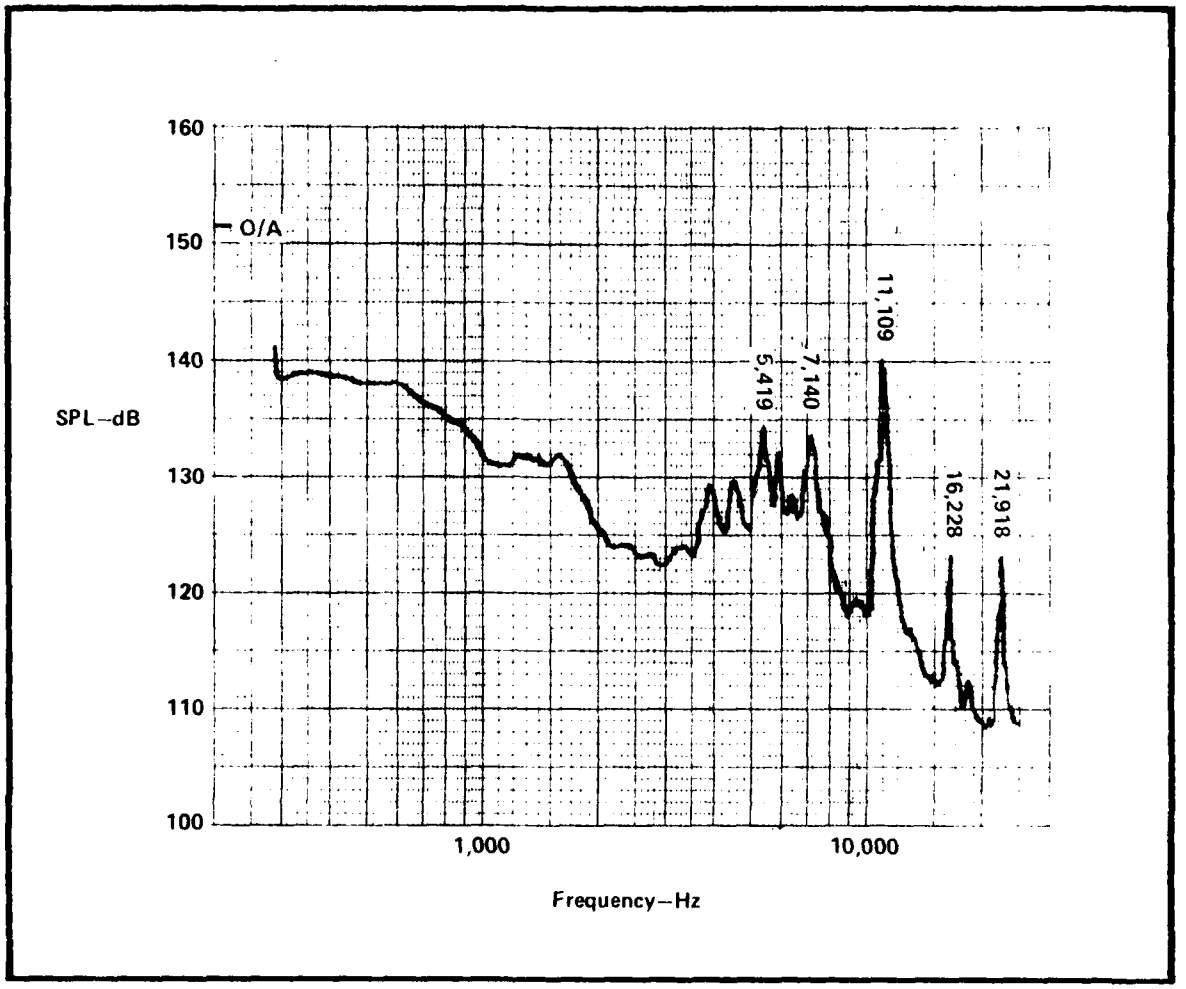

Figure 9. Spectrum at 33 psig for AR = 16 Nozzle Showing Maximum SPL at the First Harmonic Frequency

represented by Equation (1) using the rectangular coefficient of five. However, there are four points which fall far from the prediction. A detailed analysis of the frequency spectrum for a case in this region (Figure 9) shows that the dominant frequency is not the fundamental frequency but rather the first harmonic. This can be contrasted with the pressure spectrum (Figure 10) for a position outside this range (i.e., at 40 psig) where the dominant frequency is the fundamental frequency.

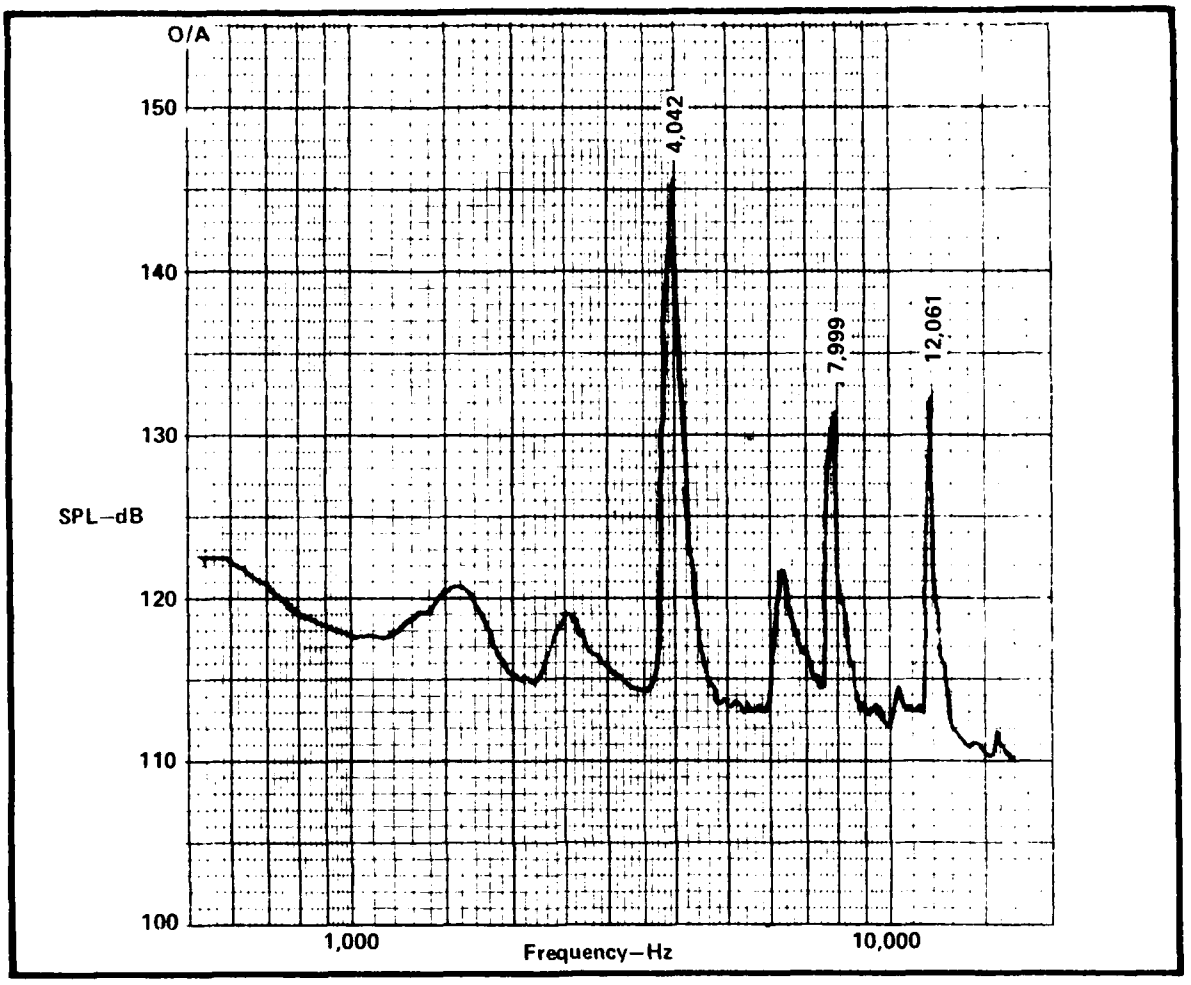

Figure 10. Spectrum of 40 psig for AR = 16 Nozzle Showing Maximum SPL at the Fundamental Frequency

If the other identifiable peaks in the acoustic spectra were plotted, then the frequency effect may be seen as in Figure 11 for the AR = 16 case. The fundamental frequency dominates everywhere except the region between 31 and 34 psig. All three modes are reasonably represented by the Powell equation (Equation (1)). The same is true of the higher order harmonics involved in the AR = 5 case and plotted in Figure 12. However, in this case the flow is dominated by the fundamental mode, with the exception of the very low chamber pressures. At these pressures there appears to be a shift in dominance from the fundamental to the first harmonic. In addition, the first harmonic data deviate strongly from the empirical predictions.

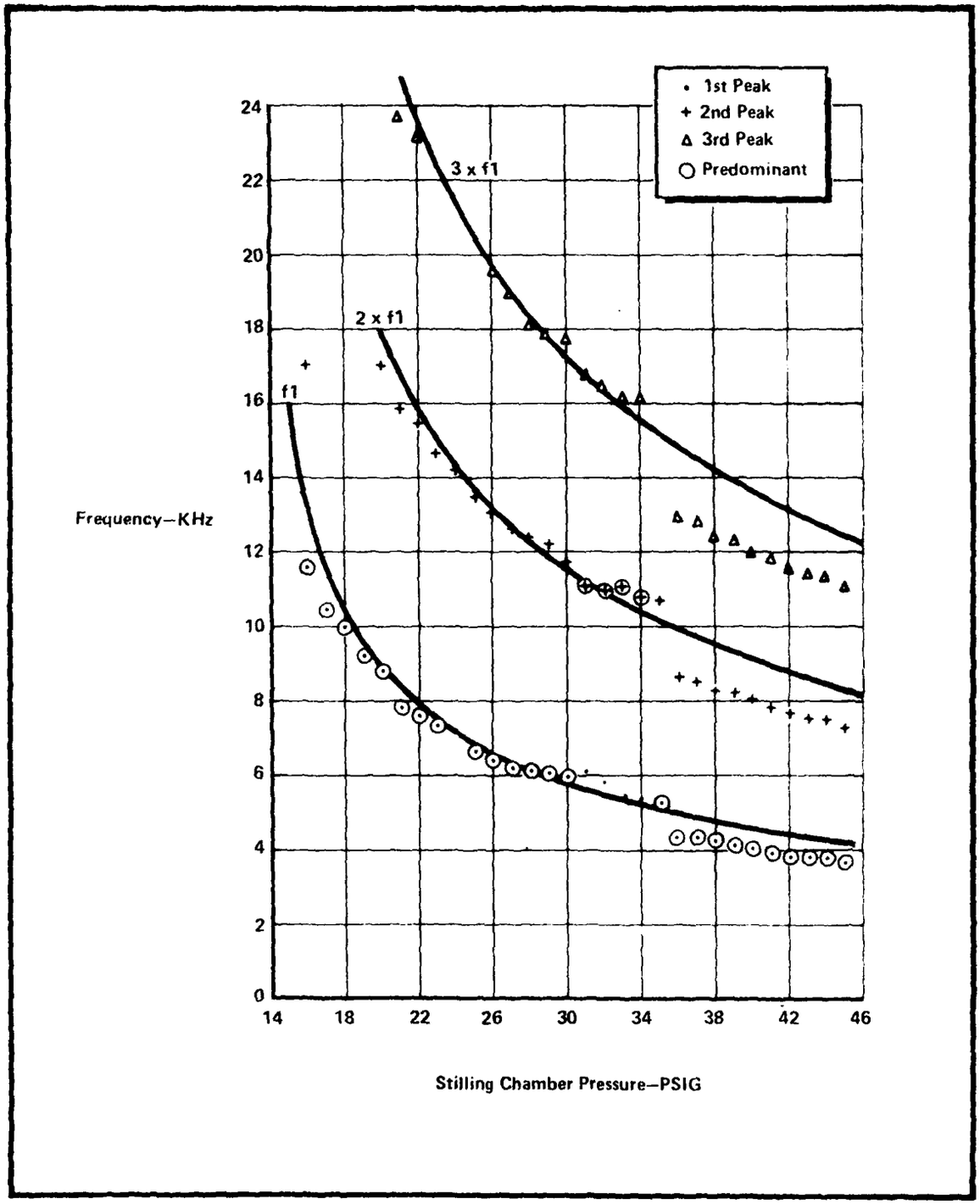

Figure 11. AR = 16 Frequency Data

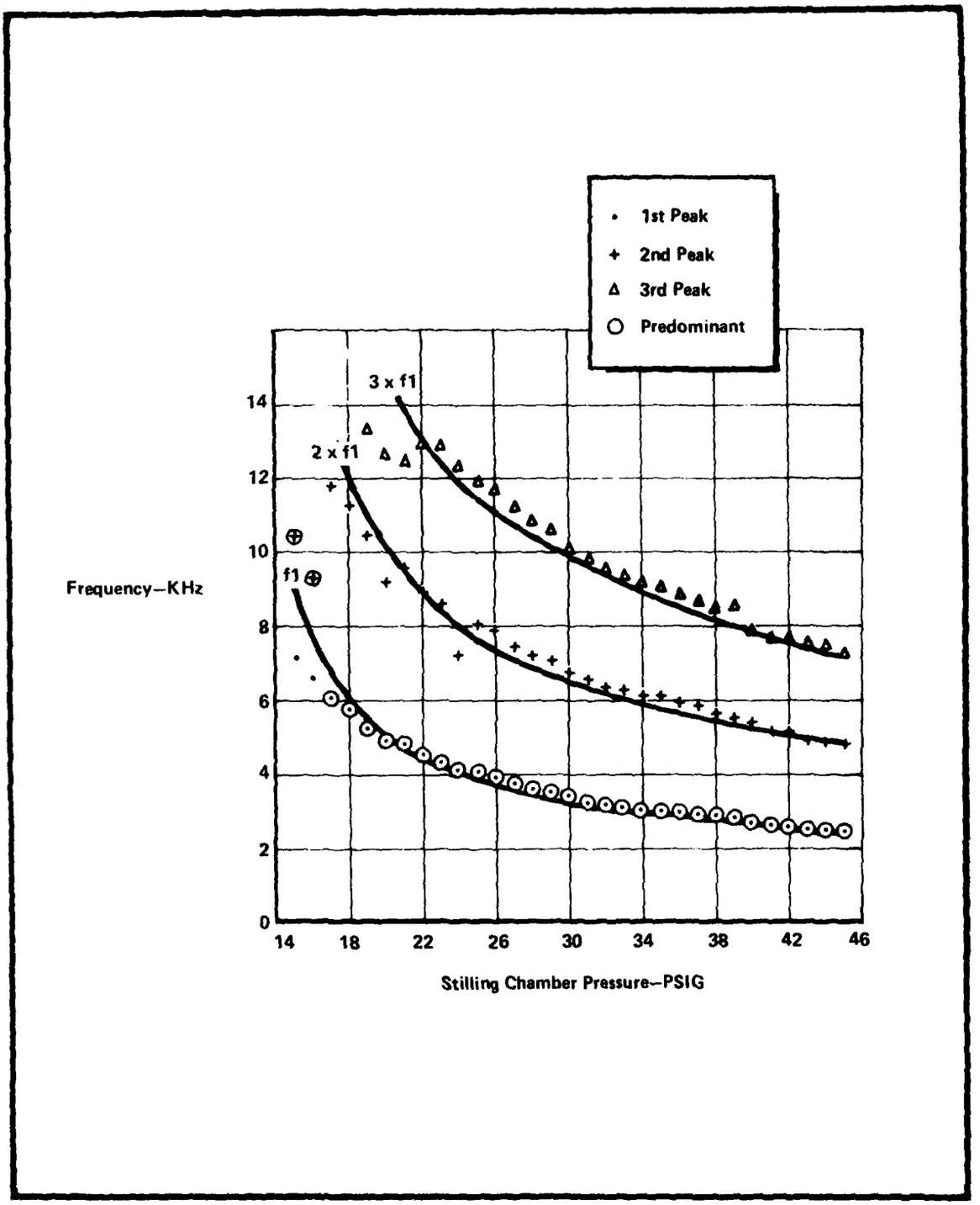

Figure 12. AR = 5.0 Frequency Data

Effect of Microphone Position

In these free jet experiments, the microphone was located at the exit plane in the center of the long side of the jet. In order to examine the effect of probe position on the measured acoustic data, the microphone was relocated to the center of the short side of the AR = 5.0 nozzle. In addition, the outer surfaces of the nozzle were insulated with four inches of foam from the base to the nozzle exit plane. The frequency spectrum produced by this arrangement is shown in Figure 13 with the empirically predicted fundamental mode and higher harmonics indicated.

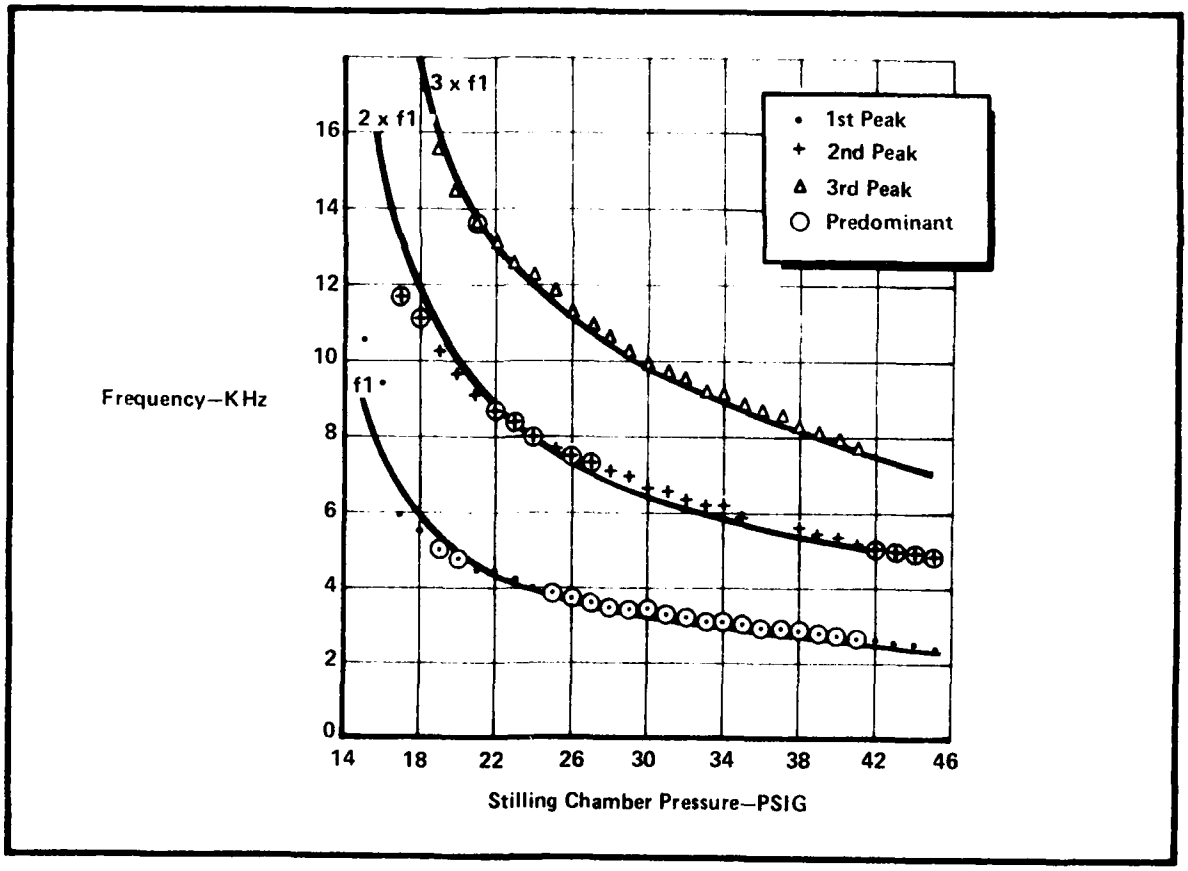

Figure 13. AR = 5.0 Frequency Data Microphone Repositioned Plus 4 Inches of Foam

Comparing the results of Figure 13 (insulated nozzle with microphone on the short side) to Figure 12 (bare nozzle with microphone on the long side), reveals two differences. One is that, whereas in Figure 12 the spectrum was dominated almost completely by the fundamental mode, the other order modes dominate at some pressure levels in Figure 13. The change in the dominant modes is probably due to a difference in the sound radiation in each direction and the addition of the foam. For the ejector application, the dominance of the different modes is probably less important than the fact that the frequency spectrum is only slightly changed (i.e., the fundamental frequencies are all evident with only minor changes in the amplitude). Thus, the frequency spectrum which will interact with the duct geometry is reasonably well defined by the isolated nozzle tests.

Spreading Characteristics

Having determined the acoustic characteristics of the three rectangular nozzles, the next objective is to examine the jet flow fields to identify the effect of any acoustic interaction on the mixing properties of the jet. The gross spreading properties are found by first identifying the aerodynamic center of the jet and then taking a family of pressure profiles across the nozzle, parallel to the short nozzle side. Typical pressure profiles exhibit no unusual behavior, being of maximum amplitude near the jet centerline and decreasing in the major axis direction. However, comparing centerline non-dimensionalized pressure profiles at a typical streamwise station, 44 short side lengths downstream, yields the results shown in Figures 14 through 16 for various settling chamber pressures.

The information in Figures 14 through 16 can be used as a guide to determine relative mixing rates. A wide pressure profile with a relatively low maximum pressure has been mixed more successfully than a narrow pressure profile indicative of a relatively large maximum pressure. With this criterion, it appears that the best settling chamber pressure (at least from the point of view of mixing) is equal to 31 psig (PR = 3.1) at AR = 2.0 and for the AR = 5.0 nozzle two points, 33 psig (PR = 3.24) and 43 psig (PR = 3.93), provide improved mixing.

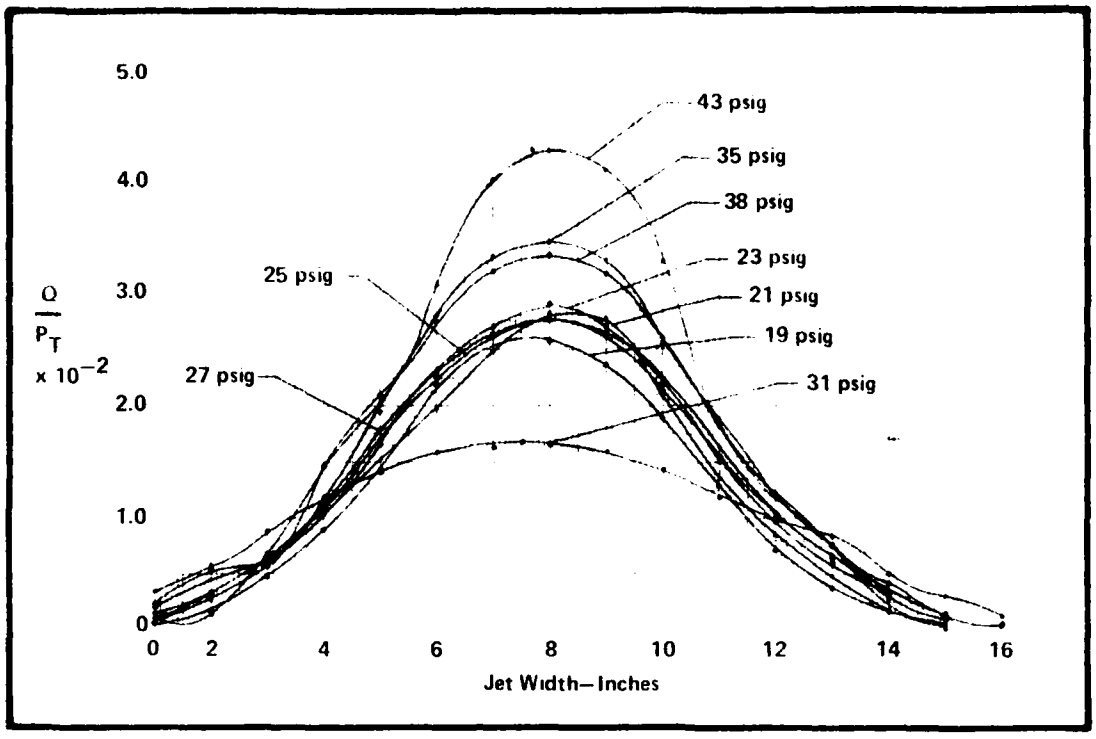

Figure 14. AR = 2.0 Nozzle Centerline Pressure Profile at x/d = 44

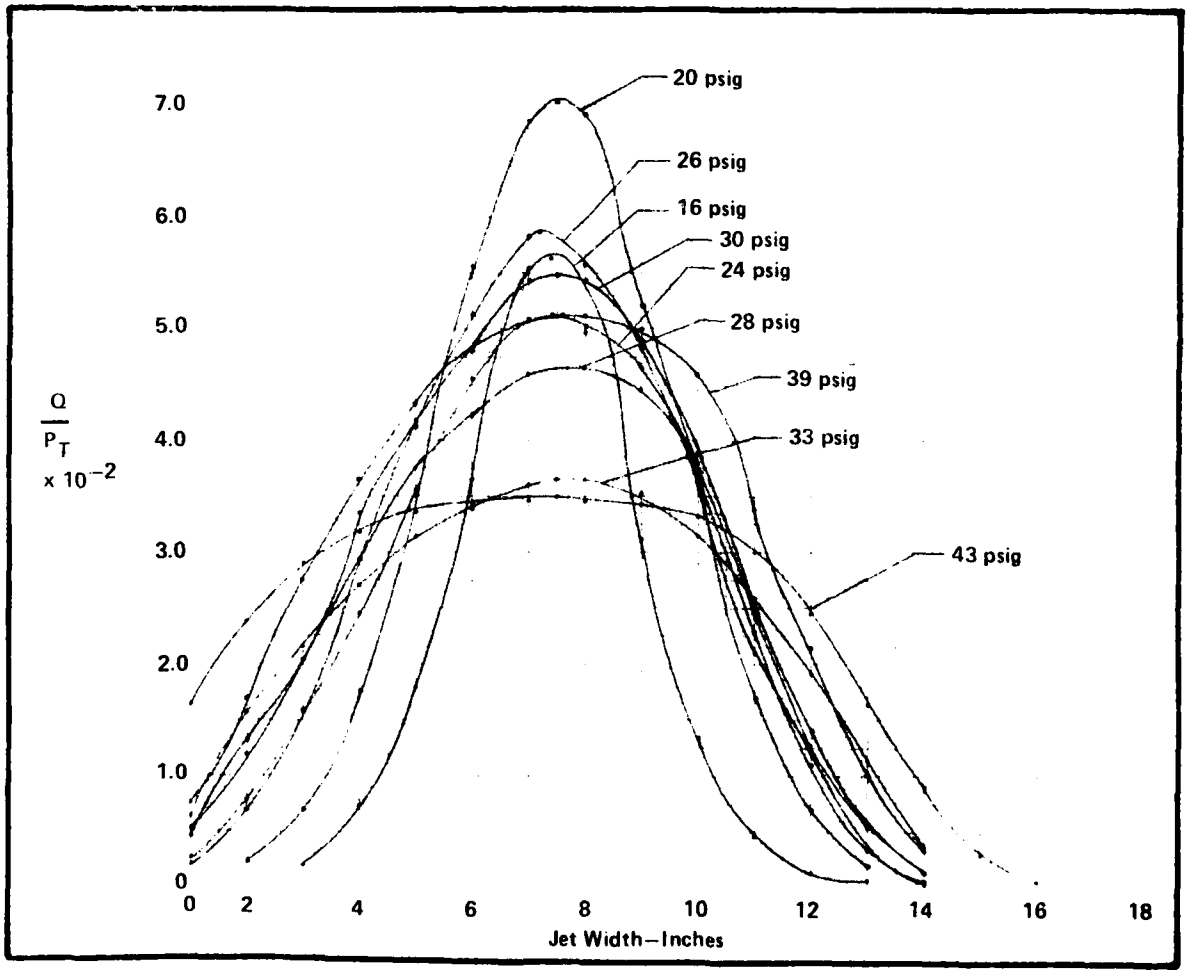

Figure 15. AR = 5.0 Nozzle Centerline Pressure Profile at x/d = 44

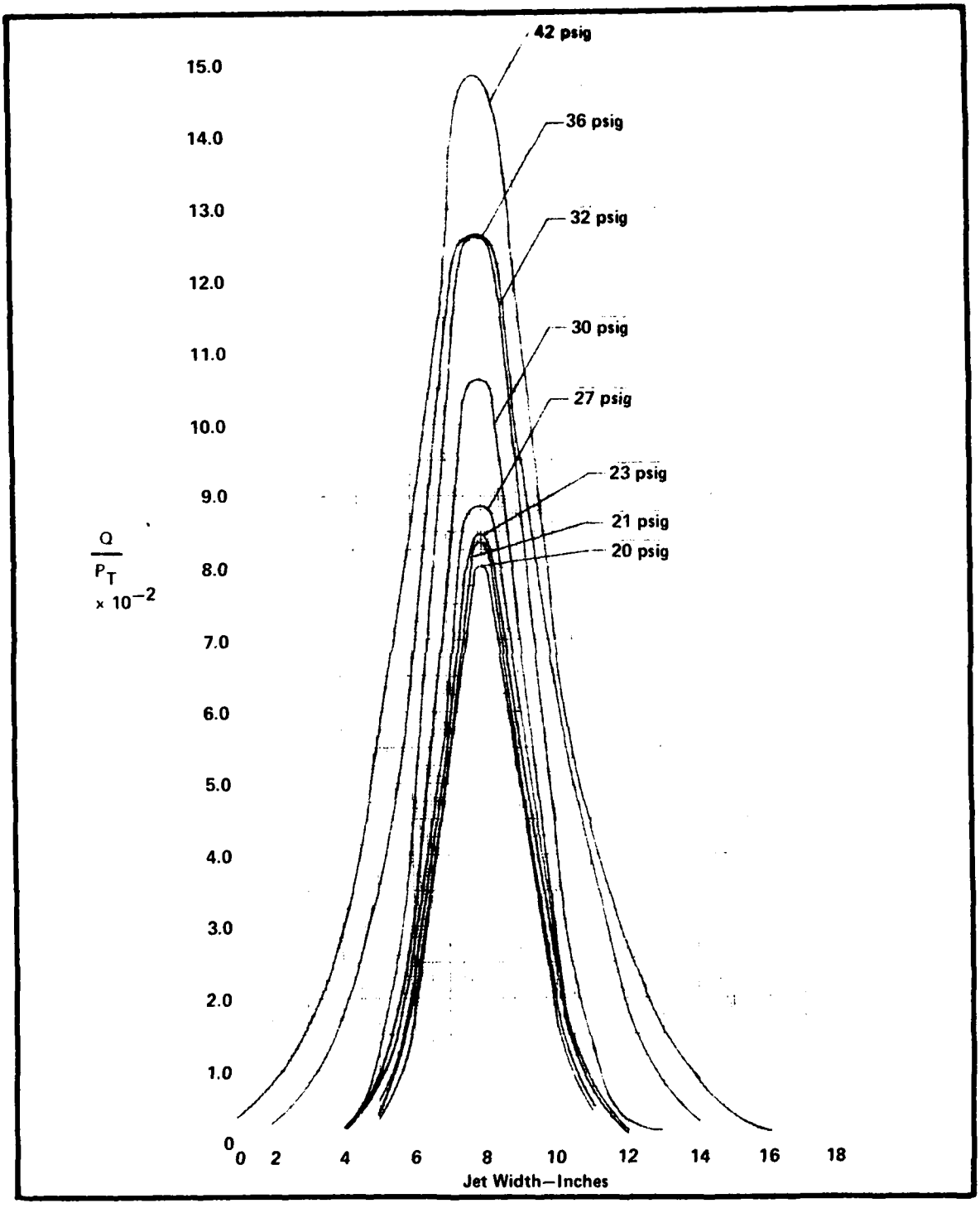

Figure 16. AR = 16 Nozzle Centerline Pressure Profile at x/d = 44

Since an entire family of pressure profiles is available, they can be numerically integrated to yield the mass flow rate passing the chosen streamwise station ($\bar{x}$ = 44), as shown in Figure 17. The general trend in the curves is positive due to the increase of the primary (jet) mass flow rate with settling chamber pressure and hence to an increase in the mass flow rate passing any streamwise position.

More interesting, however, are the local peaks on the AR = 2.0 and AR = 5.0 curves. These peaks correlate exactly with the flattest and widest pressure profiles in Figures 14 and 15. This indicates that an improved mixing rate exists at these two nozzle pressures. Examining the screech frequency curves, Figures 5 and 13, at the pressures which lead to the improved mixing, leads to no definite proof of acoustic interaction but in each case the pressure lies near the middle of a relatively constant frequency screech region. The mass flow results for the AR = 16 case exhibit only a monotonic behavior.

Integrating the total momentum flow rate yields the thrust of the various jets as measured at x/w = 44 (see Figure 18). Since the thrust of the jet is conserved in the streamwise direction, the monotonic increase in thrust with stagnation pressure for AR = 2 and 5 confirms the validity of the mass flow peak. For the AR = 16 case, the low thrust value at 36 psig suggests a measurement error at that pressure. If so, this would suggest the possibility that a mass flow peak also exists at 36 psig for the AR = 16 nozzle.

Integrating the pressure profiles taken in planes parallel to the short side of the jets results in a determination of the mass flow per unit length along the major nozzle axis passing the measuring station. An example is shown in Figure 19 for the AR = 5.0 nozzle. Normally, a Gaussian type of distribution would be anticipated for the mass flow, highest in the center and decreasing to zero at the edge of the jet. The case which had been identified as leading to increased overall mass flow in Figure 17 (P = 33 psig in the settling chamber),

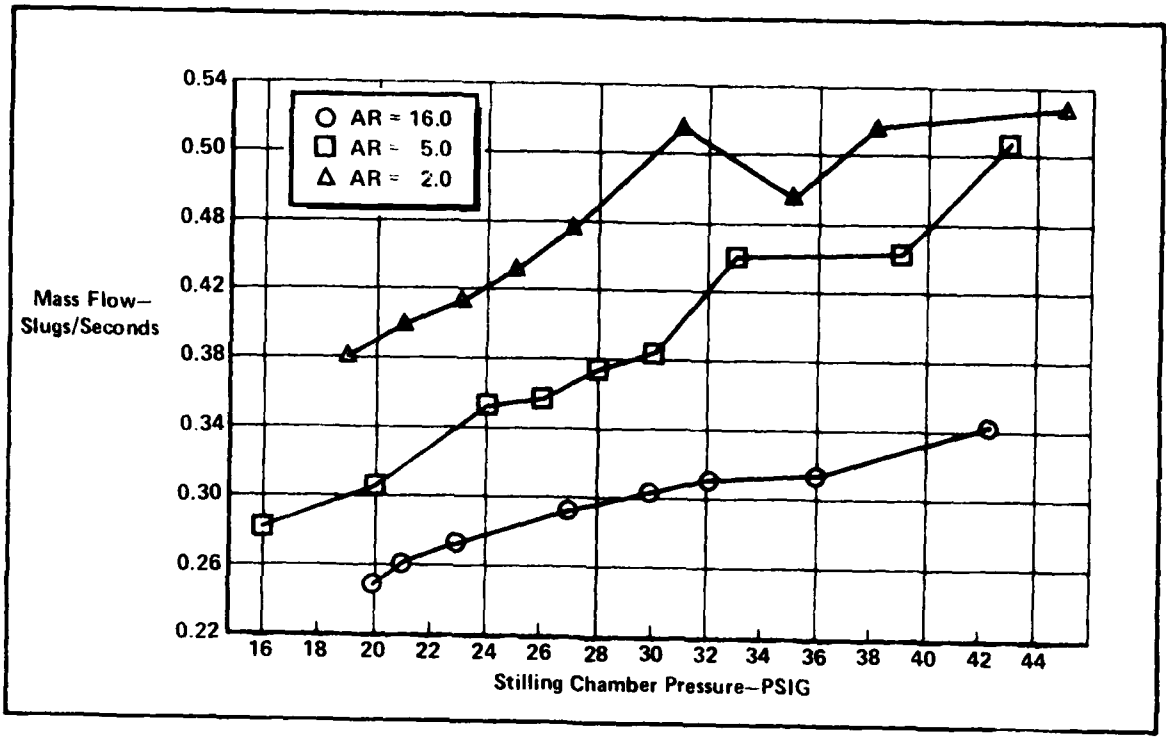

Figure 17. Calculated Mass Flow X/W = 44

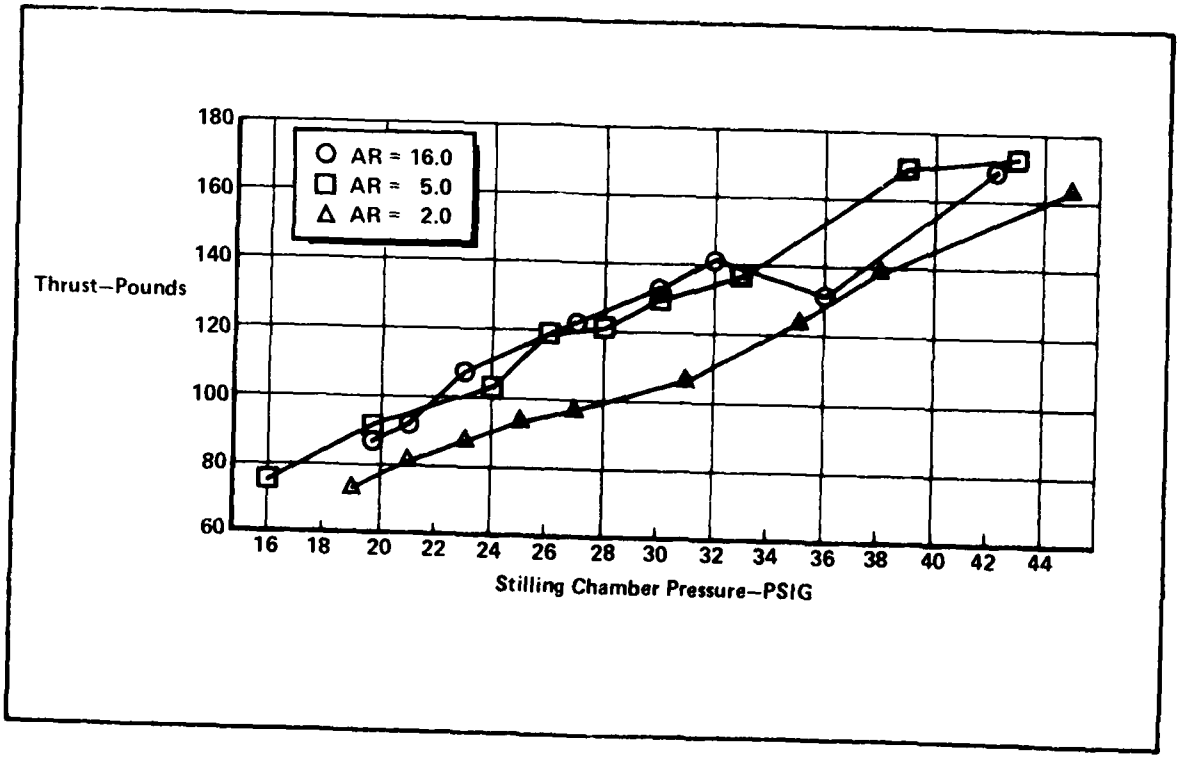

Figure 18. Calculated Thrust X/W = 44

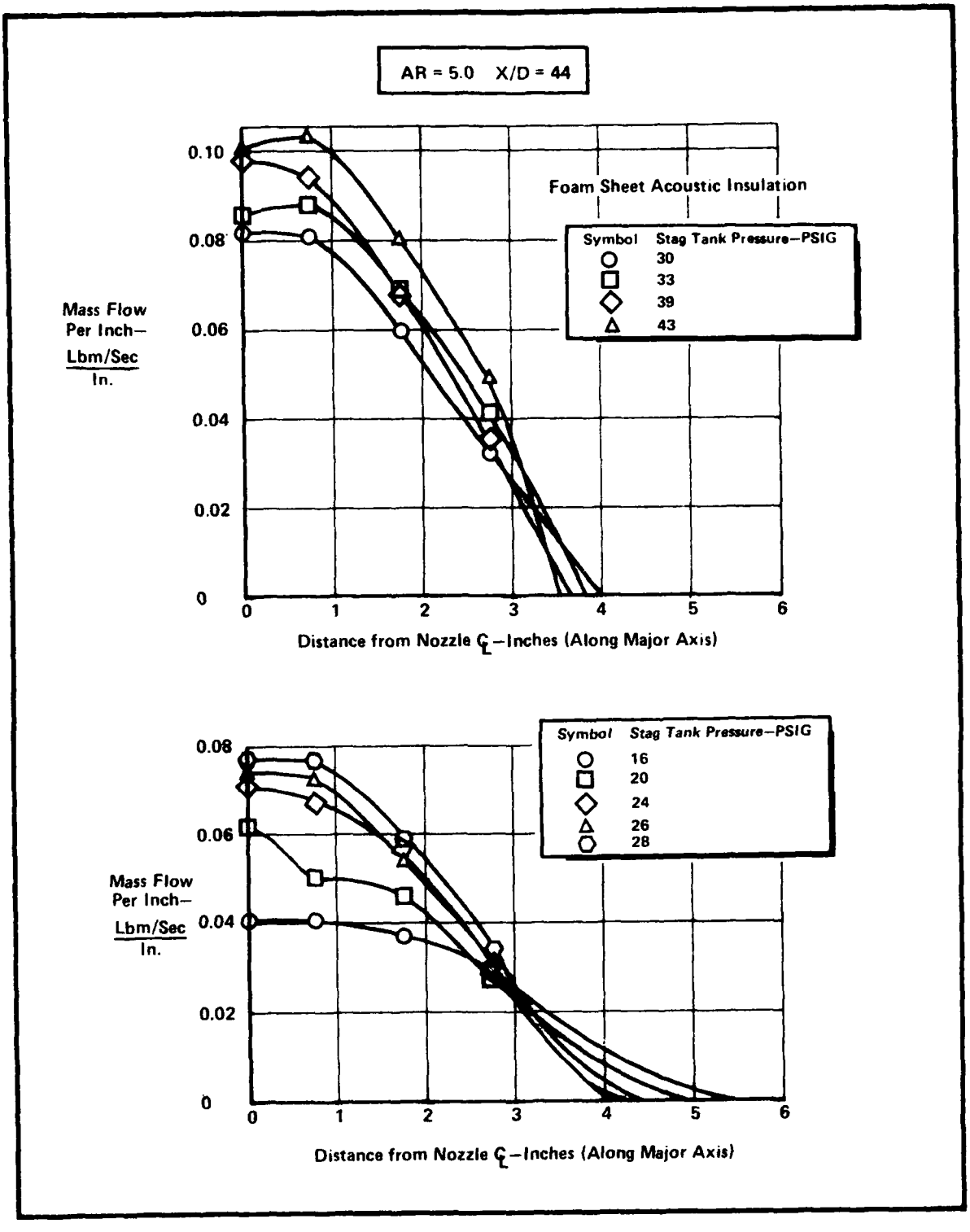

Figure 19. Isolated Nozzle Acoustic Interaction Jet Mass Flow Integrated Across Major Axis

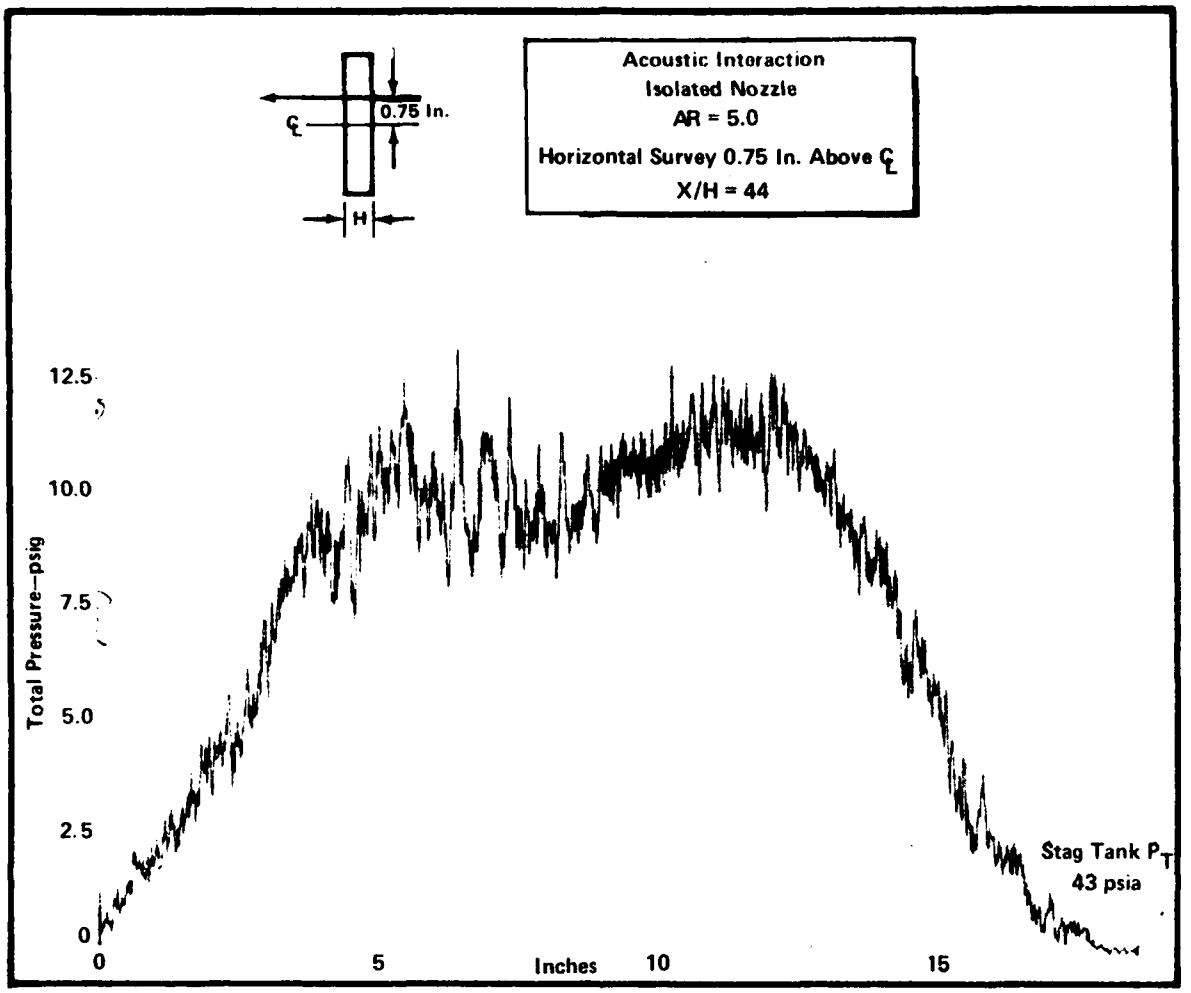

Figure 20. Dynamic Pressure Profile with Off Axis Peaks, P = 43 psig, $\bar{x}$ = 44

also leads to an odd shape in Figure 19. The maximum mass flow per unit dimension at 33 and 43 psig is not highest on the axis but rather at an off axis position. This is due to the maximum velocity position at times being located off axis, as seen in Figure 20. Such profiles may be due to jet oscillations or to the presence of vortices[16] shed by the orifice or nozzle. The presence of acoustic waves increases the probability of vortex growth and improves the mixing properties of the jets.[1-3] Thus, the appearance of twin velocity peaks in the jet (Figures 19 and 20) is consistent with the improved mixing characteristics of the jet which lead, in turn, to an improved mass flow rate (Figure 17) all of which occurs at a pressure of 33 psig. A similar acoustic interaction appears at a pressure of 43 psig. The remaining mass flow rate profiles do not indicate such a behavior.

Conclusions

The free jet results presented indicate that acoustic interactions do exist for the jets from choked rectangular nozzles. In addition, the fundamental mode is predicted reasonably well by Powell's[5] equation, and the higher harmonics are simple multiples of Powell's fundamental mode. At some pressure ratios there is a change in the dominant frequency from the fundamental to the first harmonic. However, since both frequencies are present at nearly the same amplitude, it is expected that either frequency may interact with the ejector shroud.

Thus, we concluded that the screech frequency of rectangular jets is correlated with the shorter nozzle dimension; that is, there is no effect of aspect ratio for aspect ratios greater than 5. There also seems to be a significant increase in the jet entrainment at certain critical pressure ratios.

On this basis we decided to determine if there was an acoustic effect on ejector performance; and, if there was, if it was a result of this increase in free jet entrainment or some interaction between the jet and duct acoustics.

EJECTOR TESTS

The objective of the ejector tests is to determine the acoustic effects of a rectangular nozzle mounted in a rectangular shroud. Based on the results of the isolated jet tests, a high aspect ratio nozzle was chosen for the rectangular ejector configuration. Thus, the chosen configuration is a rectangular analog of Quinn's axisymmetric configuration.

Experimental Facilities

These tests were performed at the Ohio State University Aeronautical Research Laboratory. The augmenter test facility consists of a welded steel frame which supports an augmenter mounting plate by means of four cables. The augmenter is enclosed by an acoustic chamber constructed of 3/4-inch plywood in the form of a cube 8 feet on a side and lined with a 2-inch

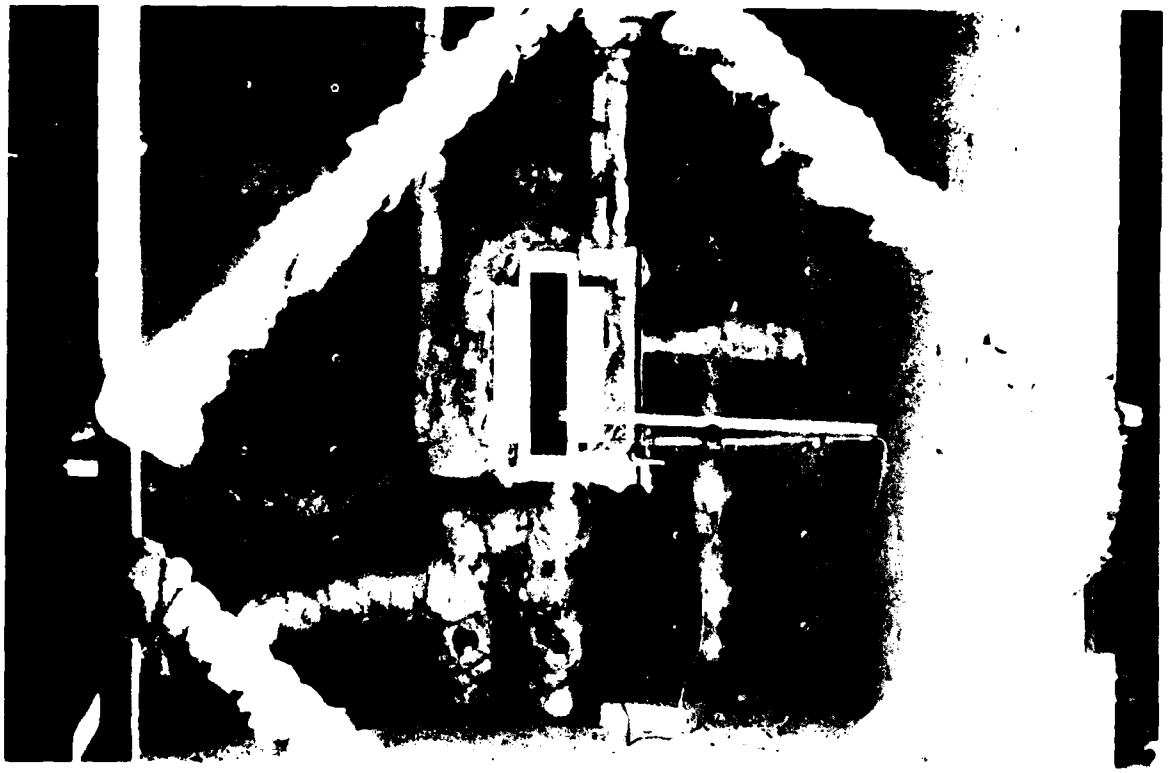

Figure 21. Ejector Thrust Augmenter Facility

layer of unfaced Owens/Corning 703 fiberglass as shown in Figure 21. In order to prevent acoustic reflections, the upstream walls and floor are also covered with fiberglass and, upon calibration, it was found necessary to insulate the supporting frame, cables, and air supply hoses.

The thrust of the ejector was measured by three strain gauges located at the top center of the augmenter and at the forward left and right hand corners of the mounting plate. The mass flow rates of air through the centerbody and the Coanda nozzles were measured by venturi meters in the supply lines as well as thermocouples and total pressure probes. The ejector was insulated from the thrust of the incoming mass flow by a flexible coupling on the primary feed duct. A schematic of the air supply system for the ejector is shown in Figure 22.

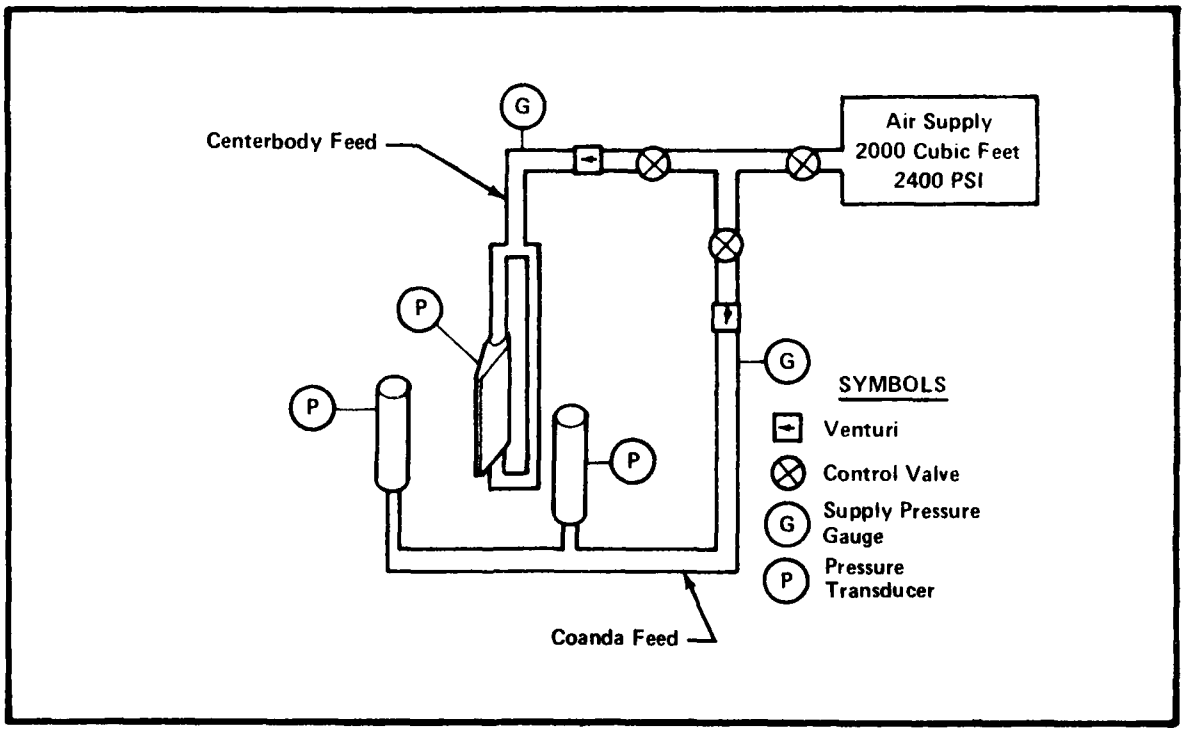

Figure 22. Air Supply System Schematic

A Bruel and Kjaer (B&K) Type 4136 1/4-inch pressure/random condenser microphone was employed to measure sound pressure levels (SPL), based on a (B&K) supplied calibration curve. This microphone has a frequency range from 3.9 Hz to 70 KHz (±2 dB), and the output is checked with a B&K Pistonphone Type 4220, which generates a pure tone of 250 Hz (±1%) at 123.8 dB (re 2 x 10^{-5} Pa). The microphone was powered by a Type 2801 B&K microphone power supply. A Type 2618 B&K preamplifier is also used with a sensitivity of 1.6 mV/Pa having a dynamic range of 67 to 172 dB.

The signal was sent via coaxial cable to a patch panel where it was amplified by a factor of 10 and sampled with a high speed A/D converter at 100 KHz. The high sampling rate is necessary since in the Fast Fourier Transform (FFT), the maximum frequency that is valid is approximately one-half that of the sampling rate. It was anticipated that frequencies of the order of 50 KHz would be encountered; therefore, sampling at 100 KHz would provide this information. This digital data was then stored and is available to be processed when desired.

High Aspect Ratio Nozzle

In the preceding section, rectangular nozzles of aspect ratio 2, 5, and 16 were examined. Since the high aspect ratio nozzles were found to screech, it was decided to study the behavior of a simple rectangular nozzle. An AR = 133 (20 by 0.15 inches) nozzle was employed in the ejector tests. The driving screech frequency generated by the nozzle at choked conditions is shown as a function of pressure ratio in Figure 23. Also included for comparison in the figure are the rectangular form of Powell's empirical fundamental screech frequency equation (given in Curve 5c) and the first harmonic thereof. The data is obtained from a numerical Fast Fourier Transform (FFT) and is reasonably predicted by Powell's equation for the fundamental mode. There are clearly no shifts to the higher harmonics seen in the data of Figure 23.

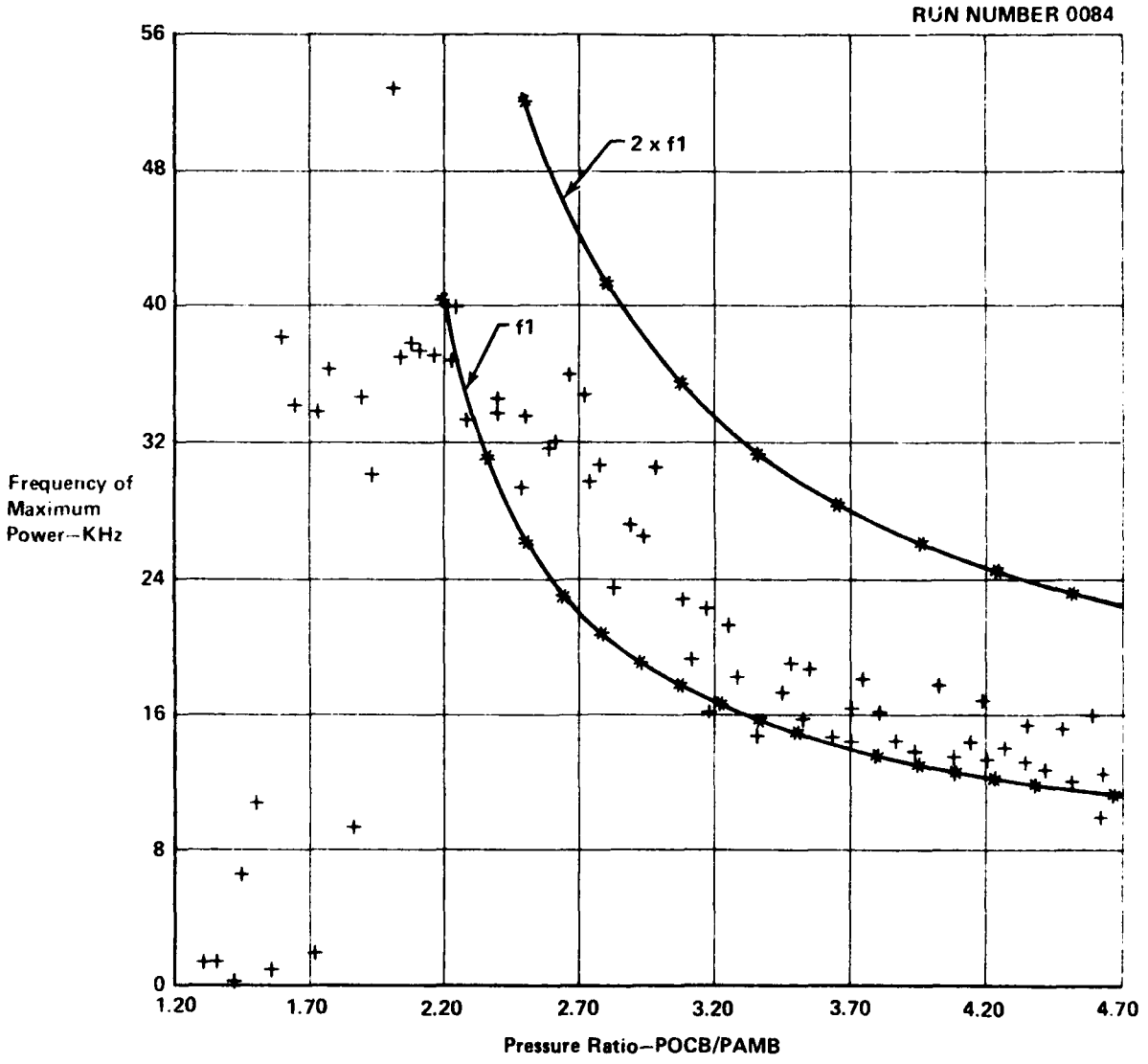

Figure 23. Comparison of Recorded and Estimated Screech Frequency Isolated Centerbody

Duct Acoustics

The acoustic characteristics of the AR = 133 nozzle were described in the preceding section. In order to obtain an interaction with an ejector duct, the dominant jet frequencies must match the natural frequencies of the duct. These duct frequencies can be predicted by a classical solution of the wave equation subject to the boundary condition of no flow normal to the walls of the duct, as follows.

According to Succi[14] and Morse,[17] the acoustic pressure disturbance in a region without sources or flow is described by the wave equation

$$\nabla^2 P - \frac{1}{C_o} \frac{\partial P}{\partial t^2} = 0 \tag{2}$$

Assuming a sinusoidal time dependence, $P = pe^{i\omega t}$ results in

$$\nabla^2 p + \left(\frac{\omega}{C_o}\right)^2 p = 0 \tag{3}$$

where $p = p(x,y,z)$ is the spatial pressure distribution. An exponential pressure decay or growth in the streamwise direction is assumed,

$$p = \psi(x,y)\, e^{ik_z z} \tag{4}$$

Substituting this form into Equation (3) eliminates the streamwise dependence and yields the governing equation for the transverse modes

$$\nabla^2 \psi + K^2 \psi = 0 \tag{5}$$

where

$$K^2 = \left(\frac{\omega}{C_o}\right)^2 - k_z^2 \tag{6}$$

The boundary condition is the fact of no flow normal to the solid wall, ie,

$$\left.\frac{\partial P}{\partial n}\right|_{\text{walls}} = 0 \tag{7}$$

or,

$$\left.\frac{\partial \psi}{\partial n}\right|_{\text{walls}} = 0 \tag{8}$$

The general solution to Equation (5) with the boundary condition, Equation (8) is

$$\psi = \sum_m \sum_n A_{mn} \cos\left(\frac{m\pi x}{b}\right) \cos\left(\frac{n\pi y}{d}\right) \tag{9}$$

where b and d are the transverse duct dimensions in the x and y directions, respectively. Substituting this form into Equation (5), results in an expression for the natural modes available in the duct,

$$K^2 = \left(\frac{m\pi}{b}\right)^2 + \left(\frac{n\pi}{d}\right)^2 \tag{10}$$

The frequencies, ν, corresponding to these mode shapes are

$$K = \frac{2\pi\nu_{m,n}}{C_o}$$

or

$$\nu_{m,n} = \frac{C_o}{2}\sqrt{(m/b)^2 + (n/d)^2} \tag{11}$$

So $\nu_{m,n}$ is the natural frequency of the various possible modes associated with the integer values m and n.

As seen in Equation (4), in order for the waves to propagate in the z-direction, the factor k_z must be real.[18] For this to be true, from Equation (6)

$$K^2 < \left(\frac{\omega}{C_o}\right)^2 \tag{12}$$

or

$$\omega > C_o\sqrt{\left(\frac{m\pi}{b}\right)^2 + \left(\frac{n\pi}{d}\right)^2} \tag{13}$$

Thus, any mode m,n will propagate only if the driving frequency is large enough to satisfy Equation (13). If the driving frequency is lower than this minimum, no waves will be propagated. From an alternate point of view, a given driving frequency, ω, may produce propagating waves in only those lower frequency modes which satisfy Equation (13).

Ejector Geometry and Natural Modes

A schematic of the ejector geometry employing the AR = 133 nozzle is shown in Figure 24. For the sake of simplicity, no diffusion was considered so the ejector flow channel was of constant cross sectional area and shape. The ejector area ratio (ejector inlet area to nozzle area) was 26.6, which is close to Quinn's[12] value of 25.8.

The natural transverse modes can then be calculated from the ejector geometry as described by Equation (11) in the previous section. The predicted modes are based on the assumption of no flow in the ejector. However, Quinn's[12] acoustic tests on an axisymmetric ejector geometry with and without flow yielded measured acoustic results which differed from each other in a relatively minor way. The basic effect of flow addition in the axisymmetric duct case appears to be a small reduction

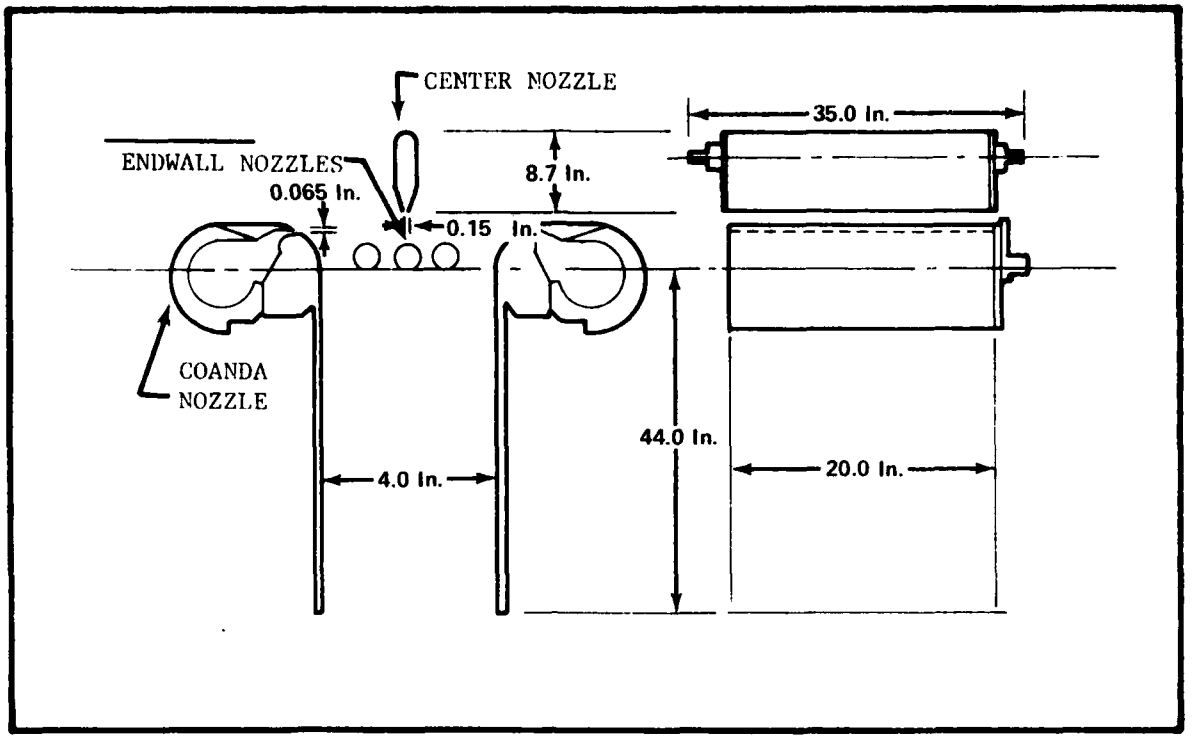

Figure 24. Acoustic Interaction Rectangular Ejector Model

in the frequencies of the identifiable modes. The same small effect is expected in the present case because the velocities are the same order of magnitude.

For the ejector geometry of Figure 24, the frequencies of the lower order modes are:

$$\nu_{1,0} = 0.33 \text{ KHz}$$
$$\nu_{2,0} = 0.66 \text{ KHz}$$
$$\nu_{3,0} = 0.99 \text{ KHz}$$
$$\nu_{0,1} = 1.65 \text{ KHz}$$
$$\nu_{0,2} = 3.30 \text{ KHz}$$
$$\nu_{0,3} = 4.95 \text{ KHz}$$
$$\nu_{1,1} = 1.68 \text{ KHz}$$

Comparing these lower order mode frequencies with the screech frequencies available in the primary jet reveals a frequency mismatch. The lowest primary jet frequency in the choked flow pressure range is approximately 8 KHz, while the lower order duct frequencies are below 5 KHz. Because the jet driving frequency is relatively high, many duct modes can be excited and propagated. However, not much energy is likely to appear in the lower order modes which are most effective for increasing entrainment. Nevertheless, because acoustic effects were observed to increase the entrainment of the isolated jet and the magnitude of interactions between the jet and duct harmonics could not be predicted, tests were conducted in order to determine what improvement in the performance of rectangular ejectors would be obtained.

Ejector Acoustic Interaction

In spite of the frequency mismatch between the driving screech frequency and the natural modes of the ejector shroud, the experiments revealed an acoustic interaction for various ejector lengths. The case of a rather long ejector L/W = 11.0 is illustrated in Figures 25, 26, and 27. An expanded plot of total ejector thrust as a function of the nozzle pressure ratio is shown in Figure 25. A pair of very small systematic deviations from the anticipated linear variation are centered about pressure ratios of approximately 3.25 and 3.55. Examining the corresponding acoustic spectrum in Figure 26, it is evident that there is considerable scatter of the data at almost every pressure ratio except in the region between 3.15 and 3.70, where the deviations from the linear thrust curve exist. In this region of pressure ratios, the interaction between the screech tone and the shroud geometry is so strong that the feedback forces the tone to assume a single strong value with very little deviation.

Additional evidence of the acoustic interaction between the choked jet and shroud geometry is shown in Figure 27 where the sound intensity

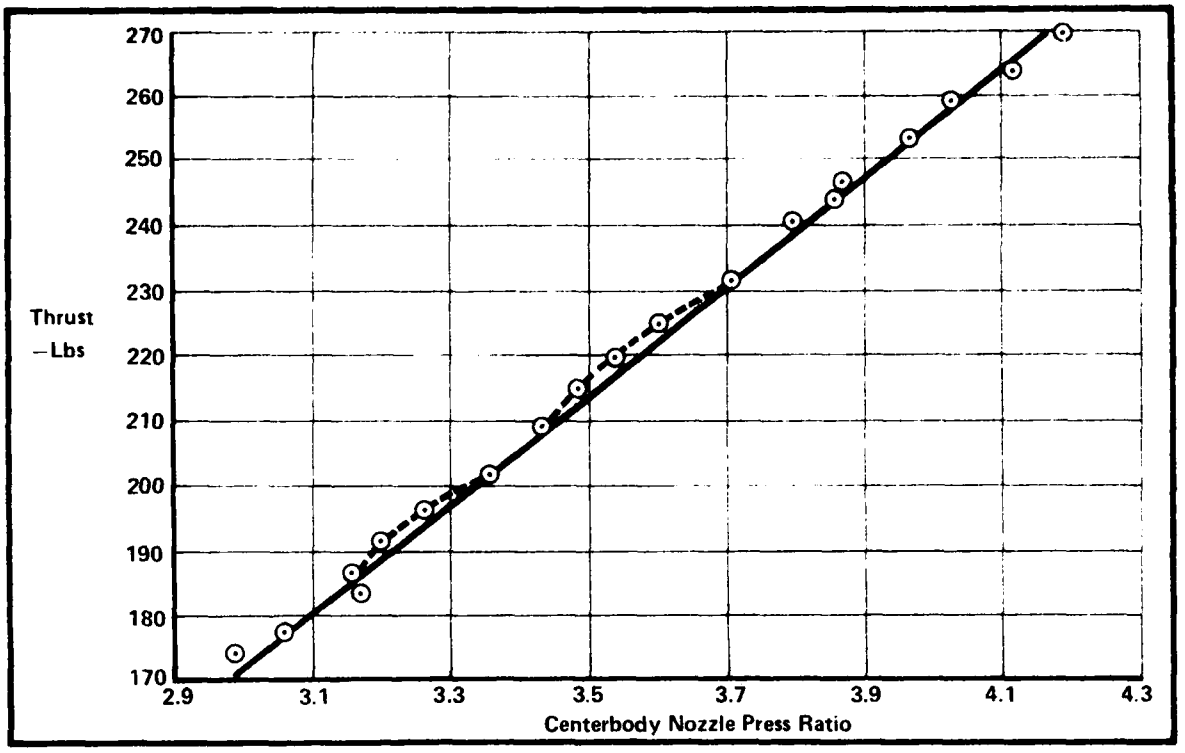

Figure 25. L/W = 11.0 Centerbody Only

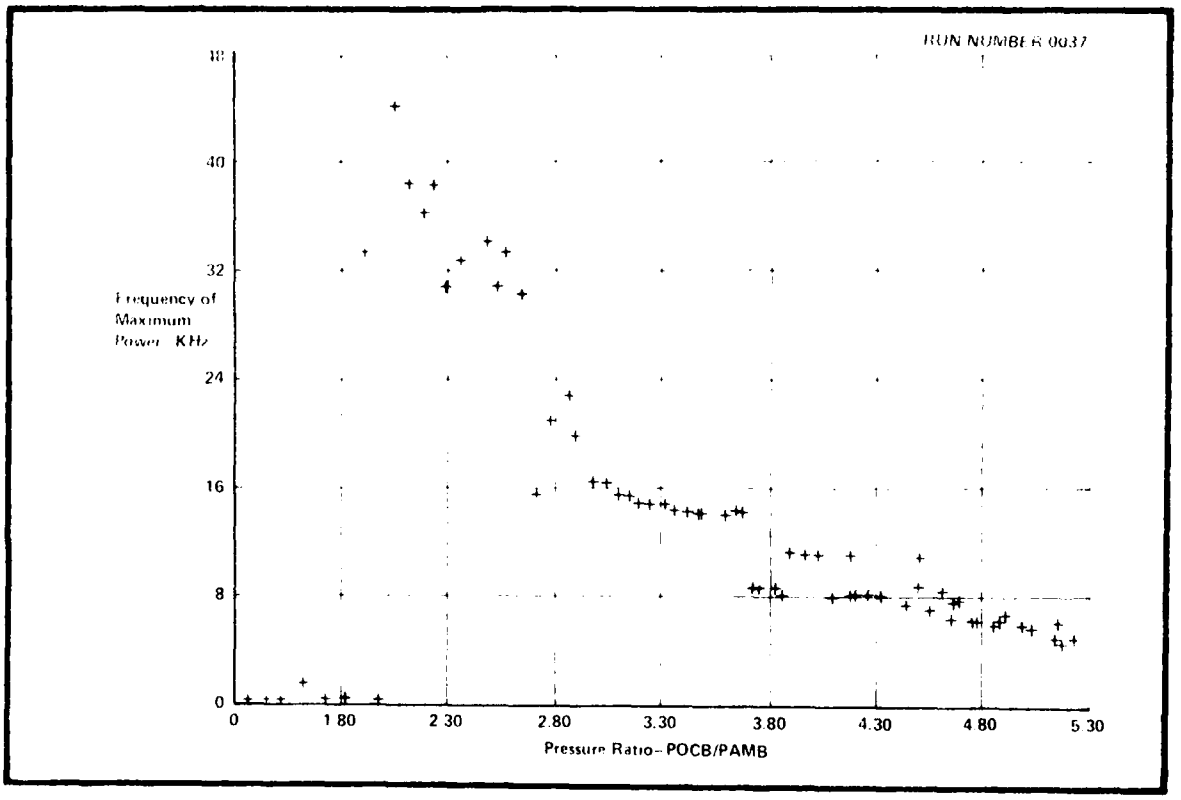

Figure 26. L/W = 11.0 Centerbody Only

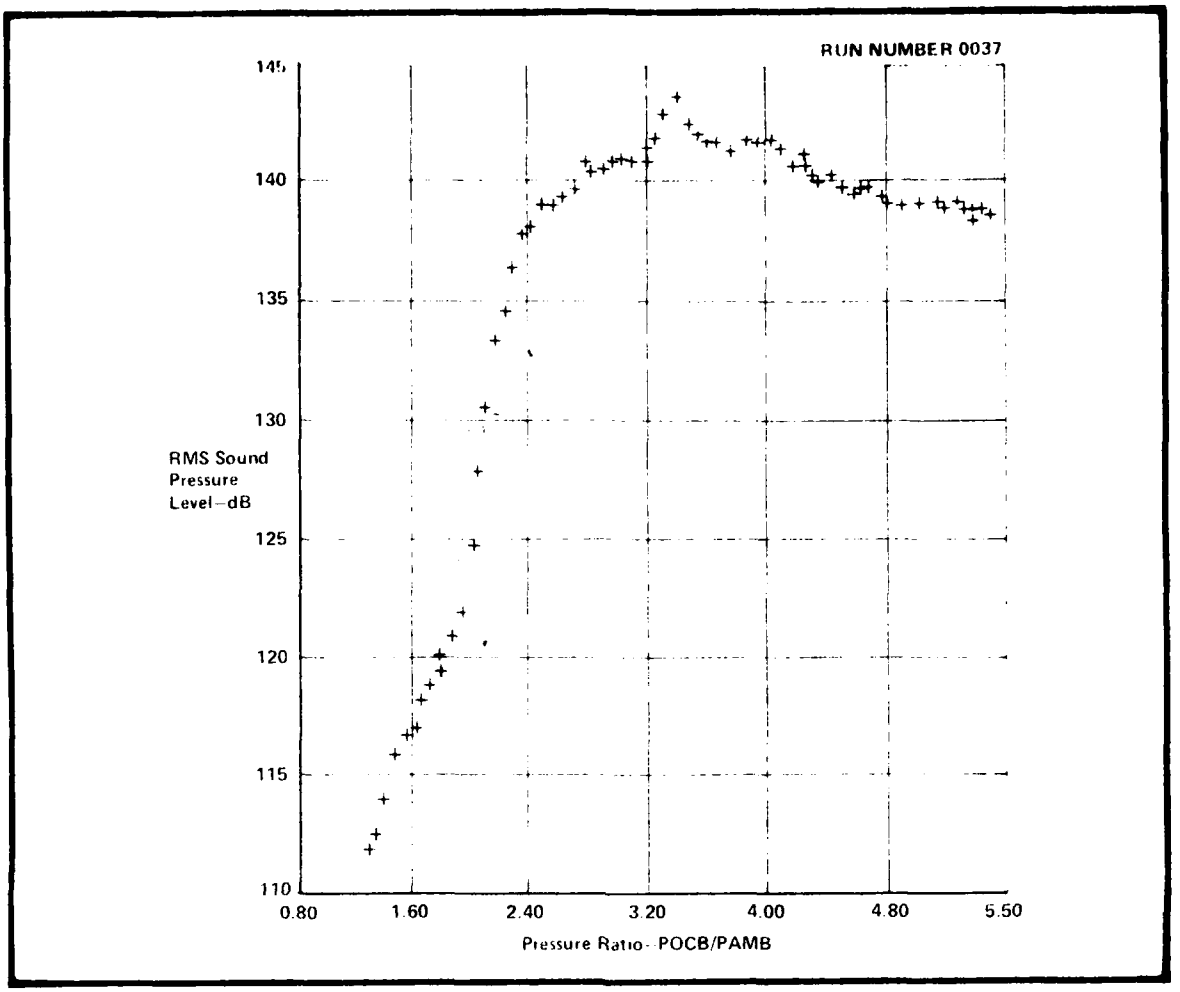

Figure 27. L/W = 11.0 Centerbody Only - Shroud Level Variation with Pressure

(as a root mean square of the sound pressure level) is presented as a function of pressure ratio. The intensity level rises with pressure ratio and then appears to level off and then decrease. The only exception to this trend is a sound intensity peak which occurs between pressure ratios of approximately 3.10 and 3.70; the same region which indicates acoustic interaction based on the measured thrust and the dominant acoustic frequencies shown in Figures 25 and 26. So over the region of interaction, not only is the frequency very coherent (Figure 26) but the total sound level is amplified (Figure 27). Additional acoustic interactions could exist but yet not be observed because they are small.

A similar behavior was observed with an ejector length of L/W = 9.5. A thrust deviation existed between approximate pressure ratios of 3.3

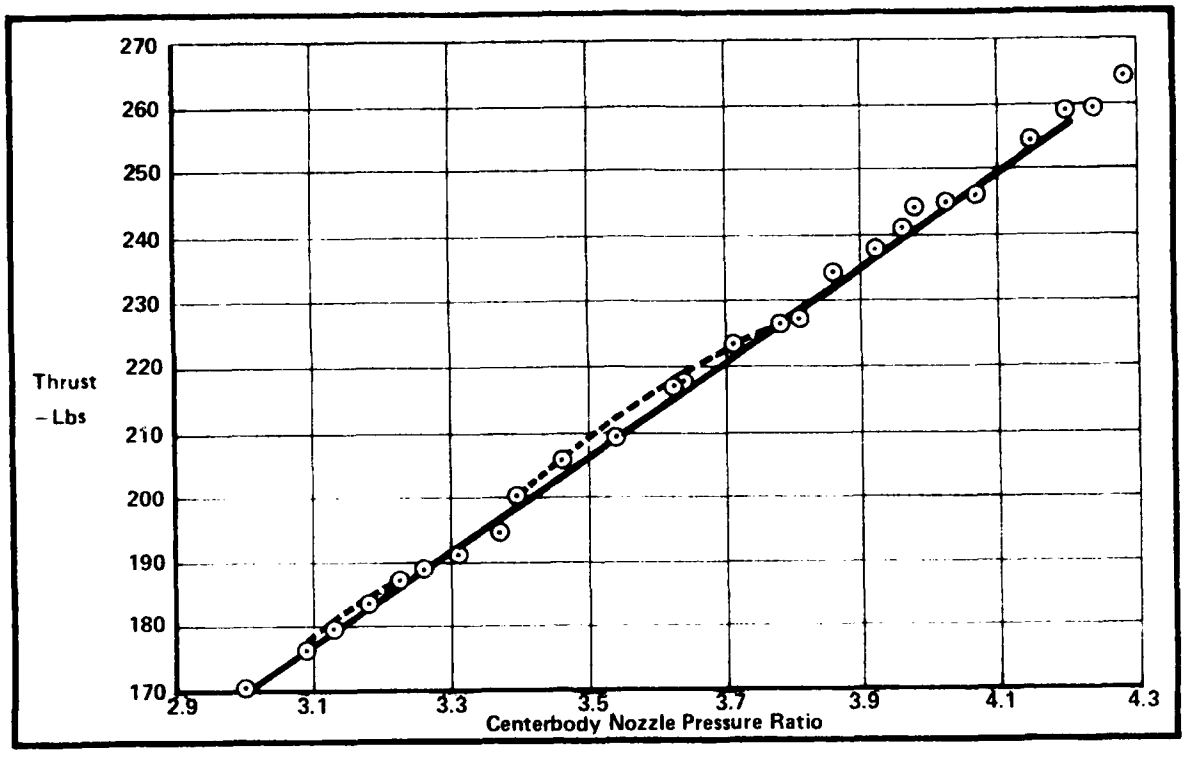

Figure 28. L/W = 5.0 Centerbody Only - Thrust Variation with Pressure

and 3.9 and the dominant acoustic frequency in that region was stable at 14 Khz. The total acoustic intensity also showed a peak in this pressure region, so the acoustic interaction model is consistent.

With the reduction in ejector length to L/W = 5.0, a multiple interaction takes place. The thrust level as a function of nozzle pressure ratio (Figure 28) shows what appear to be multiple deviations from the expected linear behavior. Examining the dominant frequencies (Figure 29), there appear to be two regions in which the dominant frequency is essentially constant, approximately between pressure ratios of 3.2 and 3.6 and again between 3.8 and 4.3. The existence of two regions of interaction is verified by the total sound intensity shown in Figure 30. The two intensity peaks are centered at pressure ratios of 3.4 and 4.1. In addition, the dominant frequencies in these two pressure ranges are

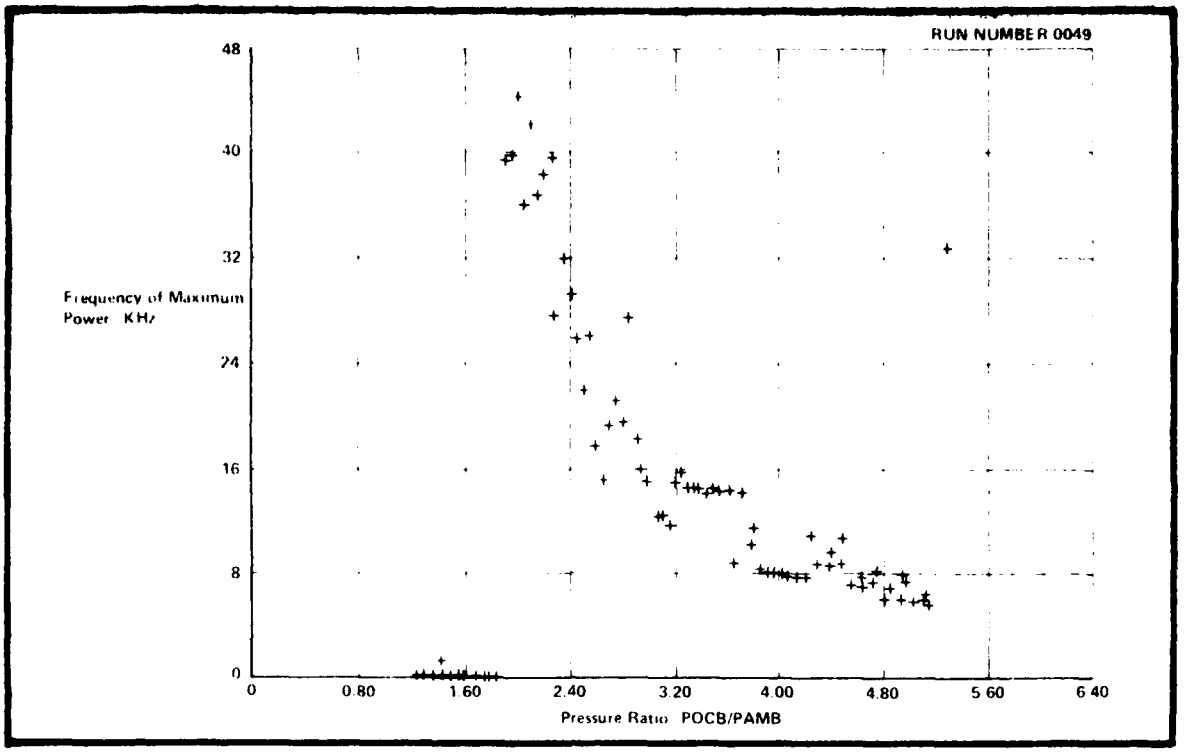

Figure 29. L/W = 5.0 Centerbody Only - Frequency Variation with Pressure

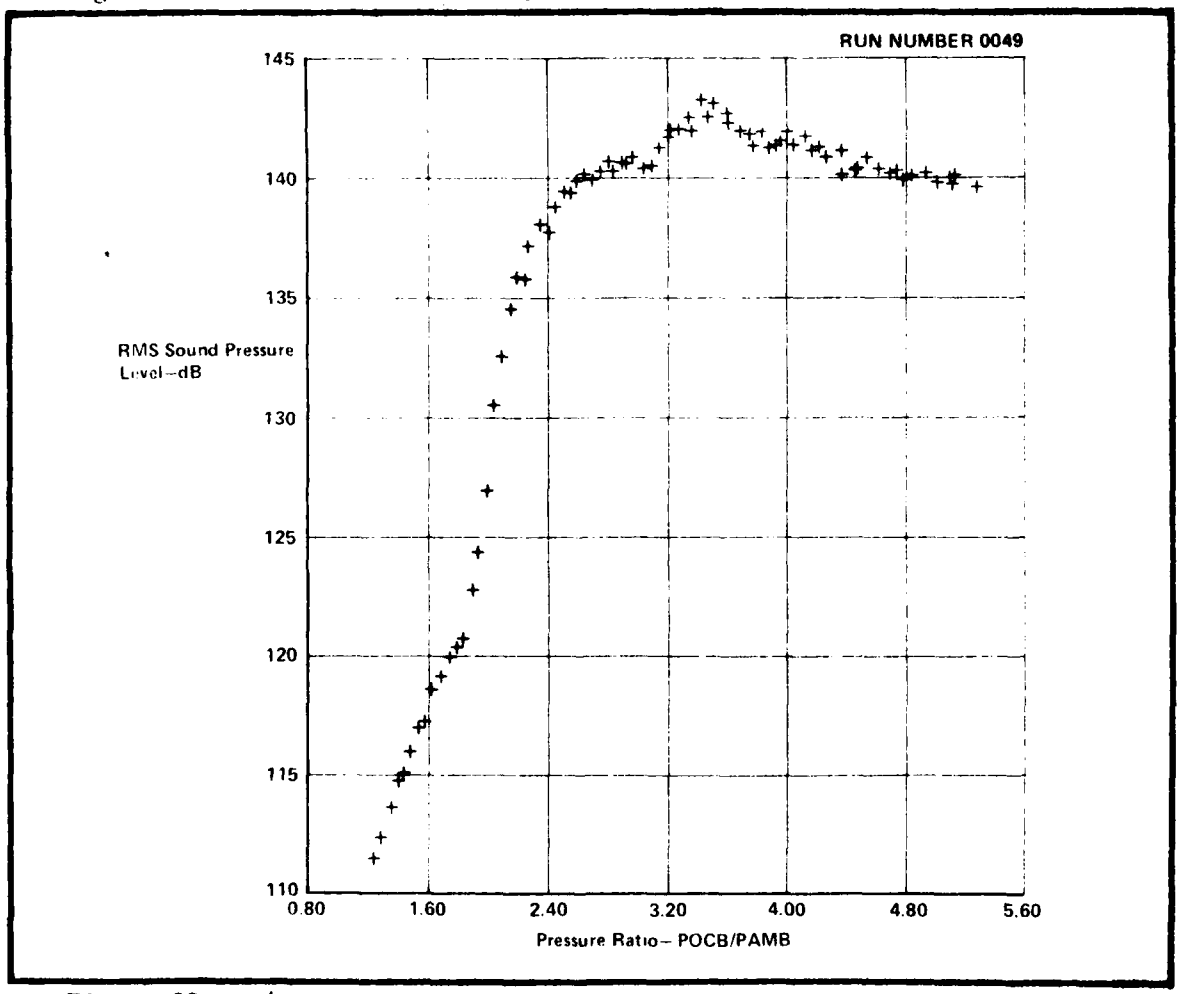

Figure 30. L/W = 5.0 Centerbody Only - Shroud Level Variation with Pressure

approximate multiples of one another. A closer examination of Figure 27 indicates that a weak second peak also exists in the L/W = 11.0 case but that its dominant frequency varies between approximately 8 and 12 KHz, making it more difficult to identify.

In the case of shorter ejector geometries, the acoustic interaction described above is not evident. The thrust rise with pressure ratio for a short ejector, L/W = 2.0, is shown in Figure 31 and shows no systematic excursions from the linear behavior. The dominant frequency behavior (Figure 32) also reveals no acoustic interaction, since there are no apparent regions of constant frequency. In fact, the dominant frequency data looks similar to that of the nozzle alone (Figure 23). In addition, the characteristic peak in the sound intensity plot is not evident for this short ejector case (Figure 33) so there is no acoustic amplification.

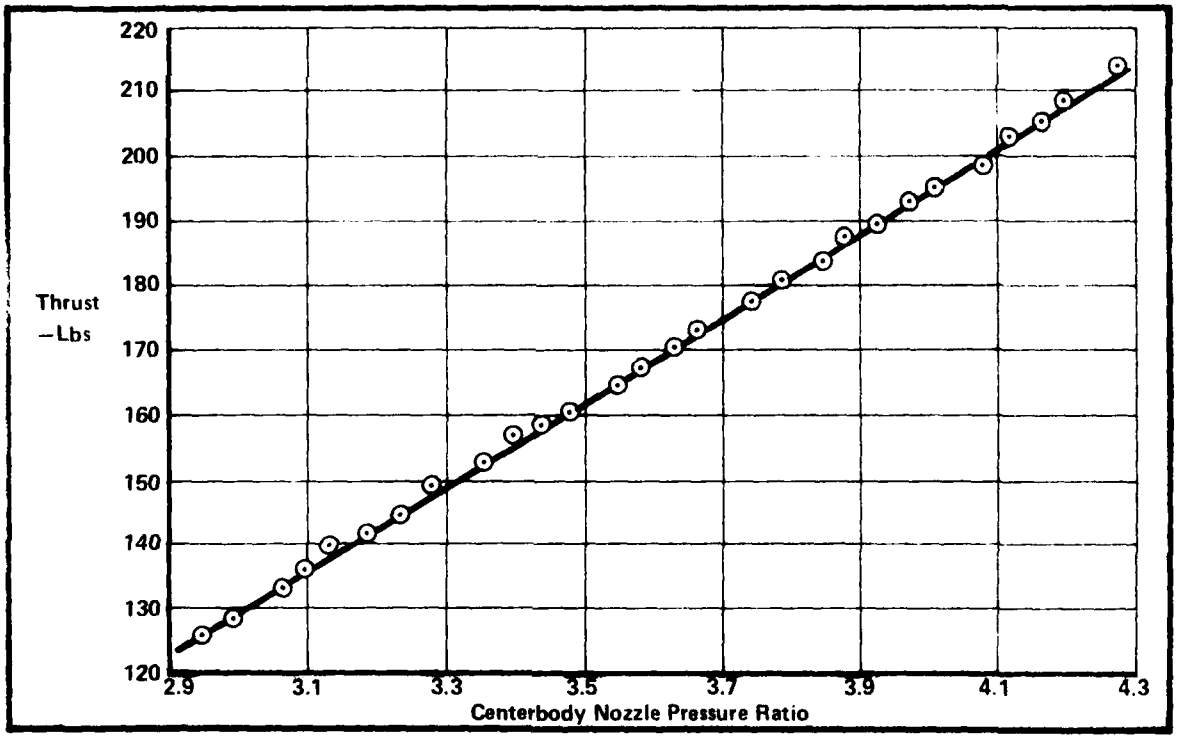

Figure 31. L/W = 2.0 Centerbody Only - Thrust Variation with Pressure

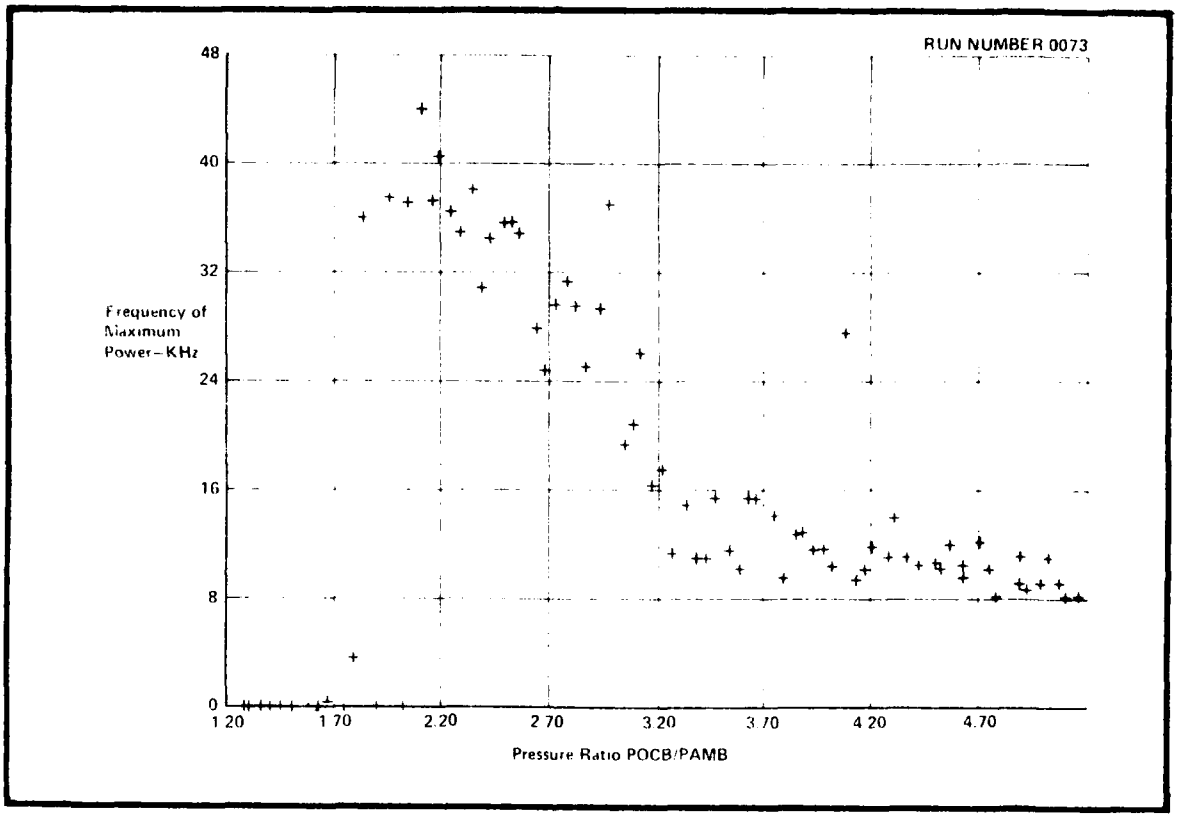

Figure 32. L/W = 2.0 Centerbody Only - Frequency Variation with Pressure

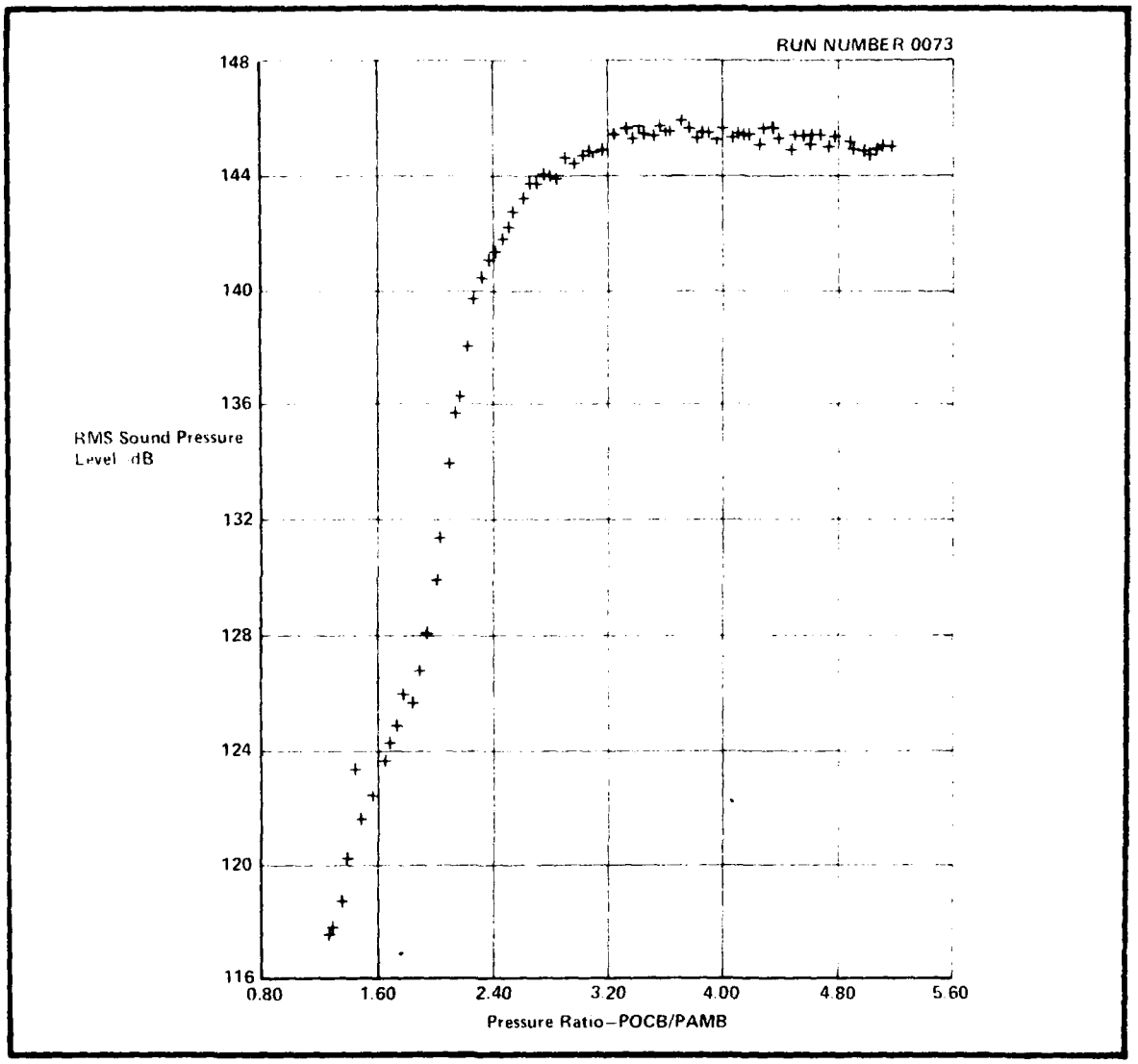

Figure 33. L/W - 2.0 Centerbody Only - Sound Level Variation with Pressure

Ejector Length Effect

Centerbody and Centerbody/Coanda

The effect of length on ejector performance has been examined by various investigators, including Quinn[8] and Bevilaqua.[19] The typical conclusion is that the effect of the addition of length to an ejector depends on the completeness of the mixing process. If the mixing between the primary and entrained flows is already relatively complete at the ejector exit, then additional length will only add a wall shear loss, and performance decreases. If the exit profile shows incomplete mixing between the two streams, then additional ejector length will result in improved performance because the improved mixing will be more important than the additional wall losses. Thus, the typical curve of performance versus length increases, reaches a maximum, and then shows a monotonic decrease with additonal length.

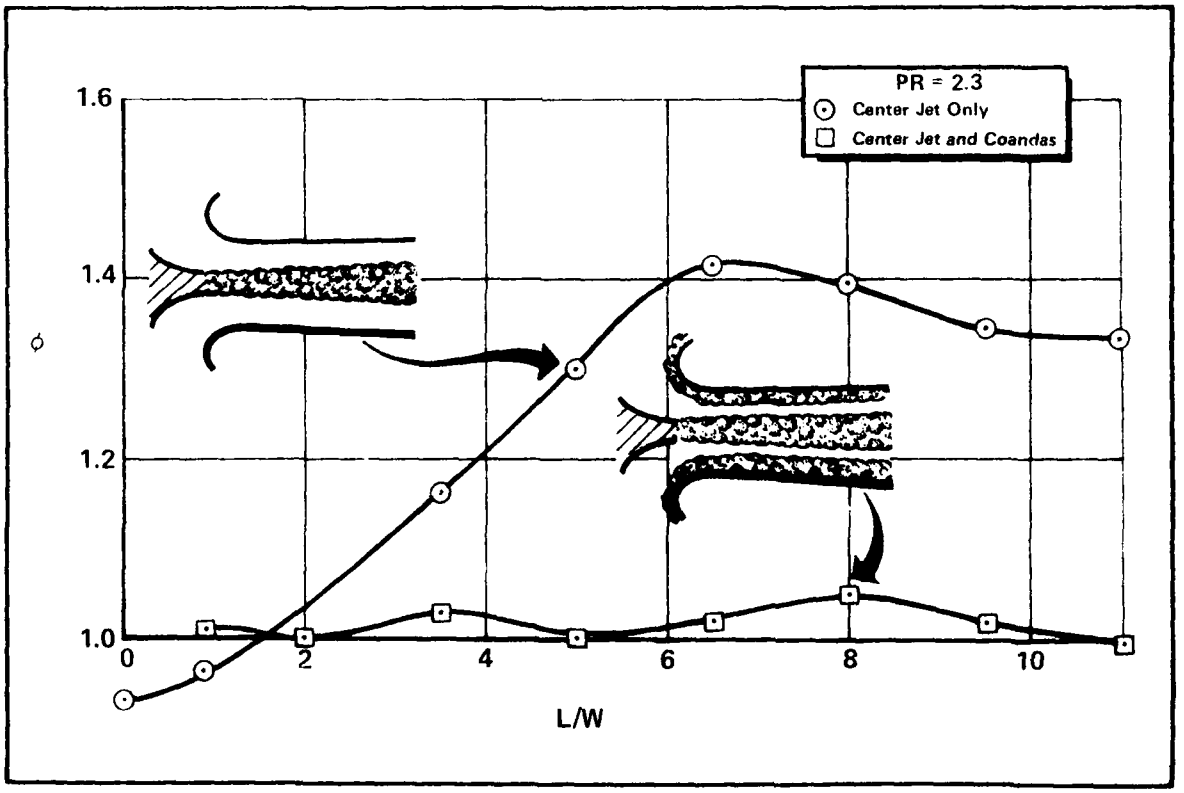

Figure 34. Effect of Length on Thrust Augmentation Ratio

The measured effect of length is shown in Figure 34 for ejector configurations with and without Coanda jets. Although the configuration with Coanda jets develops less augmentation, this is primarily due to its lower inlet area ratio.[9] Since these jets prevent flow separation if the diffuser area ratio is increased,[8] such an ejector can produce higher peak augmentation than one without wall jets. Such a change in diffuser area ratio was beyond the scope of the present study, and would not be expected to change the results.

The different trends for the centerbody ejector and the centerbody plus Coanda ejector can be explained by examining the exit velocity profiles in each case, as shown in Figures 35 and 36. For the case of long ejectors, L/W = 11 (Figure 35), both the centerbody nozzle and the centerbody plus Coanda ejectors lead to exit pressure profiles which

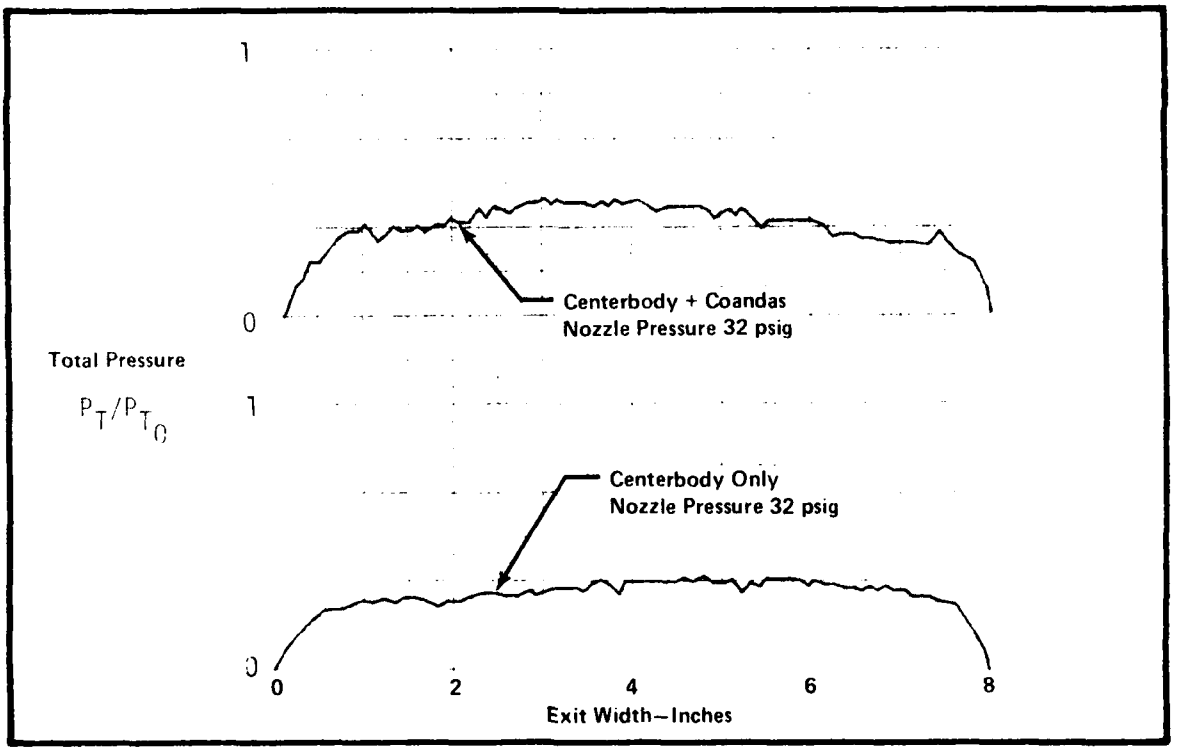

Figure 35. Total Pressure Profile L/W = 11.0 Mid Section Survey

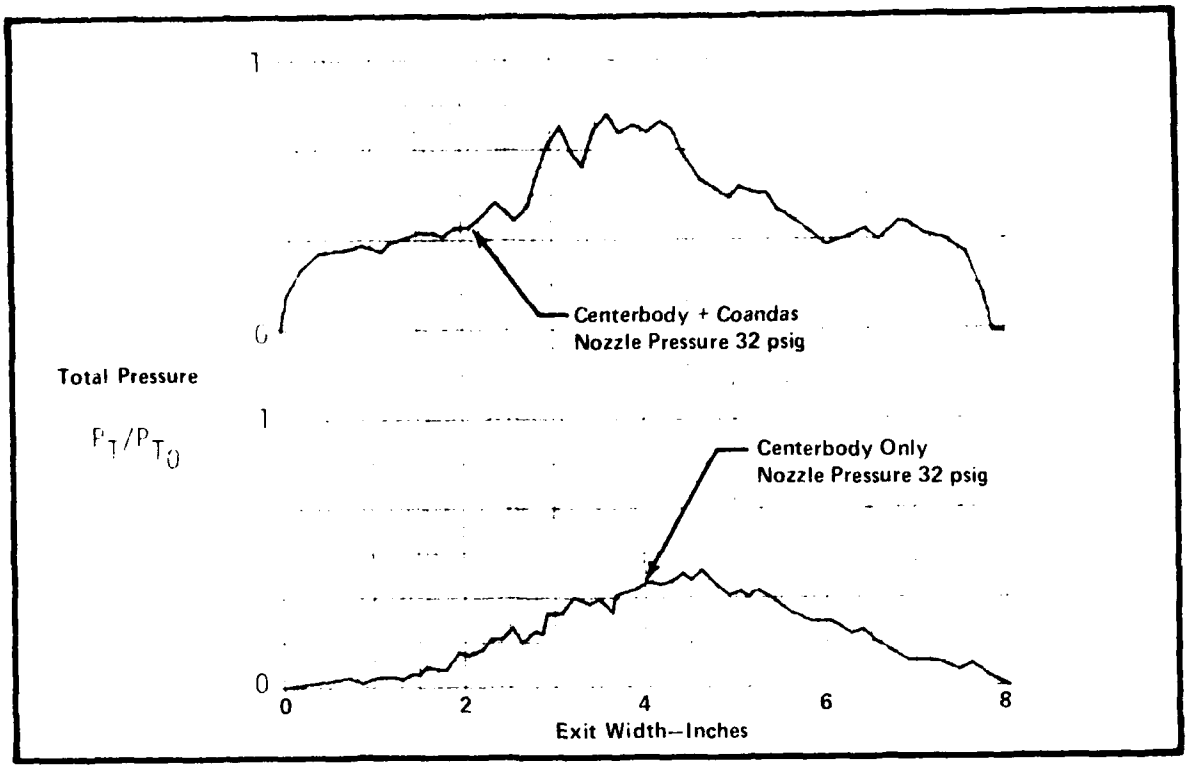

Figure 36. Total Pressure Profile L/W = 3.5 Mid Section Survey

indicate that the streams are reasonably well mixed. However in the case of short ejectors, L/W = 3.5, the exit pressure profile for the centerbody ejector is very poorly mixed as shown in Figure 36. Thus, one would expect to achieve a gain in performance by adding length to the ejector. This is verified by Figure 34 and shows that in this case the improvement in mixing overcomes the additional losses attributable to wall shear. In the case of the centerbody plus Coanda ejector geometry (Figure 36), the exit profile is reasonably well mixed even for the short L/W = 3.5 duct length. Thus, the addition of more ejector length is not justified. In fact, as illustrated in Figure 34, the small mixing advantage due to additional length is simply balanced by the disadvantage of the increased wall shear.

That the above results of length are not greatly affected by the acoustics may be seen from the fact that similar conclusions may be drawn from data at various pressure levels (corresponding to various screech frequencies).

Usefulness of Acoustics Varies with Length

The data presented clearly indicate an acoustic interaction at particular pressure ratios. However, the question of the usefulness of this interaction is also dependent upon the ejector length. For example, in the case of a long ejector, an acoustic interaction which produces improved mixing could be detrimental to the thrust augmentation because it would increase wall friction losses without substantially improving the degree of mixing at the ejector exit plane. For a short ejector, where mixing is a more severe problem, improved mixing would be expected to produce improved thrust performance.

The acoustic interactions observed in the present rectangular ejector appeared between L/D ratios of 3.8 and 11.0. At L/D = 2.0 and below, there was no evidence of the interaction. When the interaction did occur, the pressure ratio was always between 3.2 and 3.5 for the basic mode and always corresponded to a dominant frequency of approximately 15 to 16 KHz and showed very little variation.

The Effect of Size

The existence of an interaction between the jet screech modes and the duct acoustic modes is evident in the data. However, the difference in frequency between the jet screech modes and the lower natural modes of the rectangular duct reduces the effectiveness of the acoustic interaction. A high screech frequency will mainly excite the higher duct modes. Most of the energy will remain in the higher modes. Consequently, only a small fraction will appear in the lower modes, which are most effective in improving mixing. Thus, the acoustic effects in the present case are less pronounced than those observed by Quinn[12] in the axisymmetric case, where the modes were matched at low frequencies.

In order to match the modes in the rectangular case, the area of the duct must be reduced. However, the choice of jet and duct size is influenced by other factors in addition to the acoustic effect. The available primary mass flow usually dictates the nozzle area while the duct area is determined from aircraft size. The areas match well in the axisymmetric case where the area ratio is equal to the square of the ratio of duct to nozzle diameter. However, in the rectangular case, the area ratio is simply the ratio of the short side of the duct to the short side of the jet. As seen by Equations (1) and (4), the acoustics of both the nozzle and the duct also scale reasonably well with their short side dimension. Thus, the frequency mismatch is not likely to be relieved by scaling up the rectangular experiment.

Achieving a better match between the jet and duct frequencies in the rectangular case requires reducing the ejector inlet area ratio (perhaps to an unacceptable value for thrust augmenting ejectors). That is, increasing the nozzle area or reducing the duct area could improve the acoustic interaction, but there would be an unacceptable penalty in maximum thrust augmentation ratio.

Additional Effects

Krothapalli, et al.,[20] in their recent investigation of the acoustic structure of choked rectangular jets, have raised the question of the microphone's ability to correctly measure the screech amplitude. In the present experiment, the screech frequencies were all well within the measuring ability of the B&K Type 4136 microphone. Therefore, the change in dominance from the fundamental mode to the first harmonic, as shown in Figure 13, is believed to be a real effect.

From the point of view of the ejector application, as long as the magnitudes of the various modes are roughly the same, which of them is the dominant mode is not of great significance. They are capable of causing an acoustic interaction even if they are not dominant, but only slightly lower in magnitude.

Krothapalli, et al.[20] found that the maximum acoustic radiation from the rectangular jet occurred at a pressure ratio of 3.7 (at an aspect ratio of 16.7). This also corresponds to the maximum spreading rate of the rectangular jet and corresponds remarkably well with the pressure ratio of 3.8 where Quinn found the maximum acoustic effect in the axisymmetric case. For the present high aspect ratio case, AR = 133, the maximum acoustic level also occurs at approximately this pressure ratio, indicating that the intensity of the screech may be less related to the jet geometry than to the local conditions at the exit plane.

CONCLUSIONS AND RECOMMENDATIONS

The effect of jet screech on the performance of rectangular thrust augmenting ejectors has been experimentally determined. The screech frequency of the primary jet was found to be correlated with the short dimension of the primary nozzle, for nozzle aspect ratios greater than 5. For lower aspect ratios, the dominant frequency is a beat frequency due to the interaction of the tones correlated with the short and long nozzle dimensions. The entrainment of the high aspect ratio free jets was observed to increase significantly at critical pressure ratios of approximately 3.2 and 3.9. This effect was observed to produce a very small increase in the ejector thrust augmentation at the critical pressure ratios. No resonance between the jet screech tone and the natural frequencies of the ejector duct were observed to occur. This is probably due to the mismatch between the j· ;ency and the lower order duct modes. This mismatch is the result the requirement for having a large ejector duct in order to produce significant baseline levels of thrust augmentation.

Thus it can be concluded that the thrust augmentation of simple rectangular ejectors can not be significantly increased by acoustic effects. Further investigation of compound or staged ejectors, with axisymmetric or lobed nozzles will be necessary in order to realize a gain from this phenomenon.

REFERENCES

1. Brown, G. B., "Vortex Motion in Gaseous Jets and the Origin of their Sensitivity to Sound," Proc. Phys. Soc., Vol. 47, p 703, 1935.

2. Becker, H. A. and Massaro, T. A., "Vortex Evolution in a Round Jet," Journal of Fluid Mechanics, Vol. 31, No. 3, 1968, pp 435-448.

3. Crow, S. C. and Champagne, F. H., "Orderly Structure in Jet Turbulence," Journal of Fluid Mechanics, Vol. 48, Part 3, 1971, pp 547-591.

4. Powell, A., "On the Noise Emanating from a Two-Dimensional Jet Above the Critical Pressure," The Aeronautical Quarterly, Vol. IV, Part III, 1953, pp 103-122.

5. Powell, A., "On the Mechanism of Choked Jet Noise," Proc. Phys. Soc., Vol. B66, 1953, p 1039.

6. Hammitt, A. G., "The Oscillation and Noise of an Overpressure Sonic Jet," Journal of Aerospace Sciences, Vol. 28, No. 9, 1961, pp 673-680.

7. Glass, D. R., "Effects of Acoustic Feedback on the Spread and Decay of Supersonic Jets," AIAA Journal, Vol. 6, No. 10, Oct. 1968, pp 1890-1897.

8. Quinn, B., "Compact Ejector Thrust Augmentation," Journal of Aircraft, Vol. 10, No. 8, August 1973, pp 481-486.

9. Bevilaqua, P. M. "Evaluation of Hypermixing for Thrust Augmenting Ejectors," Journal of Aircraft, Vol. 11, No. 6, June 1974, pp 348-354.

10. Quinn, B. "Effect of Aeroacoustic Interactions on Ejector Performance," Journal of Aircraft, Vol. 12, No. 11, pp 914-916.

11. Rosfjord, T. J. and Toms, H. L., "Recent Observations Including Temperature Dependence of Axisymmetric Jet Screech," AIAA Journal, Vol. 13, No. 10, pp 1384-1386.

12. Quinn, B., "Interactions Between Screech Tones and Ejector Performance," Journal of Aircraft, Vol. 14, No. 5, May 1977, pp 467-473.

13. Quinn, B. "Ejector Performance at High Temperatures and Pressures," Journal of Aircraft, Vol. 13, Dec. 1976, pp 948-954.

14. Succi, G. P., Baumeister, K. J., and Ingard, K. U., "Interaction of a Turbulent-Jet Noise Source with Transverse Modes in a Rectangular Duct," NASA Technical Paper 1248, June 1978.

15. Trentecoste, N. P. and Sforza, P. M., "Further Experimental Results for Three-Dimensional Free Jets," AIAA Journal, Vol. 5, No. 5, May 1967, pp 885-891.

16. Trentecoste, N. P. and Sforza, P. M., "Some Remarks on 3-D Wakes and Jets," AIAA Journal, Vol. 6, No. 12, December 1968.

17. Morse, P. M. and Ingard, K. U., Theoretical Acoustics, McGraw-Hill, 1968, p 495.

18. Ribner, H. S., "The Generation of Sound by Turbulent Jets," Advances in Applied Mechanics, Vol. 8, H. L. Dryden and T. von Karman, Eds., Academic Press, 1964, pp 103-182.

19. Bevilaqua, P. M., "Analytical Description of Hypermixing and Test of an Improved Nozzle," Journal of Aircraft, Vol. 13, No. 1, Jan. 1976, pp 43-48.

20. Krothapalli, A; Baganoff, D/; Hsia, Y.; and Karamcheti, K., "Some Features of Tones Generated by an Underexpanded Rectangular Jet," AIAA Paper No. 81-0060, Aerospace Sciences Meeting, St. Louis, January 1981

APPENDIX A

CENTERBODY ONLY BLOWING - SCREECH FREQUENCY DATA

APPENDIX A

This appendix contains the centerbody blowing actual recorded and reduced "frequency of maximum power (amplitude) versus centerbody nozzle pressure ratio" data with the predicted "screech" frequency superimposed.

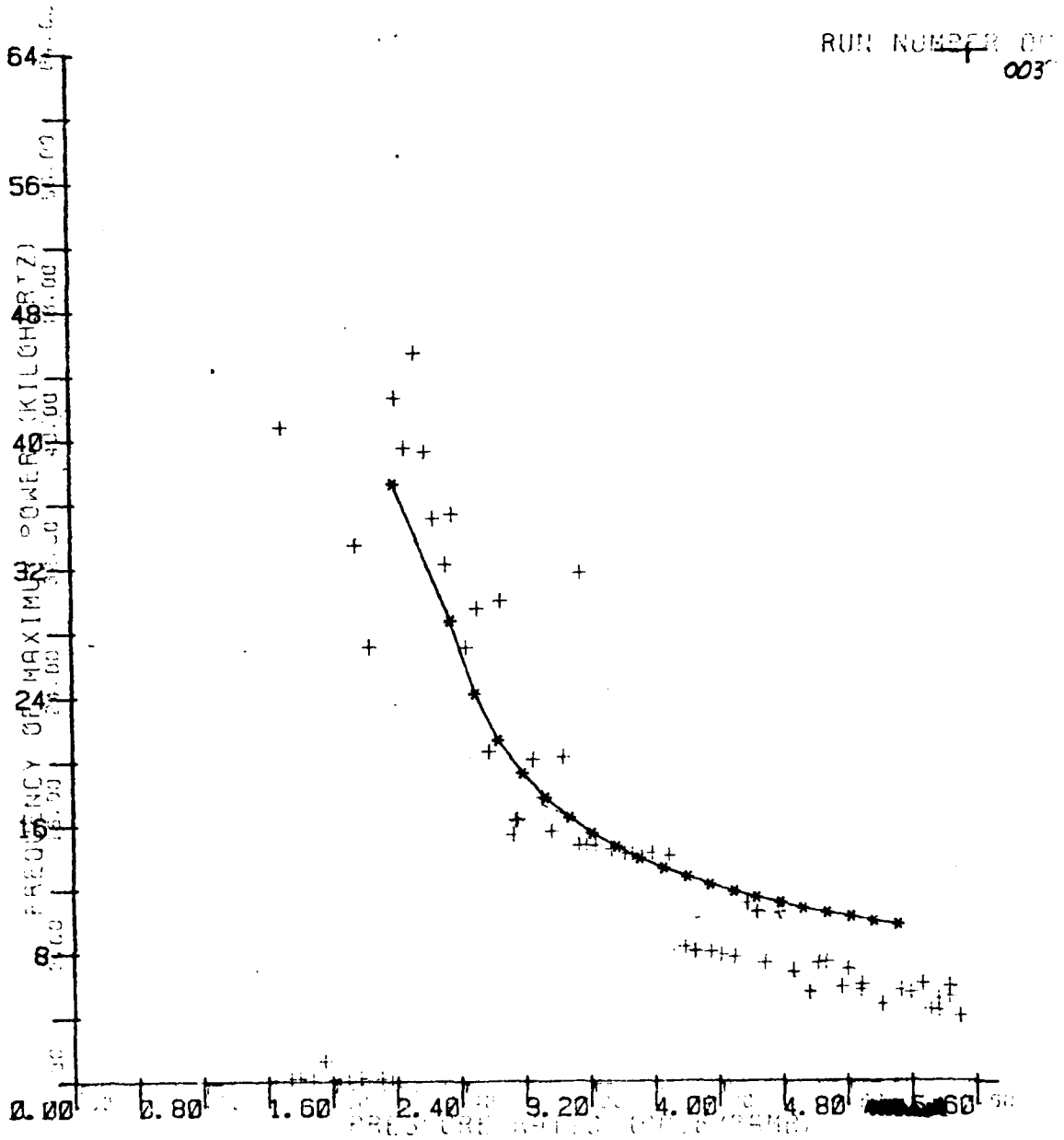

Figure A-1 L/W = 11.0

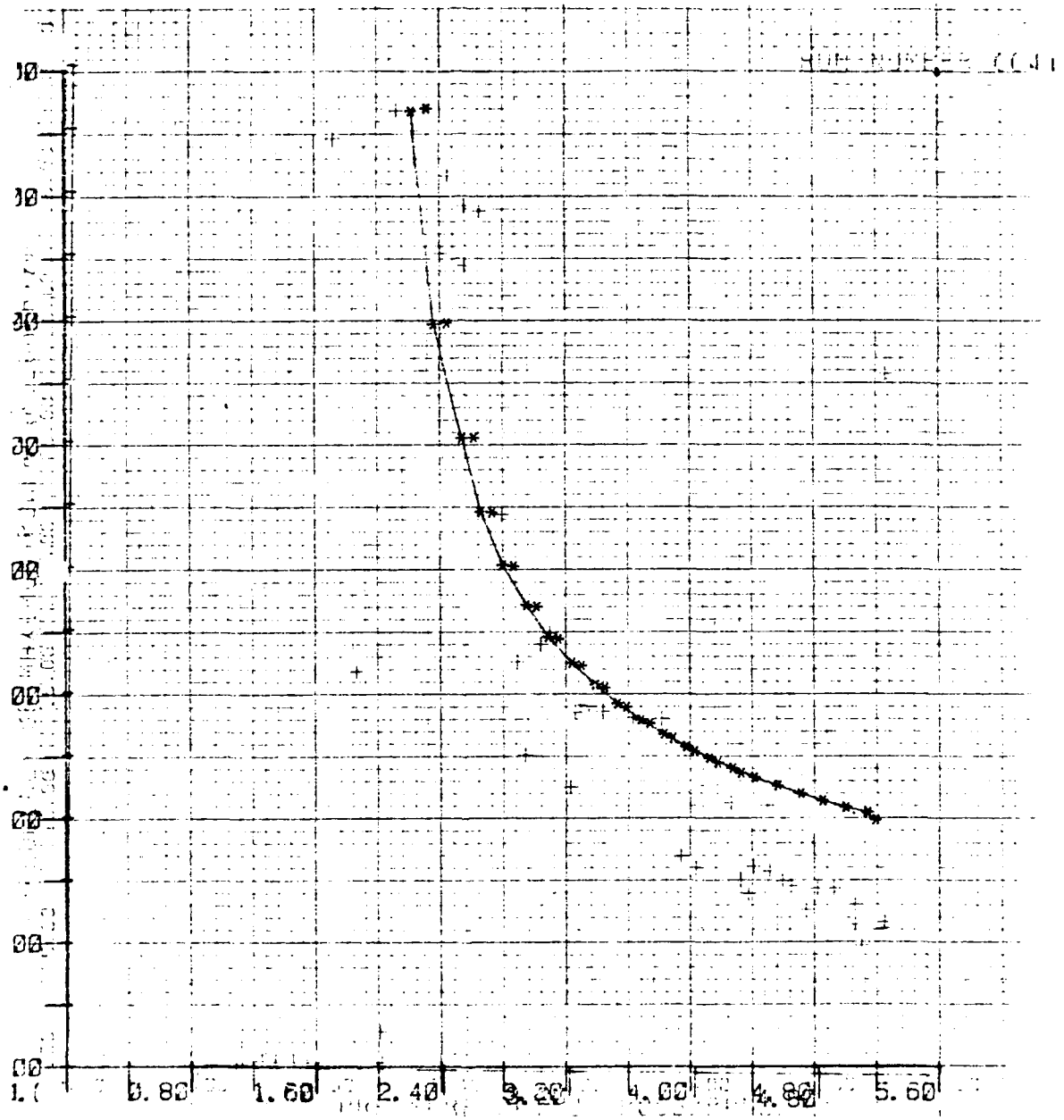

Figure A-2 L/W = 9.5

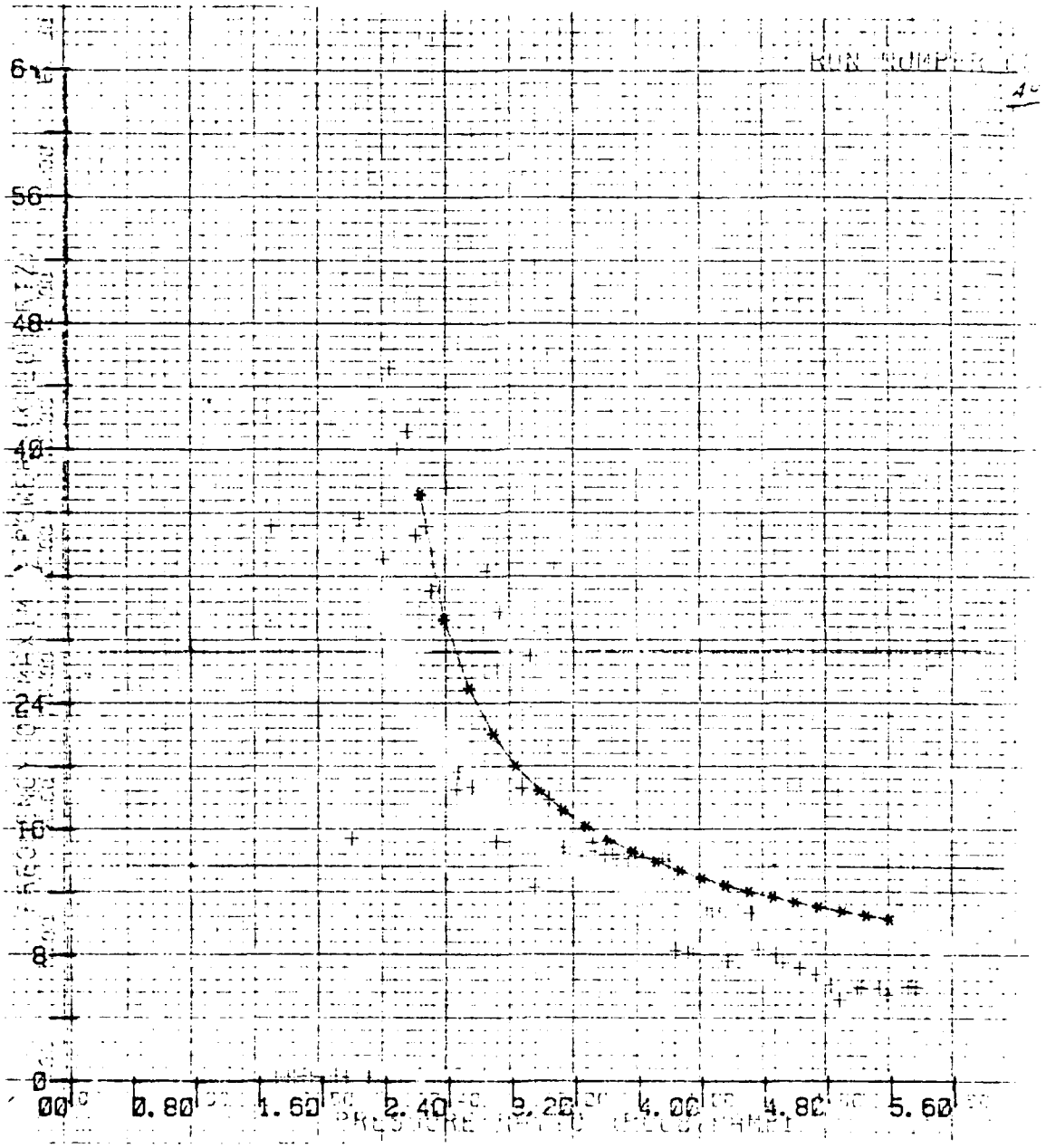

Figure A-3 L/W = 8.0

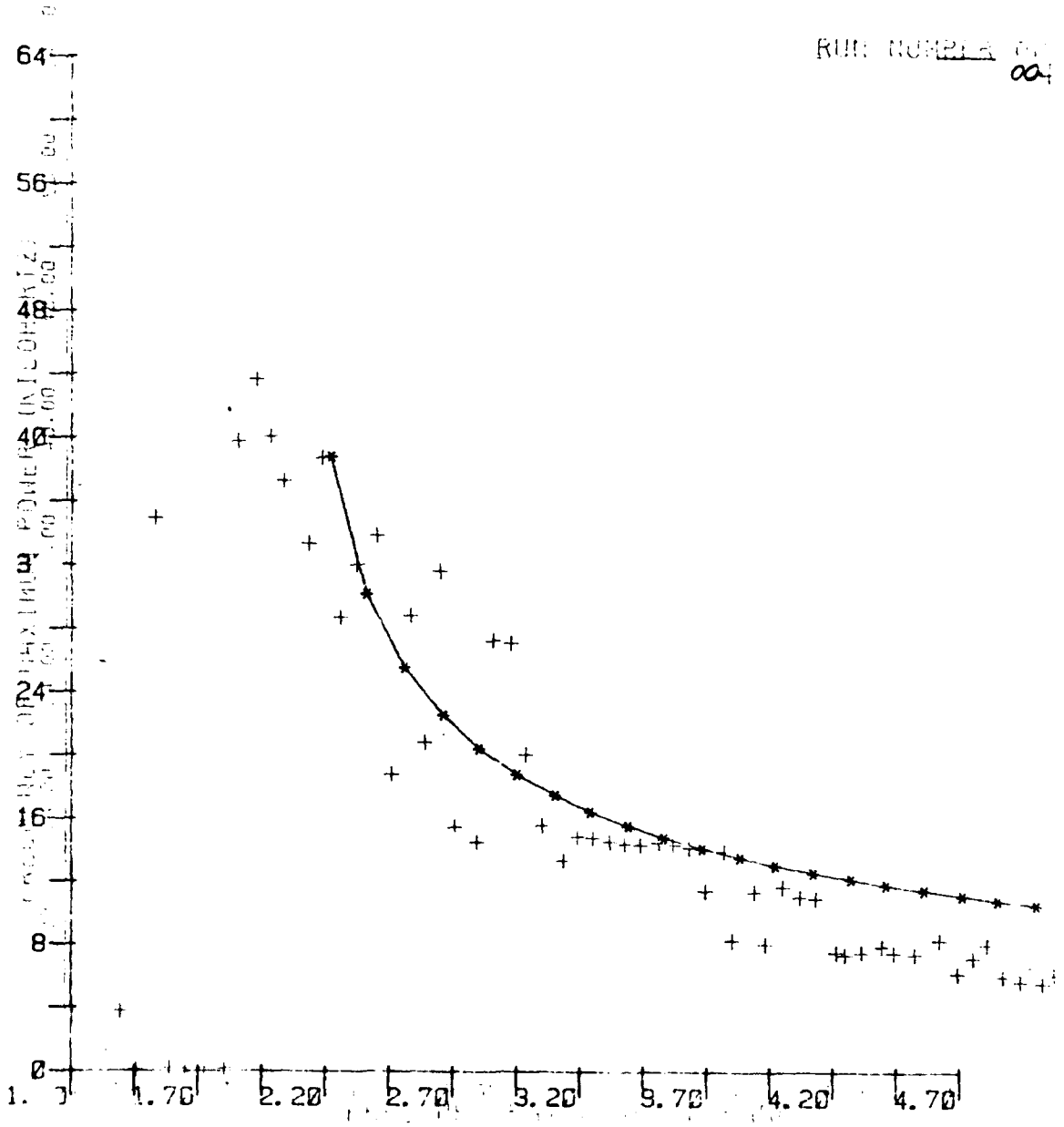

Figure A-4 L/W = 6.5

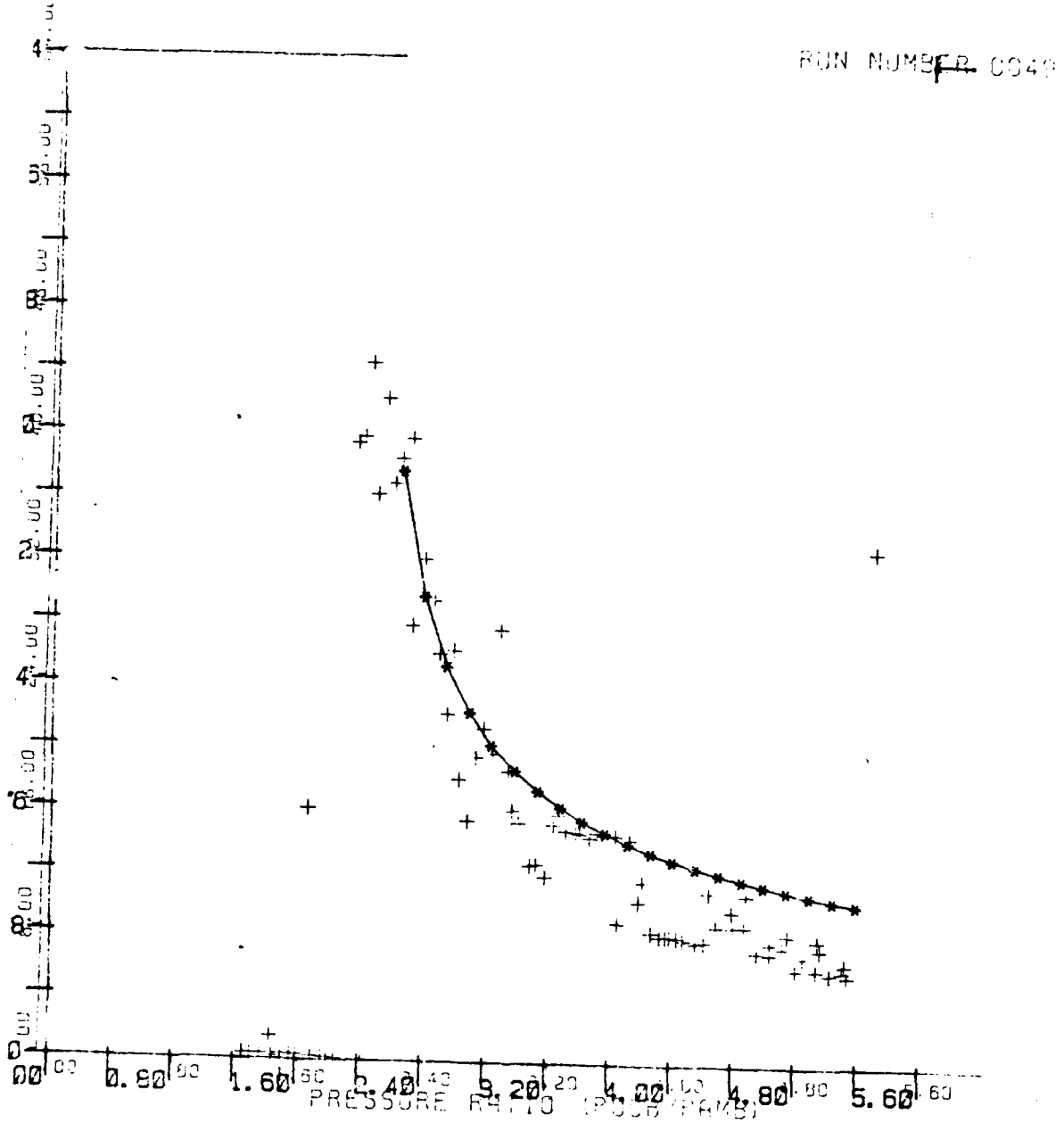

Figure A-5 L/W = 5.0

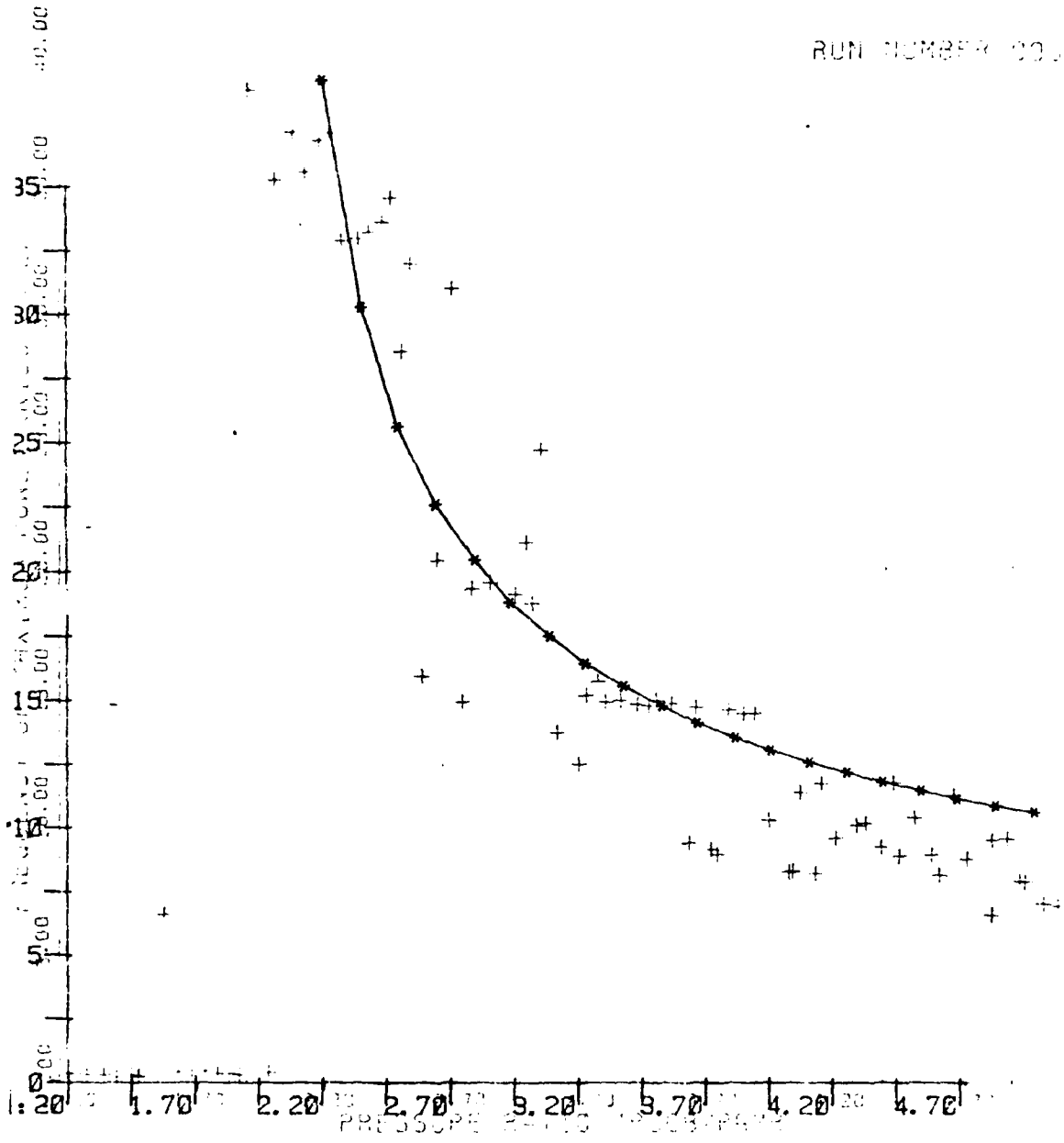

Figure A-6 L/W = 3.5

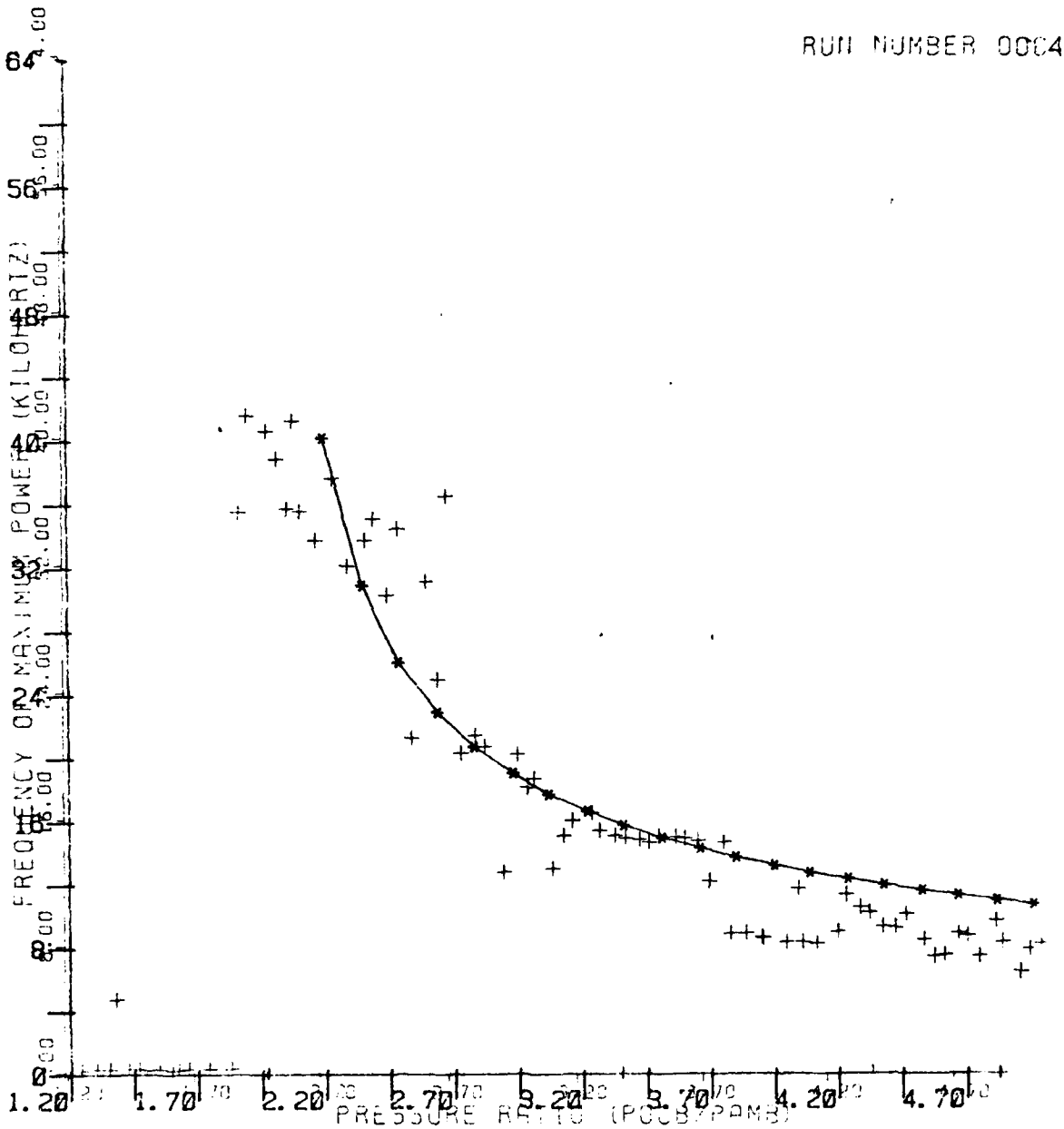

Figure A-7 L/W = 3.5 Repeated Test

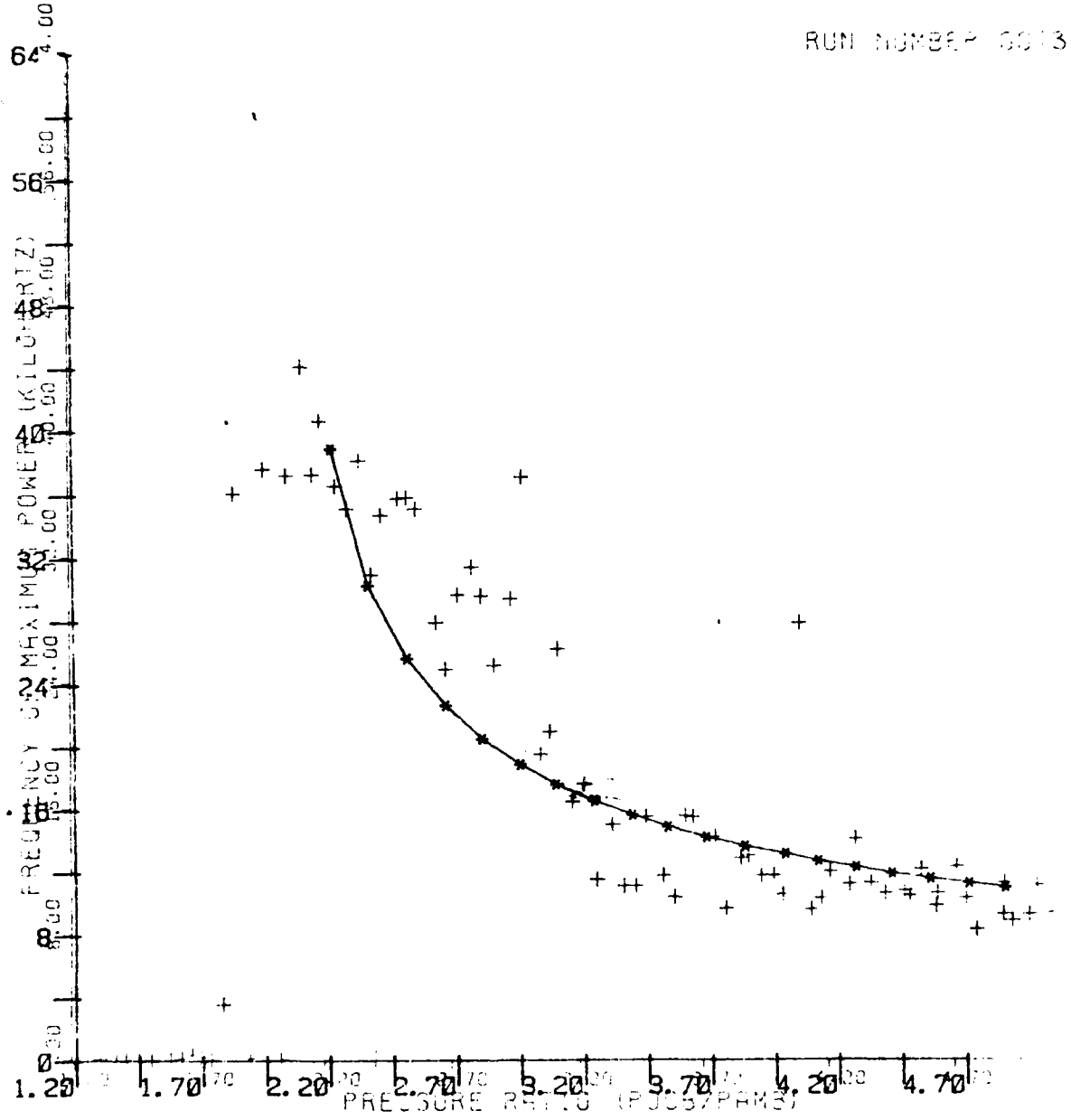

Figure A-8 L/W = 2.0

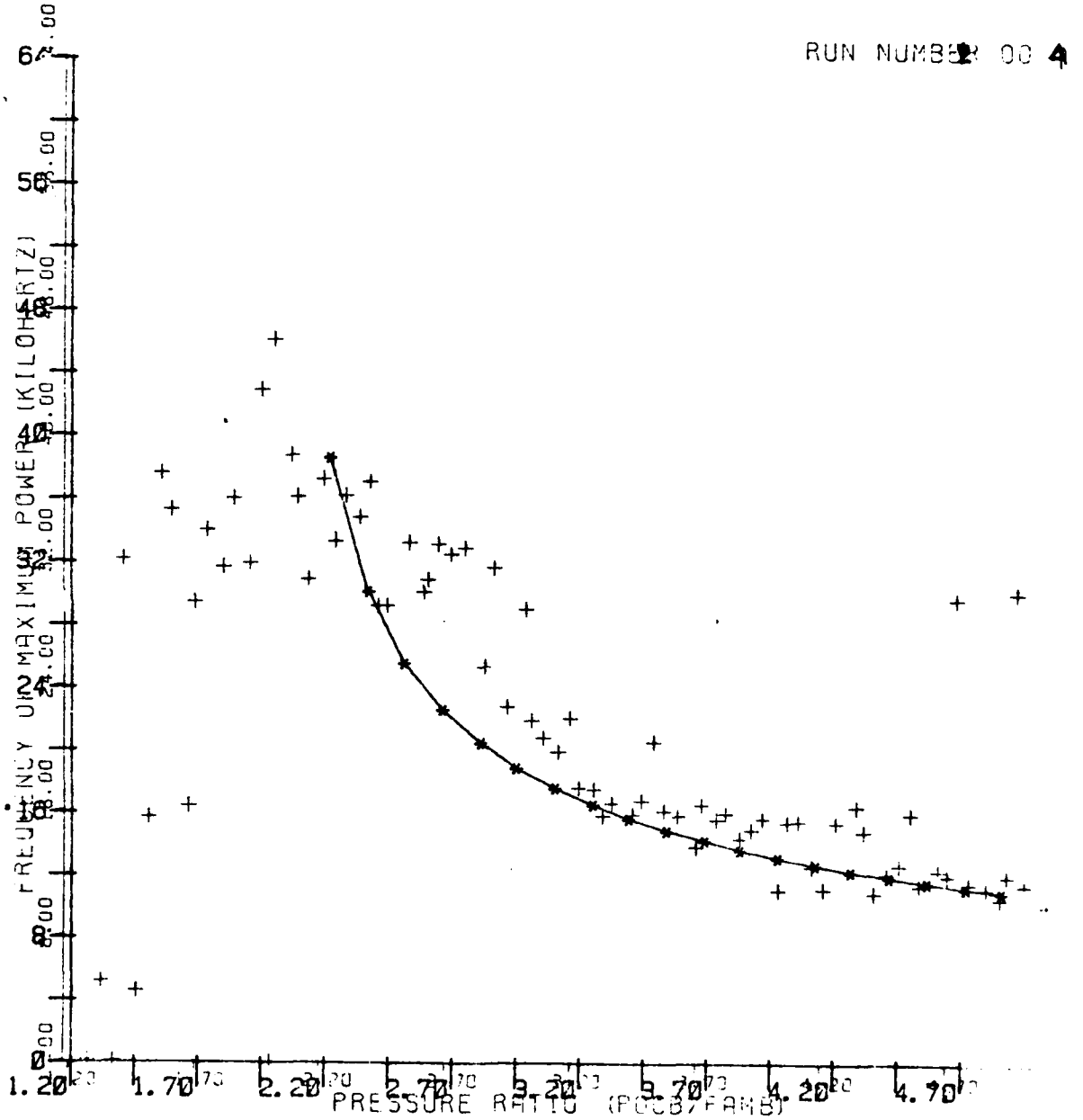

Figure A-9 L/W = 0.2

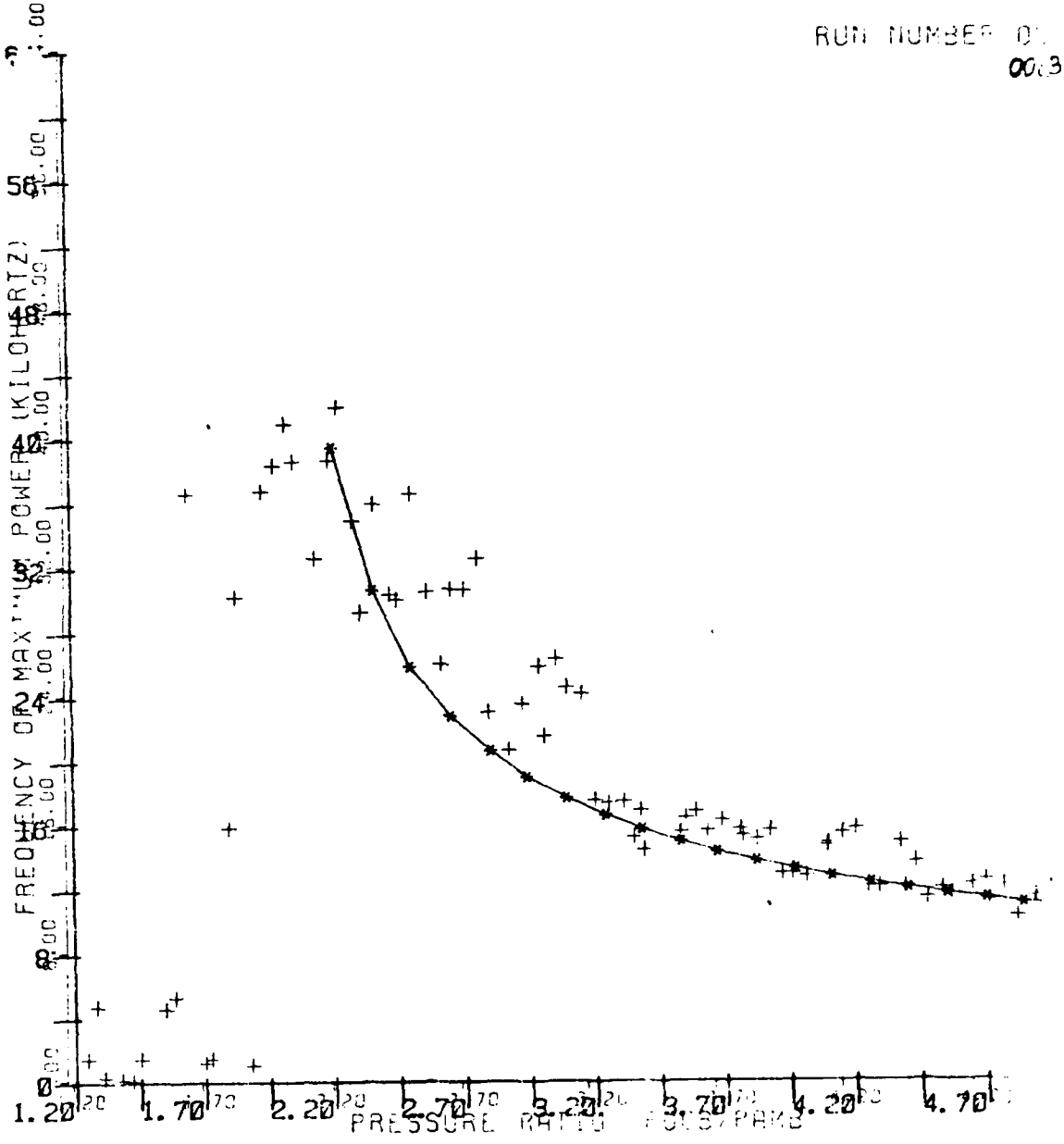

Figure A-10 L/W = 0.9

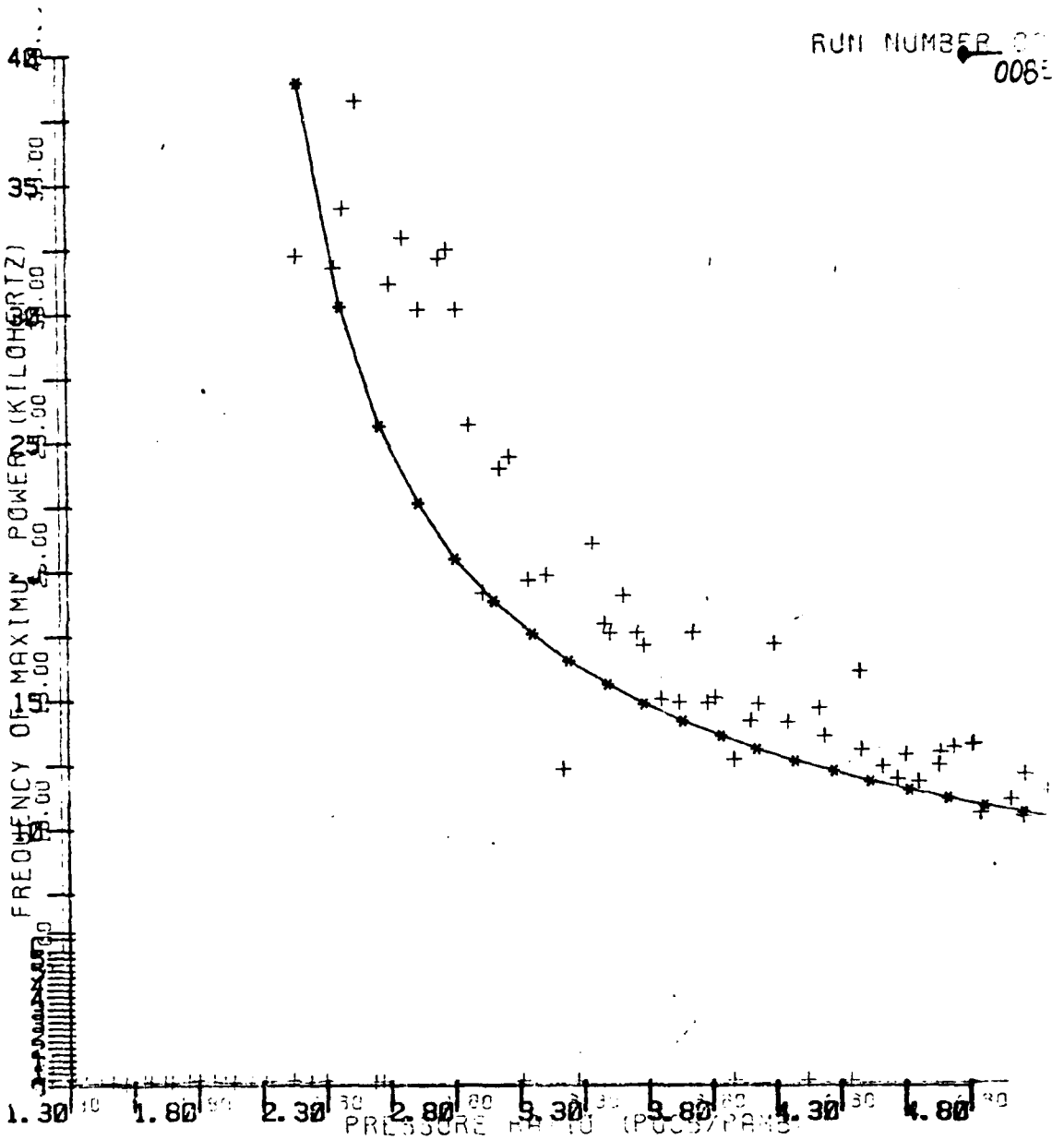

Figure A-11 Centerbody Only - Added Insulation

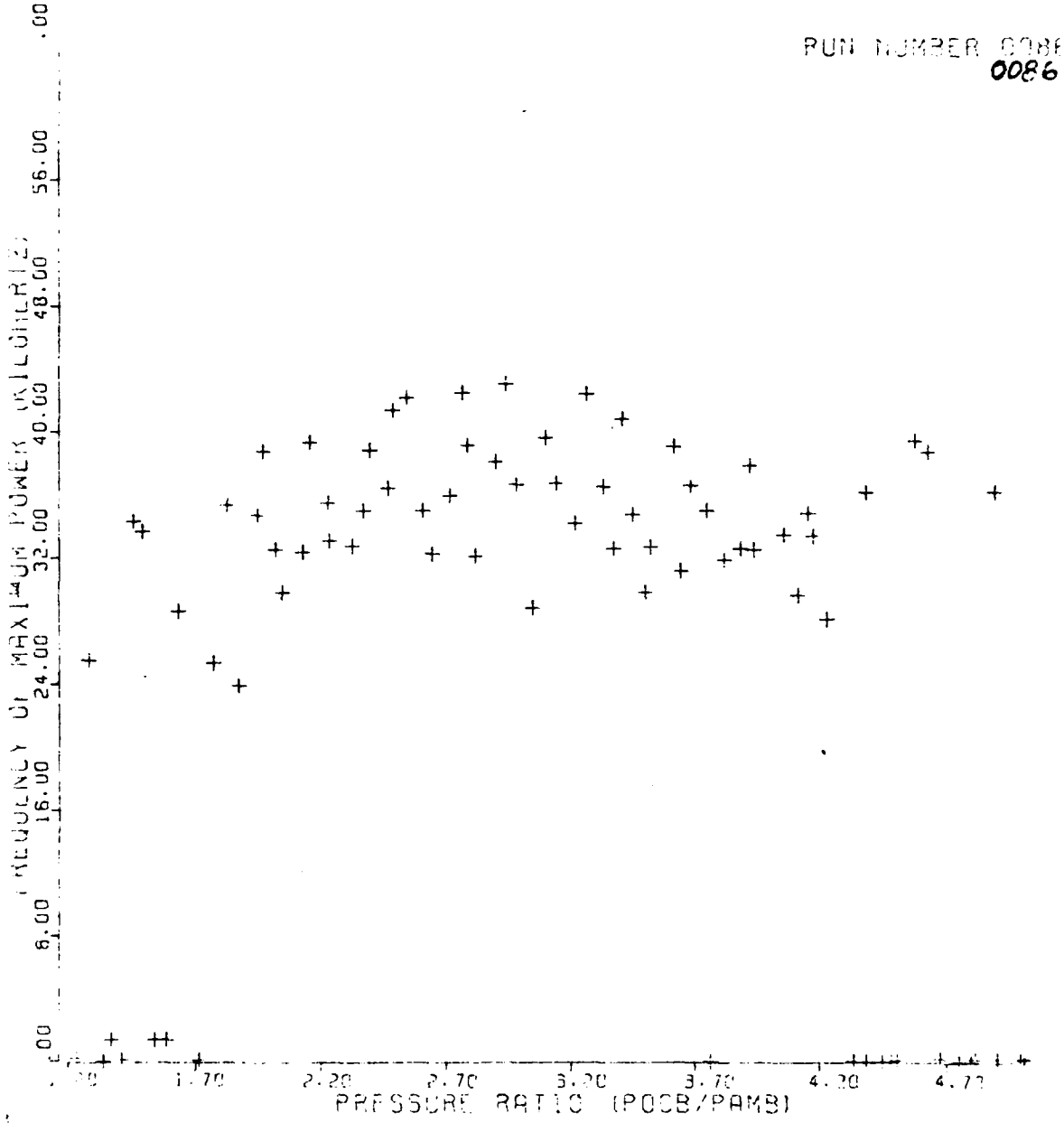

Figure A-12 **Centerbody Only/Added Insulation/New Microphone Location**

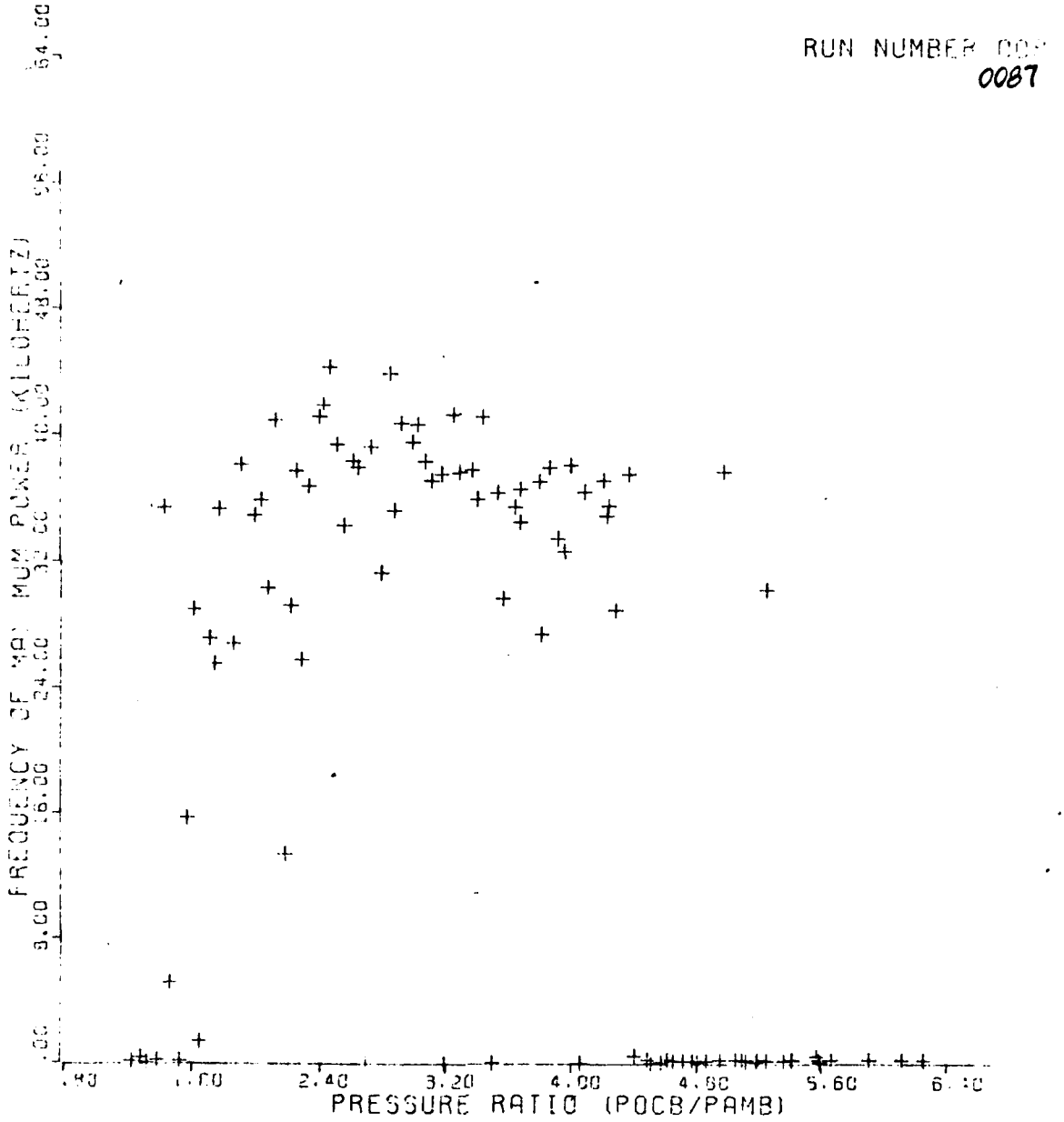

Figure A-13 **Centerbody Only Run 86 Repeated to Pressure Ratio of Approximately 6.3**

APPENDIX B

CENTERBODY ONLY BLOWING - THRUST AND AUGMENTATION RATIO (Ø) DATA

APPENDIX B

This appendix contains the centerbody blowing actual recorded and reduced thrust versus centerbody nozzle pressure ratio data (Figures B-1 through B-29).

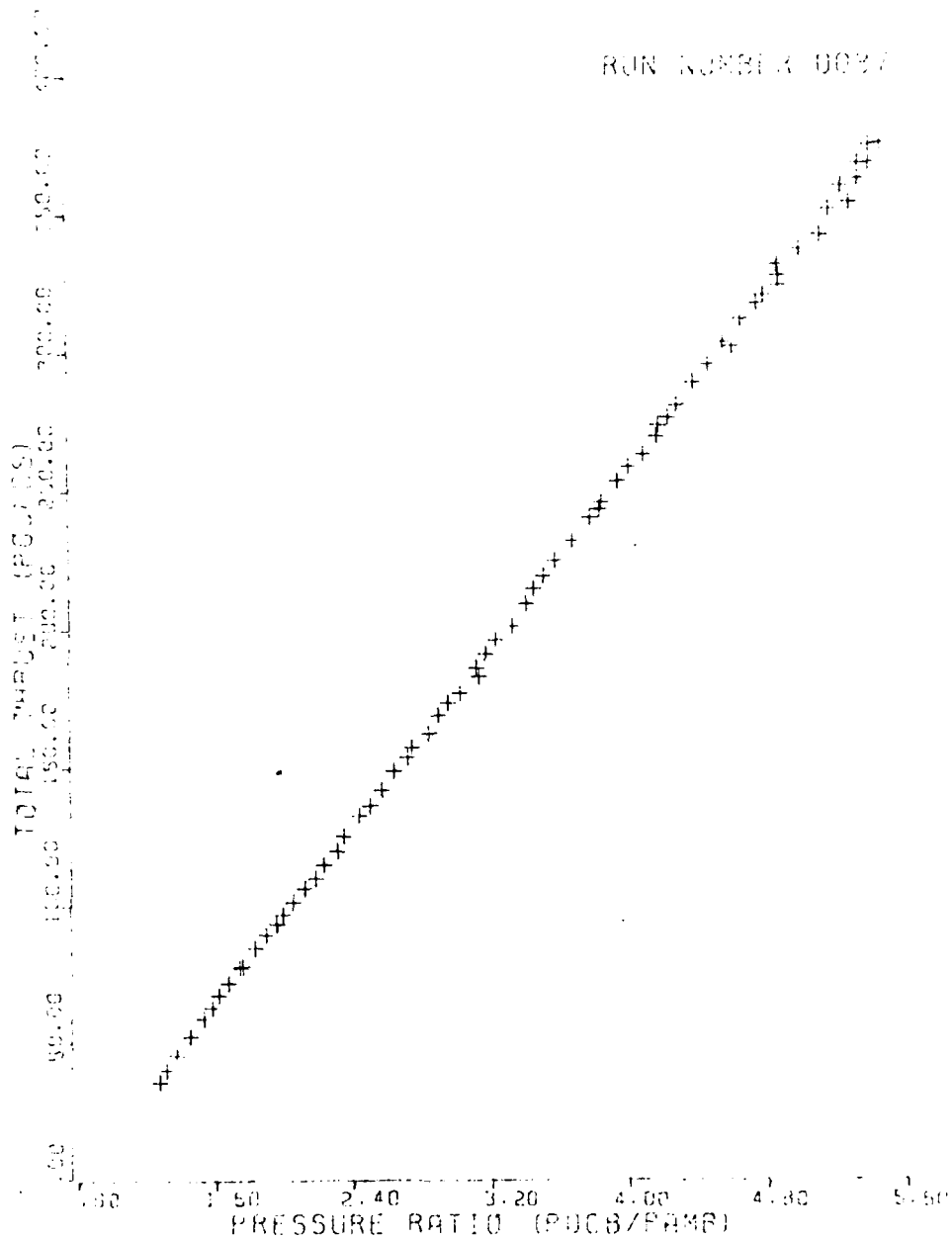

Figure B-1 L/W = 11.0

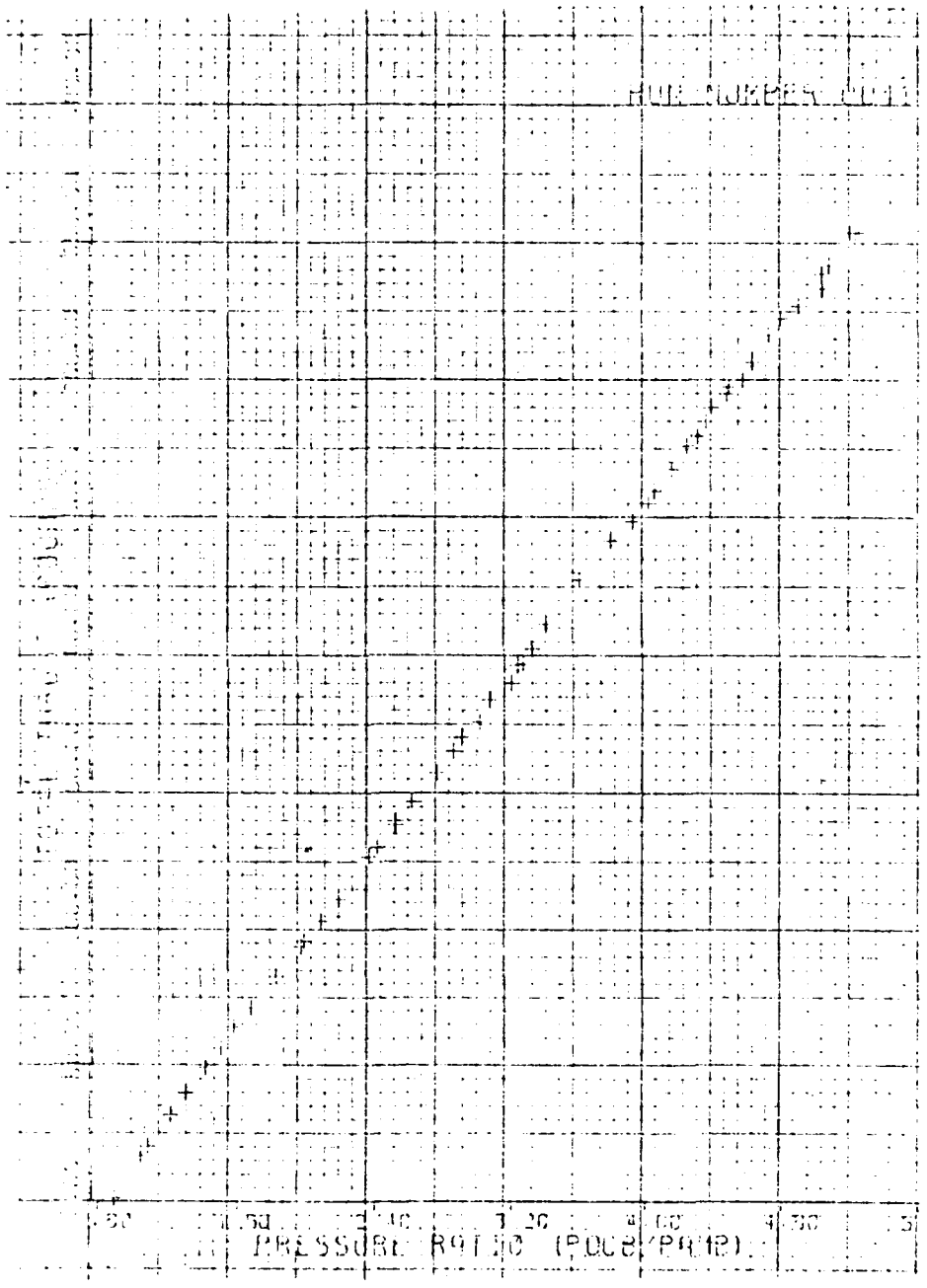

Figure B-2 L/W = 9.5

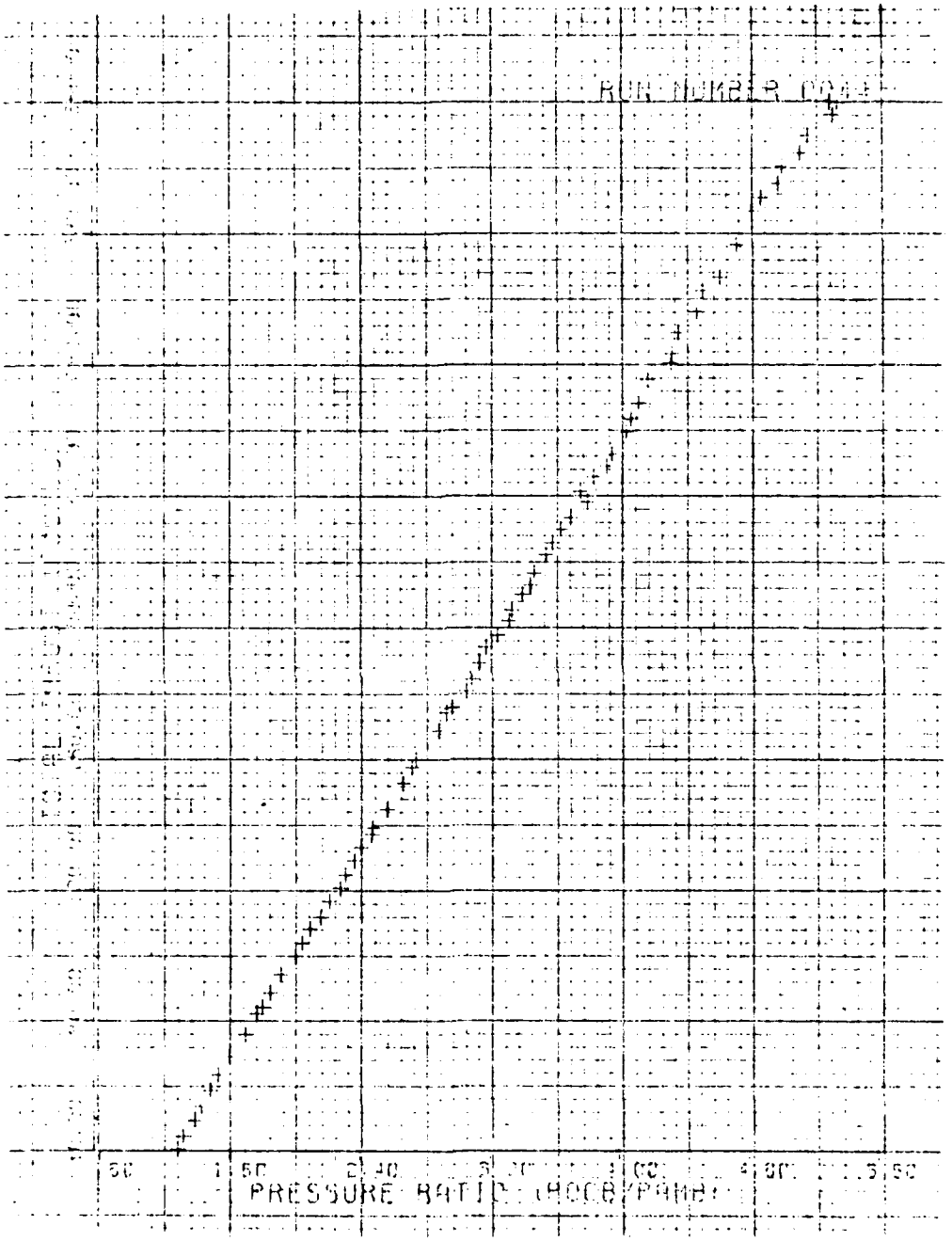

Figure B-3 L/W = 8.0

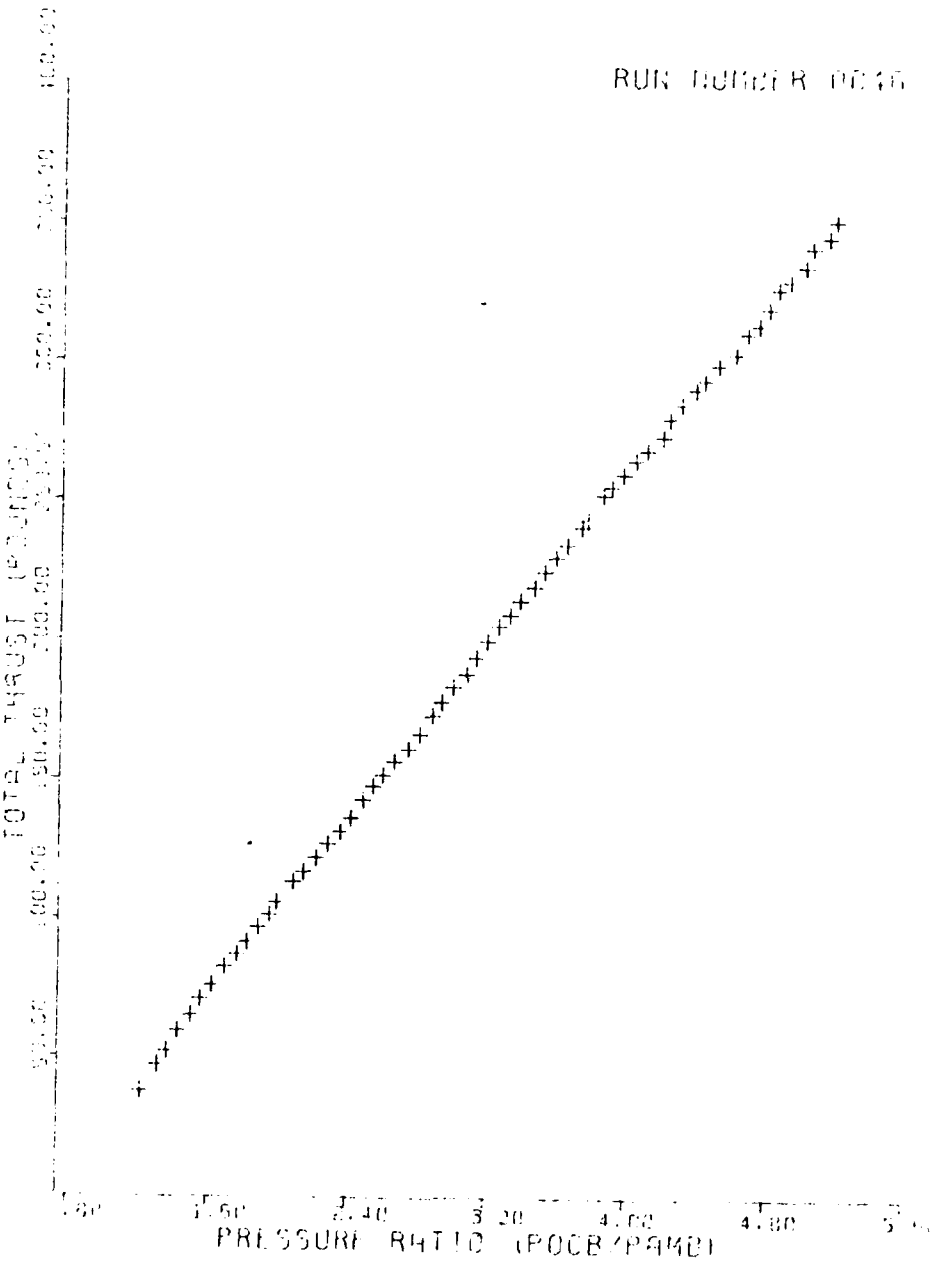

Figure B-4 L/W = 6.5

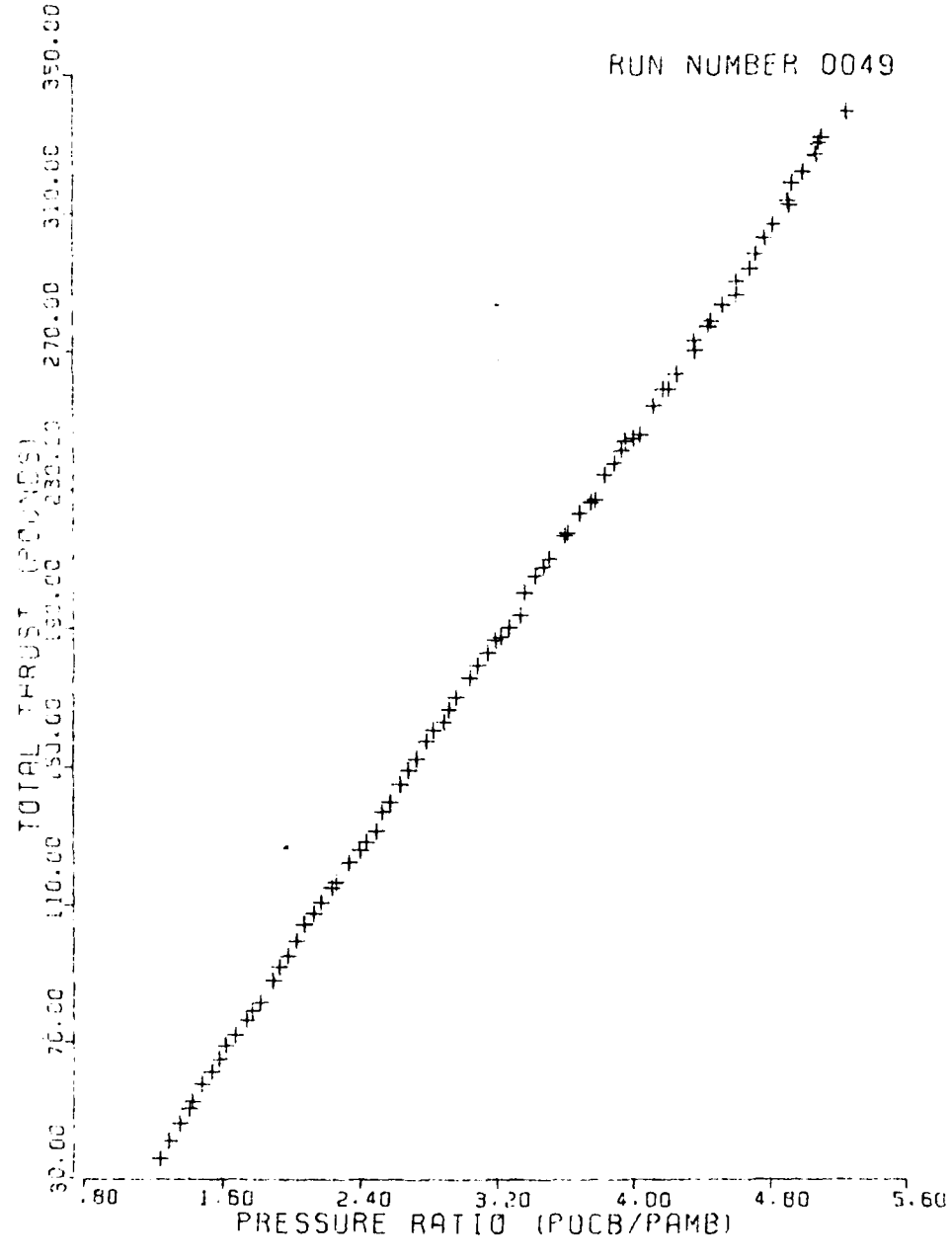

Figure B-5 L/W = 5.0

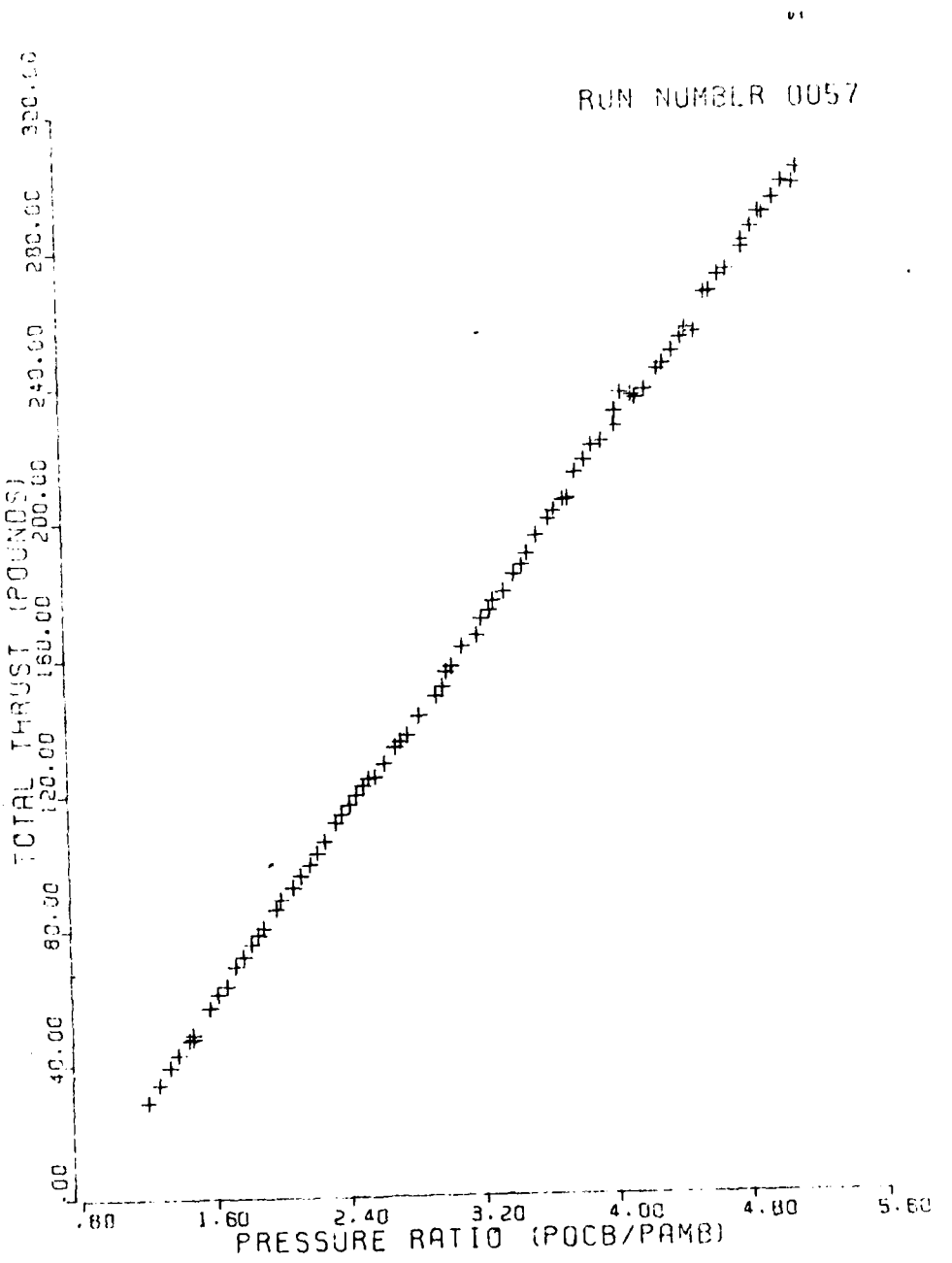

Figure B-6 L/W = 3.5

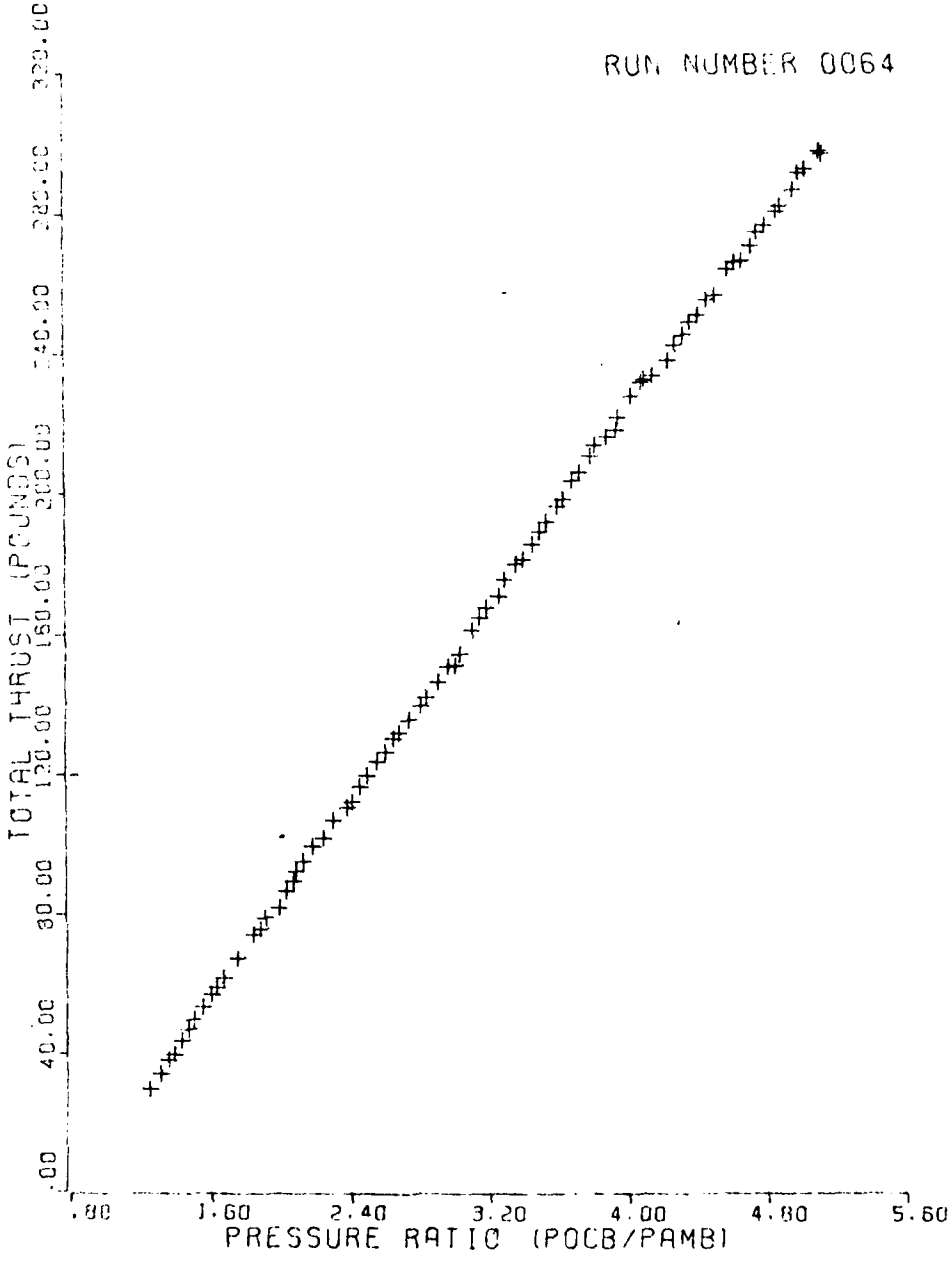

Figure B-7 L/W = 3.5

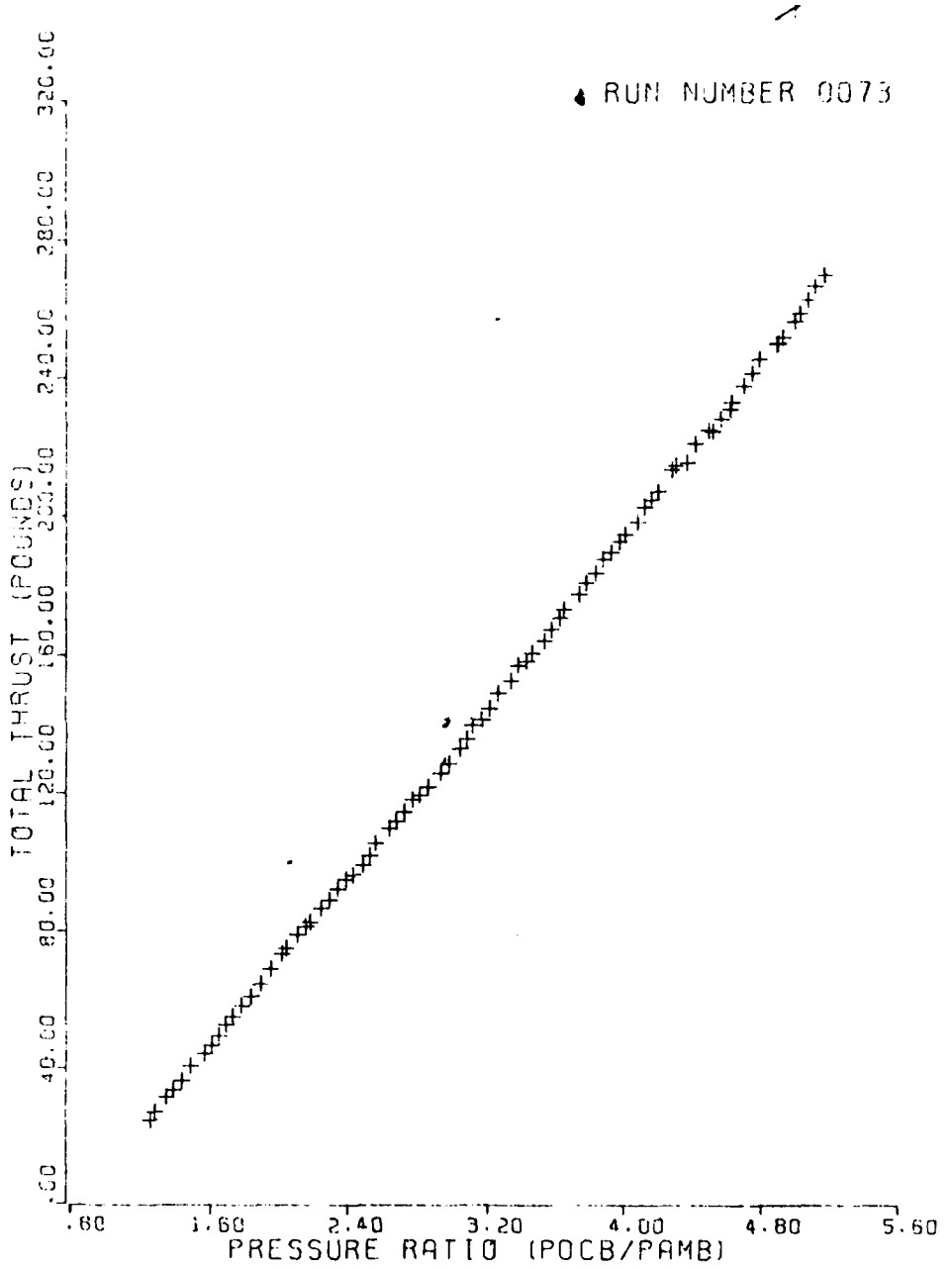

Figure B-8 L/W = 2.0

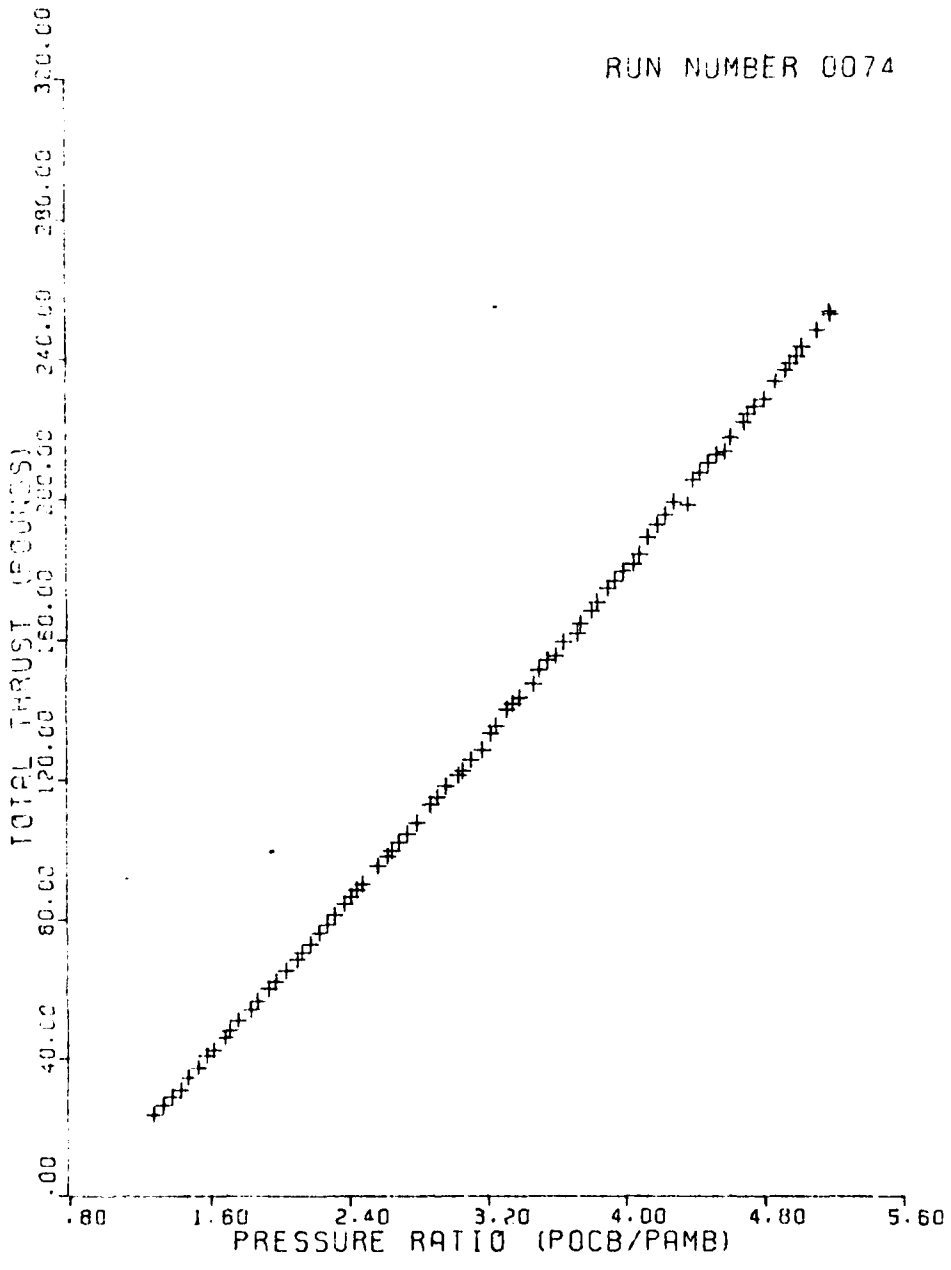

Figure B-9 L/W = 0.2

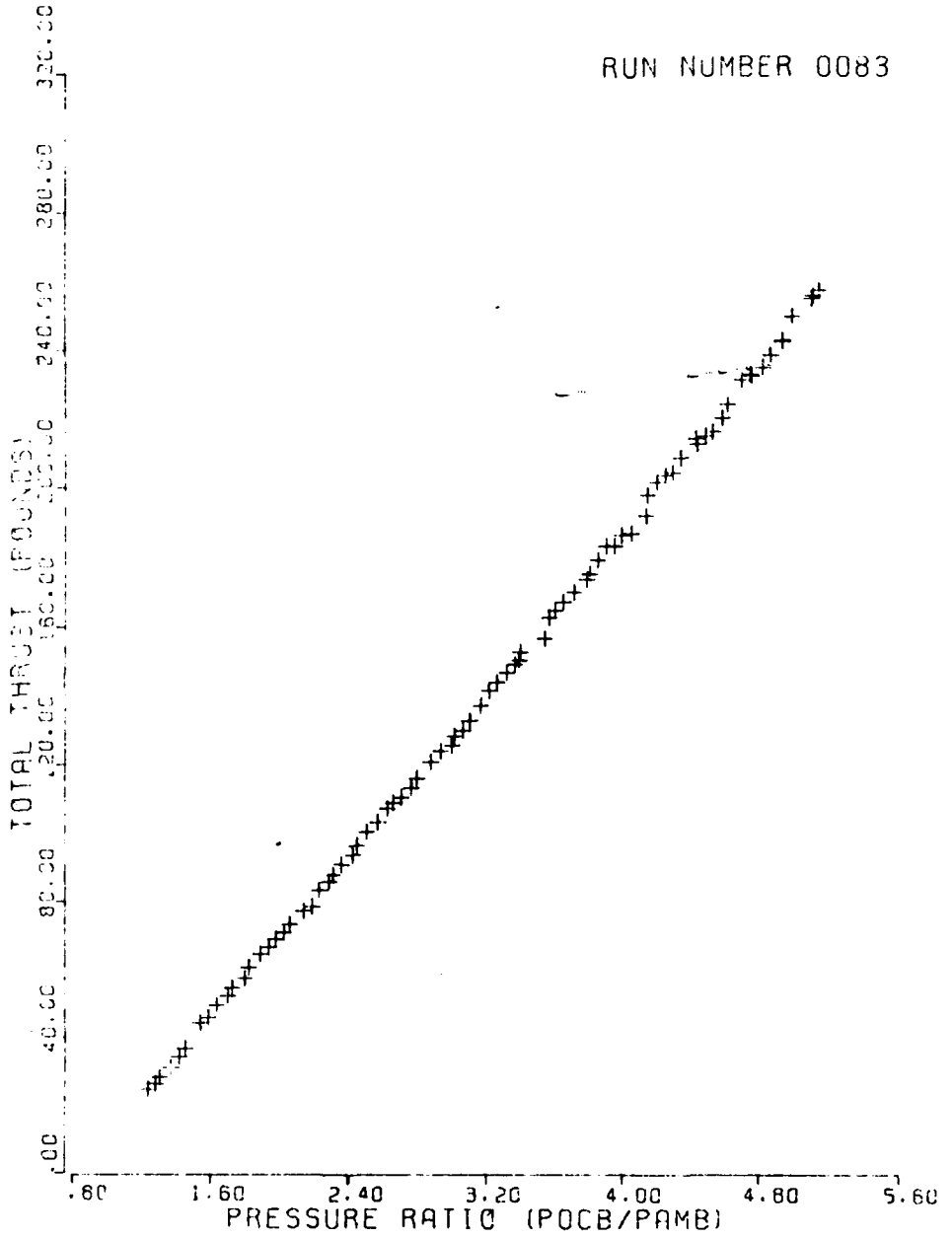

Figure B-1C L/W = 0.9

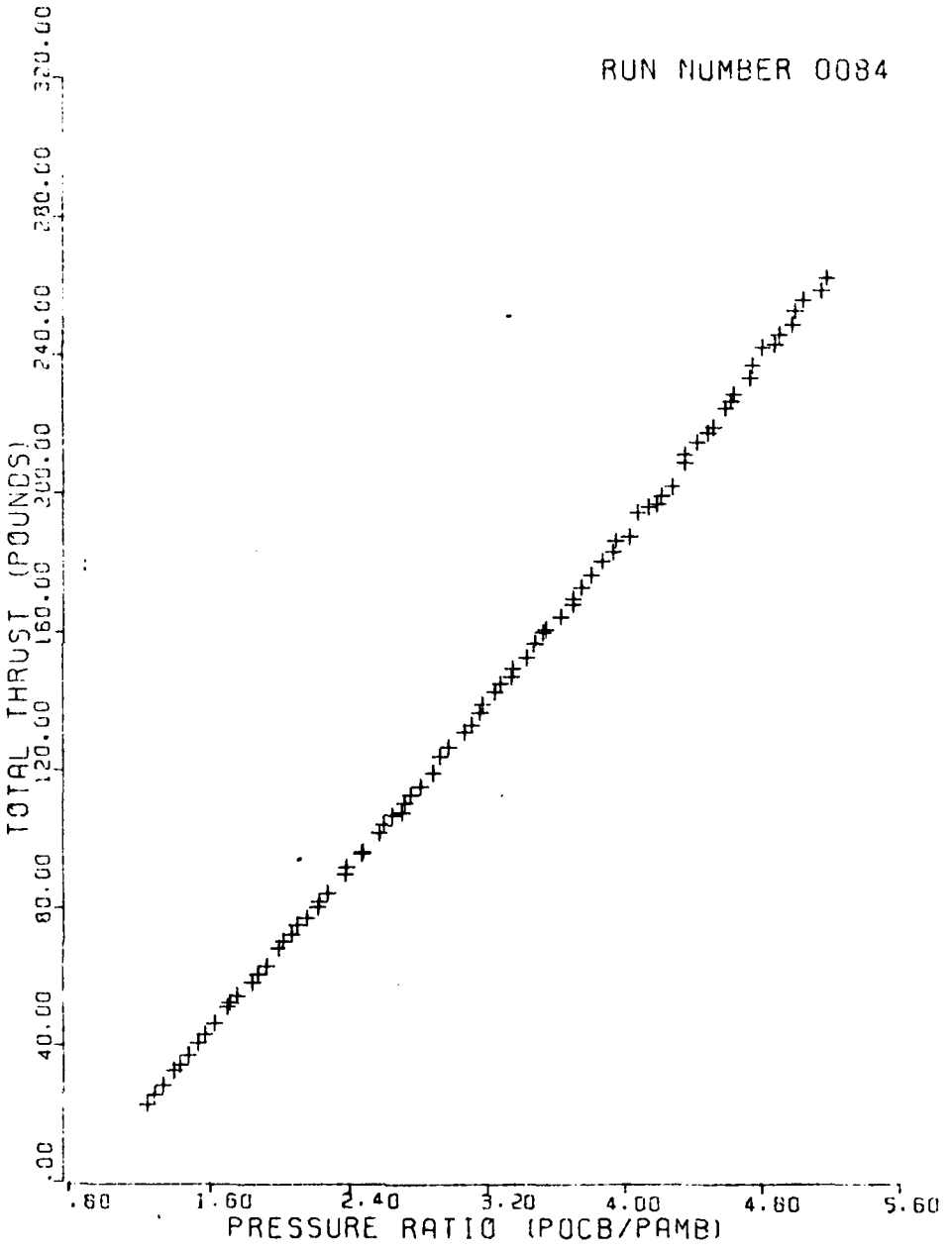

Figure B-11 Centerbody Only

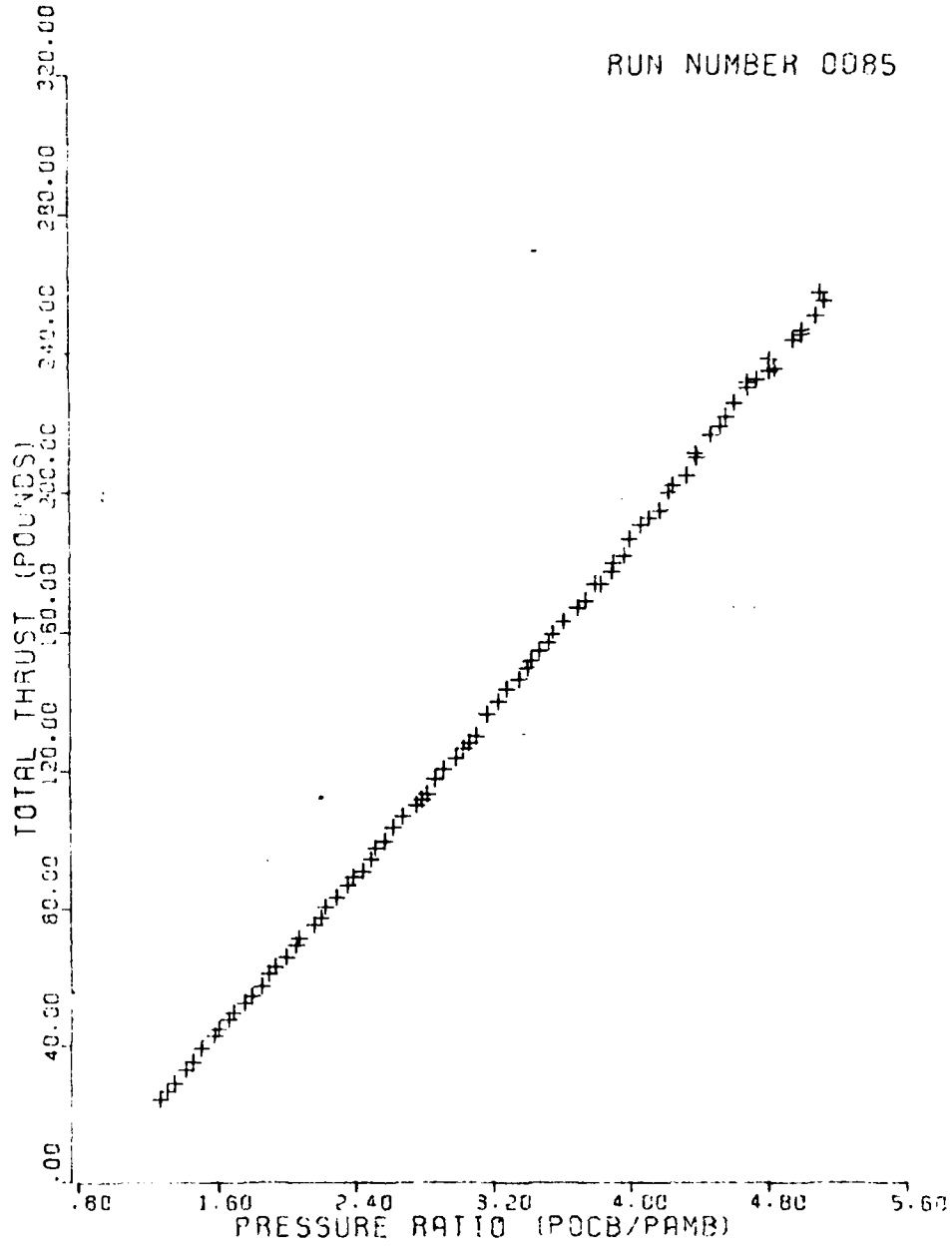

Figure B-12 **Centerbody Only - Added Insulation**

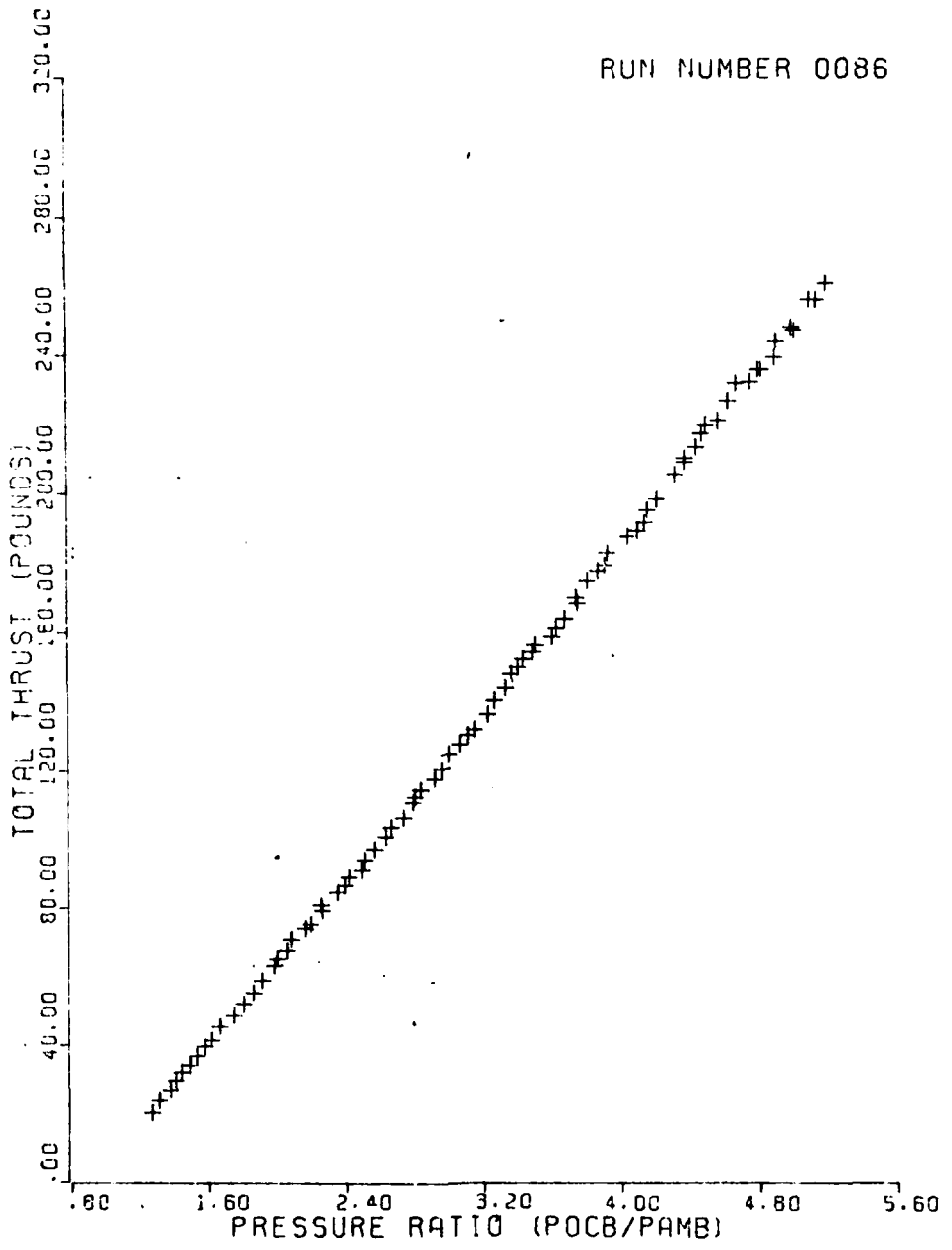

Figure B-13 Centerbody Only/Added Insulation/New Microphone Location

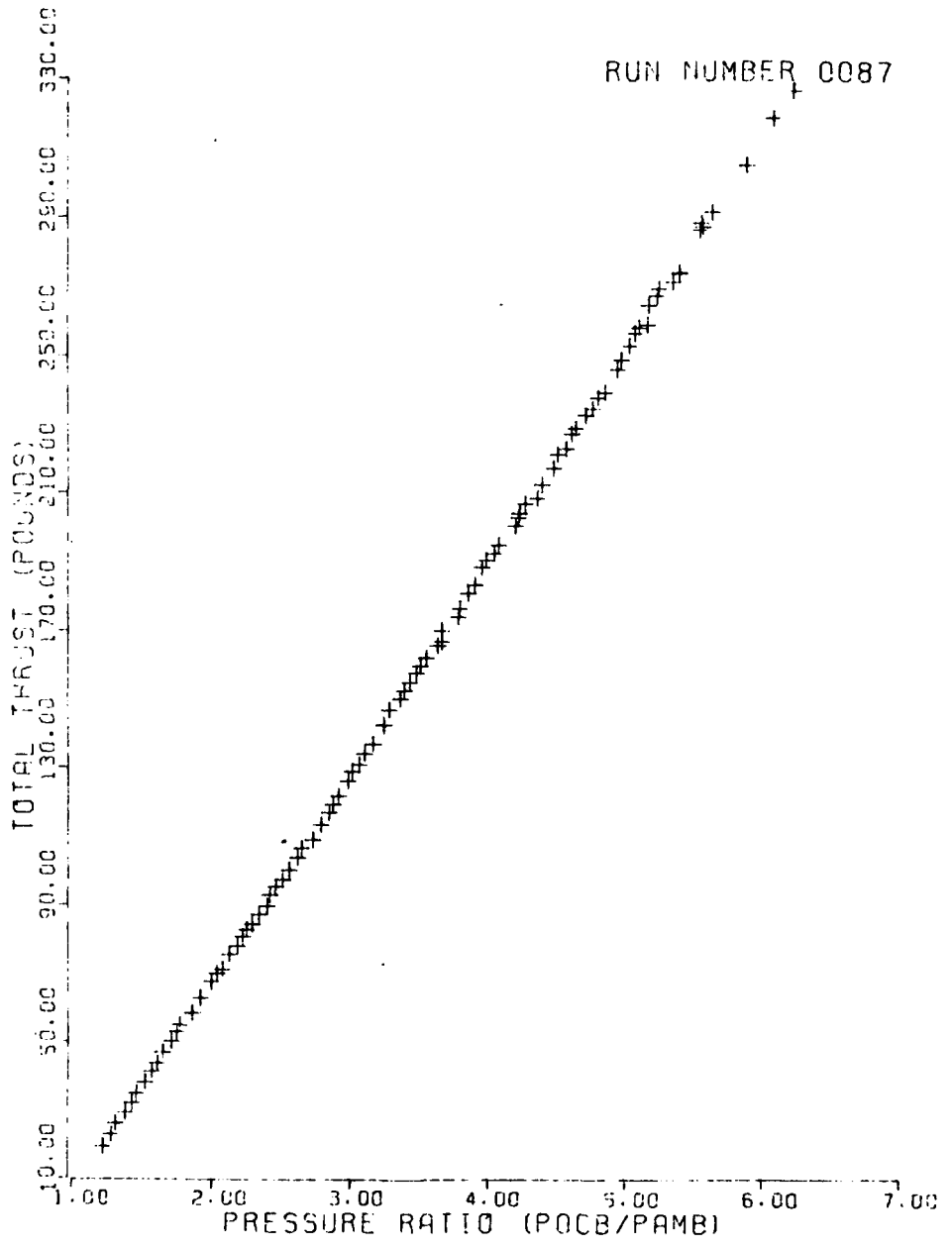

Figure B-14 Run No. 86 Repeated Increasing Pressure Ratio to Approximately 6.3

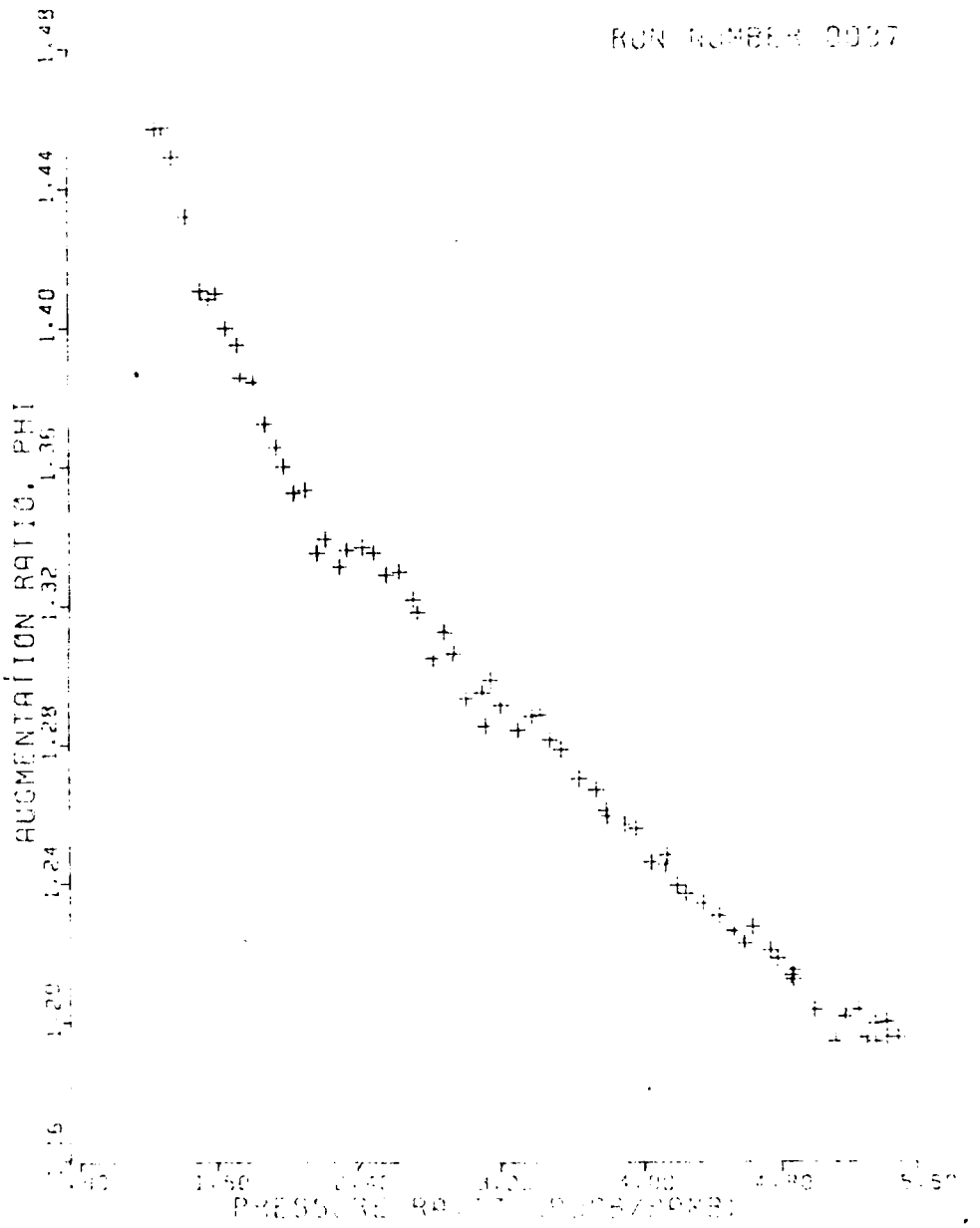

Figure B-15 L/W = 11.0

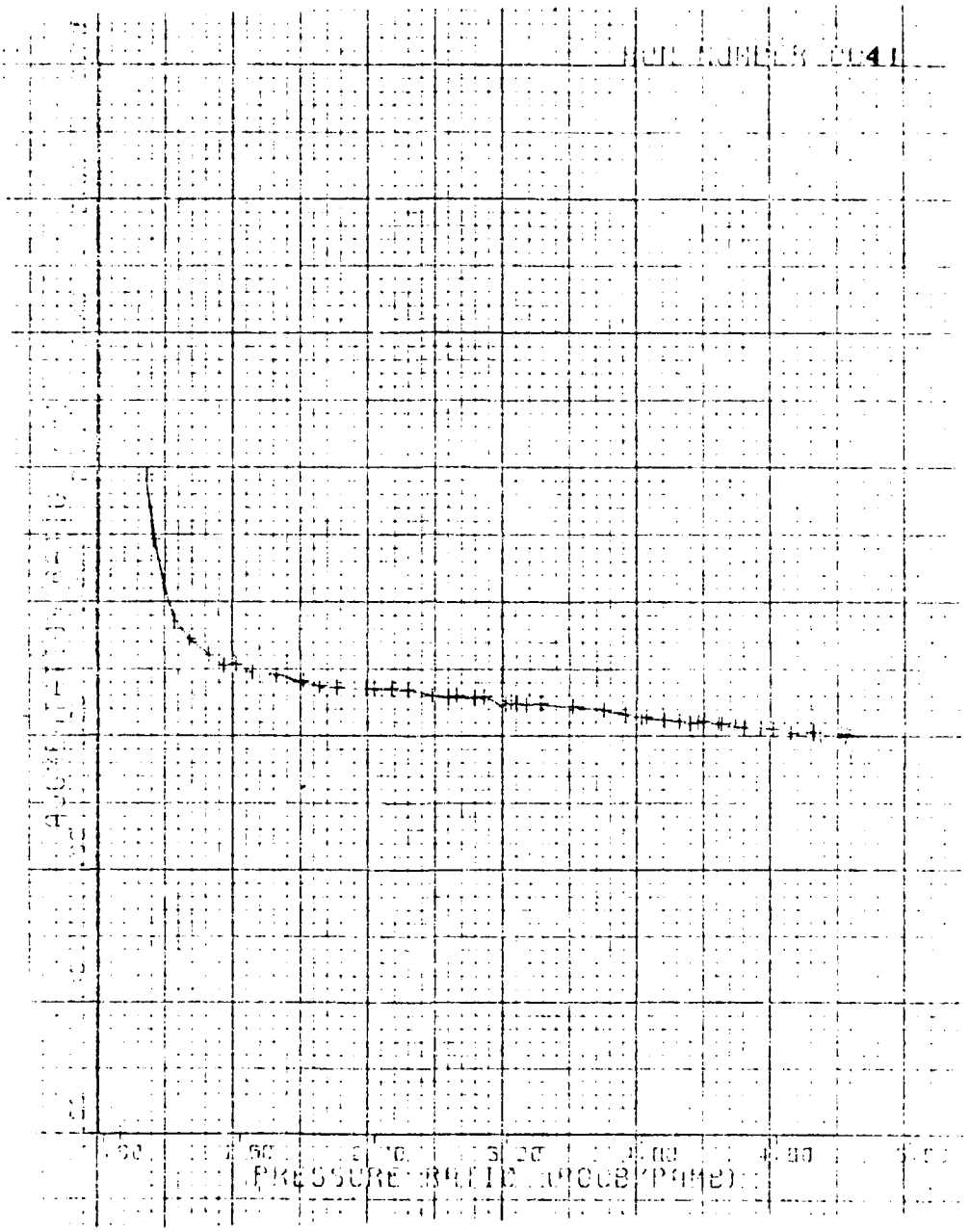

Figure B-16 L/W = 9.5

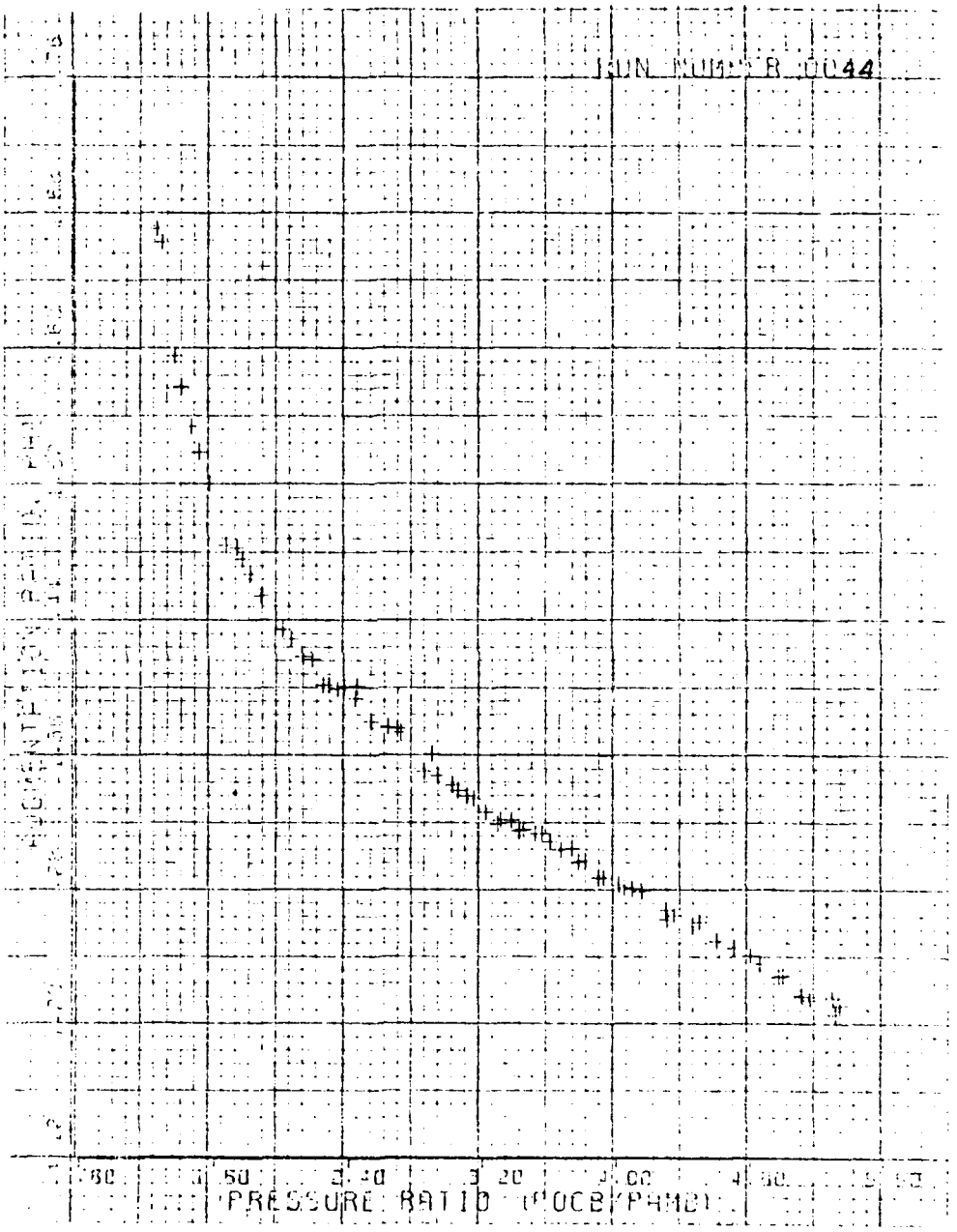

Figure B-17 L/W = 8.0

AD-A106 083 ROCKWELL INTERNATIONAL COLUMBUS OH NORTH AMERICAN AI--ETC F/G 20/1
INVESTIGATION OF ACOUSTIC INTERACTIONS IN JET THRUST AUGMENTING--ETC(U)
MAR 81 J R CAMPBELL, K D KORKAN, H VIETS N00019-79-C-0225
UNCLASSIFIED NR80H-50 NL

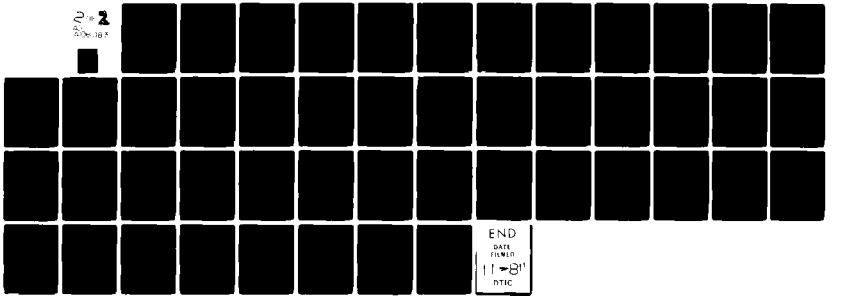

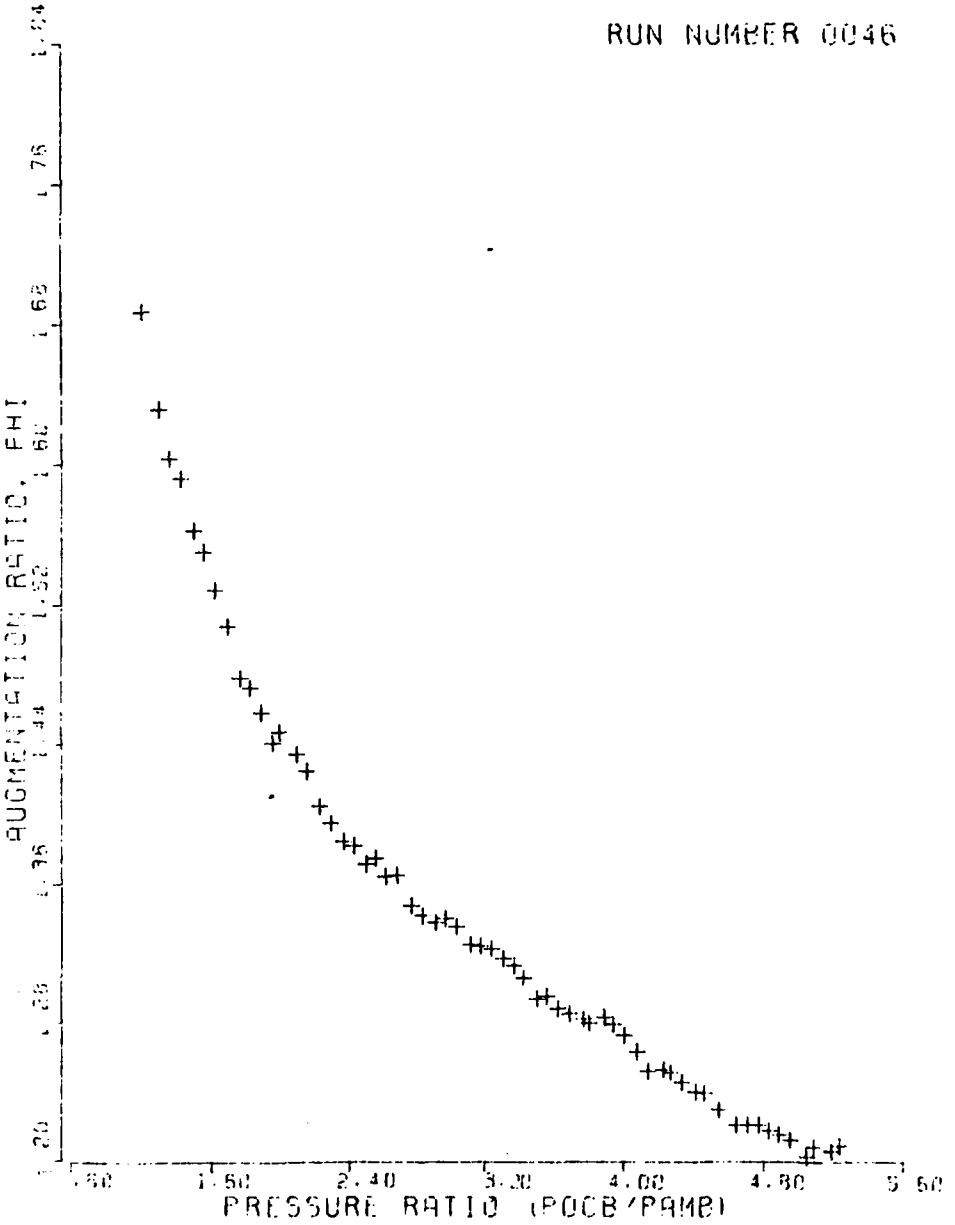

Figure B-18 L/W = 6.5

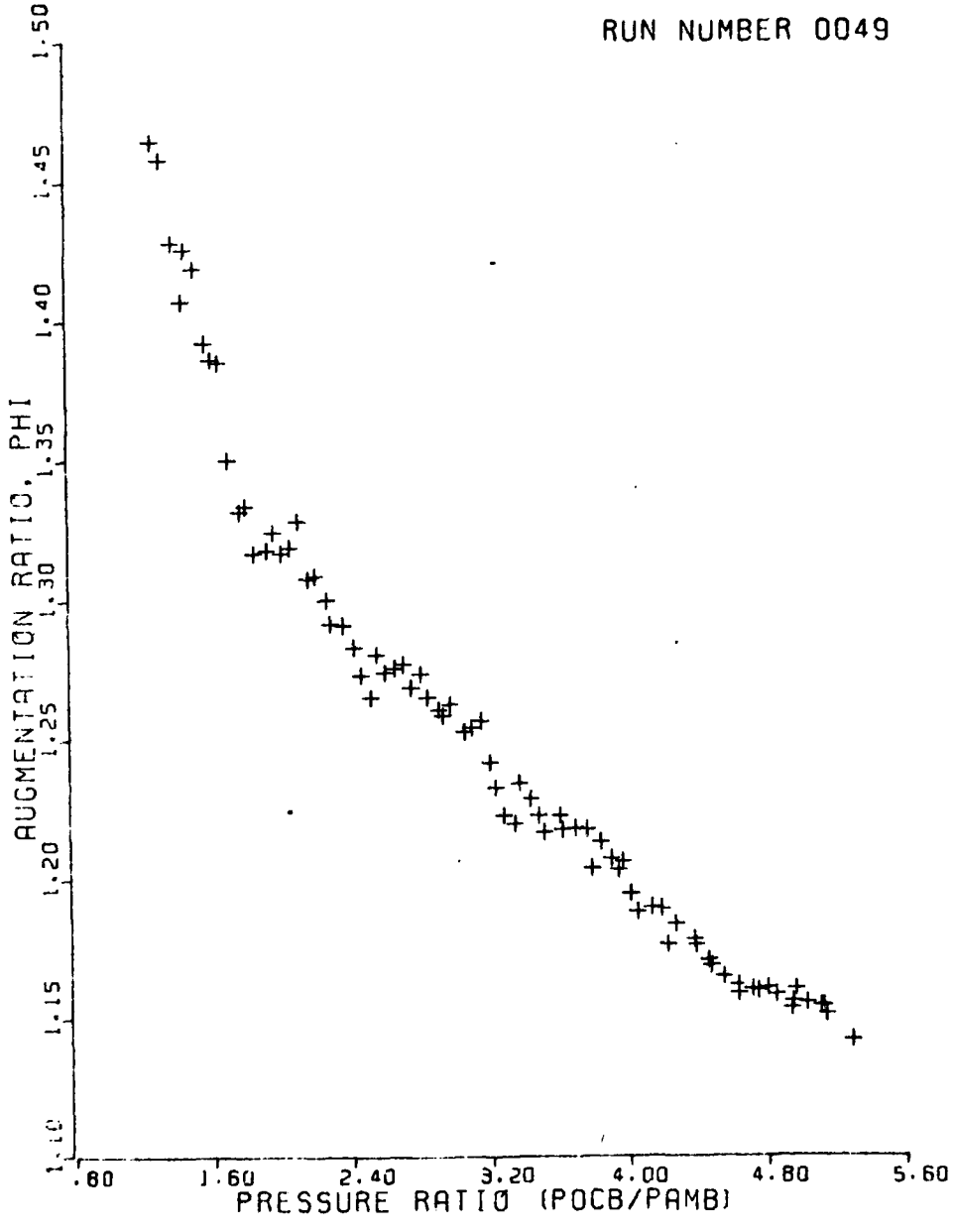

Figure B-19 L/W = 5.0

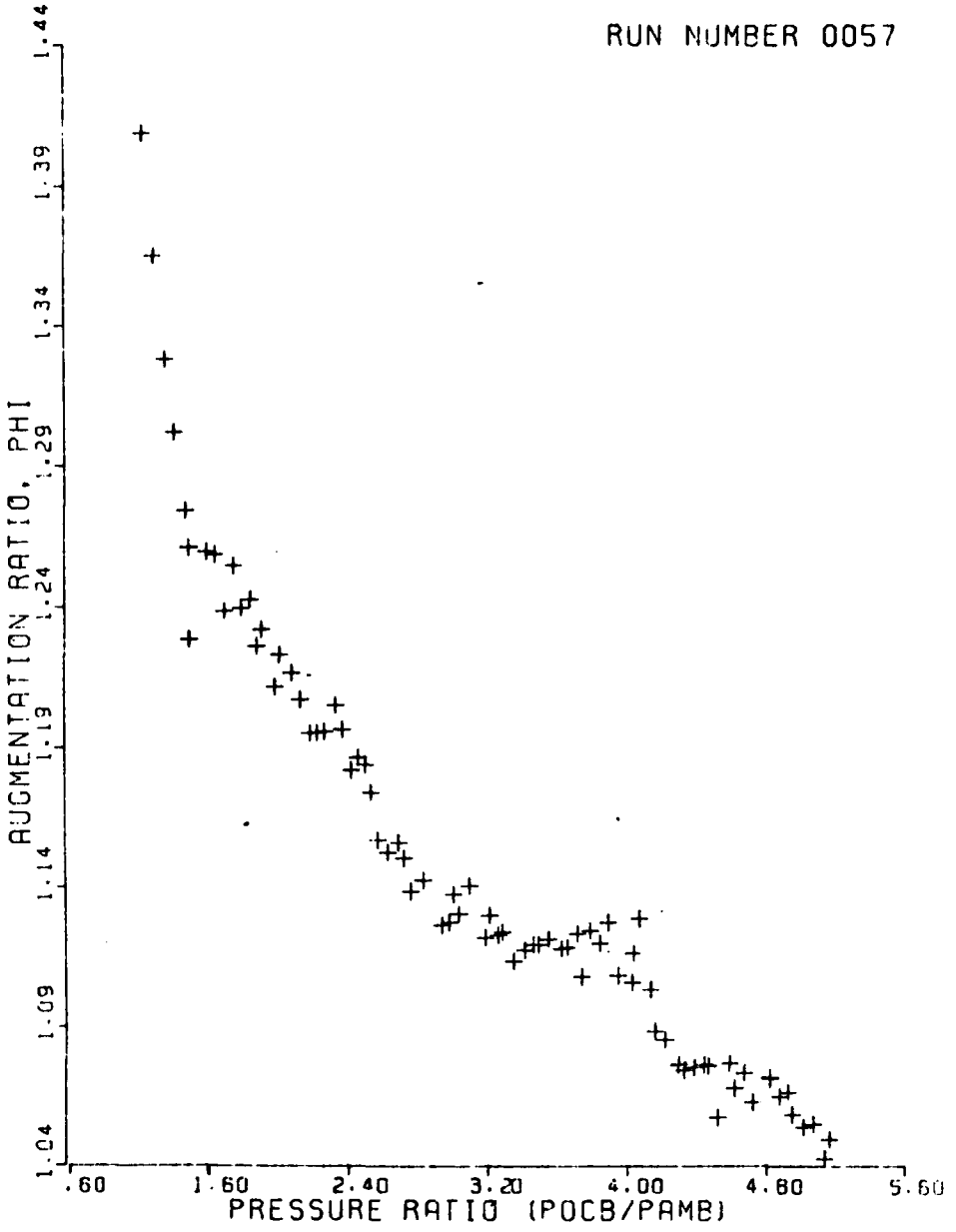

Figure B-20 L/W = 3.5

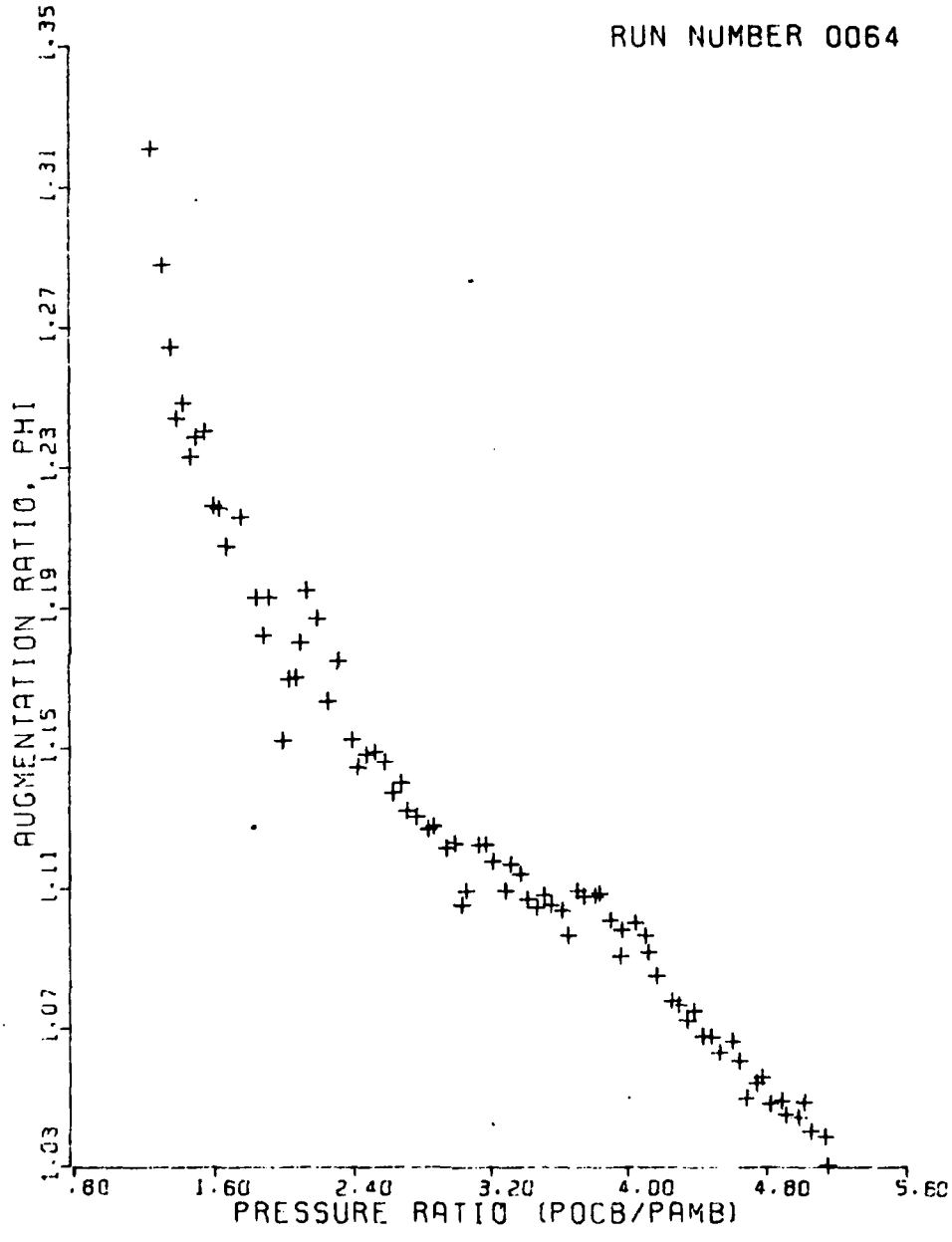

Figure B-21 L/W = 3.5 Repeated Test

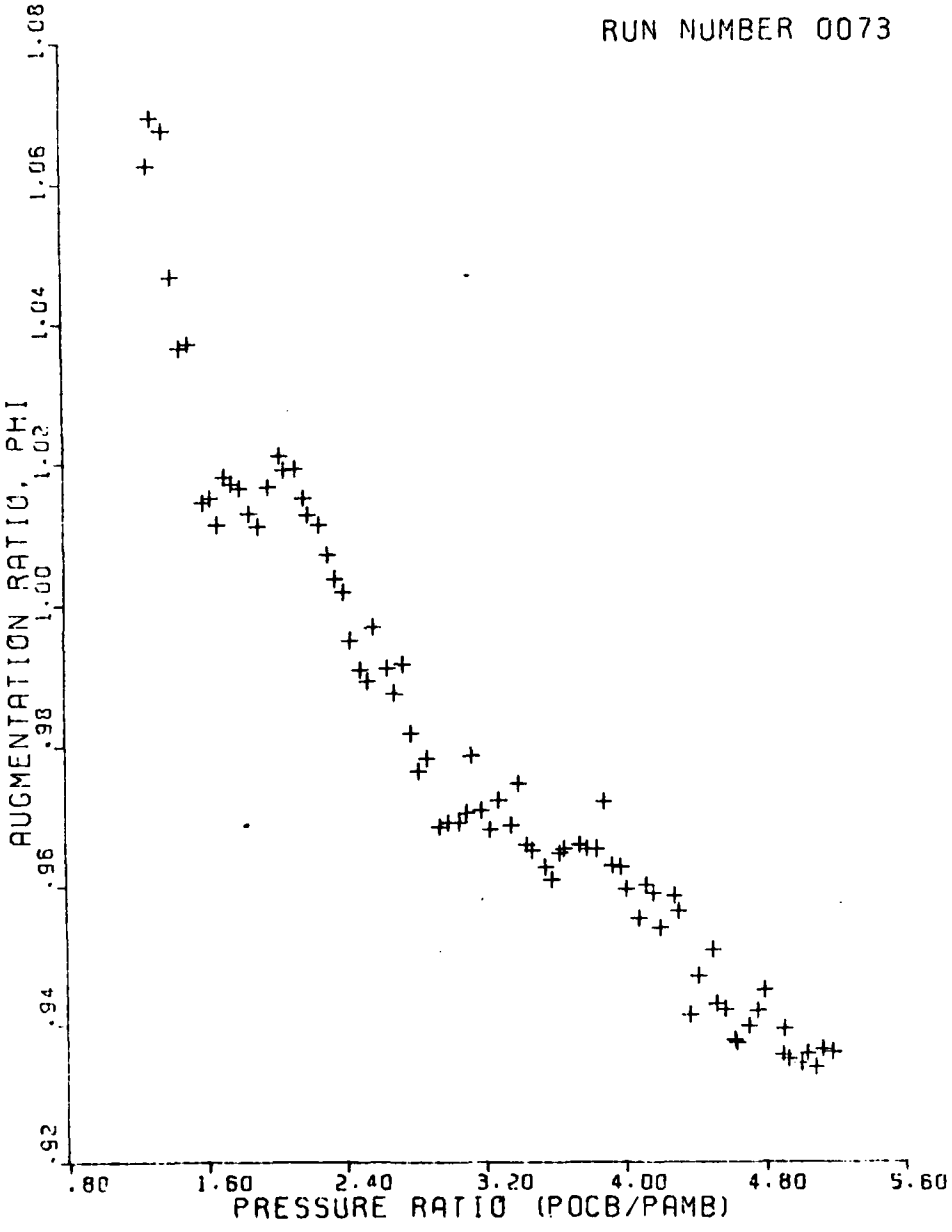

Figure B-22 L/W = 2.0

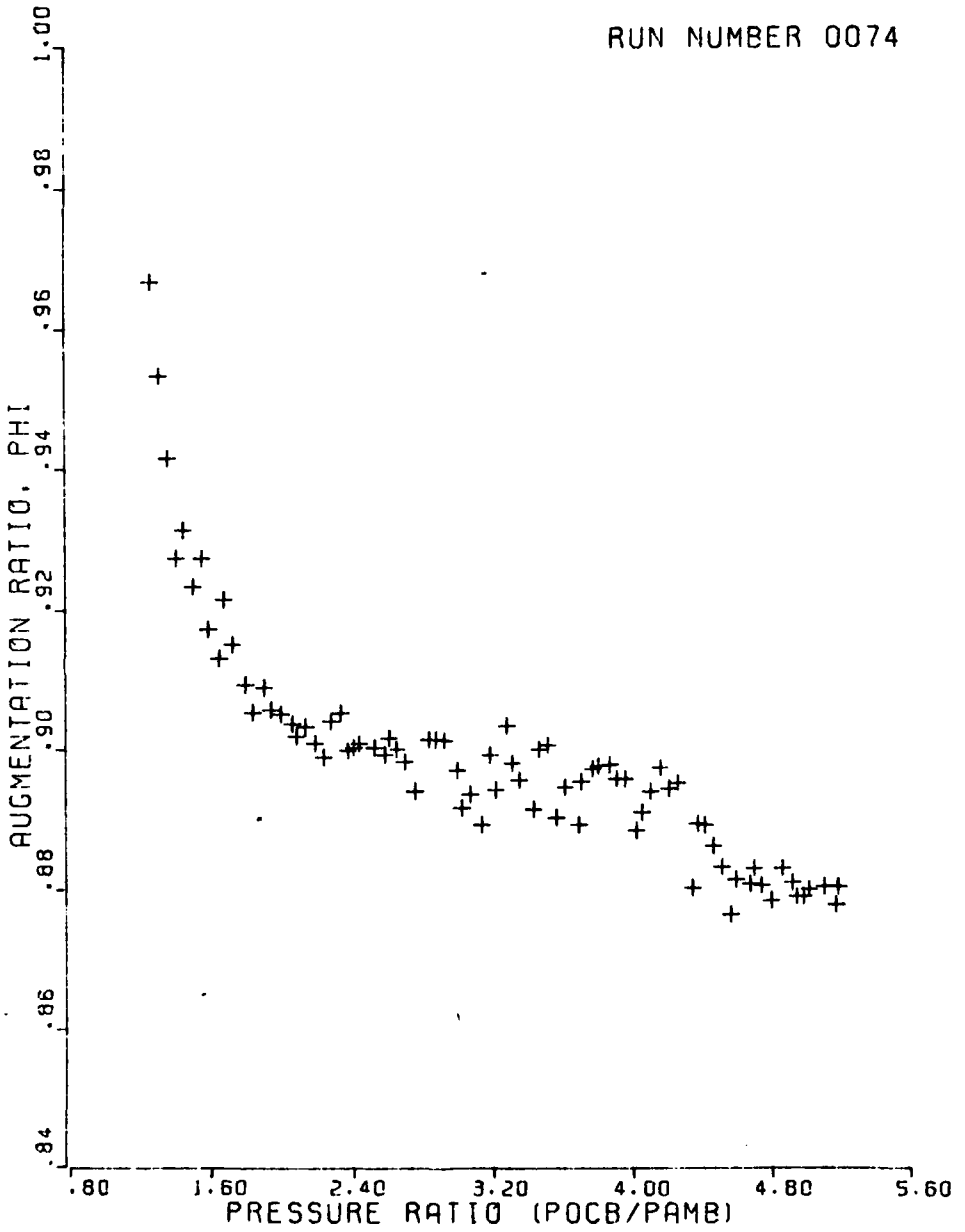

Figure B-23 L/W = 0.2

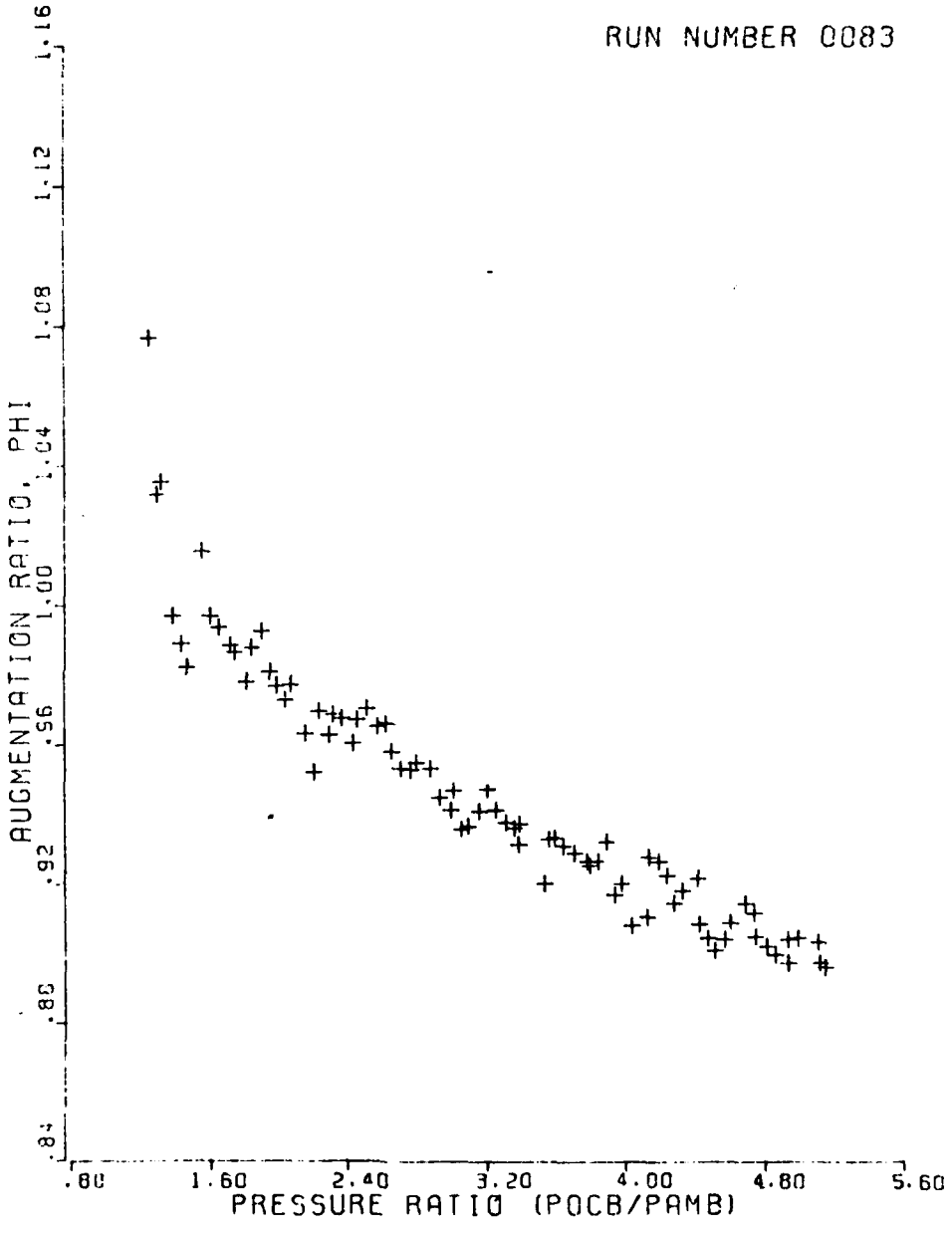

Figure B-24 L/W = 0.9

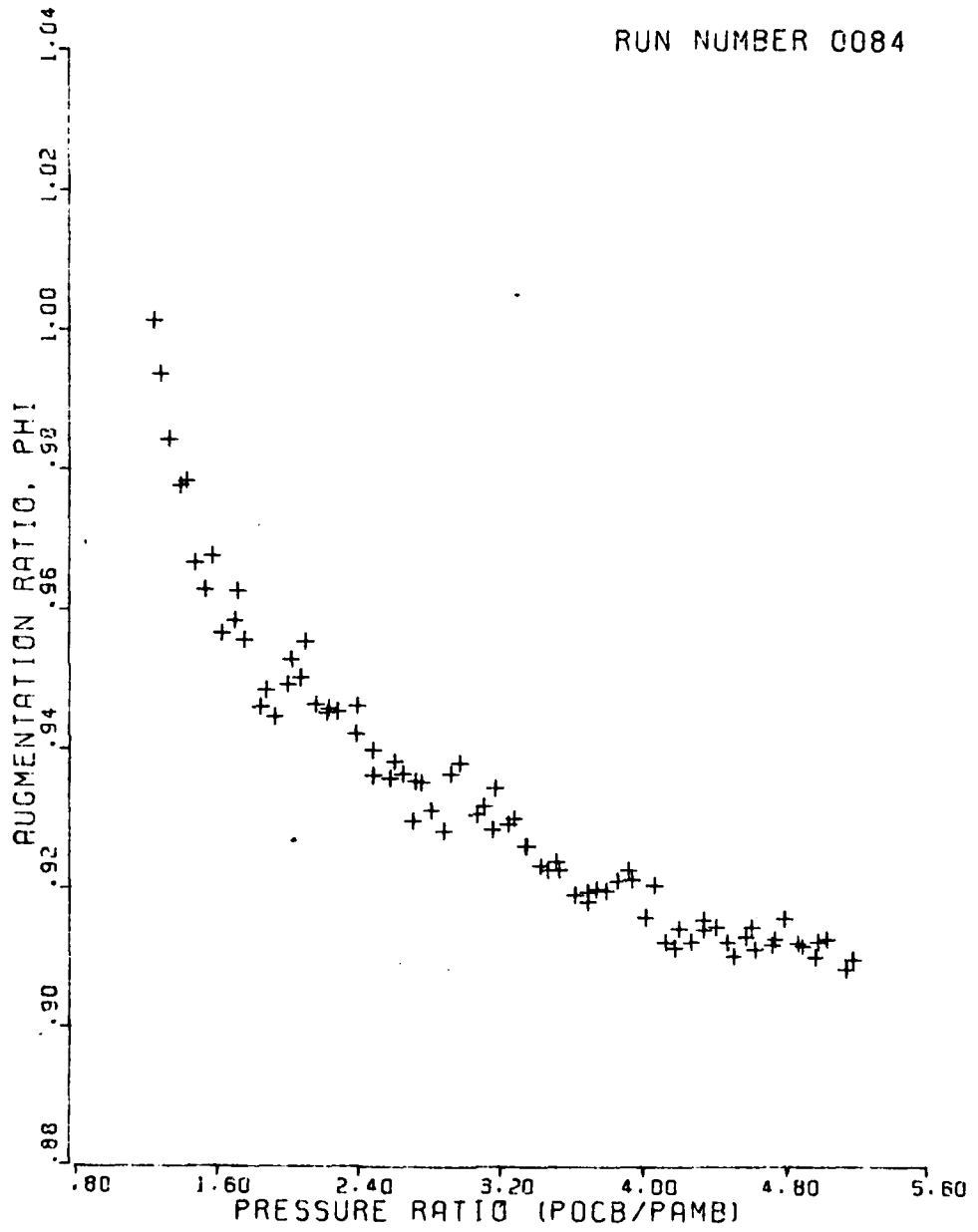

Figure B-25 Centerbody Only

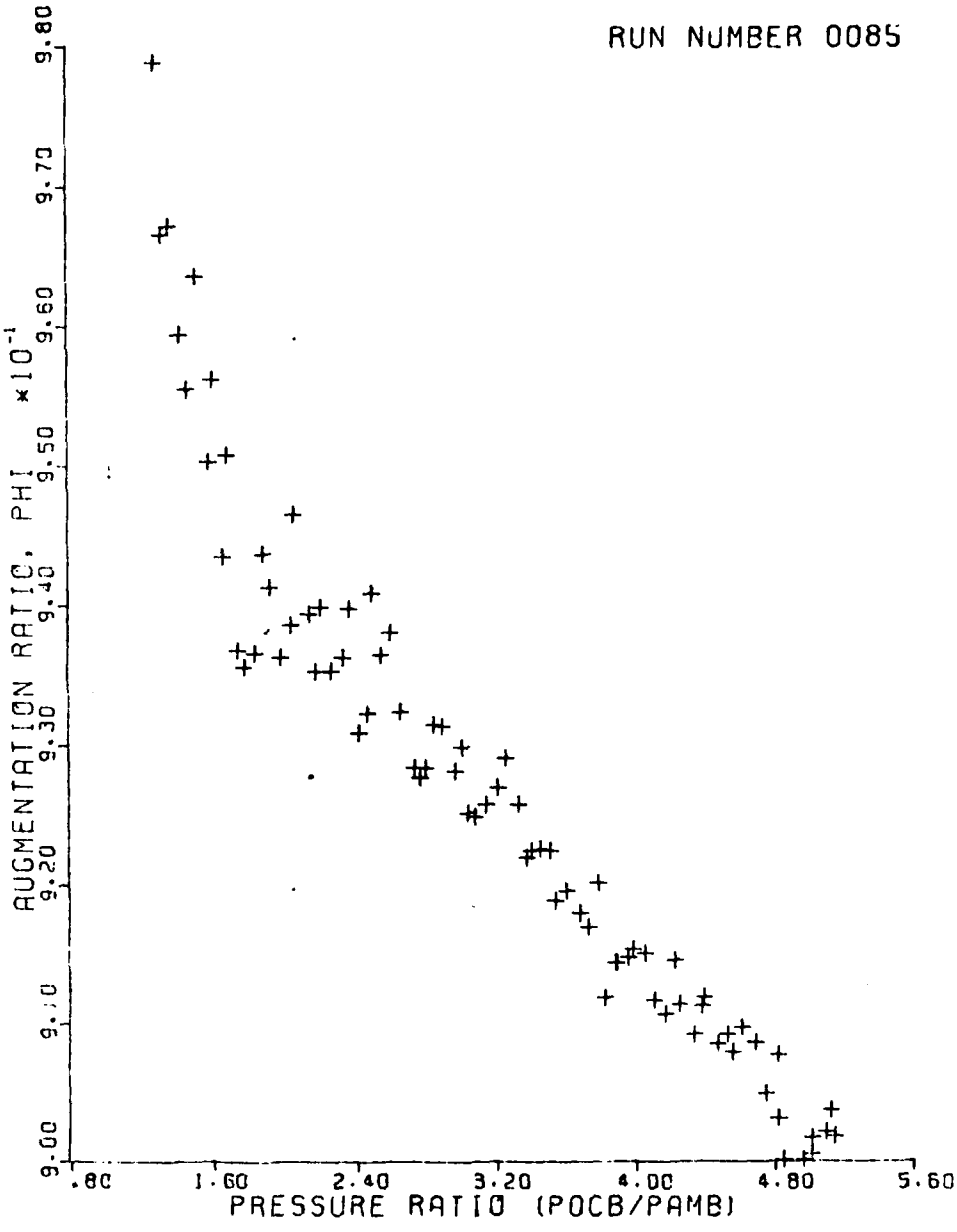

Figure B-26 Centerbody Only - Added Insulation

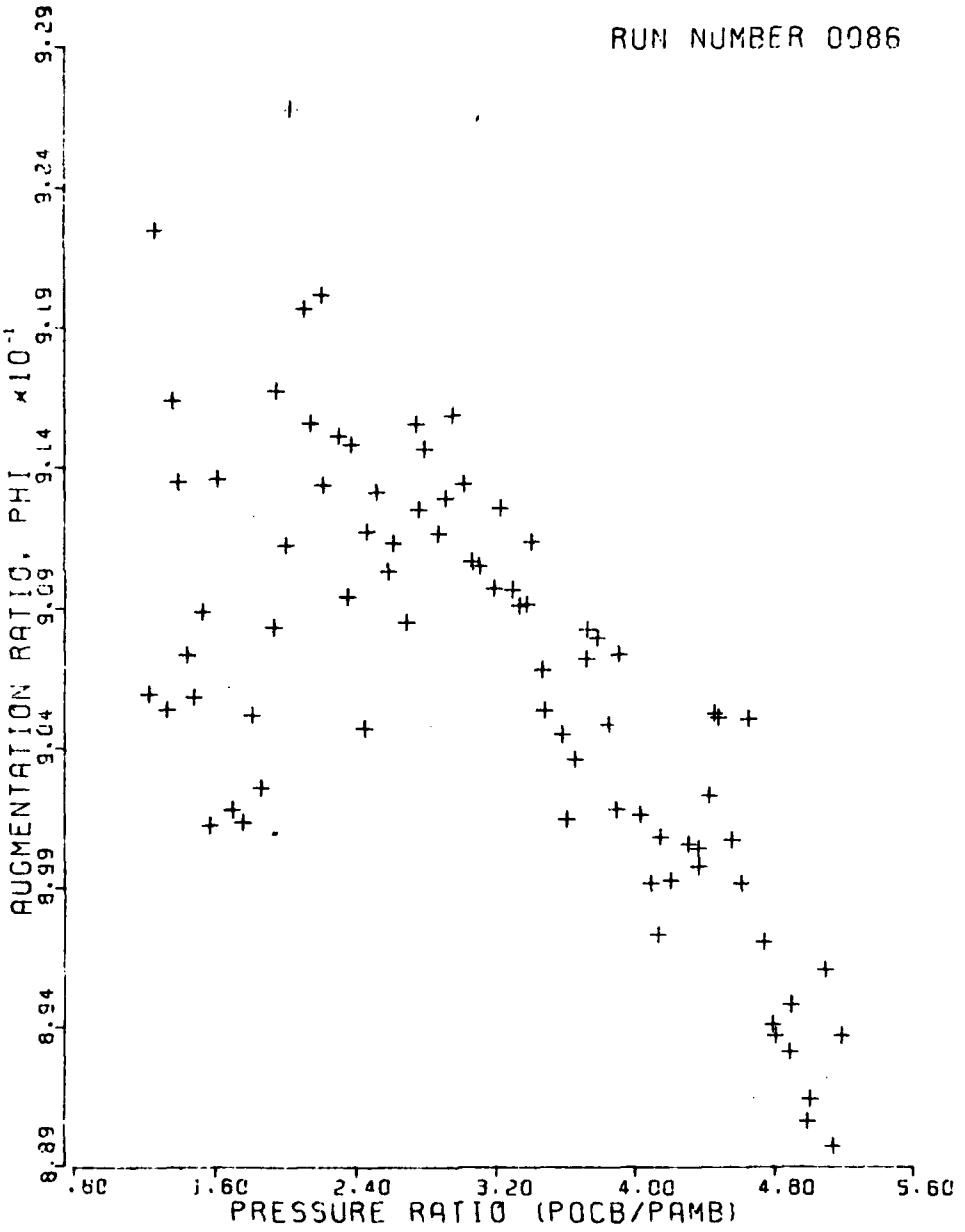

Figure B-27 Centerbody Only/Added Insulation/New Microphone Location

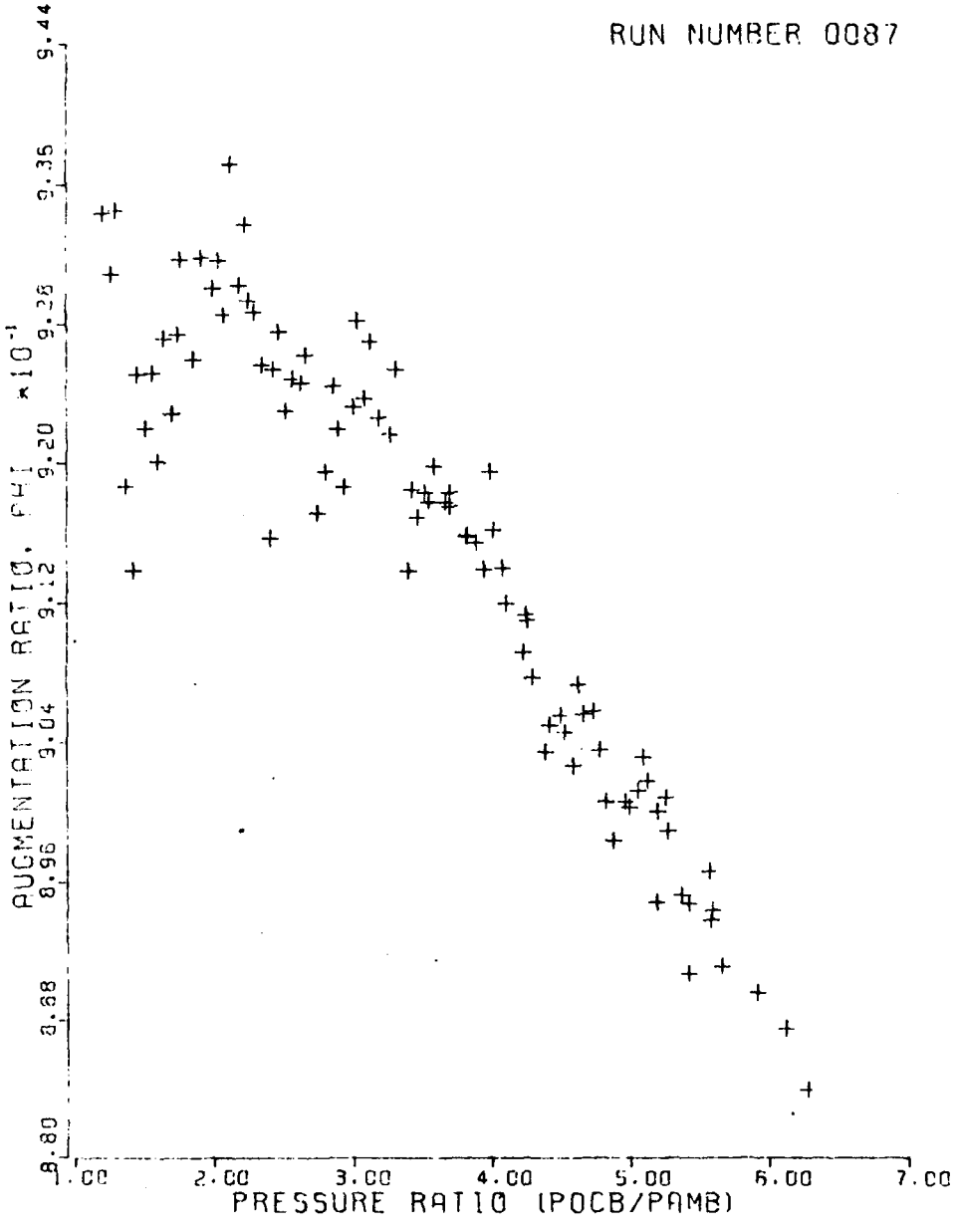

Figure B-28 **Centerbody/Added Insulation/New Microphone Location Nozzle Pressure Ratio Increased to Approximately 6.3**

APPENDIX C

CENTERBODY PLUS COANDA'S BLOWING - THRUST/Ø/FREQUENCY DATA

APPENDIX C

This appendix contains the centerbody plus Coandas blowing actual recorded and reduced "frequency of maximum power (amplitude)" and "thrust" versus "centerbody nozzle pressure ratio" data. The thrust data is provided by Figures C-1 through C-11. The frequency data is provided by Figures C-12 through C-22. The calculated "augmentation ratio (Ø)" versus "centerbody nozzle pressure ratio" data is also included in Figures C-23 through C-33.

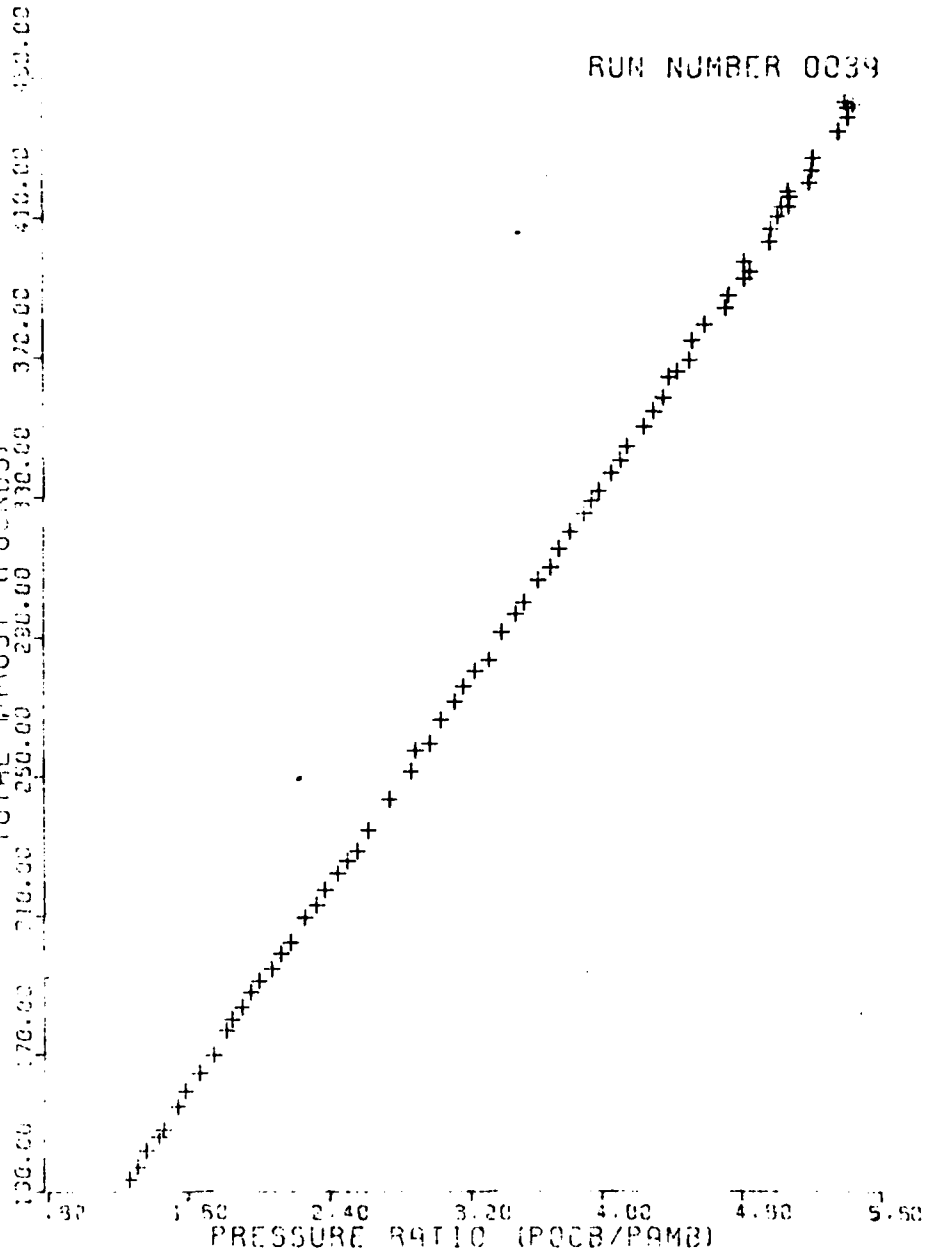

Figure C-1 L/W = 11.0

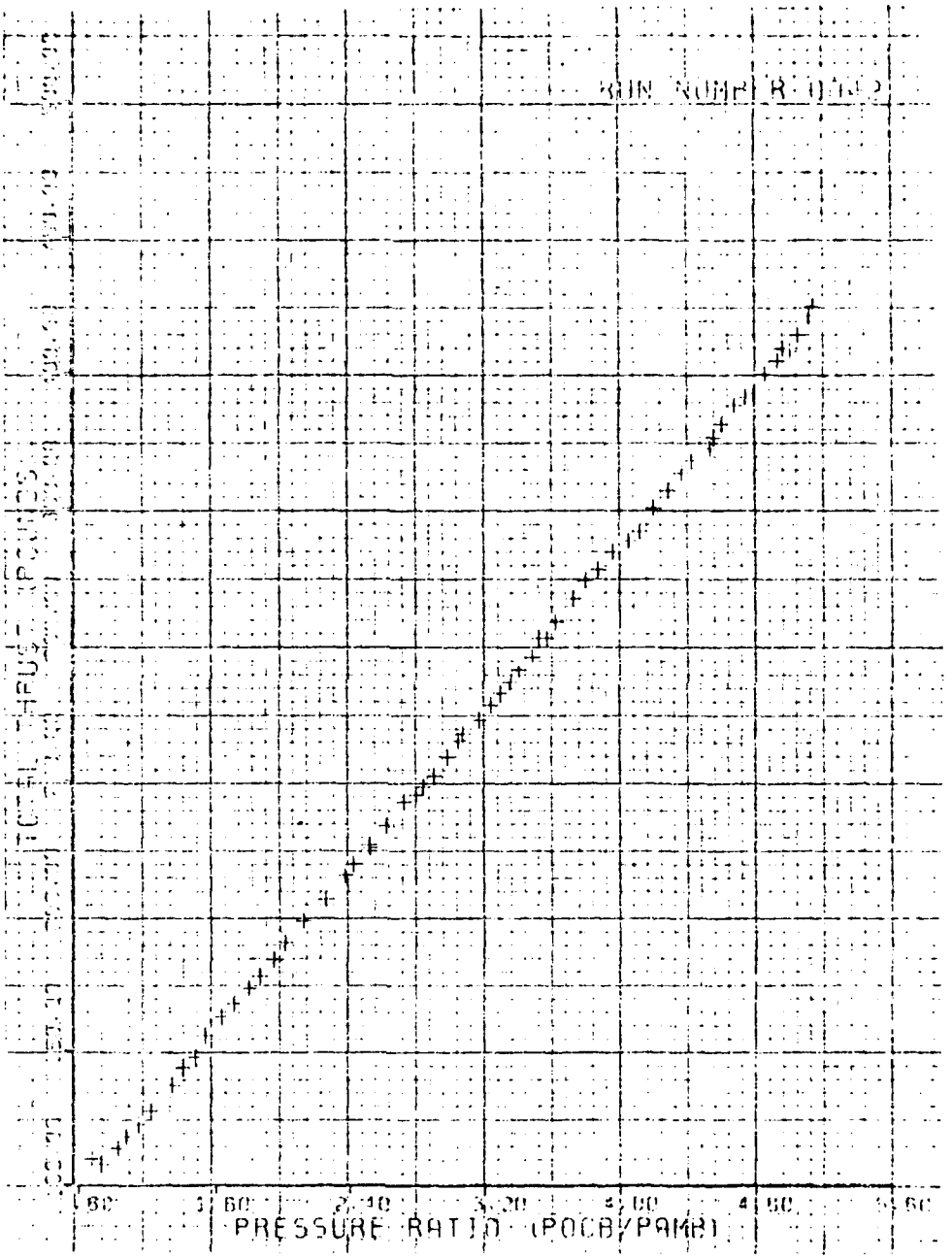

Figure C-2. L/W = 9.5

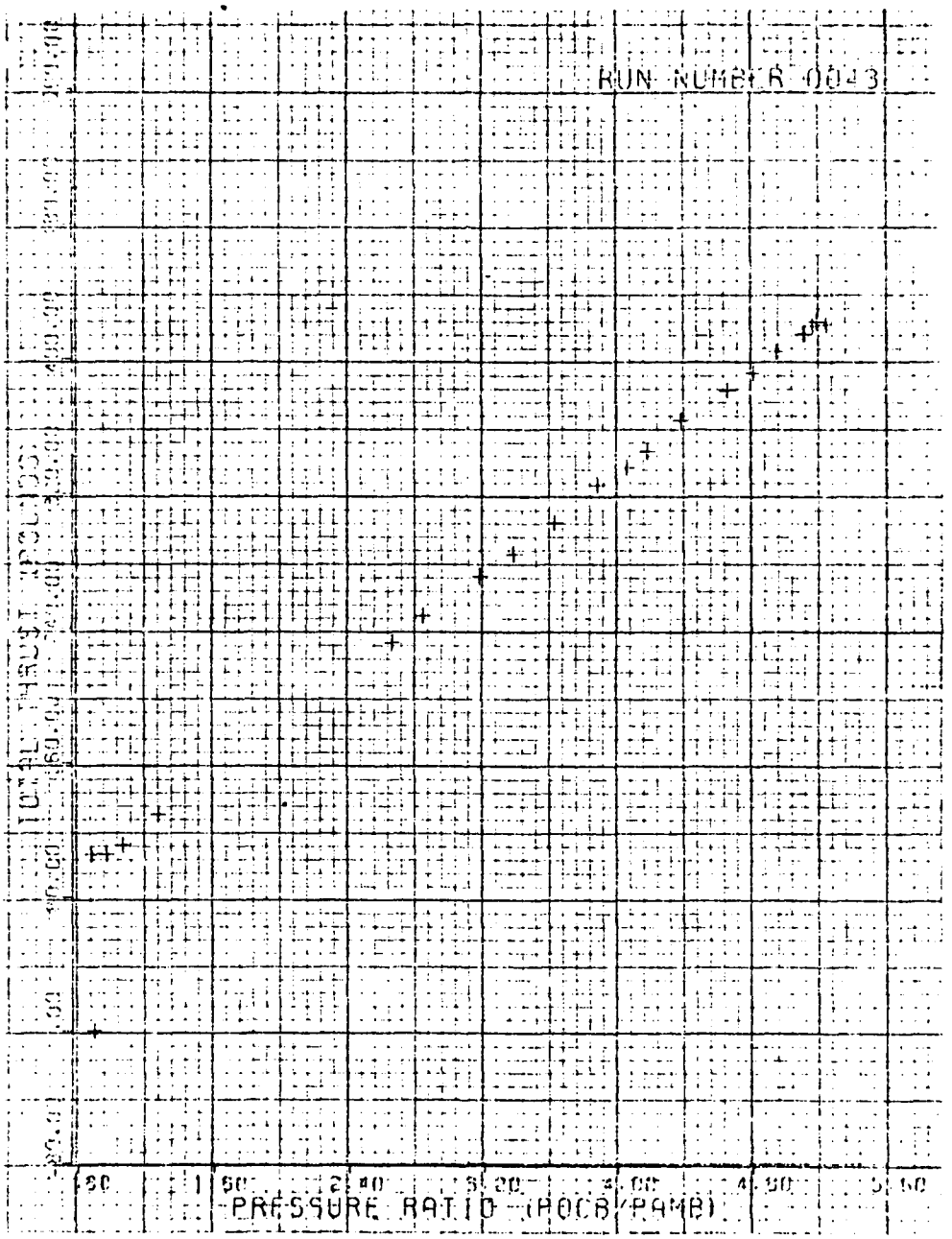

Figure C-3 L/W = 9.5 Repeated

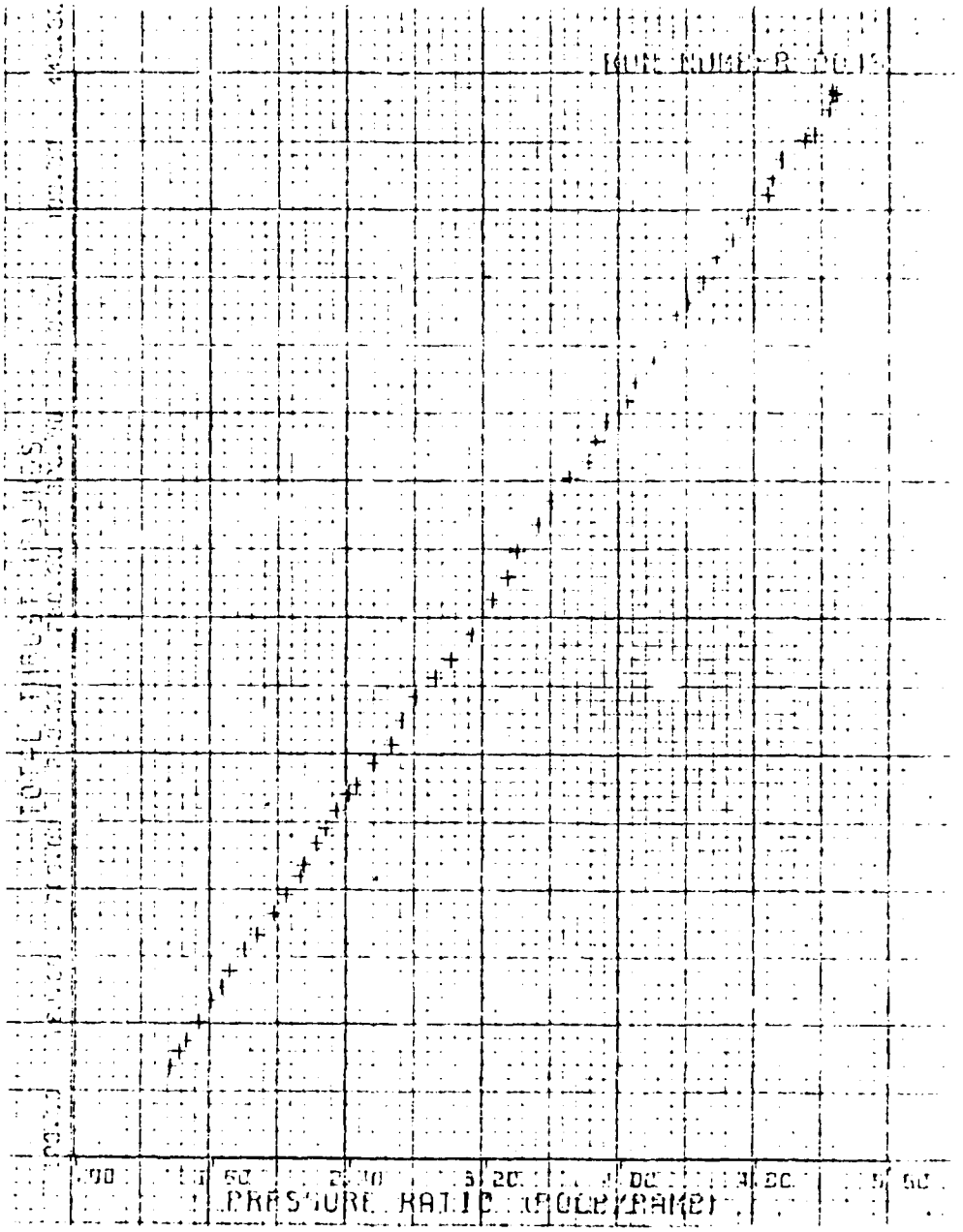

Figure C-4 L/W = 8.0

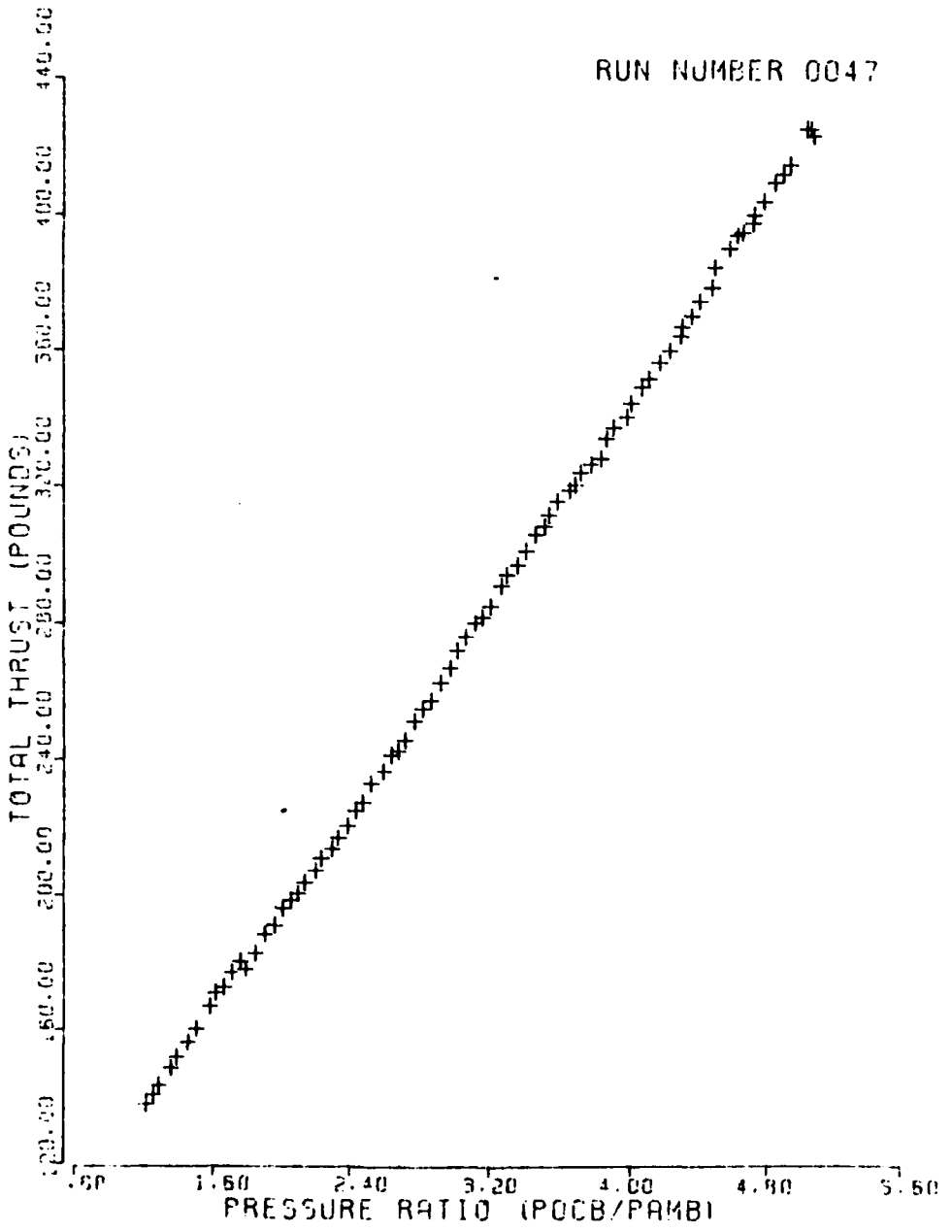

Figure C-5 L/W = 6.5

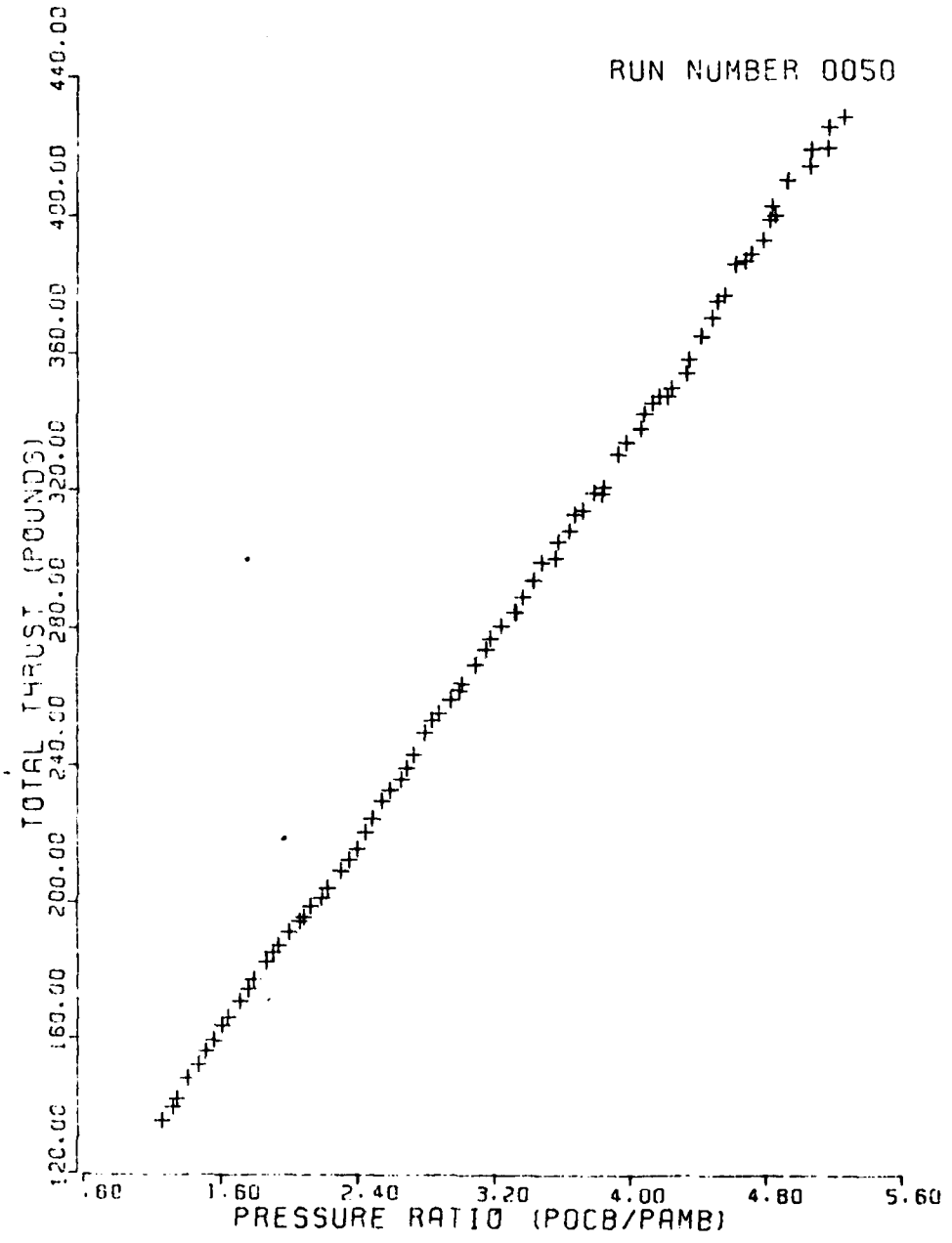

Figure C-6 L/W = 5.0

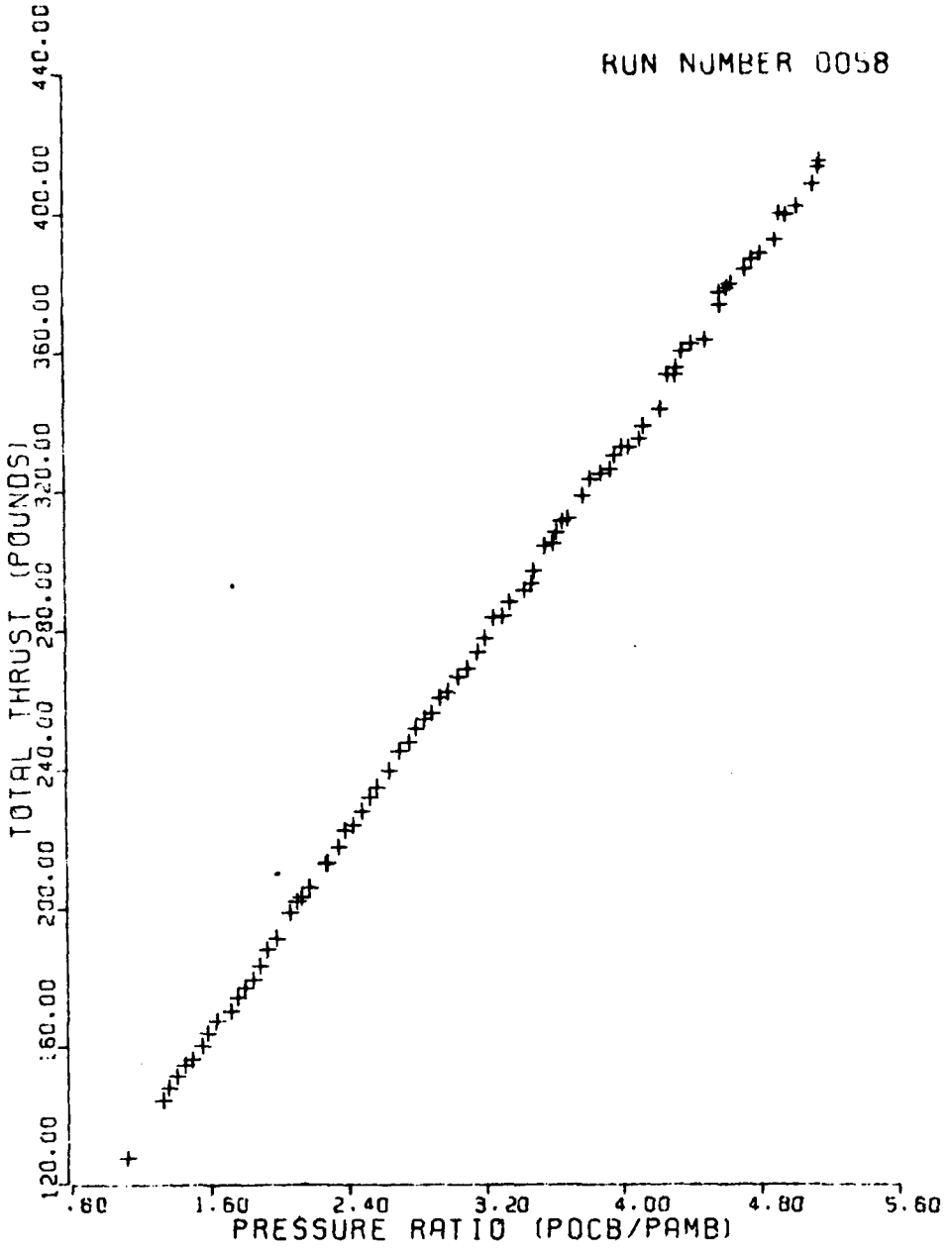

Figure C-7 L/W = 3.5

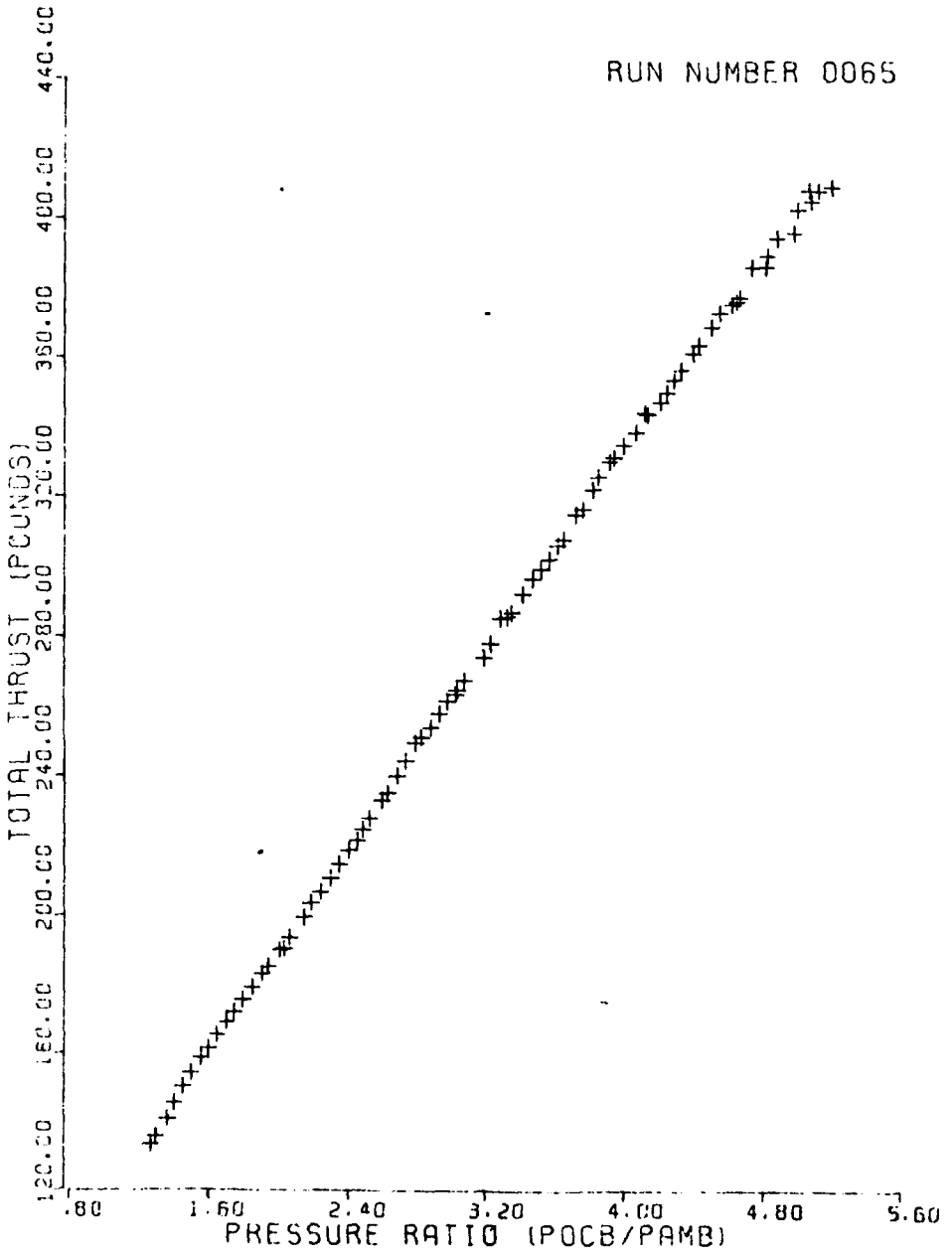

Figure C-8 L/W = 3.5 Repeated

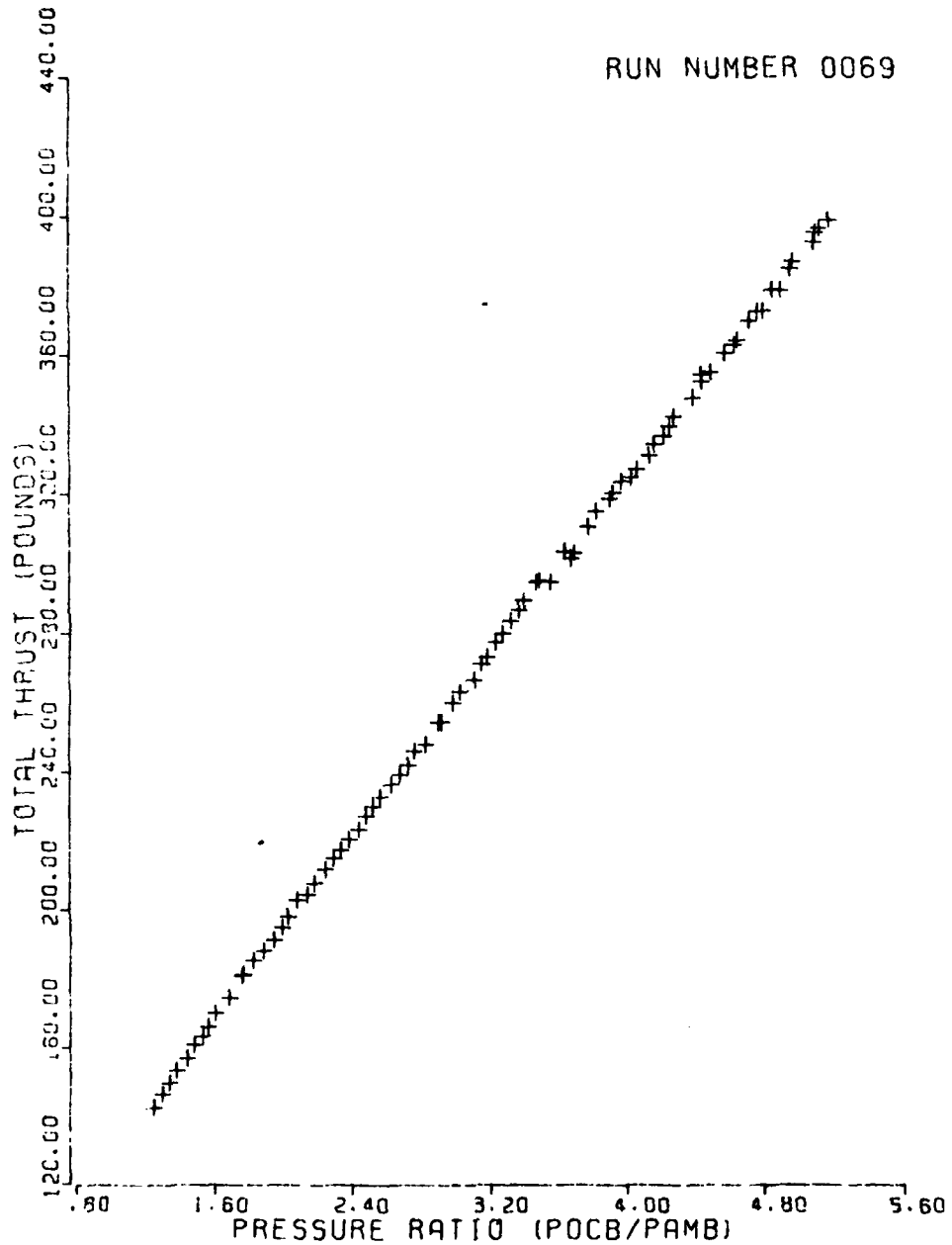

Figure C-9 L/W = 2.0

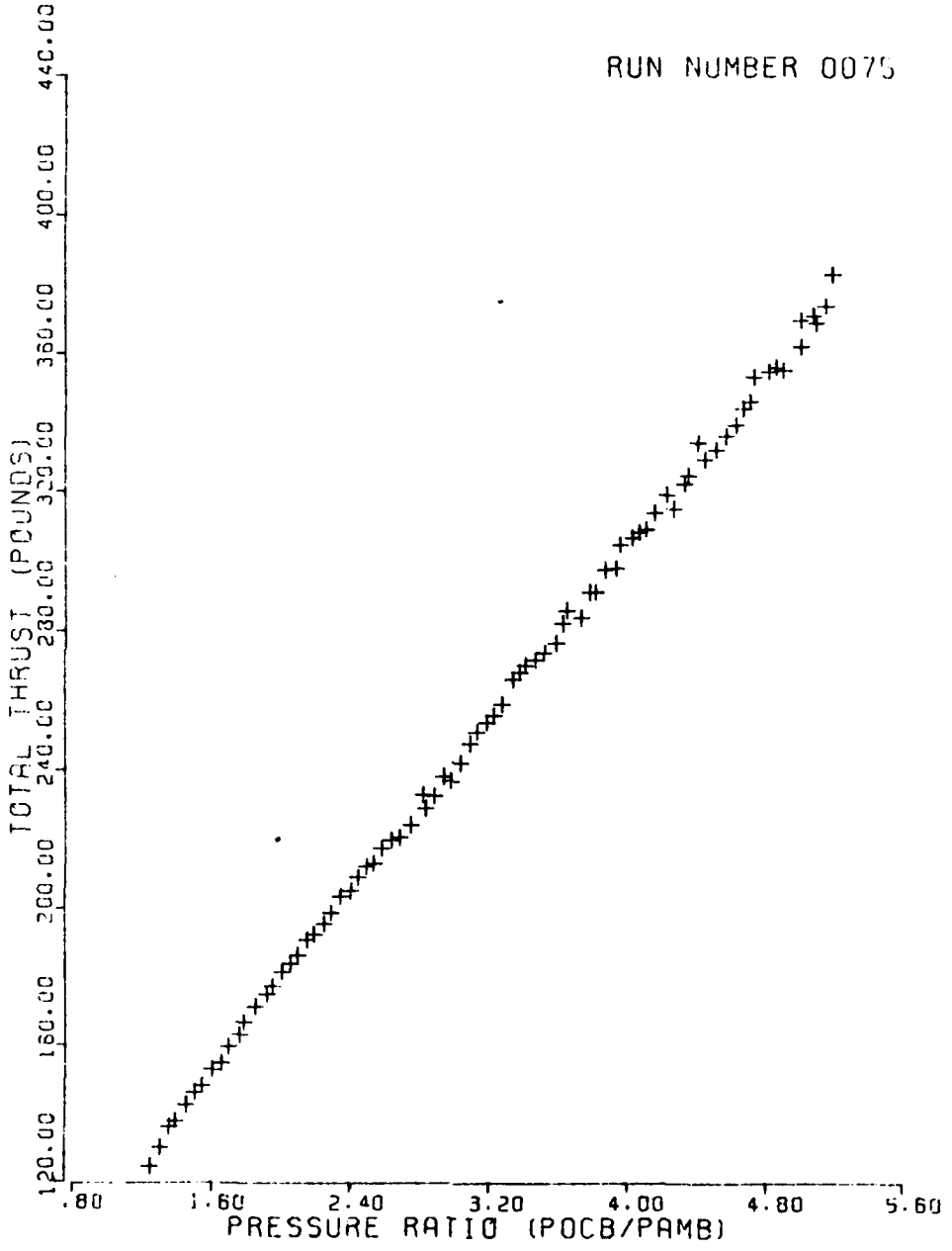

Figure C-10 L/W = 0.2

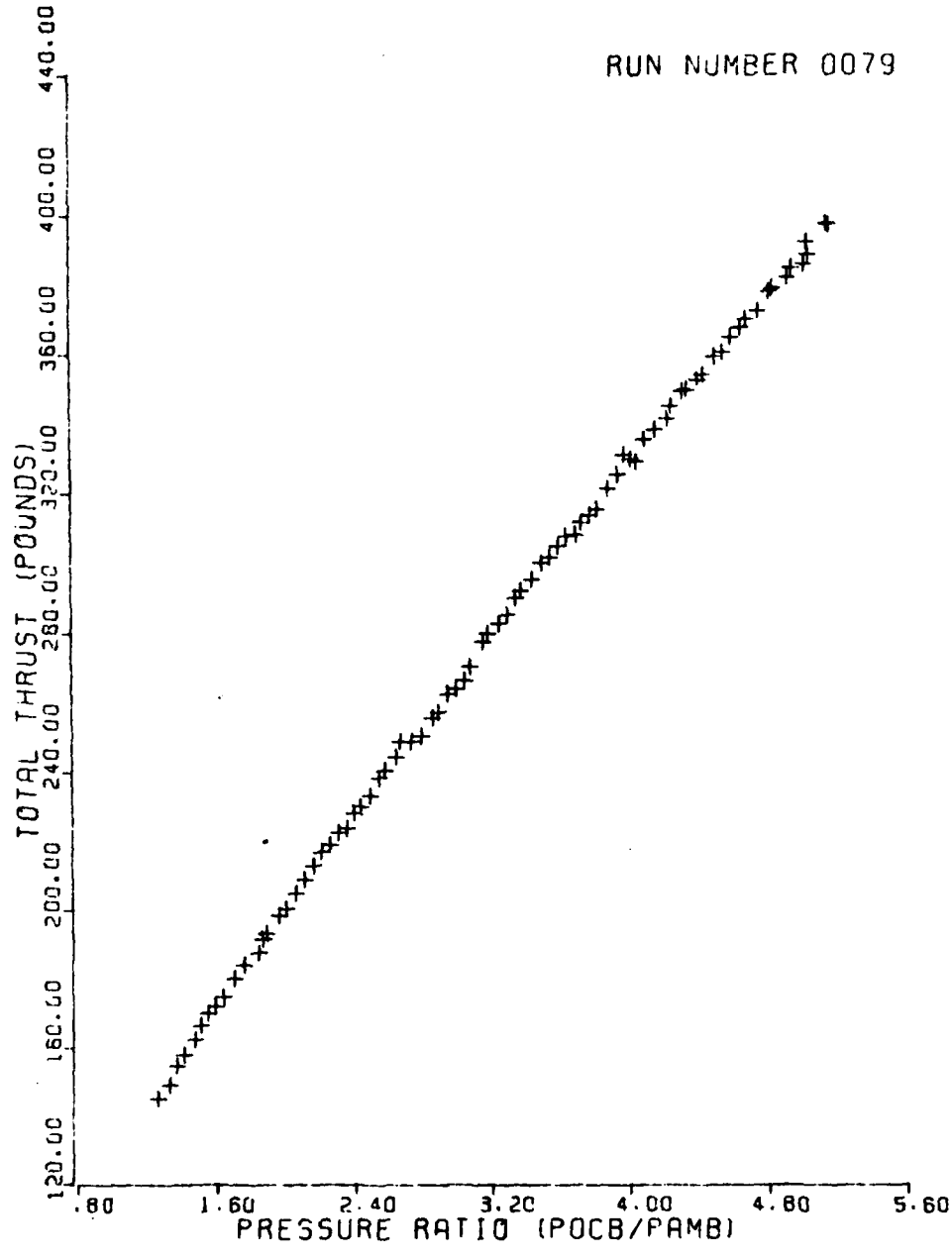

Figure C-11 L/W = 0.9

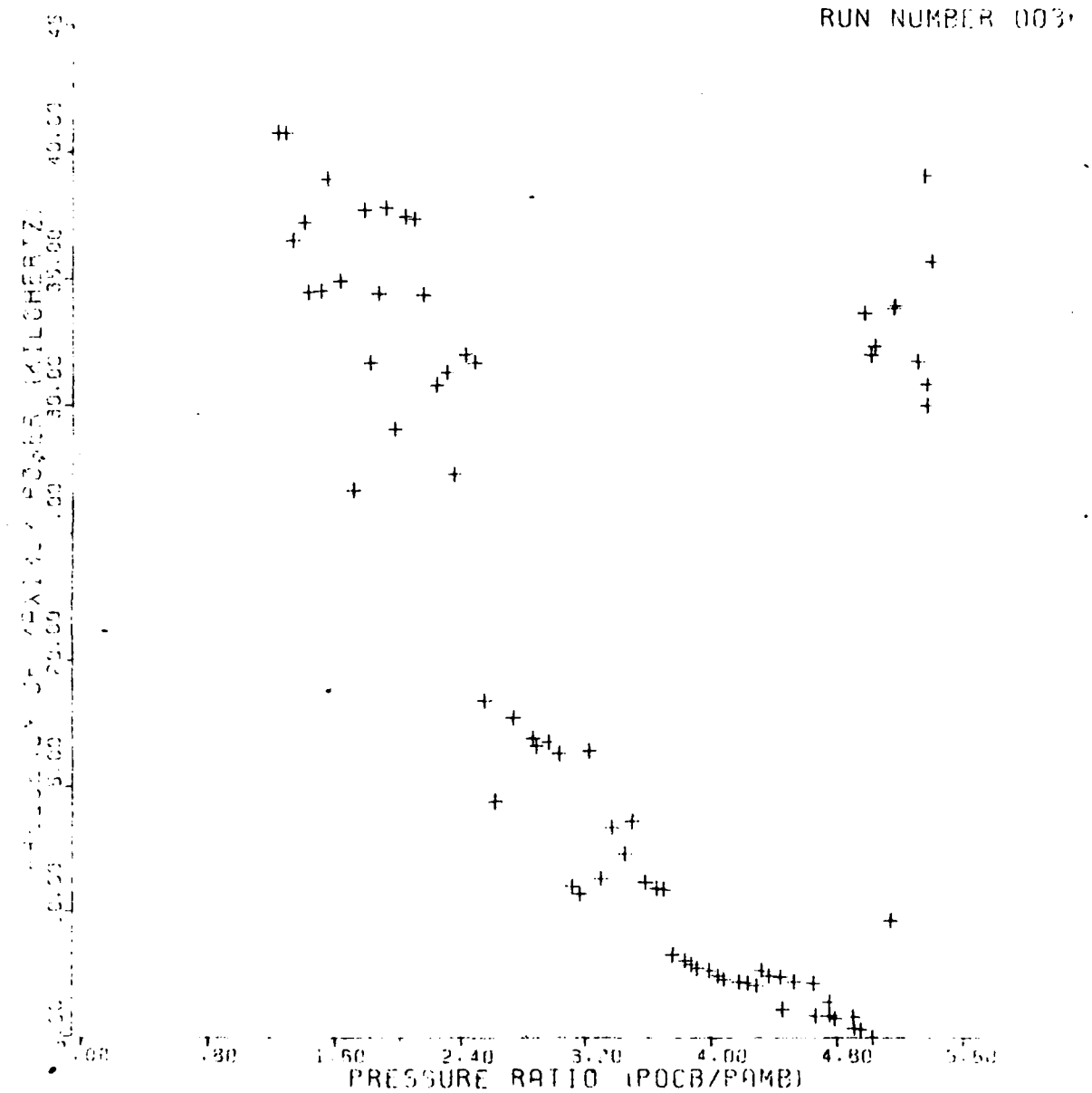

Figure C-12 L/W = 11.0

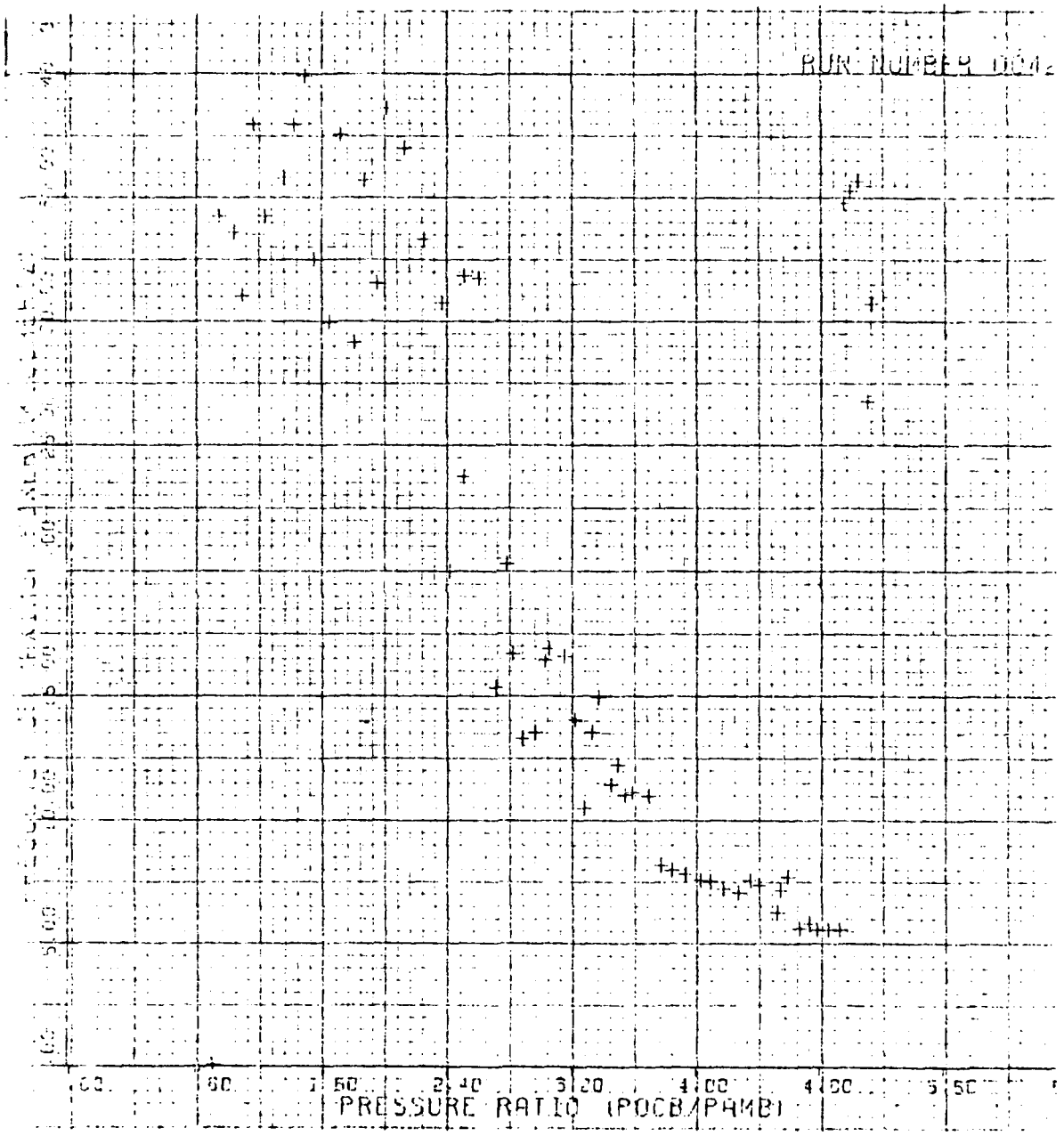

Figure C-13 L/W = 9.5

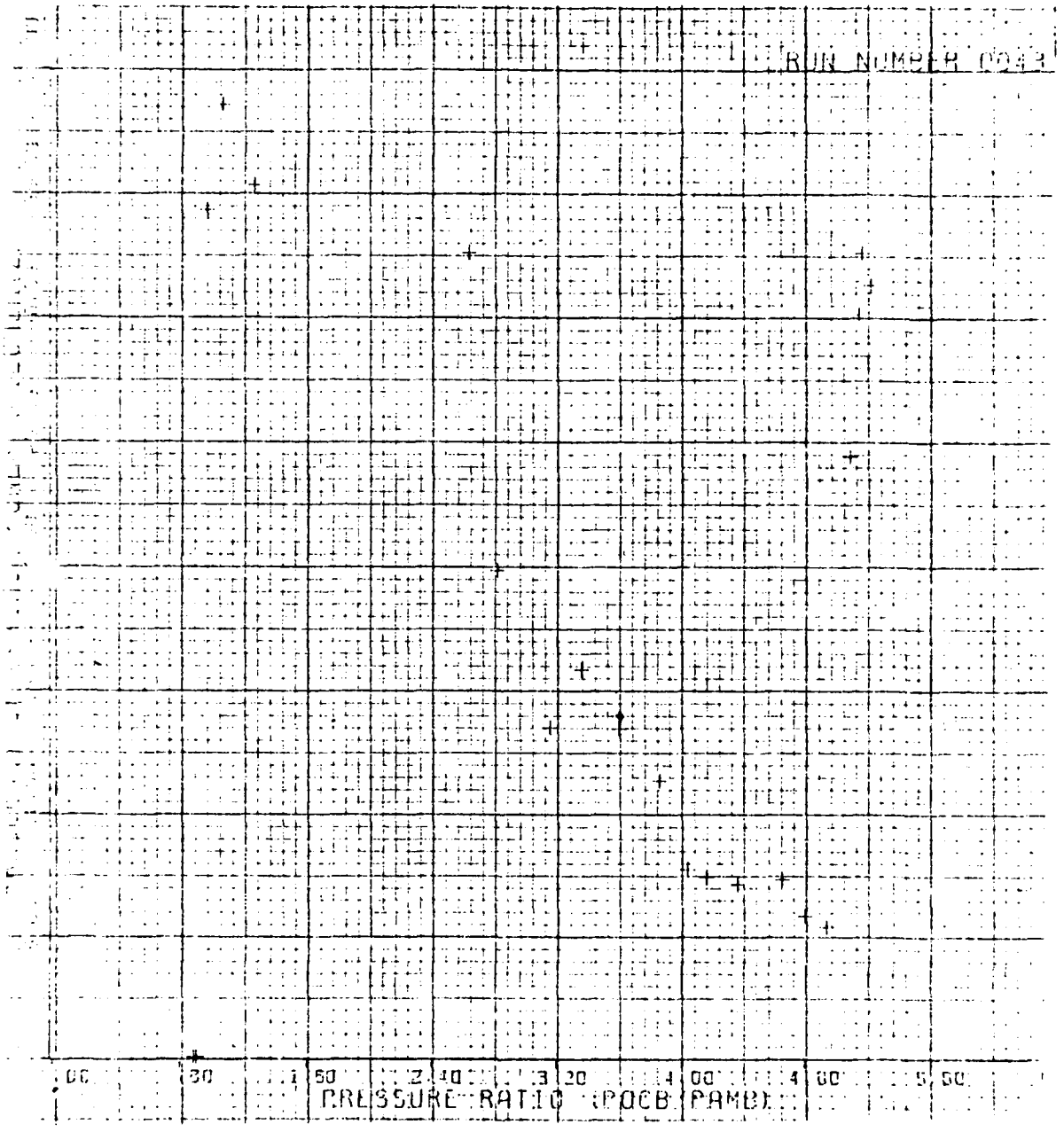

Figure C-14 L/W = 9.5 Repeated

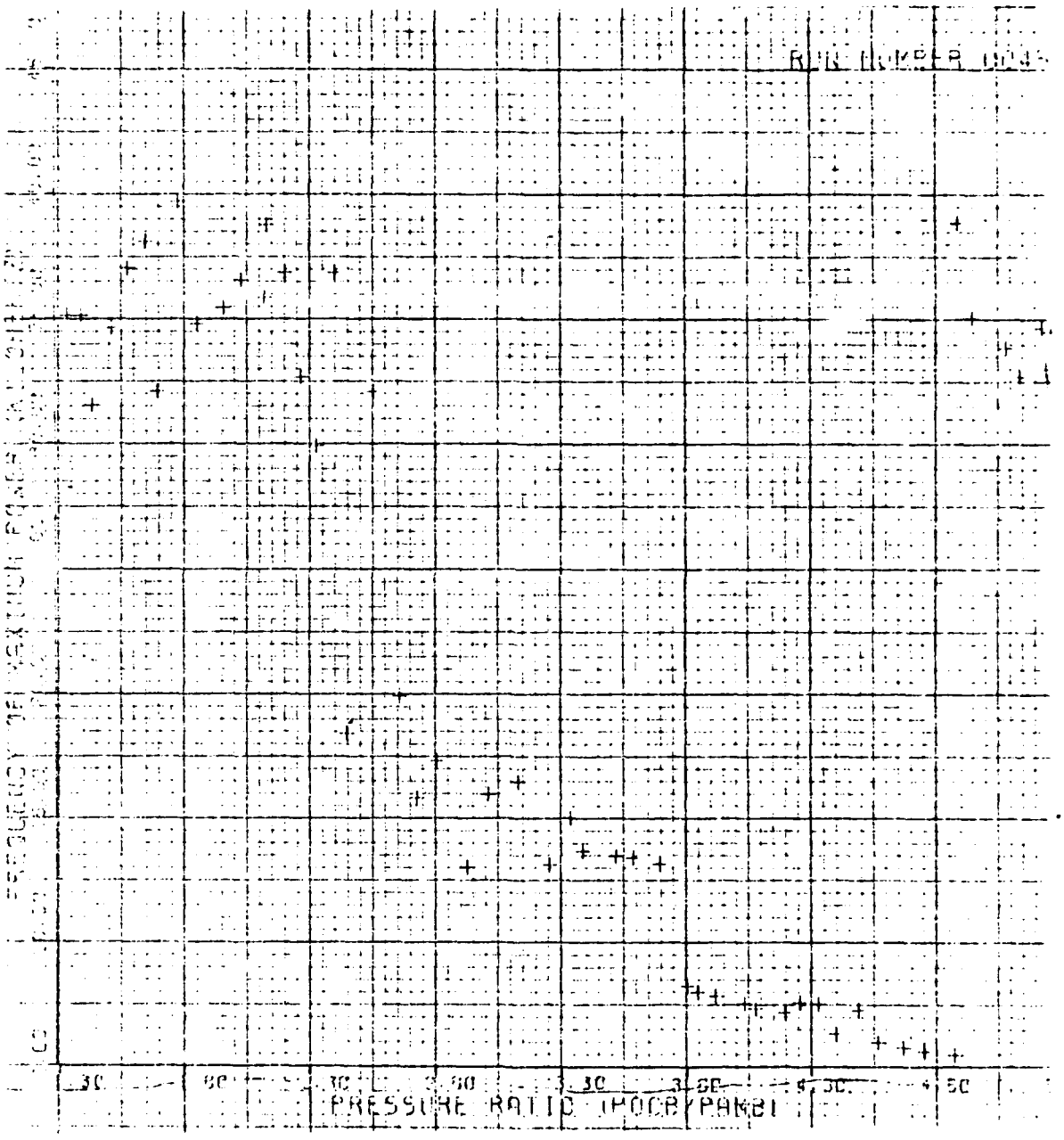

Figure C-15 L/W = 8.0

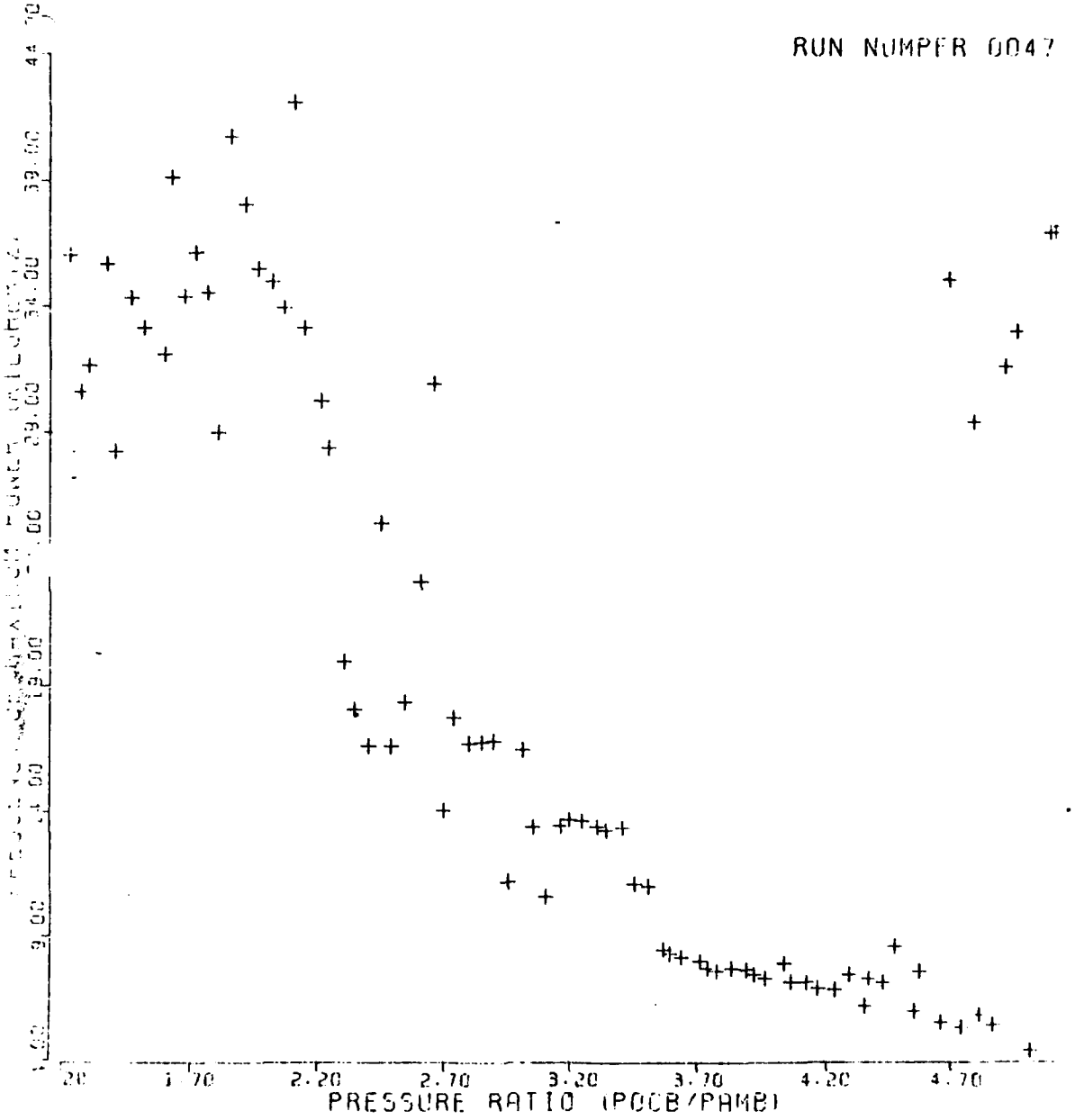

Figure C-16 L/W = 6.5

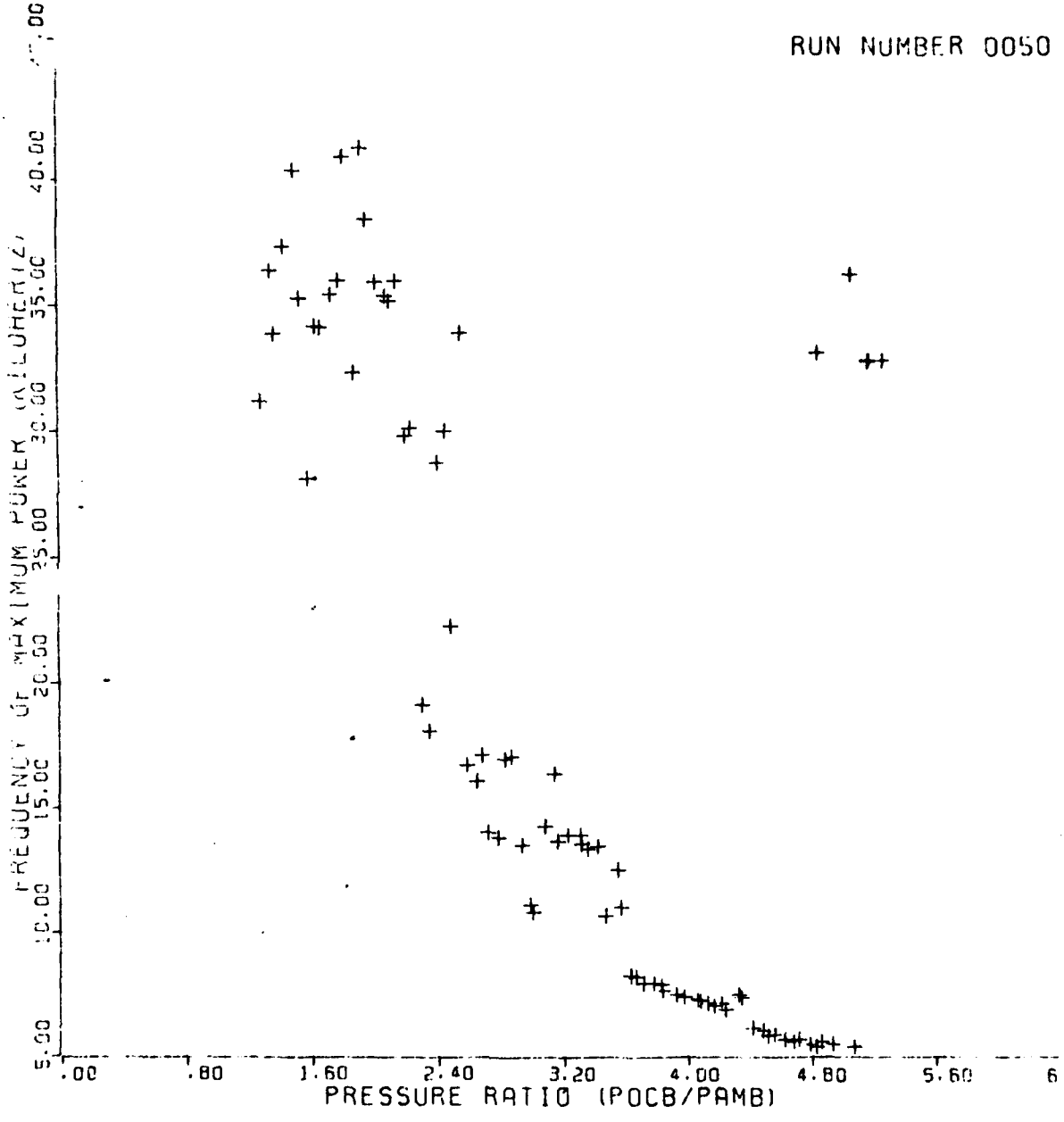

Figure C-17 L/W = 5.0

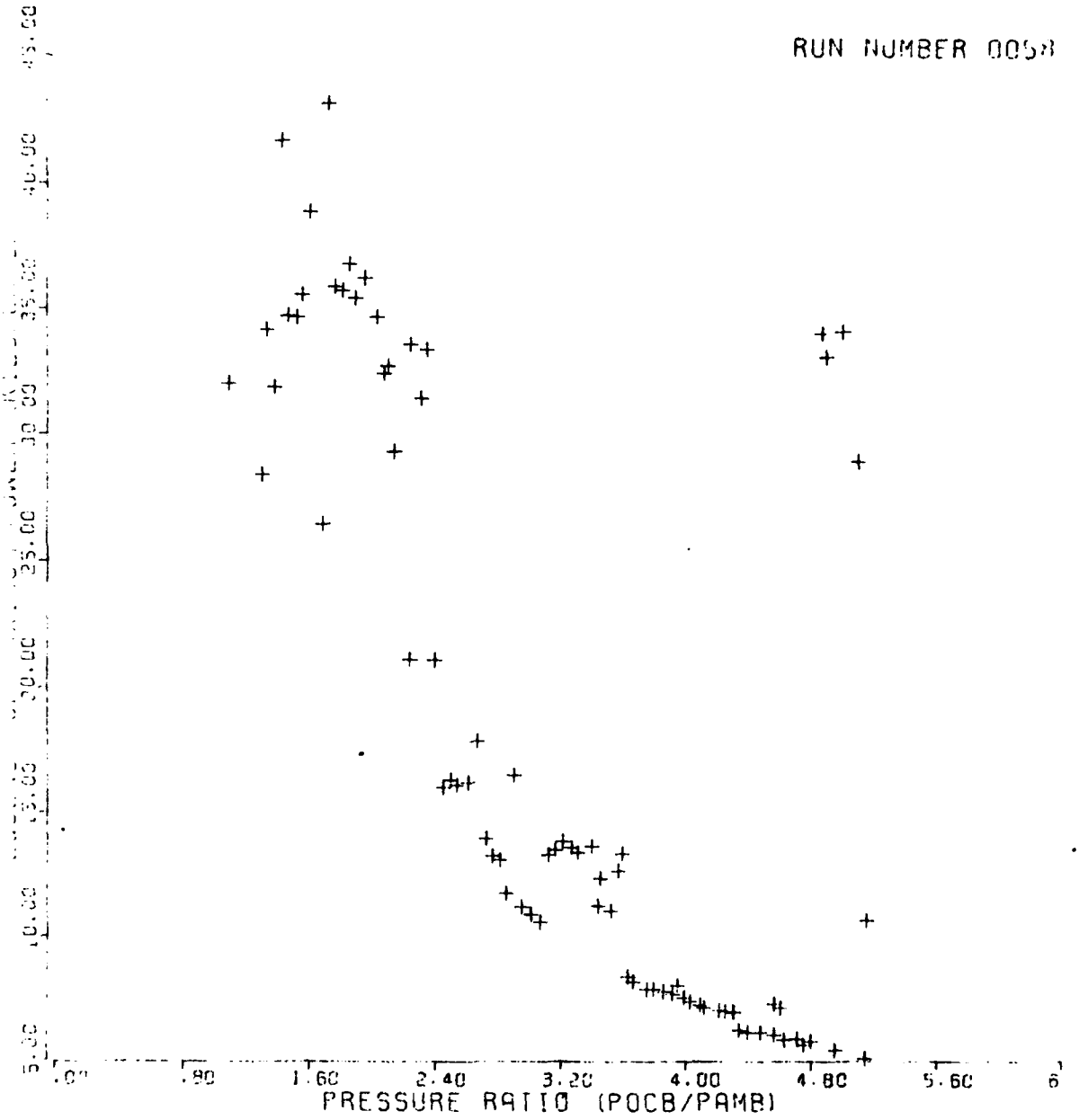

Figure C-18 L/W = 3.5

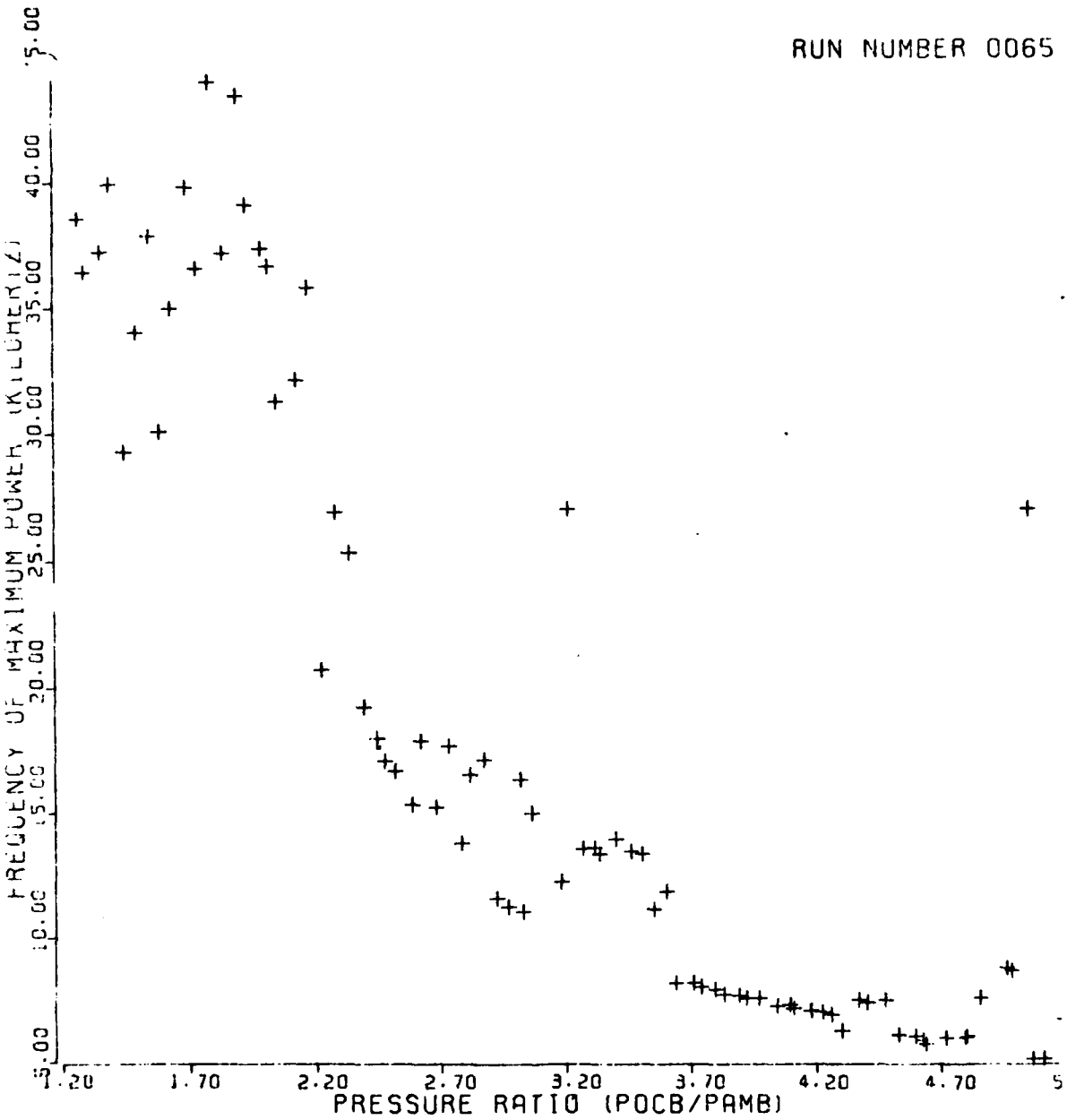

Figure C-19 L/W = 3.5 Repeated

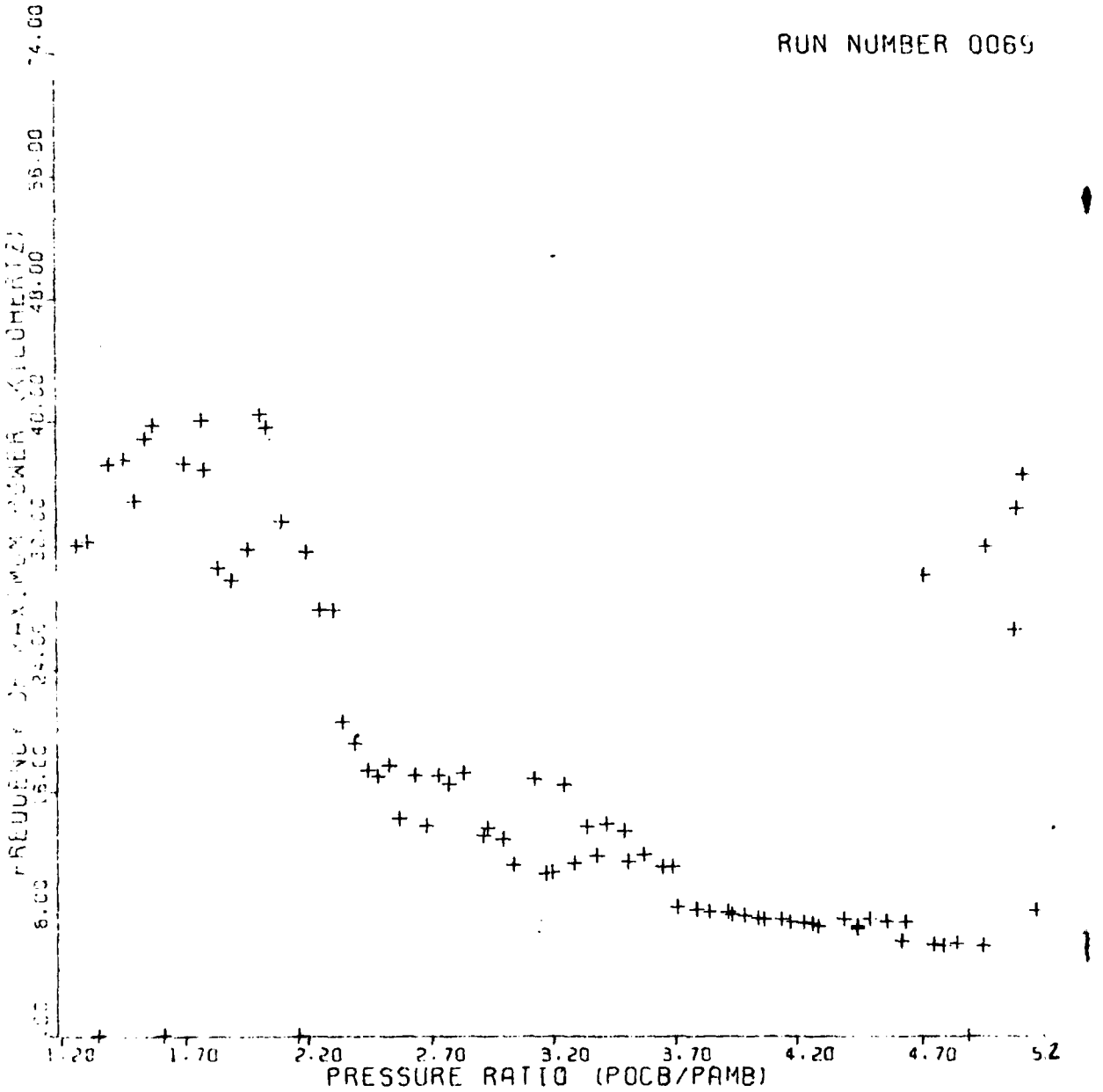

Figure C-20 L/W = 2.0

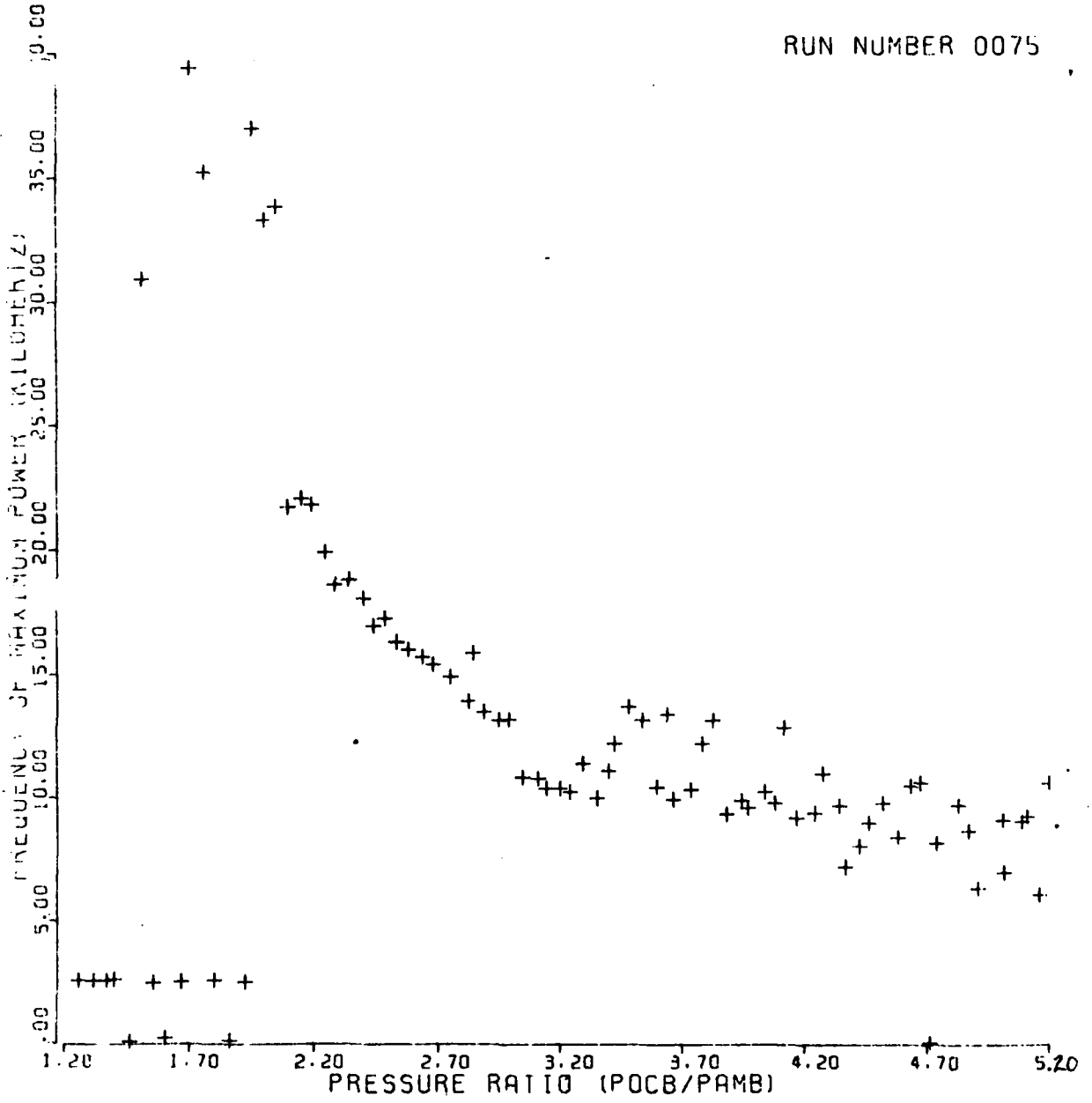

Figure C-21 L/W = 0.2

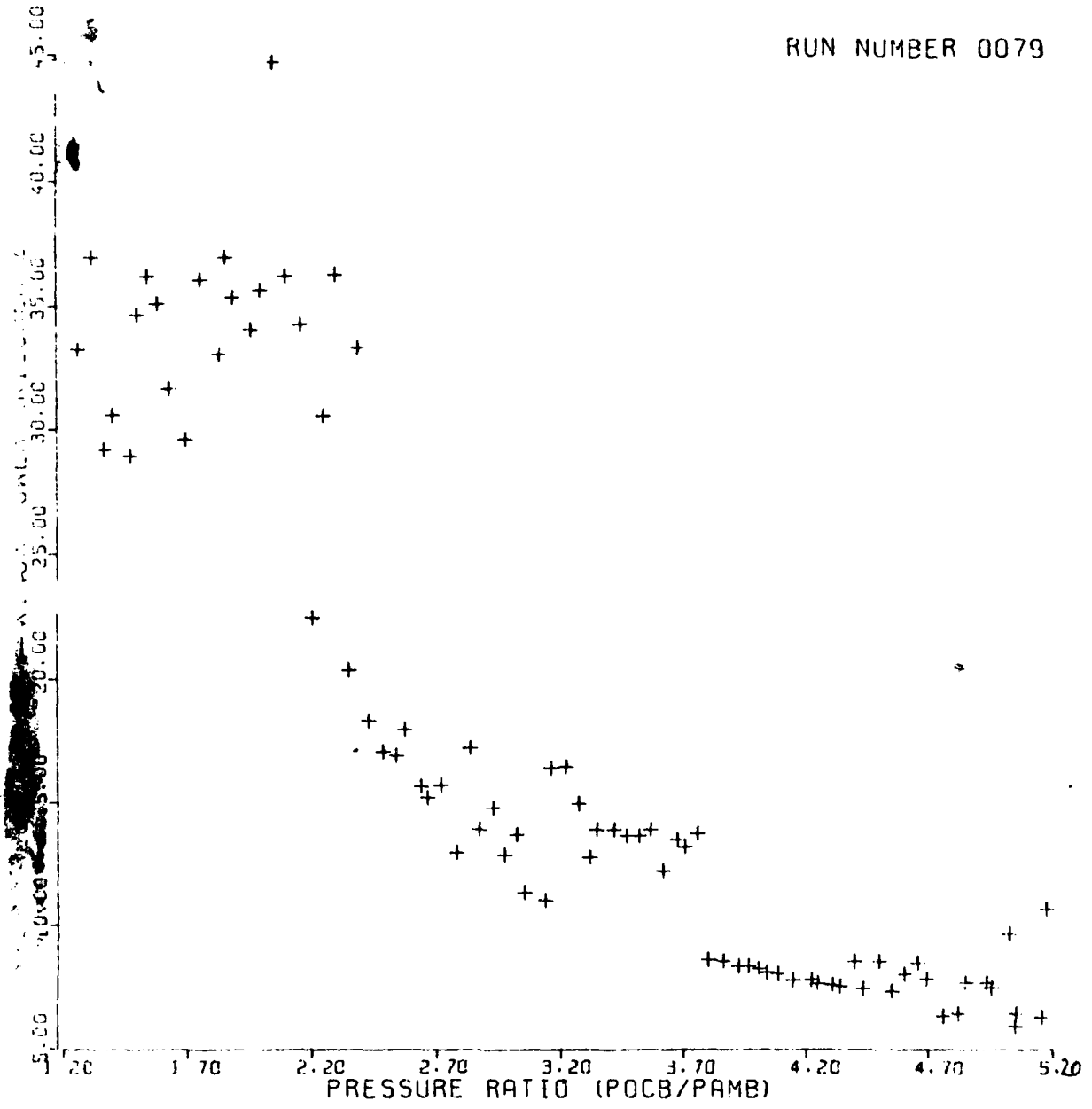

Figure C-22 L/W = 0.9

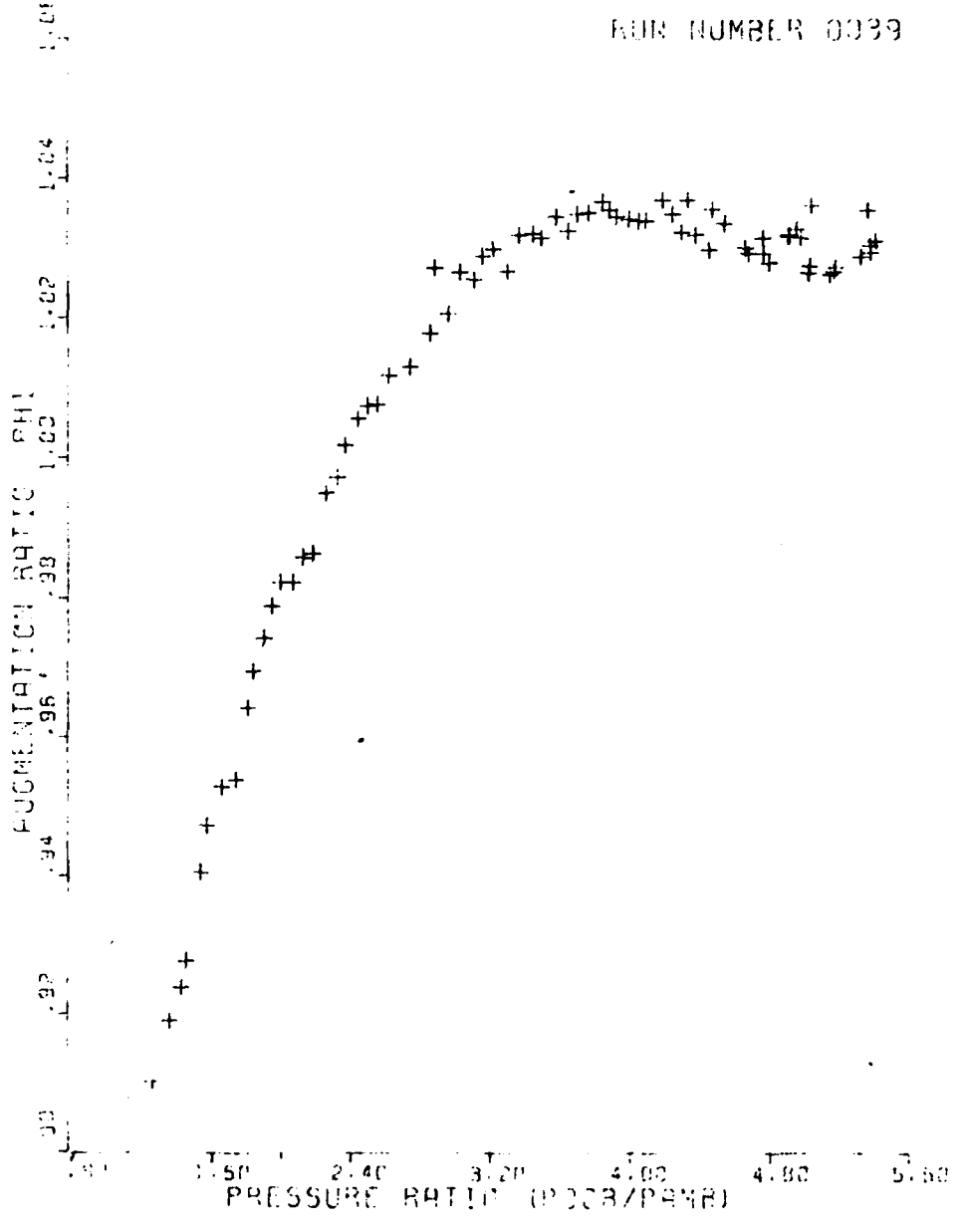

Figure C-23 L/W = 11.0

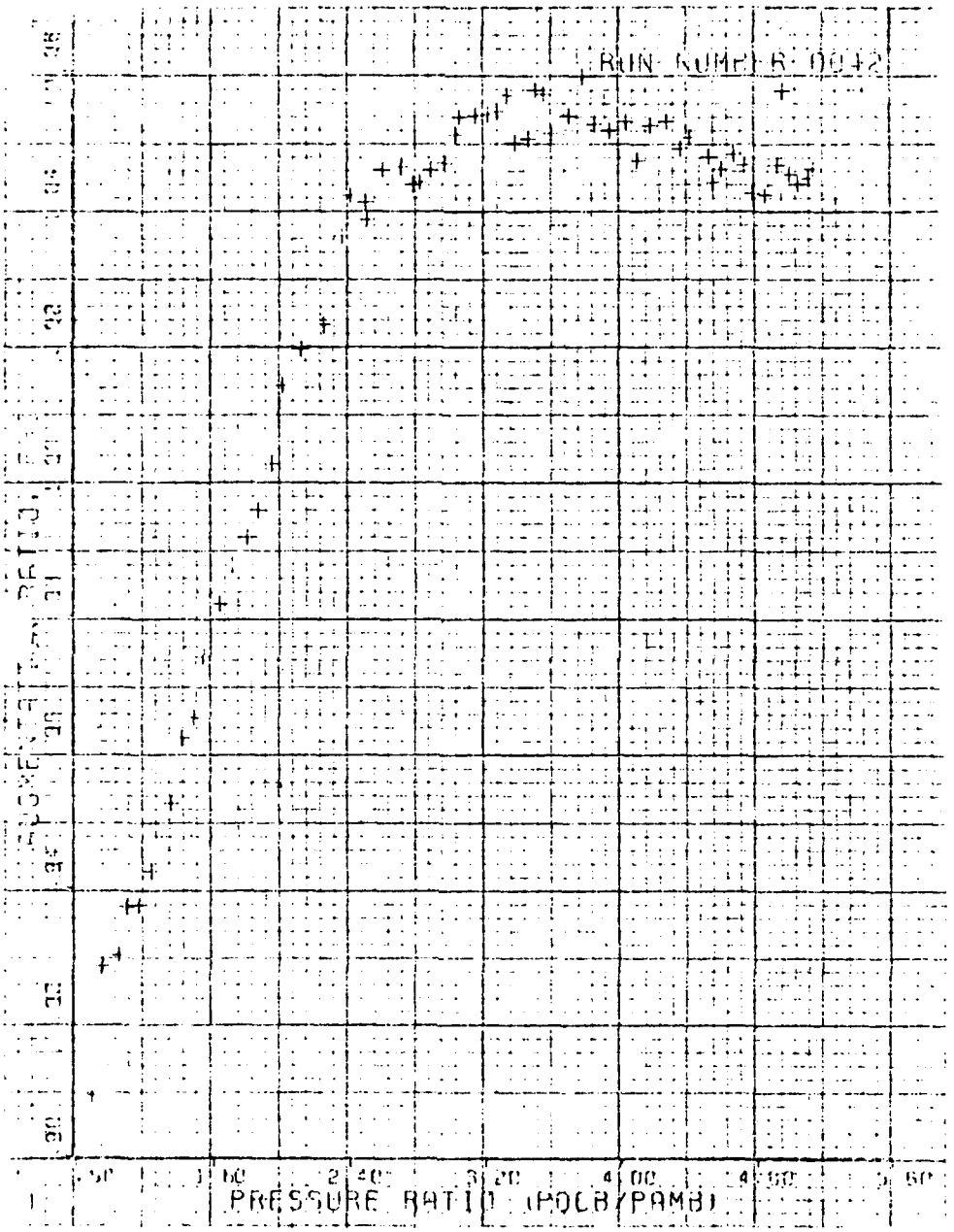

Figure C-24 L/W = 9.5

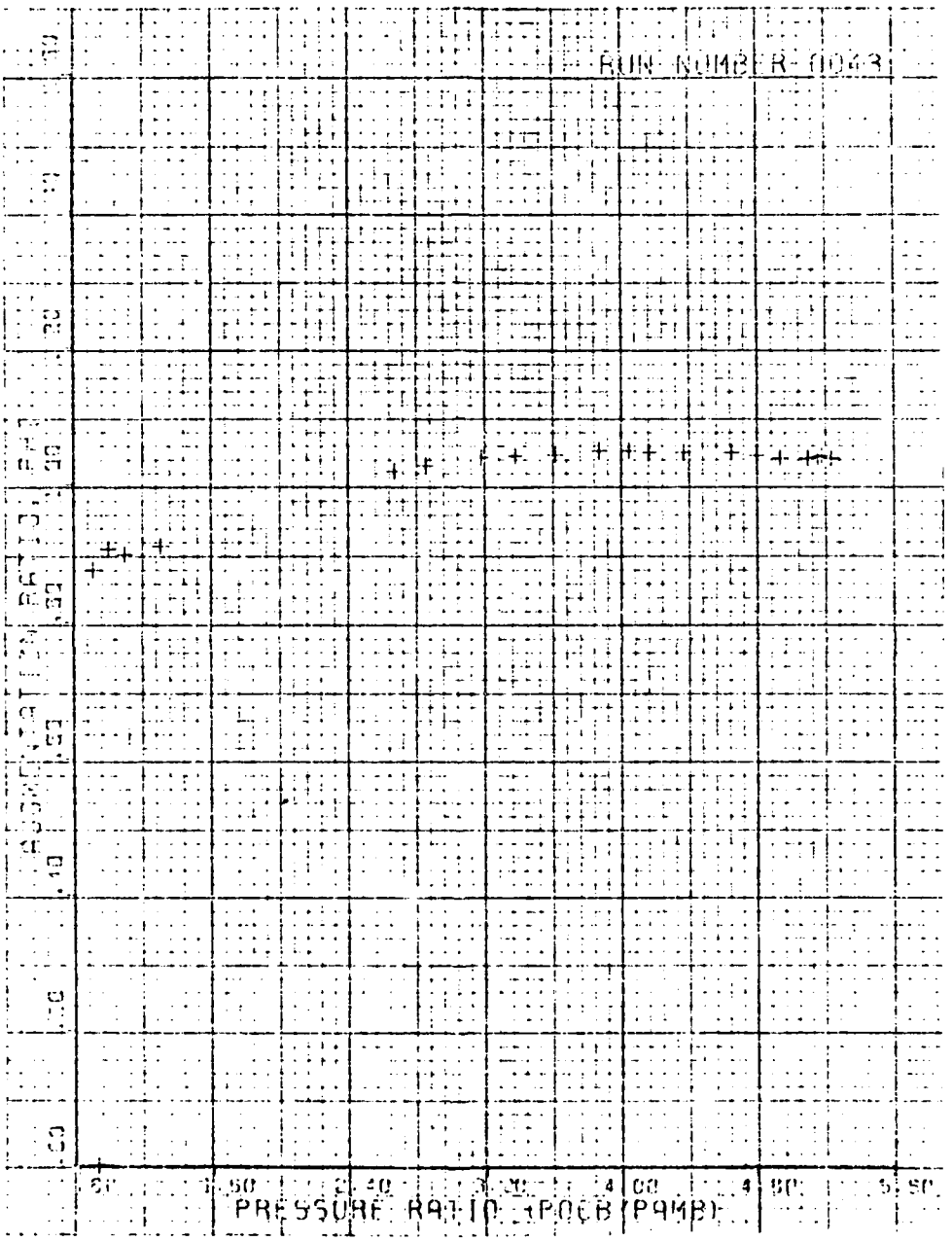

Figure C-25 **L/W = 9.5 Repeated**

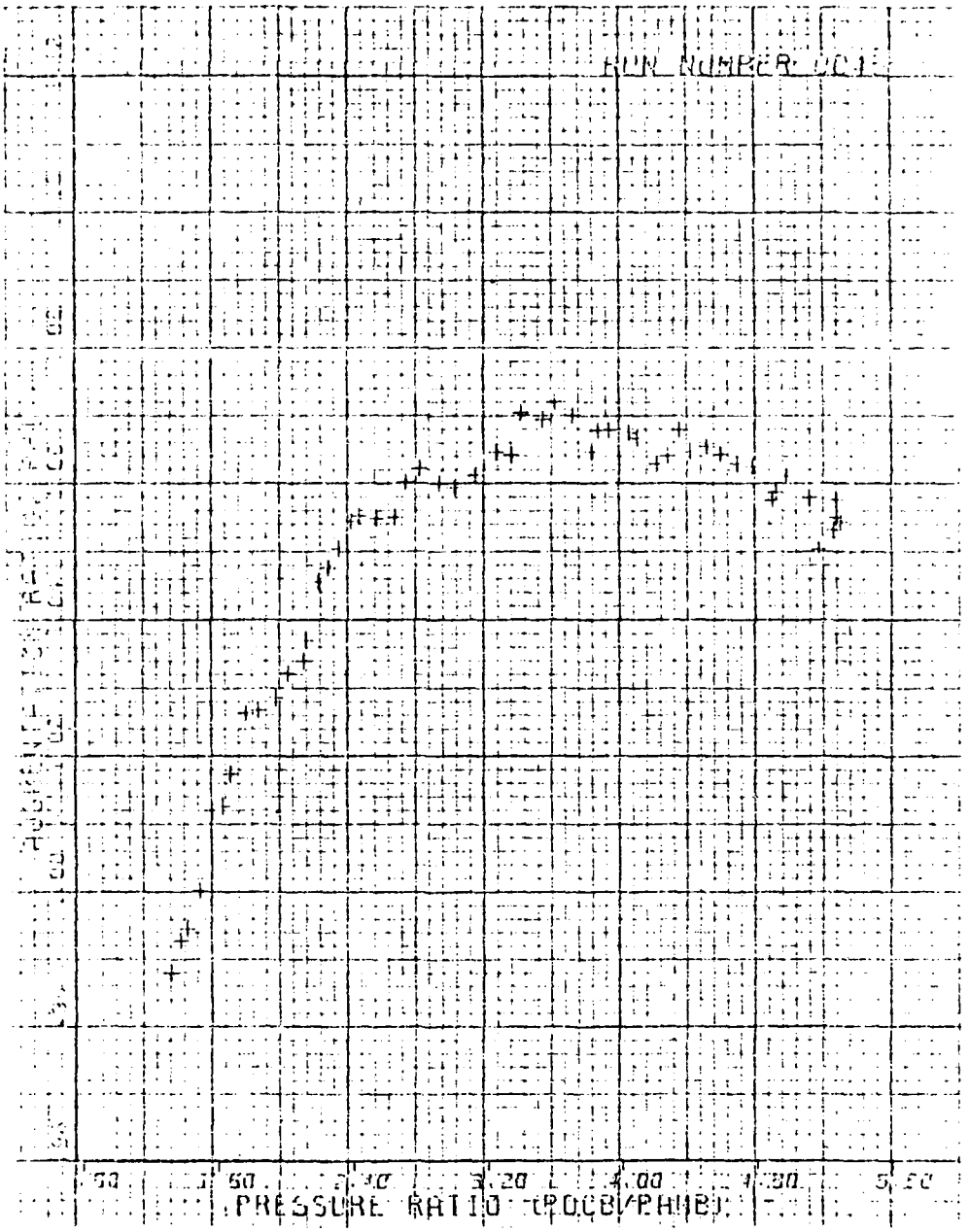

Figure C-26 L/W = 8.0

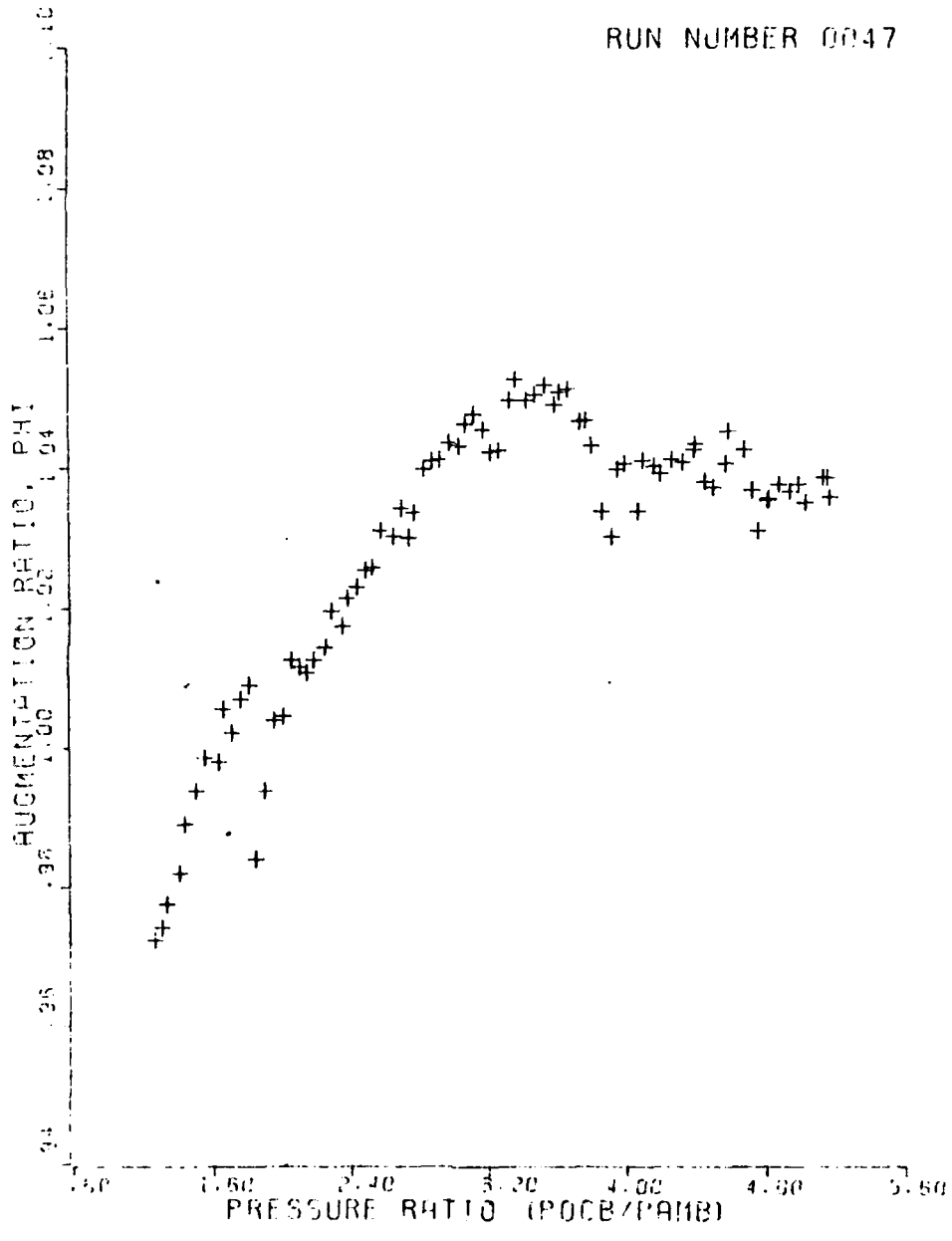

Figure C-27 L/W = 6.5

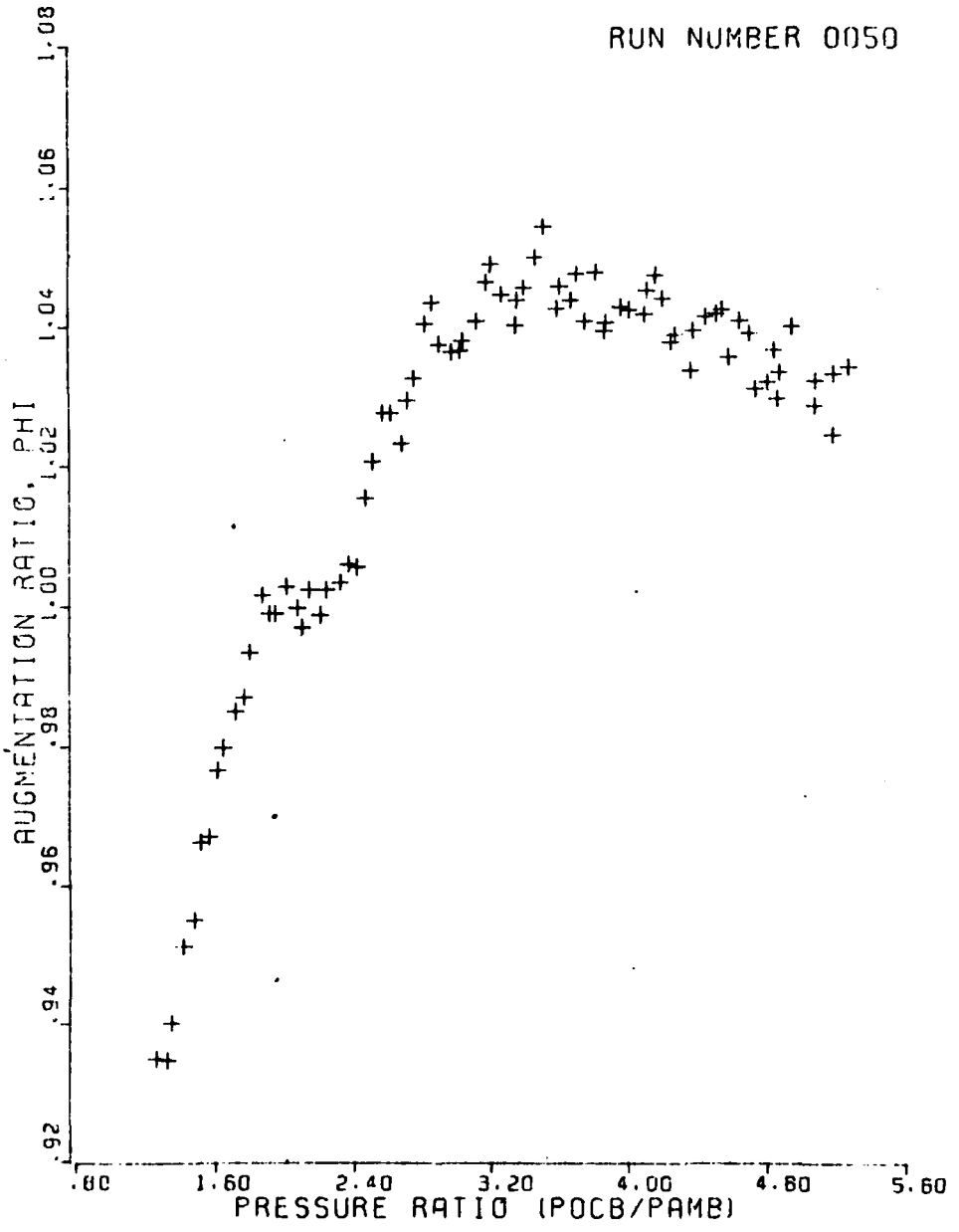

Figure C-28 L/W = 5.0

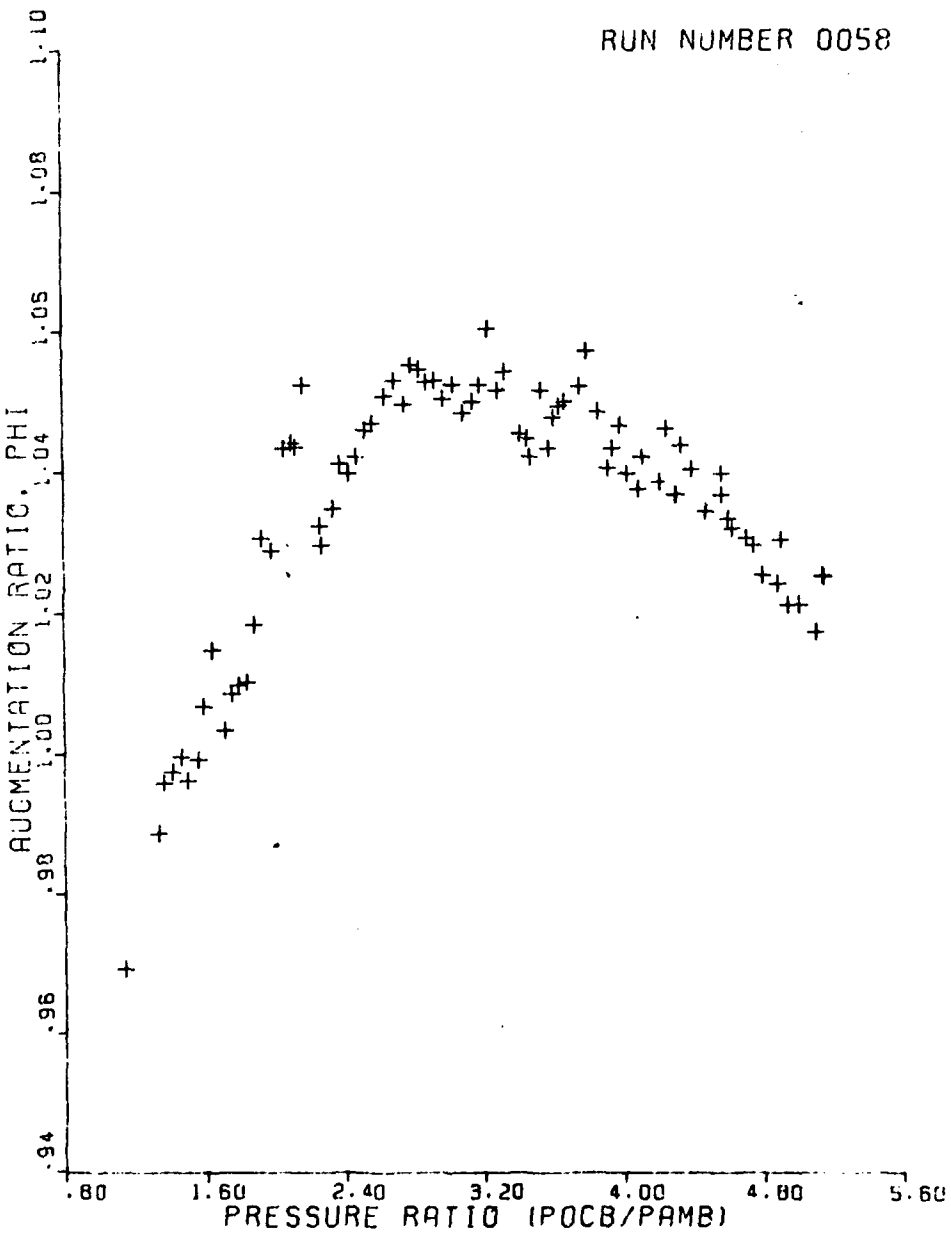

Figure C-29 L/W = 3.5

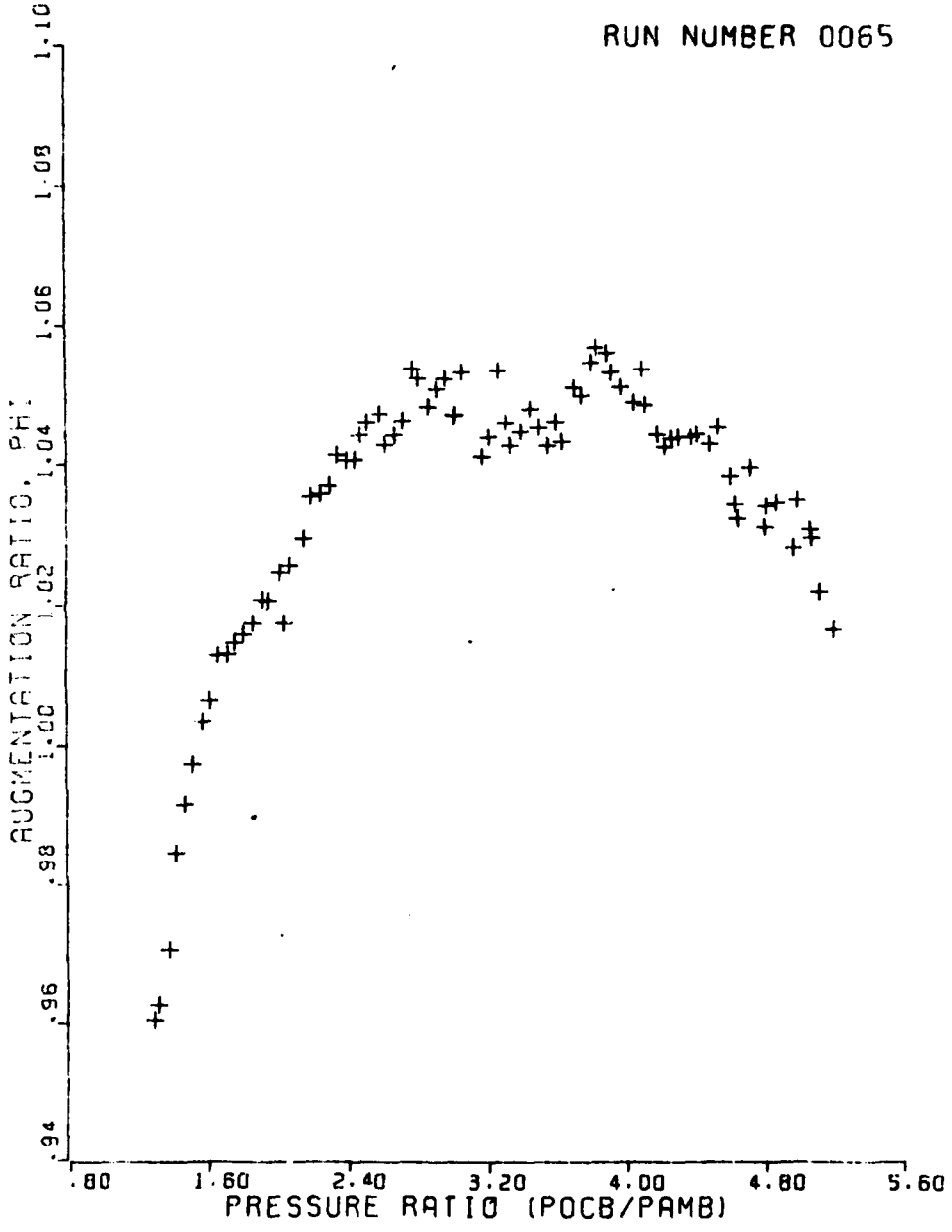

Figure C-30 L/W = 3.5 Repeated

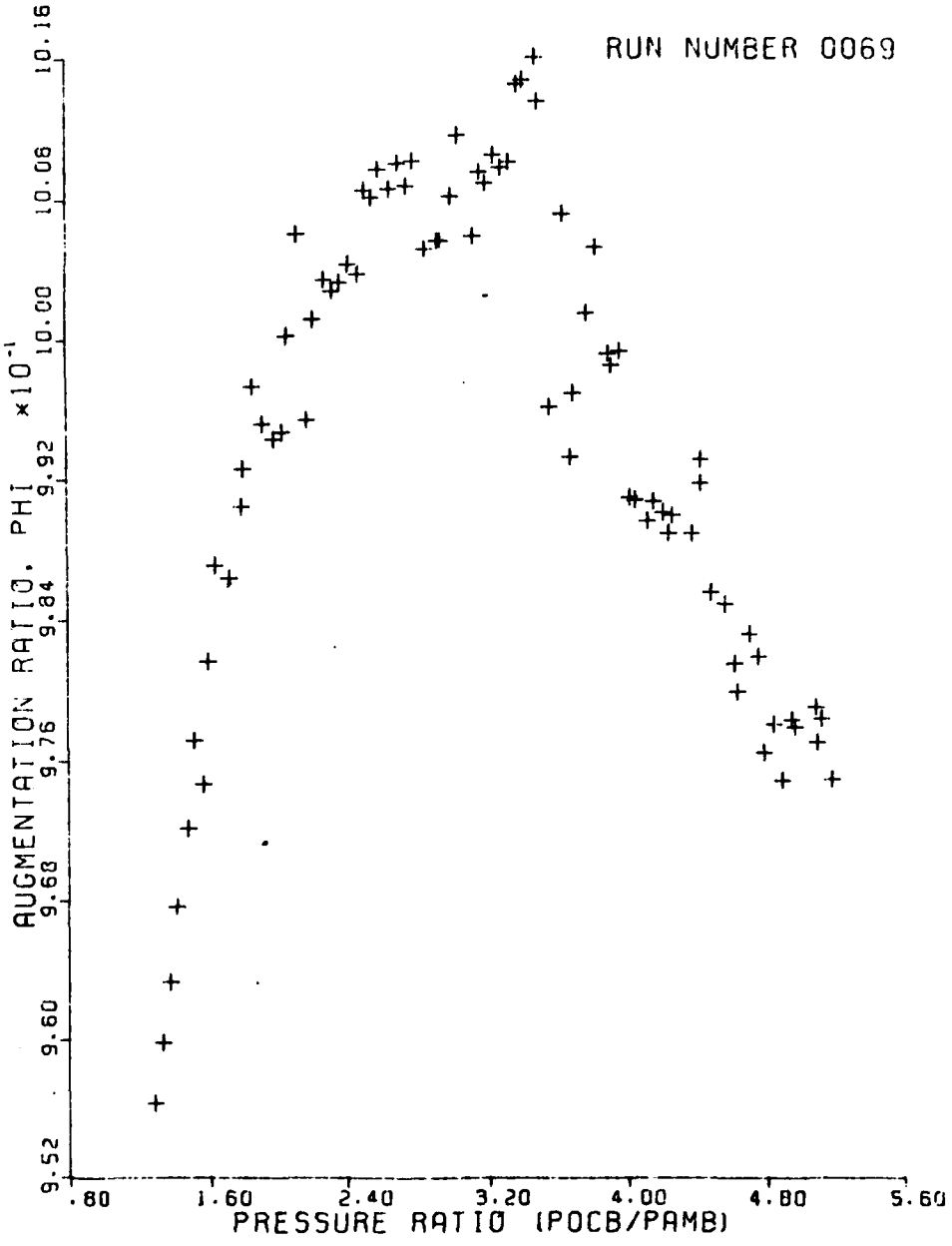

Figure C-31 L/W = 2.0

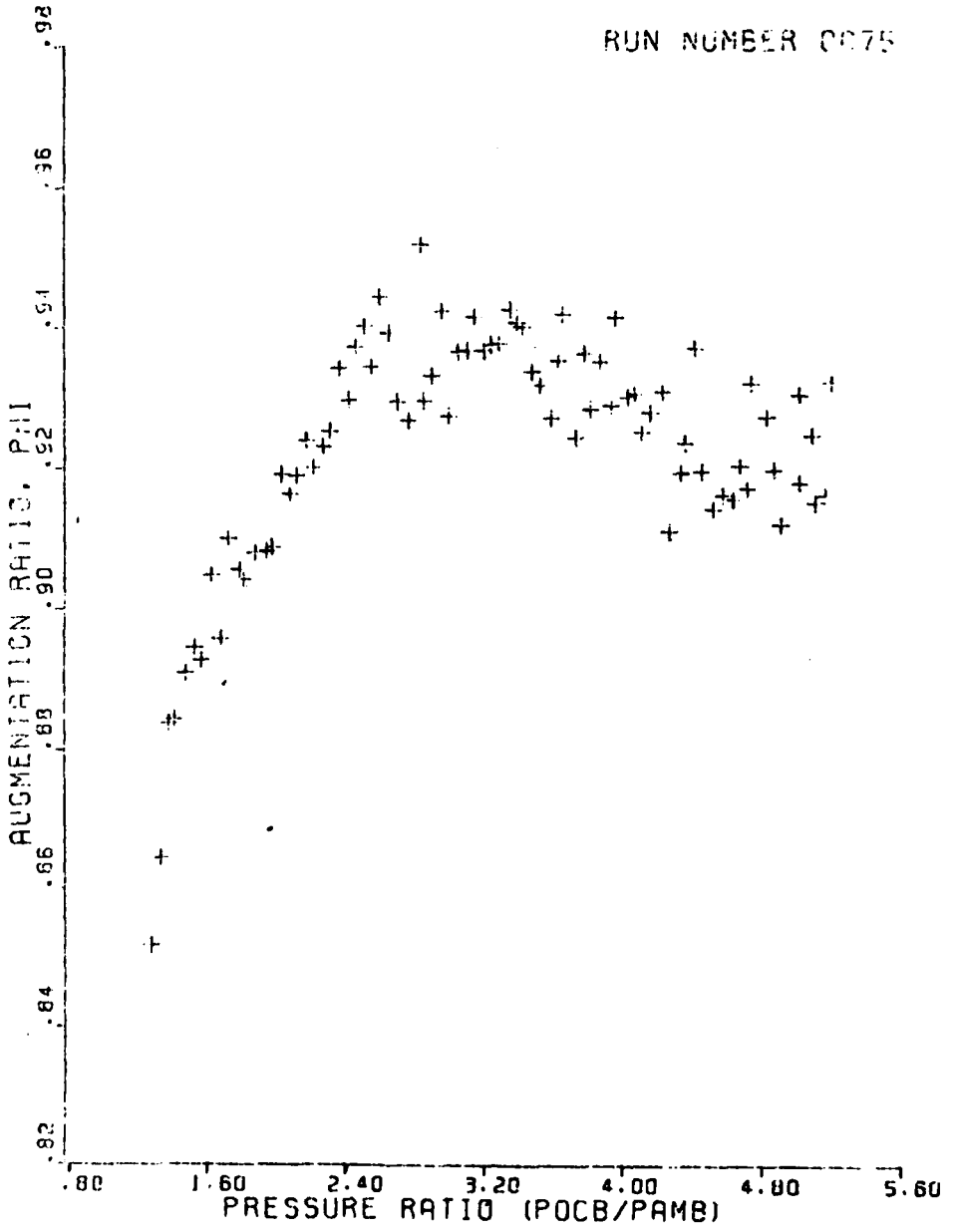

Figure C-32 L/W = 0.2

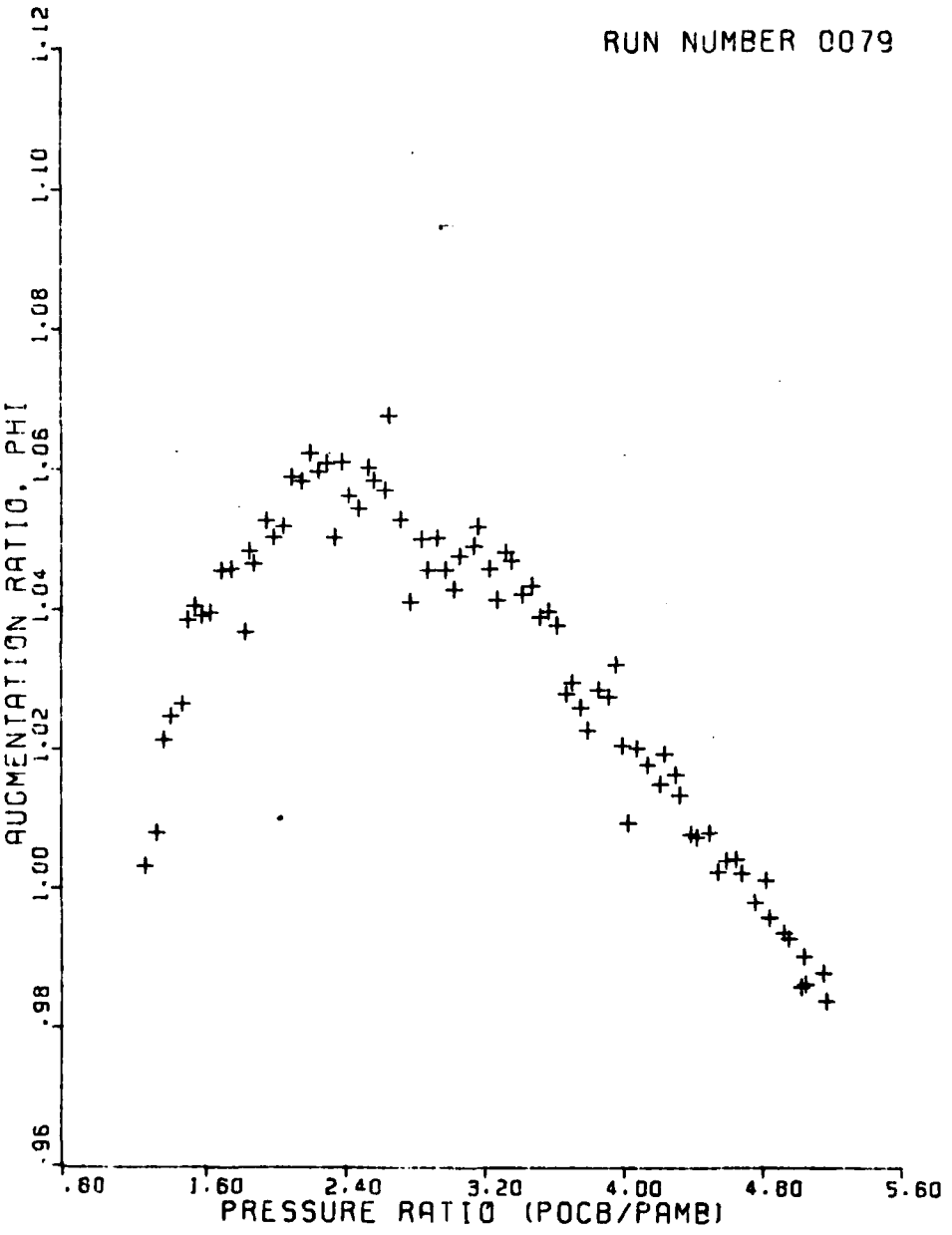

Figure C-33 L/W = 0.9

DISTRIBUTION LIST

Office of Naval Research
800 N. Quincy St.
Arlington, VA 22217
- ONR 211 — 4
- ONR 430B — 1

Office of Naval Research Branch Office
1030 E. Green St.
Pasadena, CA 91106 — 1

Office of Naval Research Branch Office
536 South Clark Street
Chicago, IL 60605 — 1

Office of Naval Research Branch Office
Bldg 114 Section D
666 Summer St.
Boston, MA 02210 — 1

Naval Research Laboratory
Washington, DC 20375
- Code 2627 — 1
- Code 2629 — 1

Defense Documentation Center
Bldg 5 Cameron Station
Alexandria, VA 22314 — 12

Naval Air Systems Command
Washington, DC
- NAIR 5301 (Mr. R. Weinraub) — 1
- NAIR 03PA (Mr. H. Andrews) — 1
- ADPO-14 (CDR J. Farley) — 1

U. S. Naval Postgraduate School
Monterey, CA 93940
- Dept. of Aeronautics (Code 57) — 1
- Library — 1

David Taylor Naval Ship Research and Development Center
Bethesda, MD 20084
- Code 16 (Dr. H. Chaplin) — 1
- Code 1606 (Dr. T. Tai) — 1
- Code 166 (Mr. R. Murphy) — 1
- Code 1660 (Mr. J. Nichols) — 1
- Code 522.3 Aero Library — 1

Naval Air Development Center
Warminster, PA 18974
- Code 6053 (Dr. K. Green) — 1
- Code (Mr. C. Mazza) — 1

NASA Langley Research Center
Hampton, VA 23665
- Mr. R. Culpepper — 1
- Mr. R. Margason — 1

Wright-Patterson Air Force Base
Dayton, OH 45433
- AFFDL (Dr. K. Nagaraja) — 1

Air Force Office of Scientific Research
Bldg 410
Bolling AFB,
Washington, D.C. 20332
- Code NA (Dr. J. Wilson) — 1

Nielsen Engineering & Research Inc
510 Clyde Avenue
Mountain View, CA 94043 — 1

McDonnell Douglas Aircraft Co.
P. O. Box 516
St. Louis, MO 63166
- Dept. 241 (Mr. R. Jenny) — 1
- Dept. 230 (Mr. R. McDonald) — 1
- (Mr. D. Kotansky) — 1
- (Mr. J. Kamman) — 1

Office of Naval Research
800 North Quincy St.
Arlington, VA 22217
- Code 473 (Mr. Patton) — 1

Commander
Naval Air Systems Command
Washington, D.C. 20361
- AIR-330 — 1
- AIR-330B — 1
- AIR-330C — 1
- AIR-03PA1 — 1
- AIR-03PA3 — 1
- AIR-530 — 1
- AIR-5360 — 1
- AIR-5361 — 1
- AIR-03PA9 — 1

Commanding Officer
Naval Air Propulsion Test Center
Trenton, New Jersey 16828 1

Commanding Officer
Naval Air Development Center
Warminster, PA 19112
Attn: AVTD 1

Prof. M. F. Platzer
Chairman, Dept of Aeronautics
Naval Post Graduate School
Monterey, CA 93940 1

Aeronautical Research Associates
of Princeton
P. O. Box 2229
50 Washington Rd.
Princeton, NJ
Attn: Dr. B. Quinn 1

Superintendent
U. S. Naval Academy
Annapolis, MD 21402 1

Wright-Patterson Air Force Base
Dayton, OH 45433
Aero & Airframe Branch,
(Dr. T. Weeks) 1

Vought Corporation
Advanced Technology Center, Inc.
P. O. Box 6144
Dallas, TX 75222
Dr. C. S. Wells, Jr. 1

Grumman Aerospace Corporation
Bethpage NY 11714
Research Dept. (Dr. R. Melnik) 1
Adv Dev. Dept. (Mr. F. Berger) 1

University of Maryland
Dept. of Aerospace Engr.
College Park, MD 20742
Dr. J. D. Anderson, Jr. 1

United Aircraft Corporation
Research Laboratories
Silver Lane
East Hartford, CT 06108
Dr. M. Werle 1

Polytechnic Institute of New York
Long Island Center
Dept. of Aero Engr & Applied Mechanics
Route 110
Farmingdale, NY 11735 1

Lockheed Missiles & Space Co., Inc
Huntsville Research & Engineering
P. O. Box 1103
Huntsville, AL 35807
Mr. A. Zalay 1

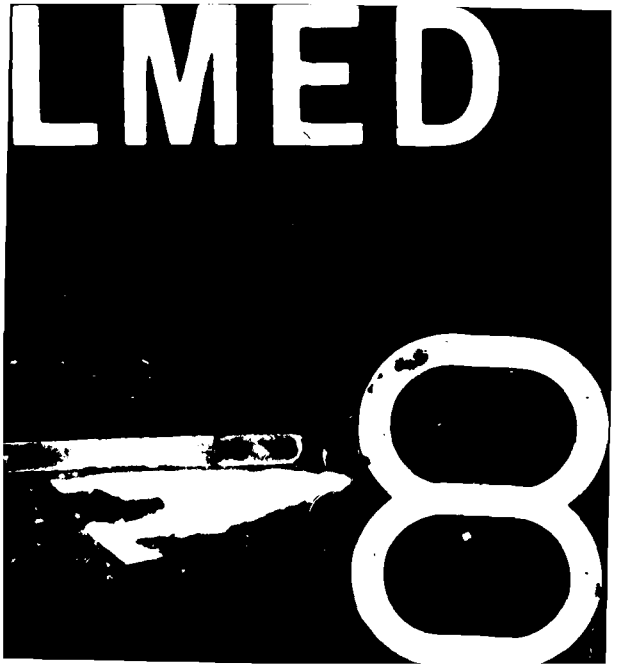
LMED
8